

INVESTIGATIONS RELATING TO THE  
APPLICATIONS OF FIELD EMISSION  
CATHODES

D.J. SWANN, M.A.

Downing College  
Cambridge

A dissertation submitted for the  
degree of Doctor of Philosophy at the  
University of Cambridge

August 1971



Frontispiece: The Scanning  
Electron Optical Column

## PREFACE

This dissertation describes the author's research at the Cambridge University Engineering Laboratories between October 1966 and January 1970, under the supervision of Dr. K.C.A. Smith, to whom I am indebted not only for suggesting the subject of this dissertation, but also for his continued help and encouragement throughout the whole of the research period.

The work was directed towards the practical application of field emission cathodes in electron optical instruments, in particular, the scanning electron microscope. Although it has been realized for many years that the field emission cathode offers the possibility of an extremely bright electron emitter, its exploitation has been prevented both by practical difficulties of operation, which normally requires an ultra high vacuum environment, and by electron optical problems arising from the extremely small size of the source.

A field emission microscope was constructed with ultra high vacuum capability, in which the behaviour of field emission cathodes was investigated over a wide range of operating conditions. The results give better understanding of the physical processes involved, and provide design data suitable for predicting emitter lifetimes and emission noise, both of which are necessary for the future development of electron optical applications.

To investigate means by which the stringent vacuum requirements for field emission might be reduced, a study was made of the operation of cathodes at elevated temperatures and under pulsed conditions. In both cases it proved possible to obtain stable emission in considerably worse vacuum levels.

A scanning electron optical column was also designed and constructed, on the basis of conventional vacuum techniques, with a differentially pumped field emission gun built to ultra high vacuum standards. A single magnetic electron lens was used to form a probe, and facilities were similar to those found in the final stages of the scanning electron microscope.

Using the apparatus, measurements were made of probe diameters, currents and brightnesses from field emission sources under particular imaging conditions. Brightnesses were obtained which were significantly greater than may be achieved with conventional thermionic emitters.

This work formed the basis of papers delivered at three conferences organized by the Electron Microscopy and Analysis Group of the Institute of Physics and the Physical Society, in 1968, 1969 and 1970.

The author gratefully acknowledges the laboratory facilities and initial funds made available by Professor C.W. Oatley, a research grant from the Science Research Council, also the loan of an ion pump power supply by GEC-AEI Scientific Apparatus Ltd., and an electron beam welding machine by the Allen Clark Research Centre, Plessey (UK) Ltd.

Thanks are due to my present employers, Cambridge Scientific Instruments Ltd., for their help and understanding during the preparation of this dissertation, also the Science Research Council for a three year maintenance grant, and the Engineering Laboratories for support during a further three months.

The author would like to express his appreciation to the staff of the Engineering Laboratories and fellow students, for their advice and for many helpful discussions during the course of the research.

Also, the author is indebted to the many assistant staff who helped with the construction of apparatus: Mr. H.C. Asplen and the laboratory staff of the North Wing, in particular Mr. G. Sayles and Mr. K. Ketteridge; Mr. A.A. Barker and the staff of the instrument workshop, especially Mr. B. Peck, Mr. J. Sayles and Mr. S. Laurence; and to Mr. H. Read and Mr. R. Holmes of the main workshops.

Finally, the author would like to thank his wife for her patience and encouragement, and for her help in the preparation and typing of the manuscript.

The contents of this dissertation are the author's original work, except where due reference is given. This dissertation has not been submitted to any other University.

*D.J. Swann*

D.J. Swann

August 1971

## CONTENTS

	<u>Page</u>
CHAPTER 1 INTRODUCTION	1
1.1 The Need For Brighter Electron Sources	1
1.2 Practical Approaches to Higher Brightness Sources	2
1.3 Field Electron Emission	5
1.3.1 The Field Emission Microscope	5
1.3.2 Field Emission Theory	6
1.3.3 Stability of Operation, and Life of Emitters	7
1.3.4 Temperature-and-Field Emission	9
1.3.5 The Energy Distributions of Emission	10
1.4 The Brightness Relationship and Field Emission	11
1.4.1 The Brightness of Field Emission Sources	11
1.4.2 Practical Limitations to Electron Probes	13
1.5 The Scope of This Research	13
CHAPTER 2 THE FABRICATION OF TUNGSTEN FIELD EMITTERS	16
2.1 Difficulties of Emitter Fabrication	16
2.2 Filament Base and Support Loop	17
2.3 Welding the Tip Wire	18
2.3.1 Emitter Welding Jig	18
2.3.2 Welding Difficulties	19
2.4 Etching of Emitter Tips	21
2.4.1 Practical Methods	21
2.4.2 Automatic Etch Control	24
2.5 Conclusions	25
CHAPTER 3 THE FIELD EMISSION MICROSCOPE	27
3.1 Introduction	27
3.2 Design and Construction of the FEM	28
3.2.1 The Viewing Screen	30
3.3 Vacuum Performance of the FEM	31
3.3.1 Bakeout and Pumpdown Cycle	32
3.3.2 Pressure Measurement	33
3.4 Operation of the FEM	34
3.4.1 The EHT Generator	35
3.4.2 The Photomultiplier	35

	<u>Page</u>	
3.5	High Voltage Pulse Generator	36
3.5.1	Experimental Requirements	37
3.5.2	Other Work	39
3.5.3	Circuit Functions	40
3.5.4	Clock Pulse Generator	40
3.5.5	Pulse Width/Delay Unit	41
3.5.6	High Voltage Pulser	42
3.5.7	Pulse Generator Performance	45
3.5.8	High Voltage Bias Unit	46
CHAPTER 4	EXPERIMENTS PERFORMED IN THE FIELD EMISSION MICROSCOPE	 47
4.1	Cold Field Emission	47
4.1.1	Preliminary Experiments	47
4.1.2	Flashing of Emitters	48
4.2	T-F Emission	50
4.2.1	T-F Emission Characteristics	50
4.2.2	T-F Emission Stability	51
4.2.3	Establishing T-F Operation in Practice	52
4.2.4	Relative Stabilities of Crystal Faces in T-F Emission	 53
4.3	Triode Gun Configuration	54
4.3.1	Field Emission Control Characteristics	55
4.3.2	T-F Emission Control Characteristics	56
4.4	Measurements of the Lifetimes of Field Emitters	58
4.4.1	Lifetime Criterion	58
4.4.2	Variation of Lifetime with Voltage	59
4.4.3	Variation of Lifetime with Emission Current and Pressure	 60
4.4.4	Factors Affecting Lifetime	61
4.5	Measurements of Emission Noise and Stability	62
4.5.1	Spectral Analysis of Field Emission Noise	63
4.5.2	Effects of Emitter Aging	65
4.5.3	Effects of Heating the Emitter	66
4.5.4	Variations with Operating Pressure and Emission Current	 66
4.6	Pulsed Emission	67
4.6.1	Lifetime of Pulsed Emitters	68
4.6.2	Noise and Stability of Pulsed Emission	70
4.7	Conclusions	70

	<u>Page</u>
CHAPTER 5 THE SCANNING ELECTRON OPTICAL COLUMN	73
5.1 General Concept	73
5.2 Electron Optical Considerations	73
5.2.1 The Conservation of Brightness	74
5.2.2 Thermionic Emission Cathodes	74
5.2.3 Field Emission Cathodes	75
5.2.4 Single Lens Imaging of F.E. Sources	76
5.3 Mechanical Design of the SEOC	77
5.3.1 Vacuum System	78
5.3.2 The Magnetic Lens	79
5.3.3 Scanning System	79
5.3.4 The Specimen Stage	80
5.3.5 Signal Detection	80
5.3.6 Antivibration Mounting	82
5.4 The Field Emission Gun	83
5.4.1 Gun Electrodes	83
5.4.2 Alignment Facilities	85
5.4.3 The Vacuum System	86
5.5 Electronics for the Probe Measuring System	89
5.5.1 The Scan Amplifiers	90
5.6 Electronics for SEM Operation	91
5.6.1 Line and Frame Generators	92
5.6.2 Scan Control	93
5.6.3 Scan Rotation	94
5.6.4 Video Amplifier	95
CHAPTER 6 EXPERIMENTAL WORK IN THE SCANNING ELECTRON OPTICAL COLUMN	97
6.1 Introduction	97
6.2 Experiments with Large Emitter to Lens Separation	99
6.2.1 Alignment	99
6.2.2 Measurements of Angular Emission Current Densities	101
6.2.3 Probe Measurements	102
6.3 Immersed Emitter Configuration	104
6.3.1 Alignment	104
6.3.2 Scan Amplitude and Linearity	105
6.3.3 Vacuum Performance	106

	<u>Page</u>	
6.3.4	Probe Measurements	107
6.3.5	Calculations of Theoretical Performance	108
6.4	Attempts to Reduce Probe Diameters	111
6.4.1	Vibration	111
6.4.2	Magnetic Materials in the Lens Field	114
6.4.3	Electron Optical Problems	114
6.4.4	Interaction of Electrostatic and Magnetic Fields	117
6.4.5	Conclusions	119
6.5	Operation as a Scanning Electron Microscope	120
6.6	Analysis of Emitters Used in the SEOC	120
6.6.1	Comparison of Wire Batches	120
6.6.2	Failure of the Second Wire Batch	121
CHAPTER 7	CONCLUSIONS AND SUGGESTIONS FOR FUTURE WORK	124
7.1	Choice of Operating Mode	124
7.2	Electron Optical Design	125
7.3	Practical Design Considerations	126
7.4	New Emitter Materials	128
7.5	Emitter Failures	128
7.6	Pulsed Emission	129
APPENDIXES		
I	The Computation of Electron Trajectories	130
II	Lanthanum Hexaboride Emitter Fabrication	131
III	Field Emission From Silicon Carbide Whiskers	133
REFERENCES		134

## CHAPTER 1

INTRODUCTION1.1 The Need For Brighter Electron Sources

High resolution electron optical instruments have, until very recently, invariably employed a tungsten thermionic cathode for their electron source. The reasons for this lie mainly with the mechanical and electrical robustness of this type of cathode, and the development of the triode electron gun, which effects an economy of heating power and beam current, whilst very nearly the full theoretical performance of the cathode may be achieved (Haine and Einstein (1952)).

In the electron microscope the electron current which may be used to illuminate a specimen, and hence to derive information, is limited fundamentally by a property of the electron source called its brightness.

The transmission electron microscope is affected only at the highest magnifications when direct observation of the image becomes difficult, requiring considerable dark-adaption of the eye, or alternatively, the use of an image intensifier.

The scanning electron microscope (SEM) suffers severely from the brightness limitation. Although the ultimate resolving power of the SEM is identical with that of the transmission instrument, direct observation of  $\lambda$  specimen  $\lambda$  is only possible with a resolution of 100nm, and the resolution of photographic recordings is limited to about 5nm (Pease and Nixon (1965)) by mechanical and electrical stabilities required for exposures of many minutes.

There is therefore considerable demand for a brighter electron source, particularly with the SEM. This is being rapidly increased by the development of new instruments and techniques, for example, in the transmission electron microscope the development of dark field and weak beam techniques, and of X-ray analysis, and in the SEM the development of Auger analysis, X-ray analysis and the use of the SEM for the fabrication of microelectronics.

The need for a higher brightness source has gained additional impetus through recent work by Crewe (1970), who has developed a high resolution scanning transmission electron microscope based on a high brightness field emission source. This instrument has demonstrated resolutions comparable with conventional transmission electron microscopes.

A scanning transmission electron microscope has several potential advantages, as no optical components follow the specimen. Thus loss in resolution due to inelastic collisions observed in the conventional transmission instrument does not take place. Characteristic energy losses may be used to identify particular materials, and under certain conditions thicker specimens may be examined for the same beam voltage. Also, flexibility in the means of collecting signal experienced with the conventional SEM is preserved, secondary electrons, transmitted primary electrons, photons or X-rays may be used to produce a picture. As the video signal is derived as a time variant, it may be readily processed, if necessary by the inclusion of an on-line computer.

## 1.2 Practical Approaches to Higher Brightness Sources

Considerable interest is currently being shown in the possibilities of electron sources of higher brightness, many published

works appearing during the latter part of this research. The approaches to a brighter source may be divided into three distinct categories.

a) Improved thermionic cathodes. Some work has been directed towards the development of new cathode materials for use in the electron microscope, e.g. Albert (1967), but most interest has been shown in lanthanum hexaboride. This material was investigated by Lafferty (1950), and is attractive because of its low work function of 2.66eV, and capability of high emission current densities, up to  $2 \times 10^5 \text{ A/m}^2$ , thus a theoretical improvement of an order of magnitude in brightness is possible compared with tungsten. It has been little used in the past because of its high chemical reactivity, but recently a successful gun has been developed by Broers (1967) and (1969), which achieves the theoretical improvement. In this gun the problem of chemical reactivity has been overcome by making an  $\text{LaB}_6$  cathode in rod form, one end is mounted in a block of cooled copper, while the other is heated by electron bombardment and forms the electron emitter.

As a result of the high reactivity of  $\text{LaB}_6$  at elevated temperatures, it has proved necessary to operate in vacuum better than  $1 \times 10^{-5}$  torr, in order to prevent poisoning of the cathodes.

b) Pointed thermionic cathodes. A tungsten cathode has normally been used, with its tip either ground or etched to a sharp point. Some workers have for several years claimed improvements of brightness by up to a factor of 10 over conventional tungsten cathodes (e.g. Fernandez-Moran (1967) and Hibi (1964)). Also a considerable improvement in beam coherence has been demonstrated in the transmission electron microscope. Pointed filaments are offered with some commercial electron optical instruments.

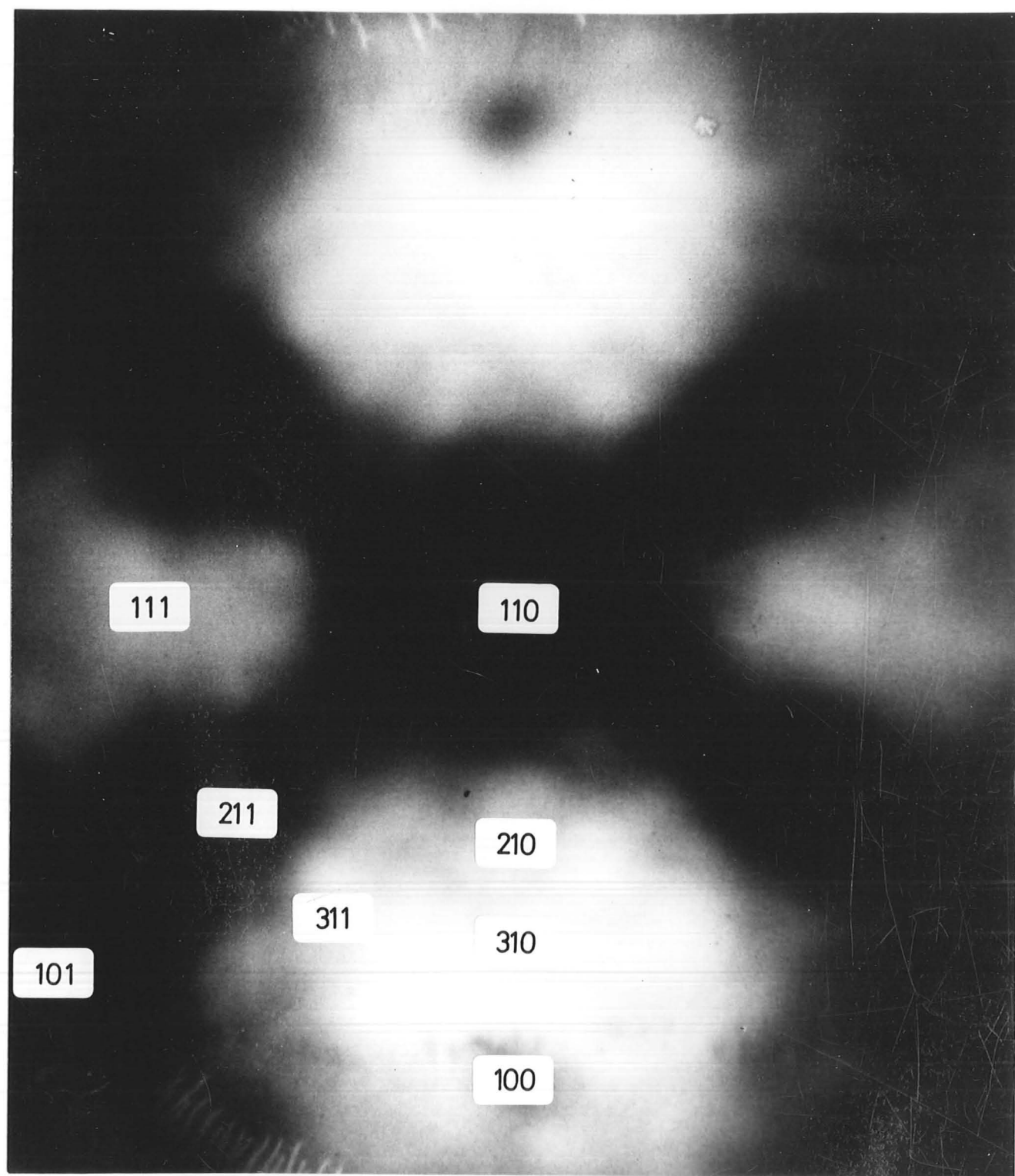


Fig 1.1 Field Emission Pattern from Tungsten

Improvements are attributed to the presence of a relatively high electric field at the tip, which may lower the potential barrier at the surface, or simply prevent the build-up of space charge at higher filament temperatures, as described by Haine and Einstein (1952). The latter seems a more likely explanation particularly in view of the results obtained with T-F emission in section 4.3.2; this is consistent with the short filament lives usually obtained.

c) Field emission cathodes. Although an order of magnitude brightness improvement is possible with thermionic emitters, and will undoubtedly be soon brought about in commercial instruments, any really significant improvement must involve the use of field emitters.

Field emission has long offered the possibility of an extremely bright source of electrons, brightnesses as much as  $10^5$  to  $10^6$  greater than those obtainable with thermionic emitters being theoretically possible.

Despite the development of much of the necessary technology with the Field Emission Microscope, field emission has remained unexploited for electron optical purposes until very recently. This has been partly due to the hitherto adequacy of thermionic sources, but the main obstacle has been the necessity for the ultra-high vacuum environment which is required to obtain stable emission.

Recently, there has been renewed interest in field emission, and the development of the first practical field emission electron gun by Crewe (1968). This gun produces a real focus which may be used directly as the probe of a scanning microscope, Crewe (1969). The performance of this instrument matches the conventional SEM with a resolution of approximately 10nm, but at a much reduced

exposure time, and has recently become available commercially as a simple scanning electron microscope.

When the probe is demagnified with a high quality magnetic lens the resolution may be further improved with transmission specimens (Crewe (1968)), and recent improvements to the system have produced point-to-point resolutions of 0.5nm at 30kV (Crewe (1970)). This is close to the theoretical resolution limit imposed by the lens aberrations and the electron wavelength.

### 1.3 Field Electron Emission

The phenomena was observed by Wood as long ago as 1897, and has since been recognized as one of the principle causes of high voltage breakdown in vacuum.

When <sup>a</sup> high electric field is applied to a conductor, the surface potential barrier is thinned. Thus electrons from the solid have a finite probability of tunnelling through the barrier and being emitted. This is called Field Electron Emission or more simply Field Emission.

#### 1.3.1 The Field Emission Microscope

The invention of the Pointed Projection Field Emission Microscope has resulted <sup>in</sup> its development as a useful tool for the study of metallurgical and physical phenomena. The emitters used take the form of wire etched to a fine point, typically less than 1  $\mu\text{m}$  diameter, so that <sup>the</sup> local field at the tip is considerably enhanced and emission takes place with a few kilo-volts applied to the cathode. The anode is a conducting phosphor screen.

As the tip is so small, it invariably consists of a single crystallite of the bulk material. The work function, and hence the height of the potential barrier, varies over the different

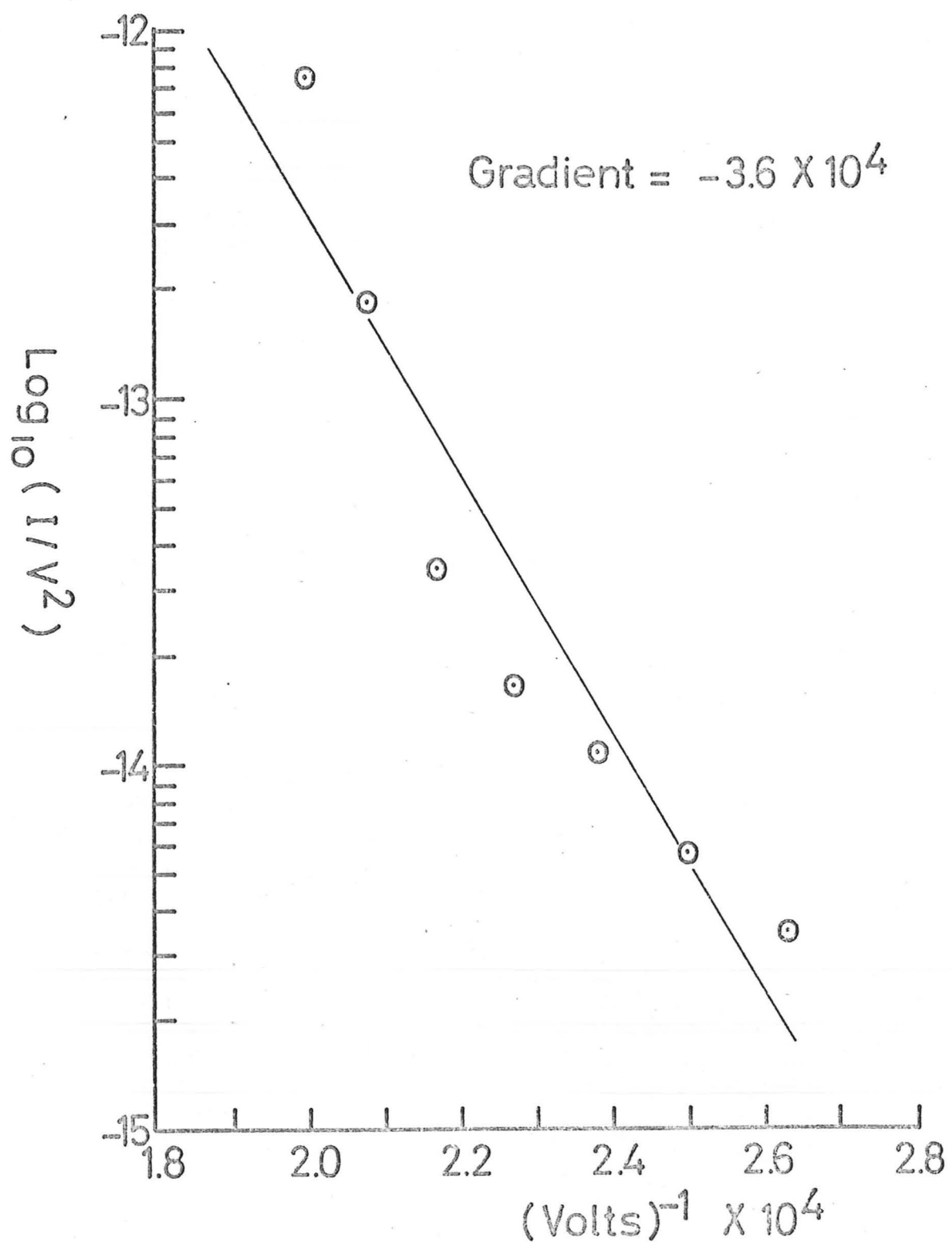


Fig 1.2 A Fowler - Nordheim Plot.

faces of the crystal, thus the emission pattern on the screen may be used to identify crystallographic directions. The manufacturing processes for normal tungsten wire invariably result in the (110) axial orientation. This face has a high work function and consequently gives little emission as may be seen in Fig. 1.1.

### 1.3.2 Field Emission Theory

The development of a satisfactory field emission theory by Fowler and Nordheim (1928), Nordheim (1928), provided a useful test of the newly developed theory of wave mechanics. The full expression for emission current density  $J$ , was given as:

$$J = \frac{e^3 E^2}{8 h \bar{\phi} t^2(y)} \exp - \left[ \frac{4(2me)^{1/2} \bar{\phi}^{3/2} f(y)}{3 h e E} \right]$$

where  $E$ , is the electric field strength at the surface of the emitters, and  $\bar{\phi}$  the work function. Functions  $t(y)$  and  $f(y)$  are both near unity, and have been tabulated.

Work by Dyke (1956) and recently van Oostrom (1966) amongst other has established the accuracy of the above relationship.

Field emission current/voltage data is often presented in the form of a Fowler-Nordheim plot, which is a plot of  $\log(I/V^2)$  against  $(1/V)$ . An example is shown in Fig. 1.2 for a field emission diode over the limited range of emission currents which could be measured in the field emission microscope. Experimental conditions will be described later in section 4.1.1.

The significance of the Fowler-Nordheim plot is that it is almost linear, and its gradient is proportional to  $\bar{\phi}^{3/2}$ , thus relative values of work function may be measured over the surface of an emitter. Also, using methods devised by Charbonnier (1962) and Gomer (1961), an estimate of emitter size and emission current densities may be made from the  $I/V$  data only, with an accuracy

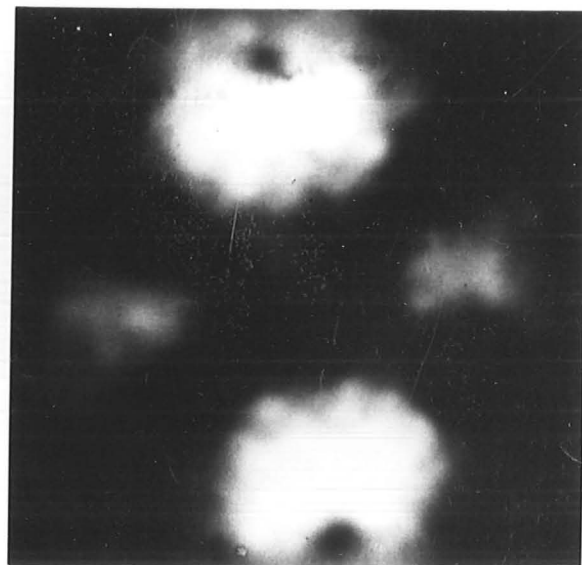
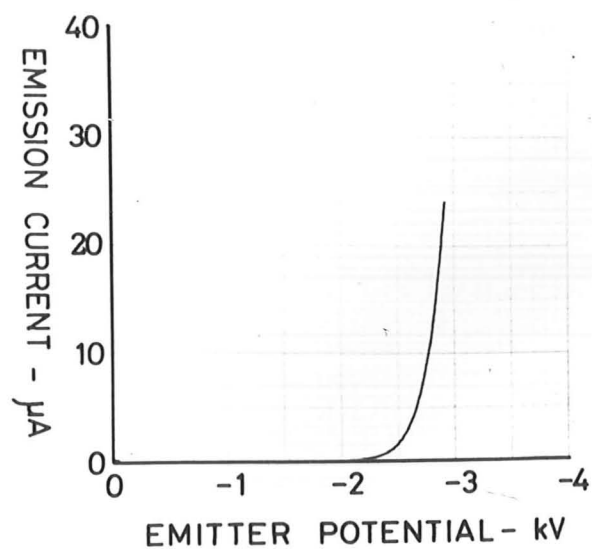


Fig 1.3 Cold Field Emission.

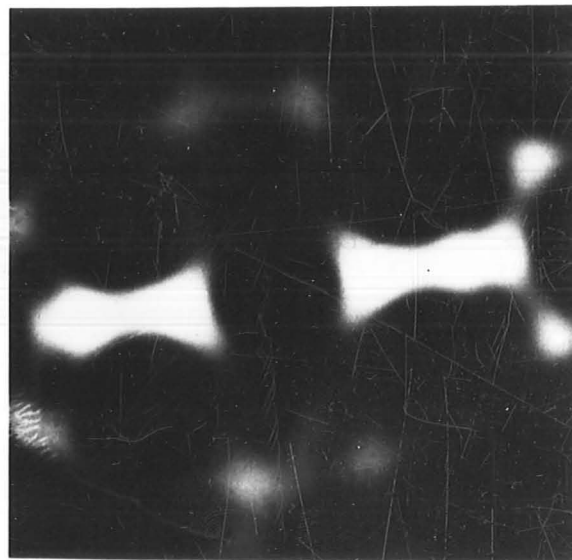
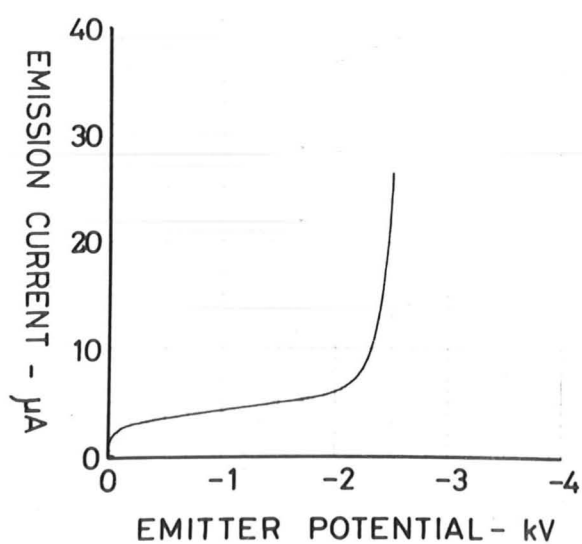


Fig 1.4 T - F Emission.

of approximately  $\pm 20\%$ . In the example of Fig. 1.2, we find that at  $V = 5.0\text{kV}$ ,  $J = 2 \times 10^7 \text{A/m}^2$ , and the effective emission area is  $9 \times 10^{-13} \text{m}^2$ .

An example of the way in which the current from a tungsten emitter varies with voltage is shown in Fig. 1.3. This illustrates the very rapid rise of emission current with voltage once the threshold level has been passed. The rapid rise of emission current coincides with the appearance of the characteristic emission pattern.

### 1.3.3 Stability of Operation and Life of Emitters

A field emitter is subjected to attack by residual gas atoms (or molecules), and ion bombardment. Both of these mechanisms affect the stability of the field emission current from the region on the surface of the emitter at which the collision takes place.

a) Residual gas attack. An atomically clean field emitter is not at equilibrium with its vacuum environment. The emitter may be heated to a temperature which is sufficient to remove any adsorbed matter,  $2000^\circ\text{K}$  for tungsten. Thereafter, residual gas atoms are reabsorbed at a rate determined by their partial pressures in the system. Thus the surface coverage follows an exponential variation towards equilibrium, which will normally be at a significant fraction of a monolayer.

When an atom is adsorbed onto the surface of a field emitter its effect is two-fold:

- i) the local field is enhanced,
- ii) the local work function may either increase or decrease.

Both of these effects cause changes in the local intensity of emission, which lead to continuous fluctuations of the total emission current.

b) Ion bombardment. Collisions between emitted electrons and residual gas atoms generate positive ions which are accelerated towards the emitter. The resulting ion bombardment damages the surface of the emitter, causing a local change of geometry and consequently a change in the local electric field. Also the ion may be adsorbed on the emitter surface. Thus local changes of emission current occur as before.

The sputtering damage is cumulative, and as surface roughening and local field enhancement take place preferentially at the sites of previous ion damage, electron emission, and hence ion bombardment are enhanced in these regions. The result is an irregular increase of emission current, which eventually leads to a vacuum arc and the destruction of the emitter.

Whereas both the effects described above may in principle be reduced to any desired level by improving the vacuum in the system, it is very seldom practicable to do so. The study of field emission cathodes has involved the development of sophisticated vacuum techniques producing pressures of the order of  $10^{-15}$  torr, in which stable operation for many thousands of hours is possible, Dyke<sup>et al.</sup> (1960). However, in a practical, demountable electron optical system, the best pressure which can be achieved in the vicinity of an emitter is about  $1 \times 10^{-9}$  torr. At this pressure the time taken for a clean emitter to reach equilibrium with the surrounding vacuum is about 30 minutes, and with an emission current of 10  $\mu$ A, about 10 hours operation is possible before the emitter is destroyed by vacuum arc.

It should be noted that the onset of severe ion bombardment damage can readily be detected from the resulting increase of emission current, and the emission stopped before catastrophic

failure occurs. Ion damage may be repaired by heating the emitter, which increases the mobility of surface atoms. Under the influence of surface tension the smooth surface is regenerated. This operation, known as "flashing", also serves to remove adsorbed gases.

#### 1.3.4 Temperature-and-Field Emission

When a tungsten field emitter is heated to around 1800K, not only are surface contaminants thermally desorbed, but also the mobility of the tungsten emitter atoms is increased, so that any small surface irregularities caused by ion bombardment are smoothed over and do not accumulate. Thus the two mechanisms described above which lead to emitter failure may be countered by operating at an elevated temperature.

This mode of emission is normally called T-F emission after Dolan and Dyke (1954), who have successfully obtained stable emission in sealed ultra-high vacuum tubes for several thousands of hours. Its application in vacuum conditions which are much worse than those required for stable cold-field emission is an obvious application which has been suggested by, among others, Drechsler et al. (1958), though experimental work seems lacking. However, Dyke<sup>et al.</sup> (1960) has reported stable T-F operation in a pressure of  $10^{-6}$  torr of helium.

In the region of 1800K, the thermionic emission coefficient of tungsten is very low, and in high electric fields the principle mechanism of electron emission is by tunnelling through the potential barrier as in field emission. Fig. 1.4 gives typical I/V characteristics and the T-F emission pattern obtained from a tungsten emitter, which shows variations of work function with crystallographic orientation on the tip. At low applied voltages

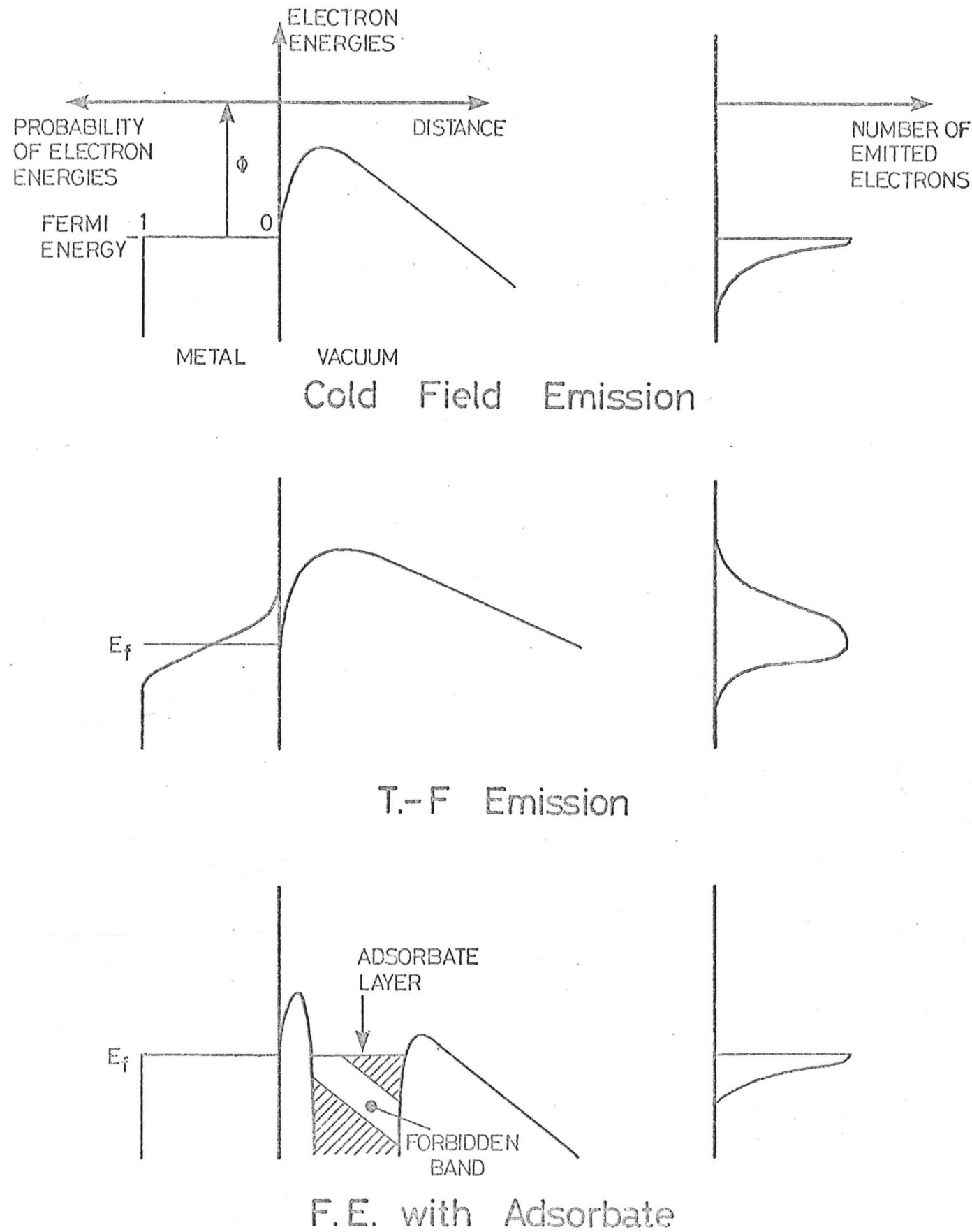


Fig 15 Illustrating Modes of Emission

the emission current is due to thermionic emission from the relative bulk of the tip support and heating loop, at higher fields the emission pattern emerges and the I/V curve shows the steep rise of current characteristic of electron tunnelling.

At the elevated temperatures required for T-F emission, the highly mobile surface atoms experience both surface tension and electrostatic forces, the former tending to blunt the emitter and the latter to sharpen it. These mechanisms have been investigated by Dyke et al. (1960), who found that there is a practical operating range of tip radii and surface fields at which a balance occurs. The effect is, however, to limit the maximum current density available from the cathode at  $10^7$  to  $10^8 \text{ A/m}^2$ .

1.3.5 The Energy Distributions of Emission

An important consequence of operating field emitters at elevated temperatures, is that it results in a larger energy spread of the emitted electrons. To see how this occurs, we refer to the models of surface potential distributions shown in Fig. 1.5, which are based on those published by Dyke and Dolan (1956).

In cold field emission, there are no electrons in the metal with energies greater than the Fermi energy. The surface potential barrier is thinned by the presence of the high surface field. Clearly, electrons which have the Fermi energy have the highest probability of tunnelling through the barrier, and this probability decreases rapidly at lower energies. Thus the spread of energies of the field emitted electrons is very narrow and is cut off abruptly at the Fermi energy.

When the emitter is heated there becomes a finite probability for electrons to have energies greater than the Fermi energy, and these electrons see a correspondingly reduced potential

barrier, so that the probability of emission is high. Equally, emission from below the Fermi energy takes place as with cold field emission, so that the resulting spread of emitted electron energies is considerably broadened.

Measurements and calculations of emission energy spreads from cold field emitters have been reported by Young and Müller (1959), Young (1959), and show that a typical value is 0.2eV. In T-F conditions, Dyke and Dolan (1956) have calculated energy distributions of 2 - 3eV over a range of operating temperatures and applied fields.

It is worthwhile examining the effects of adsorbed gases on the emitter surface. The adsorbate layer is formed close to the metal surface, so that a very thin potential barrier exists and electrons may transfer freely from states within the metal to similar states in the adsorbate layer. In the example shown in Fig. 1.5, the adsorbate has permissible energy levels which see a much thinner potential barrier than would electrons in the clean metal, the emission is therefore greatly enhanced. With a different adsorbate, the forbidden energy band might be higher, so that there would be no exchange of electrons between the metal and states above the forbidden band, thus the emission would be reduced. It is important to note that the energy distribution of electrons in the presence of adsorbed gas is not broadened, since emission is seldom obtained from an atomically clean emitter surface.

#### 1.4 The Brightness Relationship and Field Emission

##### 1.4.1 The Brightness of Field Emission Sources

Langmuir (1937) showed that the brightness of an electron

beam cannot exceed the brightness of the electron source. This is related to the emission current density  $\rho_0$ , at the cathode and total accelerating voltage  $V$ . For thermionic emission he derived the relationship

$$B = \frac{\rho_0}{\pi} \left( \frac{eV}{kT} + 1 \right)$$

by assuming a Maxwellian distribution of energy in the emitted electrons, and obey Lambert's law.

For field emission, and T-F emission, the energy distribution of the emission is not Maxwellian. To take account of this we replace the term  $kT$ , by  $eV_t$ , where  $eV_t$  represents the transverse energy spread of emission  $\lambda$  (full width at half maximum). Thus, since  $V \gg V_t$ , we obtain

$$B = \frac{\rho_0}{\pi} \frac{V}{V_t}$$

For field emission,  $\rho_0$  may be as large as  $10^{10} \text{ A/m}^2$ , with  $V_t = 0.2$  volts. Taking  $V = 5 \text{ kV}$ , this gives

$$B_{FE} = 8 \times 10^{13} \text{ A/m}^2/\text{sr}$$

In T-F mode,  $\rho_0$  is limited to about  $10^8 \text{ A/m}^2$ , with typically,  $V_t = 3$  volts, whence

$$B_{T-F} = 5 \times 10^{10} \text{ A/m}^2/\text{sr}$$

For comparison, normal tungsten thermionic emission at  $3 \times 10^4 \text{ A/m}^2$ , gives

$$B_{TE} = 2 \times 10^8 \text{ A/m}^2/\text{sr}$$

Clearly, for an imaging system in which the probe current is limited by the brightness of the electron source, both T-F and field emission sources offer the possibility of greatly improved performance.

#### 1.4.2 Practical Limitations to Electron Probes

The brightness of an electron probe is given by

$$B = \frac{4I}{\pi^2 d^2 \alpha^2}$$

where I is the probe current, d its diameter, and  $\alpha$  the semi-angular aperture of the imaging system. By Langmuir (1937), this value of probe brightness may not exceed the brightness of the source.

At first sight it may appear that an increase in brightness will give a proportional increase in probe current. However, Cosslett and Haine (1954) have shown that a field emission source may not in practice be imaged under optimum conditions, and that the full potential advantages of field emission sources may not therefore be approached. There are considerable gains, nevertheless, in the use of field emission sources, compared with thermionic emission for producing probes of small diameter, less than 100nm approximately, whereas for larger probes, more current may be obtained by thermionic emission.

Recent calculations by Crewe et al. (1968), and Everhart (1967) for field emission systems have shown that for probes less than 10nm diameter, typically three orders of magnitude increase in current may be achieved. Field emission sources are therefore particularly suited to the high resolution operation of the scanning electron microscope.

#### 1.5 The Scope of this Research

This investigation has been directed towards the practical application of field emission cathodes in electron optical instruments.

It has been necessary to develop the basic techniques for fabricating and operating field emitters, since little or no experience of this mode of emission existed within the laboratory.

To study the basic physical processes governing the operation of field emitters, a field emission microscope has been built. In this instrument the effects of operating over a wide range of emission currents and system pressures down to the ultra high vacuum region have been investigated. Measurements made include, principally, the operating lifetimes of emitters and the emission noise.

Particular attention has been paid to techniques which might relieve the stringent operating conditions necessary to obtain stable field emission from tungsten. These include a study of the T-F mode of emission, and an investigation into the effects of pulsed operation of field emitters. An attempt was made to fabricate field emitters from single crystal lanthanum hexaboride, since Windsor (1970) has reported that this material is less sensitive to the vacuum environment than tungsten. However, this was largely unsuccessful and is described briefly in Appendix II. Also, a short investigation of emission from silicon carbide whiskers was made, and this is described in Appendix III.

A triode field emission gun was designed, which overcame some of the practical operating problems associated with the use of field emitters, by providing independent control of accelerating voltage and total emission current. Additionally, the triode geometry permitted an investigation of the pulsed emission mentioned above.

Initially it was intended to study field emission systems both experimentally and theoretically by the use of the University computer facilities. However, it soon became clear that both

courses represented major projects, and the computational work was discontinued. Some plots of electric field and electron trajectories for a simple triode gun were obtained and this is described in Appendix I.

For the experimental study of field emission systems, a single lens scanning electron optical column was built. It had a differentially pumped electron gun which permitted all but the gun components to be operated in much higher pressures than were required in the emitter region. The instrument was used to measure the brightness of electron probes from a number of column configurations. Brightnesses were obtained which were considerably greater than may be achieved with conventional thermionic cathodes.

Towards the end of the research, development of the facilities in the scanning electron optical column enabled it to operate as an independent, scanning electron microscope, with a field emission electron source.

## CHAPTER 2

THE FABRICATION OF TUNGSTEN FIELD EMITTERS

Several accounts of techniques for producing tungsten field emitters have been reported in the literature (eg. Crewe (1968), Dyke (1953), Dyke and Dolan (1956), Earnshaw (1965), Gomer (1961), Hibi (1964), Martin (1960), van Oostrom (1966), and Swift (1960)), though in general no more than a brief descriptions of the processes have been given.

The basic requirements are for a suitably oriented wire (eg. (111)) to be etched to a fine point which forms the actual field emitter. This must be rigidly supported in a manner which is compatible with heating the tip. A number of possible geometries have been discussed by Swift (1960). Of these, the most suitable construction is achieved by welding a short length of the oriented wire to a supporting tungsten wire loop. This was the method chosen by Swift. An additional important factor in favour of this construction is that it uses the minimum length of oriented wire\*.

2.1 Difficulties of Emitter Fabrication

When attempting to produce emitters by methods described in the literature, it soon became clear that results would depend very much on the skill of the operator, and that even with considerable practice a low success rate would have to be tolerated.

---

\* At present, single crystal tungsten wires, .005" diam., 2" long are available from Field Emission Corporation, McMinnville, Oregon 97128, USA at £100 each.

The principle areas of difficulty are as follows:

- a) The welding of the tungsten tip wire to its tungsten support loop is very difficult to achieve reproducibly.
- b) Accurate positioning and orientation of the tip with respect to its support requires careful alignment in a suitable jig.
- c) The etch process must be made reproducible, and automatic control is necessary to produce consistently high quality tips.

It was clearly necessary to develop improved techniques for emitter fabrication which would be both reliable and reproducible, not only to avoid wastage of the expensive oriented wire, but also to give consistently high quality emitters.

## 2.2 Filament Base and Support Loop

Tungsten wire may conveniently be bent into a smooth, reproducible radius by pressing the wire around a suitable tool in to a rubber bung. The tool in this case was parallel sided with an approximately 1mm radius edge, the bend thus produced formed the apex of the hairpin, which proved satisfactory. A sharper bend was found to harden and stress the wire making subsequent tip welding more difficult.

The legs of the hairpins were bent into a similar radius, and welded to the pins of commercially available AEI electron microscope filament bases using a small, conventional spot welder. These bases were chosen as they were readily available and convenient to use and mount, moreover the materials used, sintered glass and niolo pins, are compatible with ultrahigh vacuum use.

Little difficulty was encountered in this process other than occasional poor alignment of the hairpin. Due to the low cost of the emitter at this stage the small rejection rate was

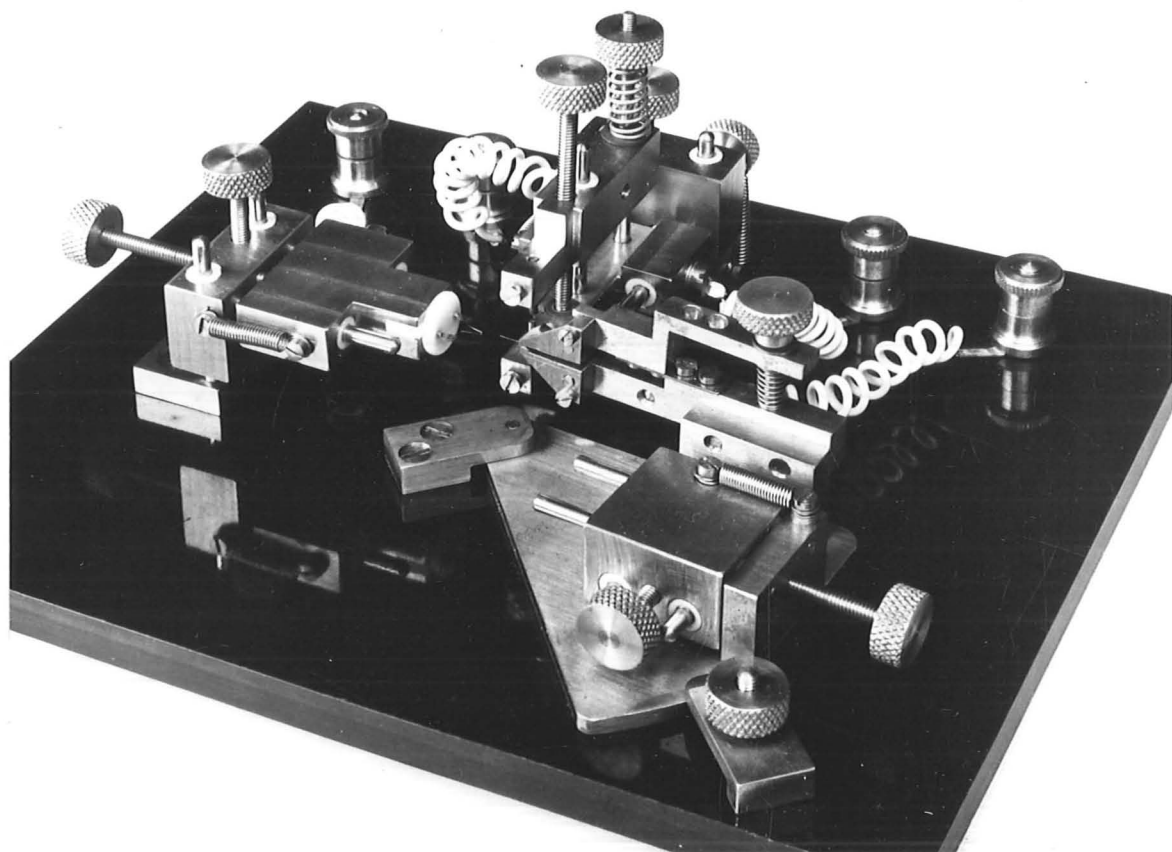


Fig 2.1 Emitter Welding Jig

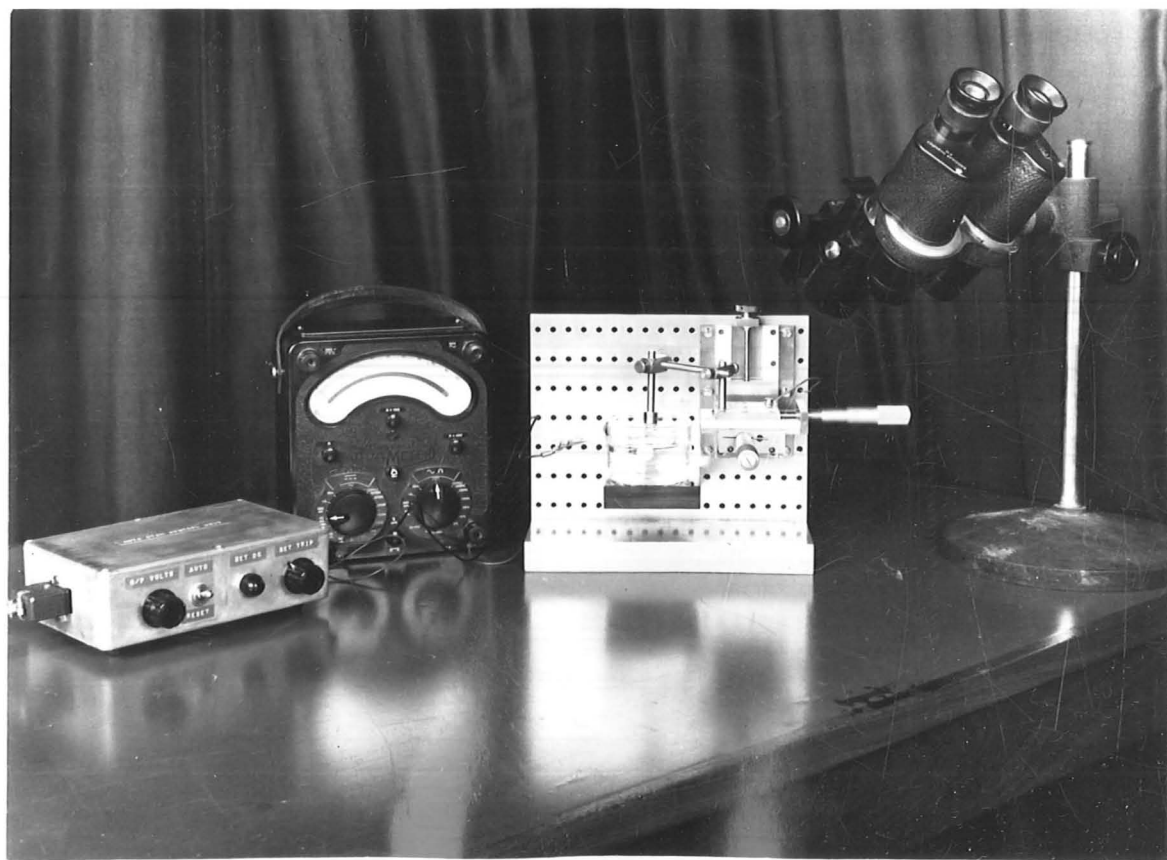


Fig 2.2 Etching Apparatus

tolerated.

### 2.3 Welding the Tip Wire

A number of methods were tried for welding the tip wires to the hairpins, including conventional spot welding, discharge welding, and electron beam welding. Only the first method gave any significant success, though the other methods were interesting as they offered a possibility of butt welding the tip to the hairpin.

#### 2.3.1 Emitter Welding Jig

When a tungsten to tungsten weld has been made, the metal near to the weld becomes very brittle. Thus, mechanical shock introduced by trying to cut the tip wire after welding with ordinary wire cutters invariably results in a fracture near to the weld.

Although methods could clearly be devised for cutting the wire without damaging the weld, e.g. the whole area could be encased in hard plastic and then cut with a diamond saw, the most convenient method found was to use short, cut lengths of oriented wire.

It is clearly necessary to accurately position and align the tip wire to the filament, and to be able to carefully control the welding electrodes so that fracture does not result after the weld has been made.

The welding jig shown in Fig. 2.1 was constructed, with which it was possible to handle lengths of oriented wire of about 3mm satisfactorily. Independent movements for the filament holder, tip wire holder and electrodes were provided, each being moveable in two orthogonal directions. Additional facilities

to separate the electrodes and wire clamp by fine controls were provided, also the wire could be rotated about the vertical axis for alignment.

The jig was set up through binocular viewers. One disadvantage was found to be that visibility of the wires was severely limited, and there is no obvious way of improving this.

Electrical connections for welding were provided to the electrodes, also to the filament holder and wire clamp. These were used for experiments on discharge welding and could also be used to test continuity of the weld before removing the clamps.

### 2.3.2 Welding Difficulties

The reliability of spot welding was not good and this could be traced to a number of causes:

a) Surface contamination on the hairpin. This was removed by electrolytic cleaning in 0.5N NaOH solution, with 10V a.c. applied between the hairpin wire and a nickel electrode for 10 seconds. Contamination did not appear to be present on the single crystal wire and treatment was not needed.

b) Nature of the tungsten wire. Tungsten wire is not a universally constant and pure material, it is fabricated almost entirely for the lamp and valve industries, and manufacturers have several techniques for producing the wire. These nearly always involve some form of additive which can severely affect the physical nature of the wire by influencing crystal formation.

Several sources of wire were explored, and the most satisfactory wire for welding was found to be soft, straight wire, which could be readily cut and formed. Suitable wire with potassium and aluminium silicate doping to promote large crystal growth, was supplied under the description "cleaned and lightly

straightened" by Mullard Ltd\*. The single crystal tungsten for the oriented tips is of a similar nature, and was found to weld well to this type of wire.

c) Oxidation at weld. This can be prevented by welding in an inert atmosphere, or under a protective liquid. Carbon tetrachloride was found to be suitable and has the further advantage that it effectively degreased the wire and electrodes ensuring good electrical contact. Also if the weld was for any reason unsatisfactory, the short length of expensive oriented wire was captured by the surface tension in the remaining liquid and was not lost.

d) Poor reproducibility of welding conditions. It was found that satisfactory welds could be produced over only a very limited range of discharge conditions. A S.T.P.\* capacitance discharge welder was found most suitable, and when operated with a capacitance of 1.2  $\mu\text{F}$  discharging 55 volts gave very good, reproducible welds.

e) Sticking to welding electrodes. By keeping the electrodes clean and polished, sticking to the wire was largely avoided. Copper and tungsten electrodes were both used with success, using a very low welding pressure, but a better combination was found to be with one electrode copper, on the hairpin side, and the other tungsten.

With reasonable care, the techniques described above produced very consistent, high quality welds almost without failure.

---

\* Mullard Ltd., Mullard House, Torrington Place, London WC1.

\* Spemby Technical Products Ltd., Trinity Trading Estate, Sittingbourne, Kent.

## 2.4 Etching of Emitter Tips

The electrolytic forming of tungsten wire into fine tips is usually described as an etch, but is in fact an electro-polishing process.

Characteristics of electro-polishing action are described by Tegart on the basis of the formation of a viscous layer of reaction products over the anode. The effect of the layer is to inhibit further attack, so that surface protrusions are preferentially removed and a smooth, polished surface results.

### 2.4.1 Practical Methods

When polishing is taking place the development of the inert surface layer may reduce the reaction to an undesirably low rate. Several means have been devised to overcome this difficulty:

a) Mechanical agitation of the electrolyte. Anode rotation is often used in commercial electropolishing system as a means of stirring the electrolyte. Stirring was tried in these experiments, however, the turbulence in the electrolyte rendered the method useless for the etching of fine tips.

b) Agitation by inert gas. A non-reactive gas may be bubbled through the solution, and over the anode surface so that it is purged of inert layers, reaction then proceeds rapidly and a new inert surface layer builds up to produce the polishing action.

This method was used to produce some early emitter tips which had very good surface finishes, however, several difficulties were encountered:

i) Etch rate and current varied rapidly as each gas bubble passed through the system, this made the etch process difficult to monitor and impossible to control with an automatic cut-off.

ii) Bubbles of electrolyte could rise up the anode wire, and unless the weld was well away from the surface of the electrolyte it came under severe attack. This effect was reduced considerably by inserting the wire through a 1mm diameter hole in the cathode, which was then mounted horizontally on the surface of the electrolyte. By this technique tips could be formed as close as  $\frac{1}{2}$ mm from the edge of the weld.

iii) Bubbles in the solution made visual observation of the process difficult, and hence determination of the completion of the etch was uncertain.

c) A.C. etching. This provides alternately attack of the metal and liberation of gas, the latter serves to purge the surface clean of reaction products and thus permits a rapid reaction.

Disadvantages are generally as given above in (b). Tips produced by the A.C. technique were generally of a poorer surface finish than those using D.C. techniques, this is probably due to the severe attack which takes place at the beginning of each etch cycle, when the surface is unprotected by an inert layer, and the applied voltage is not at the value required for a polishing action.

d) The use of strong electrolyte. Under D.C. conditions the reaction will proceed at a satisfactory rate if a sufficiently concentrated solution of electrolyte is used. A reasonable rate is obtained with 1N NaOH solution.

This method does not suffer the disadvantages encountered in (a) (b) and (c) above. As no agitation is necessary the tip forms without being subjected to mechanical stresses, the etch current varies smoothly so that a automatic control of the process is possible, and visual observation is not impaired.

Some emitters were prepared by this process, though it was found very difficult to obtain reproducible etching characteristics and emitters. The reaction was often very difficult to start, and would only proceed if the tungsten was cleaned by A.C. etching. This method is believed to be used by Crewe who reports that considerable care must be taken to isolate the etch bath from mechanical vibrations, and carries out emitter etching on a concrete block supported by antivibration mounts. As no similar precautions were taken it is likely that the lack of reproducibility was due to mechanical vibrations, however, the method was not pursued as a more satisfactory arrangement was developed.

e) The use of chemical reagents to remove reaction products.

Work at the Department of Metallurgy, Cambridge University has shown that a very high polish is possible if a tungsten wire is etched in certain photographic developers, e.g. Ilford ID 11. The use of photographic developers as electrolytes is reported elsewhere in the literature by Fasth (1967). Very highly polished surfaces were readily produced by this method, though reaction would only proceed under A.C. conditions.

The addition of developer to NaOH solution, however, provides a very useful electrolyte. Suitable concentrations were found to be obtained with equal quantities of 2N NaOH solution and ID 11 stock solution, though quite varied concentrations could be tolerated and were found to have little effect on the process.

This mixed electrolyte was found to work very well under D.C. conditions and gave very reproducible etch characteristics and emitters, it also had none of the starting problems associated

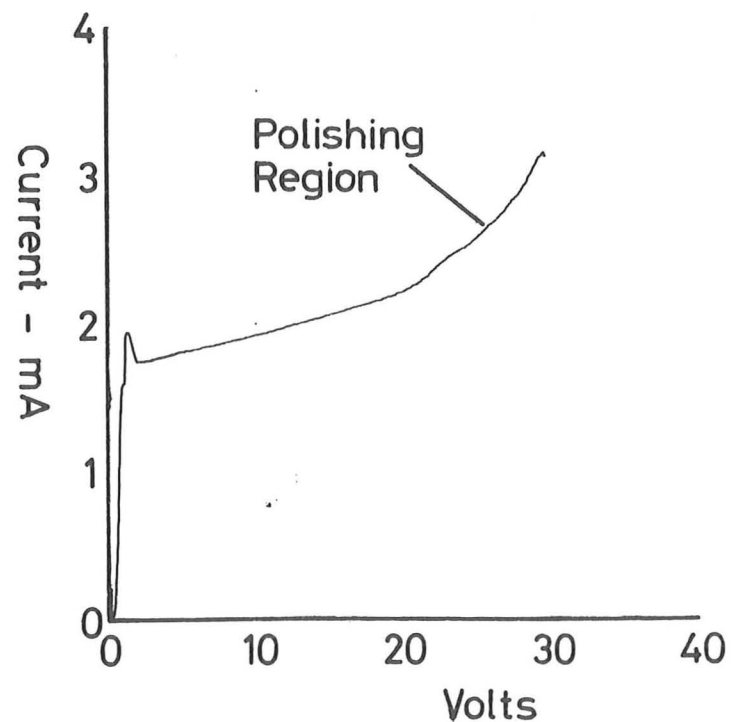


Fig 2.3 Cell Current Variation with Voltage

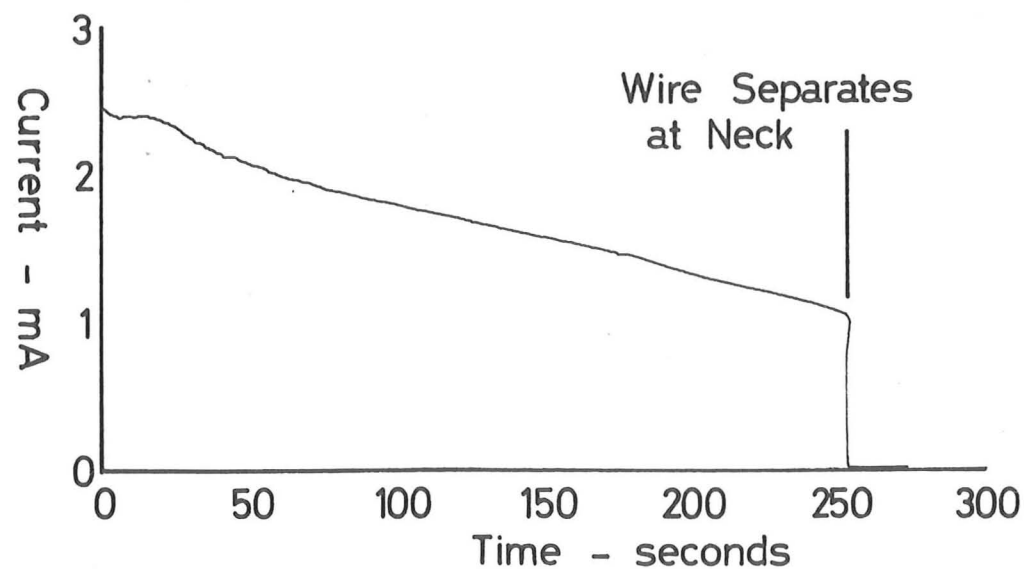


Fig 2.4 Current Variation with Time

with NaOH solution alone, nor did it require an environment free from mechanical vibrations. In addition the very highly polished surface was obtained as with the developer alone.

Cell characteristics are shown in Fig. 2.3. The polishing region may be identified from similar curves given in Tegart (1959), and a voltage of 26V was used satisfactorily.

All emitters used for serious experimental work were produced by this technique, which was completely free of the disadvantages found with others discussed above.

#### 2.4.2 Automatic Etch Control

Typical current variation during the etch process is shown in Fig. 2.4. Initially the current is very high, dropping rapidly as an inert layer of reaction products builds up. The current steadily decreases as the surface area of anode is reduced. A neck begins to form in the wire and becomes more pronounced as the reaction proceeds. Eventually the wire separates at the neck causing a sudden drop of current as the surface area is reduced. The remaining wire tip is now at its sharpest, the etch should be stopped to prevent continued attack which would blunt the tip.

A control circuit had been devised which will detect the rapid drop in current, and switch off the cell voltage, and is shown in Fig. 2.5.

Operation of the control circuit is straightforward. The cell current is sampled by a 1 k-ohm resistor and the voltage generated compared with a reference using the long tail pair comparator, T8 and 9, which is fed from the constant current source provided by T10. When the current falls below a predetermined level, the collector voltages in the comparator swing,

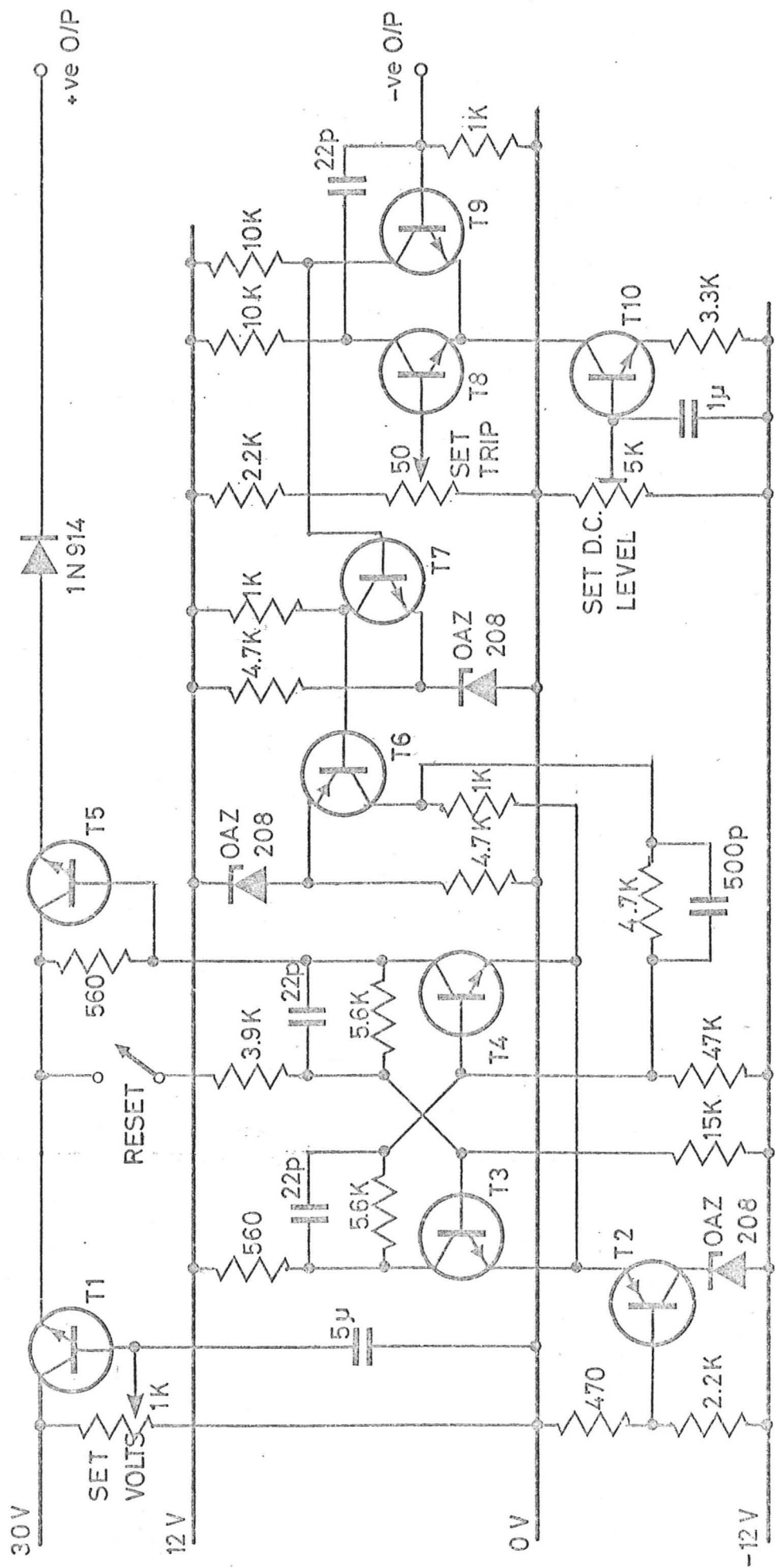


Fig 25 Etch Control Circuit.

TRANSISTORS:- T1-2N3055, T2-ACV17, T3,4,7,8,9,10-2N2926, T5-2N3053, T6-ACV17.

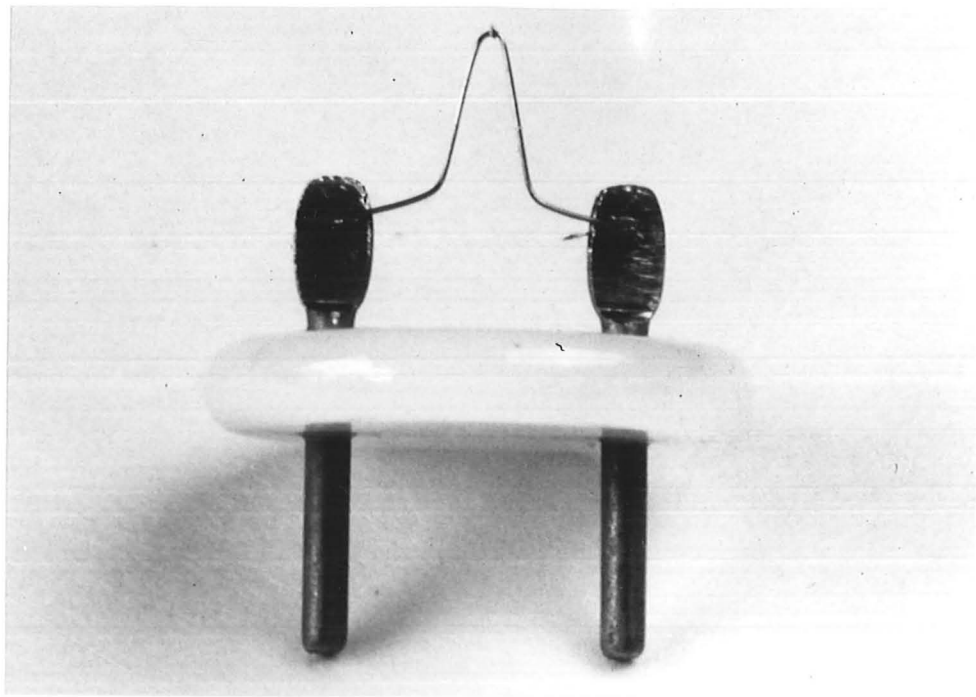
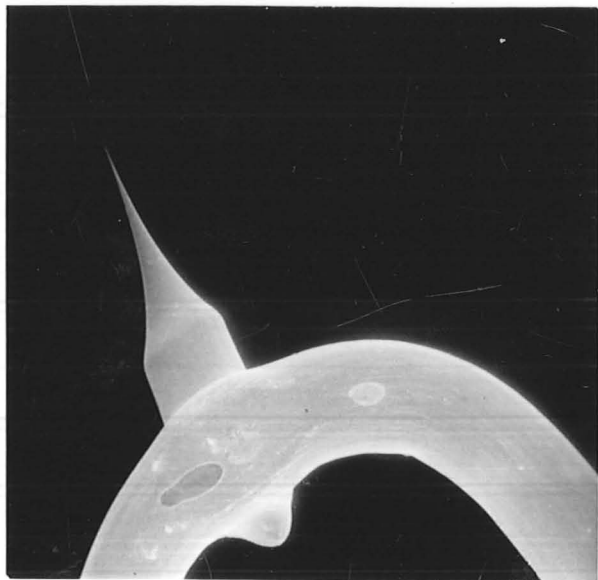
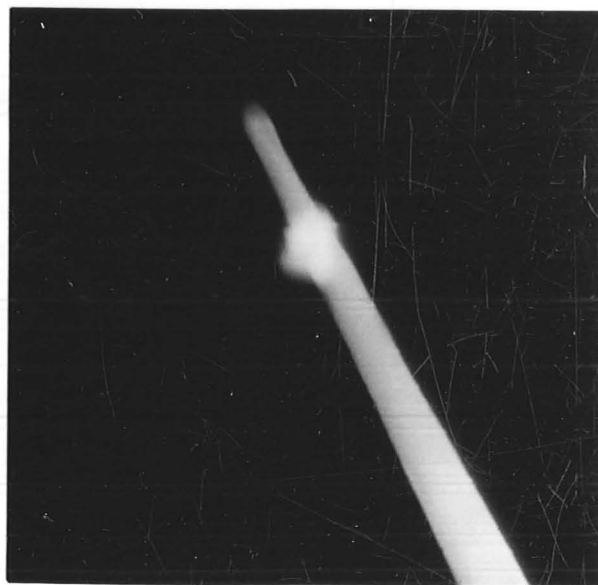
and this is amplified through T7 and T6. This signal is used to trigger the bistable T3 and T4, which acts as a memory for the state of the system. A simple series regulator, T1, controls the available voltage which is supplied to the output via a series switch, T5, controlled by the bistable to either the on or off condition. In the off state the base of the series switch transistor is held to a slightly negative line provided by T2, and reverse current is prevented by the inclusion of a low leakage series diode. The circuit is triggered to the 'on' state by momentarily closing the reset circuit, which changes the state of the bistable, cell current then flows and maintains this state.

Order of magnitude calculations show that a significant blunting of the emitter tip would occur if the etch were continued for 10 to 100  $\mu$ s after the wire separates. Measurements made on the circuit showed that the switching time was below 100 ns and clearly adequate.

2.5 Conclusions

In all, about one hundred tungsten field emitters were made by the author using the processes described above, of which about one third were of (111) oriented wire. Only three failures to make emitters from the pieces of oriented wire occurred, in all cases due to loss of the wire and not failure of the method. Occasionally a weld was not satisfactory, the oriented wire was then reversed and welded at the other end to a new base.

About 80% of the oriented emitters were sufficiently well aligned to be of use in the electron optical column, typical variations being  $\pm 5^\circ$ . The emission voltage of new emitters in the field emission microscope was found to be consistently below 3kV, indicating a tip radius less than 300nm.

Optical -  $\square$  1mm.S.E.M. -  $\square$  100  $\mu$ m.S.E.M. -  $\square$  1  $\mu$ m.

Whereas the methods described above are by no means perfect, the fabrication of emitters has been developed from a highly skilful art with a poor success rate, to a state where, with a little practice an operator may obtain a very high success rate, producing high quality emitters.

Photographs of a typical emitter at various magnifications are shown in Fig. 2.6.

Fig 2.6 A Typical Completed Emitter

## CHAPTER 3

THE FIELD EMISSION MICROSCOPE3.1 Introduction

The need for a field emission microscope (FEM) capable of performing basic emission experiments in a controlled ultra high vacuum (UHV) environment was realized at the beginning of the research. Although there had been some work on field emission at the laboratory by Earnshaw (1965), no direct experience was available on either the fabrication of emitters or the control of field electron emission.

Further, the use of field emitters for electron optical applications requires that intense emission is directed along the optical axis. Thus, as the properties of the emitters were unknown, the observation of their emission patterns in the FEM as a routine measure would enable their emission characteristics and alignment to be checked prior to use in the electron optical column.

Additionally, one of the aims of the research was to develop field emission techniques for practical application by investigating the possibilities of operating in relatively poor vacuum conditions, using T-F or pulsed field emission modes. The controlled environment of the FEM, and easy observation of the emission pattern would provide an ideal experimental arrangement.

Unfortunately, at the start of the research, funds were limited, and it was not possible to build a FEM immediately. The first part of the research period was occupied largely with

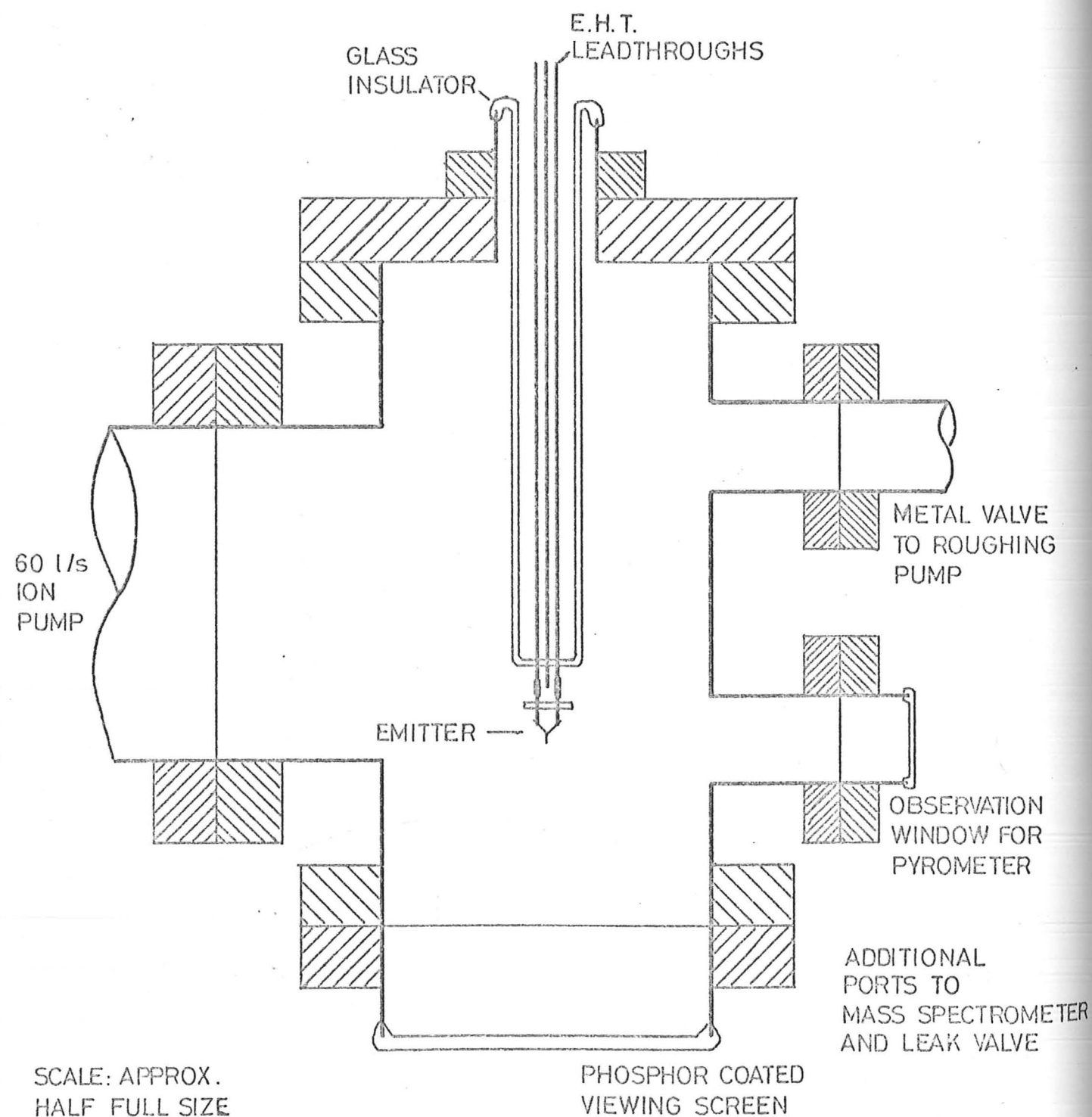


Fig 3.1 Section of the Field Emission Microscope

the fabrication of emitters and the design and construction of the electron optical column.

However, half way through the research period a grant was made by the Science Research Council which provided, among other things, for the construction of the FEM. This enabled almost all of the early field emission experiments to be performed in the FEM as had first been hoped, and an ability to operate field emitters satisfactorily was soon generated.

Throughout the remaining period of research many experiments were performed in the FEM and these are described later in Chapter 4.

The remainder of this chapter will be devoted to describing the design and construction of the FEM, its vacuum performance and the associated electronics which include, in particular, a high-voltage pulse generator which was built for experiments with pulsed field emission.

### 3.2 Design and Construction of the FEM

It was decided to base the design of the microscope on the range of commercial UHV flanges and equipment which were becoming readily available. This would enable the system to be produced rapidly, it would be versatile and could readily be adapted to other applications in the future.

The basic design of the FEM is shown schematically in Fig. 3.1. The design was based on a standard 'T' section supplied by Vacuum Generators Ltd.<sup>+</sup>, which was modified by the inclusion of four small ports, two of which are not shown but rise vertically from the plane of the 'T' section.

<sup>+</sup> Vacuum Generators Ltd., Charlwoods Road, East Grinstead.

Two of the small ports were in line with the tip of the emitters. One was provided with a window to permit observation of the emitters with an optical pyrometer. The other port was fitted with an AEI\* Vacuum MS10 mass spectrometer which was used to obtain an accurate measurement of the pressures of residual gases at the emitter.

Of the remaining small ports, one was used for rough pumping via a 1" diameter all metal valve, the other was fitted with an all metal leak valve capable of introducing finely controlled gas leaks into the system, thus enabling controlled environments to be produced for experiments at higher pressures.

Field emitters were mounted from one arm of the 'T' section on a tubular pyrex glass insulator. Electrical leadthroughs were of 1mm tungsten rods sealed into uranium glass, which has a graded joint to the pyrex. At the other end the tube was joined to a standard UHV stainless steel flange fitted with a nilo tube which has been glassed and graded to pyrex. The lead-through was mounted on a small-size flange for economy, and for convenience of changing emitters.

Fitted to the other arm of the 'T' was the viewing screen which was based on a standard AEI 4½" diameter window coated with phosphor. Preparation of the viewing screen will be described in more detail below.

Main UHV pumping was provided by an AEI\* P60 triode ion pump, for which a power supply was kindly loaned by the manufacturers. The triode pump configuration is reputed to have better starting characteristics and higher pumping speeds than earlier commercial ion pumps, certainly, no difficulties were encountered in the use of this pump.

---

\* GEC-AEI Scientific Apparatus Division, Harlow, Essex.

To prevent tip destruction due to discharges from the ion pump spreading through the system, particularly when starting at high pressures, an earthed stainless steel mesh was included at the pump flange, and no emitters were lost due to this effect.

Rough pumping was by a liquid nitrogen sorption pump, through the 1" metal valve. This method of pumping was cheaper than conventional rotary pump and diffusion pump and left no possibility of contamination from vacuum oils.

### 3.2.1 The Viewing Screen

A number of techniques for depositing phosphor screens suitable for UHV applications may be found in the literature, for example, Gomer (1961) and Dyke and Dolan (1956). A method described by Gomer formed the basis of the technique used.

The surface of the glass was first rendered conducting by coating with a thin, transparent film of tin oxide. This is an established technique and was carried out by a local glass worker.

A binder for the phosphor was provided by treating the surface with a few drops of orthophosphoric acid dissolved in about 1cc of methanol. This was spread evenly over the surface by partly covering the screen with small glass balls and agitating vigorously. Excess liquid and the glass balls were tipped away and the window allowed to dry.

The phosphor used was blue P11, chosen for its high light yield and suitability for direct photography. A suspension of about one gramme of the powdered phosphor was prepared in 100mls of demineralized water, which was thoroughly agitated in an ultrasonic bath. Heavier particles were allowed to settle before pouring the suspension into the window.

When the phosphor had settled, excess water was removed by

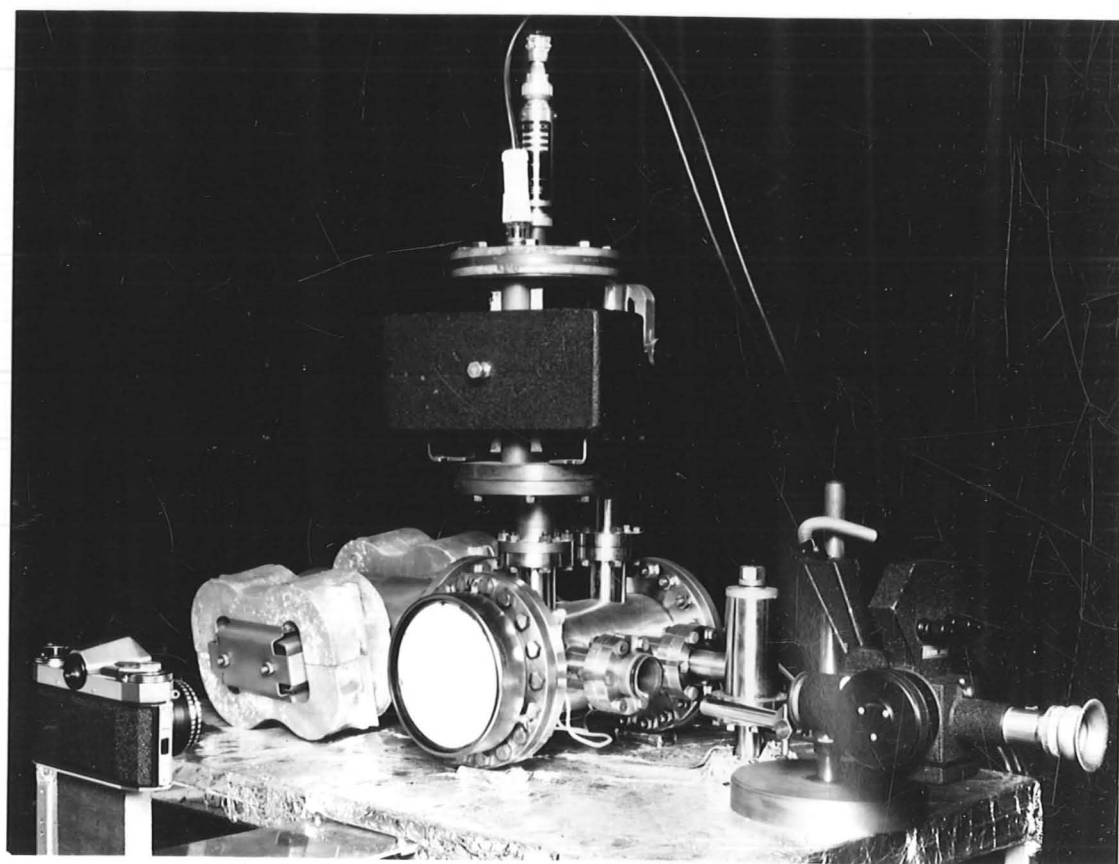
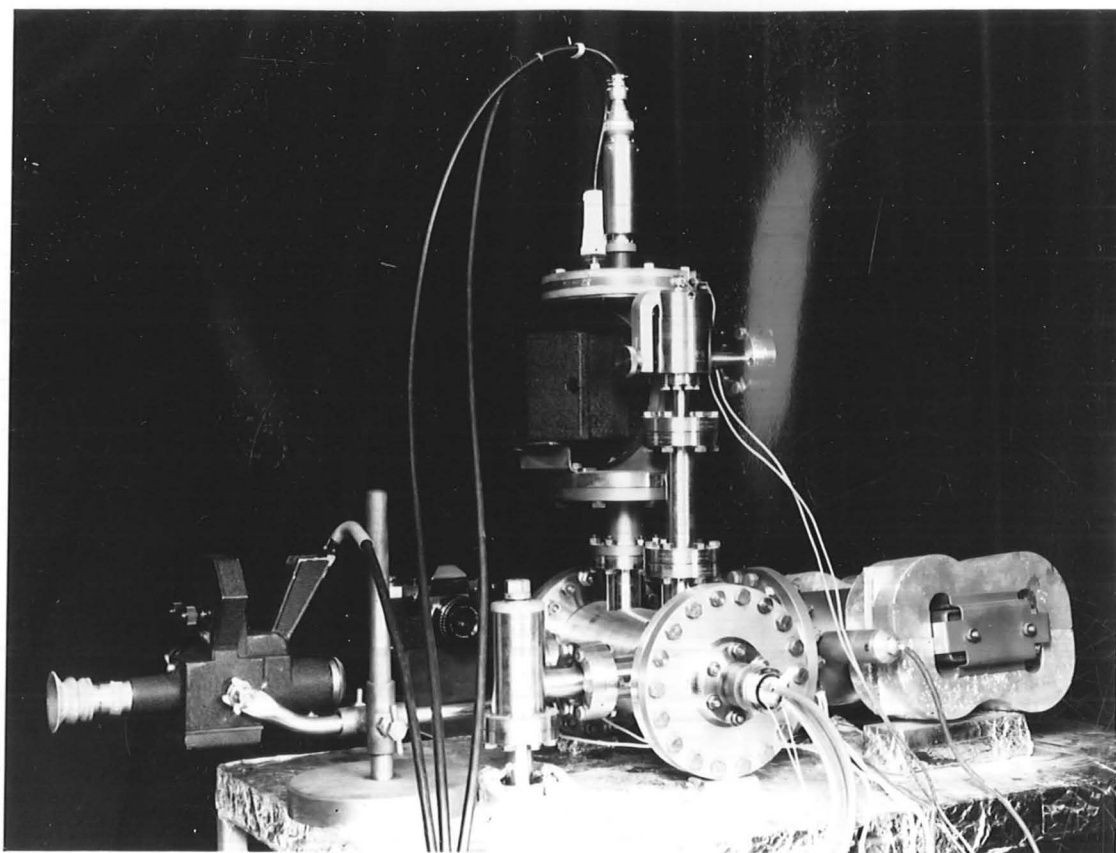


Fig 3.2 The Field Emission Microscope

siphoning until only a thin surface covering remained, which was allowed to evaporate slowly by gently warming the window on a photographic hot plate.

The method described above proved very difficult in practice due to the curvature of the glass at the edges. Several attempts at the process were necessary, the phosphor was simply washed off and the processes of applying binder and phosphor repeated. The screen eventually obtained was not perfect as the phosphor was not continuous at the edges on the curved section of the glass, however, an even deposit was obtained over the flat central region of the window.

The window was fitted directly to the FEM and baked in the normal vacuum pumping cycle without suffering any ill effects. It subsequently gave satisfactory performance for the remainder of the research period.

Fig. 3.2 shows two views of the complete FEM. The viewing screen may be seen in the lower photograph, with the 35mm single lens reflex camera used to record emission patterns. Other items of interest which may be identified include the small observation window and optical pyrometer, the ion pump, and, mounted vertically, the mass spectrometer head and leak valve.

The FEM was supported on a metal frame table. The top was made from sindanyo to give good thermal insulation during bake-out of the microscope, and was covered with aluminium foil to contain asbestos dust and to further reduce heat losses.

### 3.3 Vacuum Performance of the FEM

The FEM was cycled from air to pressures below  $1 \times 10^{-9}$  torr on a routine basis. This involved a bakeout and pumping procedure

lasting several hours, and once the procedure had been established little or no difficulty was encountered in achieving the desired pressures.

During the course of the experiments only a very few leaks were encountered, which illustrates the reliability now possible with commercial UHV equipment and crushed copper seals. Also no difficulties were encountered when starting the ion pump.

### 3.3.1 Bakeout and Pumpdown Cycle

The liquid nitrogen sorption pump rapidly roughed the system through the metal valve, to achieve a pressure better than  $1 \times 10^{-3}$  torr in a few minutes. At this stage bakeout was started, pumping all released gases into the sorption pump.

A simple box oven made from aluminium sheet was placed over the entire microscope, resting on the table top. The oven carried 4kW of heaters mounted on its sides. This was a very convenient arrangement as both oven and heaters were completely removed from the FEM in normal use.

Temperature was monitored by thermocouples clamped at various points on the microscope. A simple transistor amplifier was built to give a direct metered output of temperature up to  $400^{\circ}\text{C}$ , this was operated from a battery supply to avoid problems with earth loops. The temperature could be regulated by varying the heater power with a domestic oven type controller.

A normal bakeout cycle consisted of raising the temperature of the microscope to  $300^{\circ}\text{C}$  in about 2 hours, and by regulating the heater power this was maintained for a further 2 or 3 hours. The heaters were then turned off and the temperature would fall to  $150^{\circ}\text{C}$  in about an hour, when the oven was removed.

The ion pump was started with the system still hot to enhance

degassing of the electrodes. After the first release of gas the ion pumping was rapidly established and the pressure would begin to drop. At this stage the roughing valve was closed.

Final cooling of the microscope and pumpdown to below  $1 \times 10^{-9}$  torr was a lengthy process and took a further 5 to 6 hours. It was convenient to bake out the sorption pump at this stage in preparation for the next pump-down cycle.

### 3.3.2 Pressure Measurement

After following the above procedure the pressure in the microscope would normally be in the low  $10^{-10}$  region, which would just give a detectable current on the ion pump meter. This gave a very quick and useful check on the state of the system.

For accurate monitoring of the pressure both a mass spectrometer (AEI MS10) and the conventional Bayard-Alpert ionization gauge were used. However, at this pressure the ionization gauge was found to be very unsatisfactory, even lengthy outgassing procedures failed to give consistent measurements, due partly to steady outgassing of the gauge on the one hand, and to its tendency to act as a small ion pump on the other.

The most satisfactory way of measuring the pressure was to use the mass spectrometer. This again needed thorough degassing which was achieved by baking out the spectrometer at about  $50^{\circ}\text{C}$  hotter than the rest of the microscope, the bakeout heaters supplied with the spectrometer produced this effect during the normal bakeout cycle. By this procedure consistent readings were obtained after it had been running for about an hour. After pump-down, typical levels of residual gases would be:  $\text{H}_2 = 2 \times 10^{-10}$  torr,  $\text{N}_2 + \text{CO} = 5 \times 10^{-11}$  torr,  $\text{H}_2\text{O} = 5 \times 10^{-11}$  torr.

The mass spectrometer had the additional advantages that it

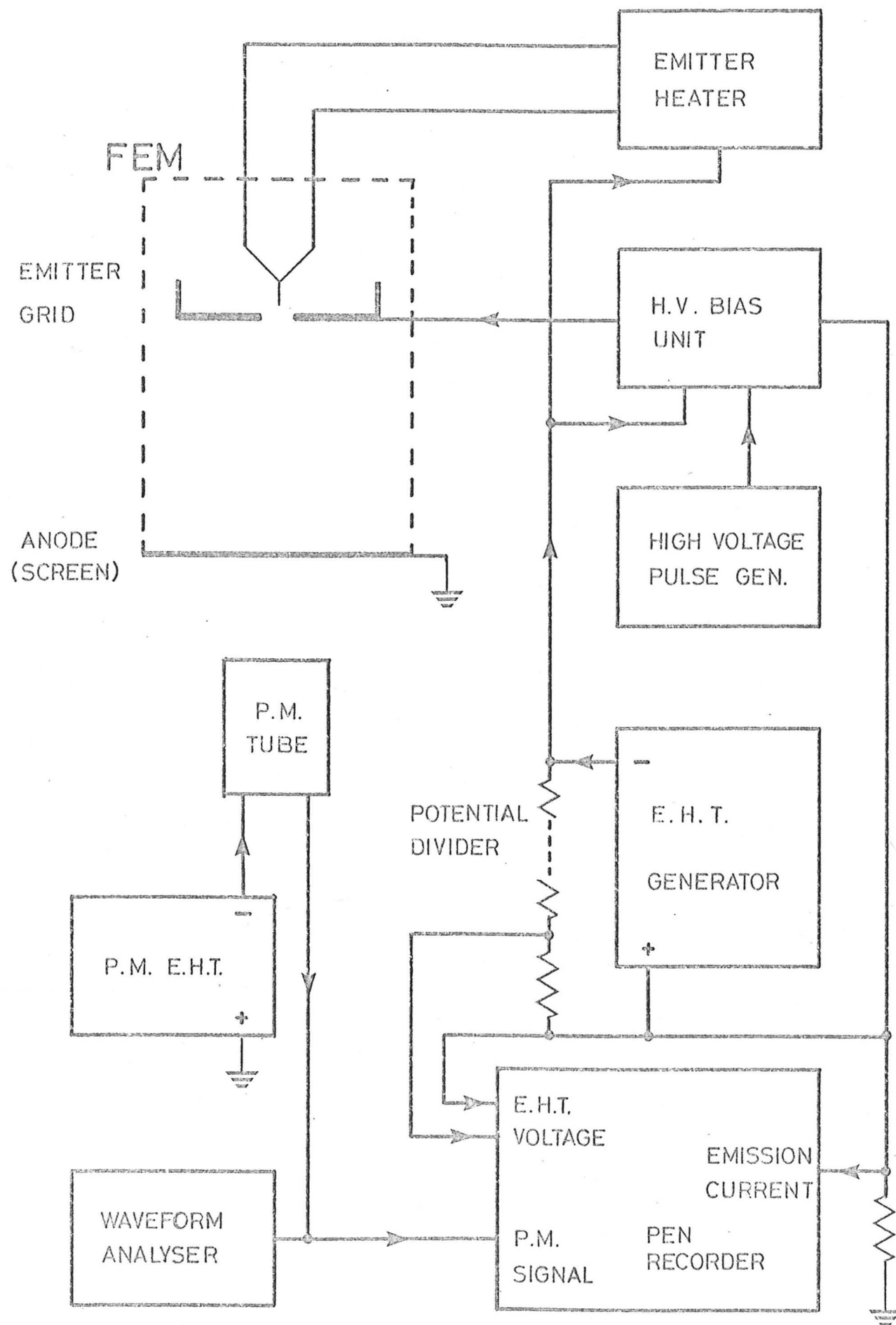


Fig 3.3 Block Diagram of F.E.M. Electronics

permitted an accurate determination of the residual gases in the system, and permitted very rapid detection of even small leaks with a helium gas probe.

#### 3.4 Operation of the FEM

The electronics used in conjunction with the FEM is shown schematically in Fig. 3.3. This provided facilities for monitoring applied potentials and emission current in addition to photographic recording of emission patterns and measurement of emitter temperature discussed above.

Provision was made for a third electrode to be used in the FEM to act as a control grid. This is an important feature as it enabled independent control of emission current and emitter potential to be obtained, in both d.c. and pulsed operation. The pulse circuitry including the bias unit will be described in section 3.5.

Facilities were provided for observation of the emission pattern with a photomultiplier, which had wide bandwidth capabilities limited by the response time of the phosphor screen, in this case to about  $50\text{kHz}$  for the P11 phosphor used. This arrangement permitted the frequency spectrum of emission current to be analysed, and in addition enabled emission from a small area of the cathode to be studied.

The recording of operating parameters centred around the pen recorder. Usually, this was either used to monitor the variations of emission current from all or part of the cathode with time, or to investigate the relationship between emission current and applied potential to emitter, or by moving the connection of the potential divider network, to the grid.

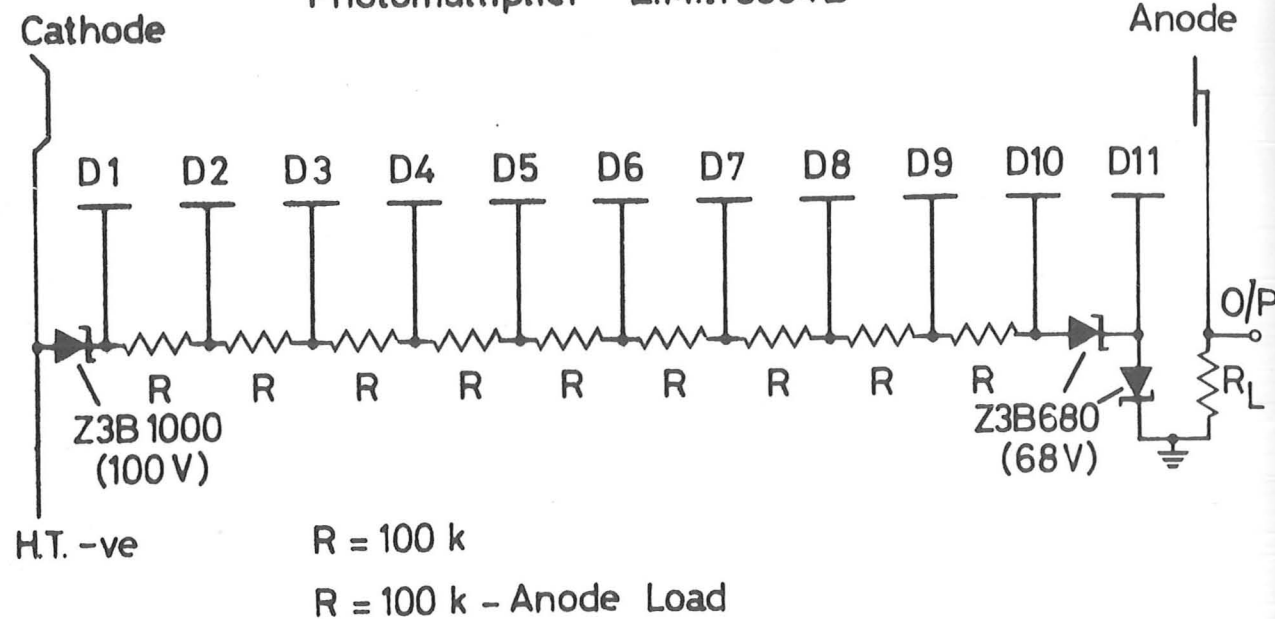


Fig 3.4 The Photomultiplier Circuit

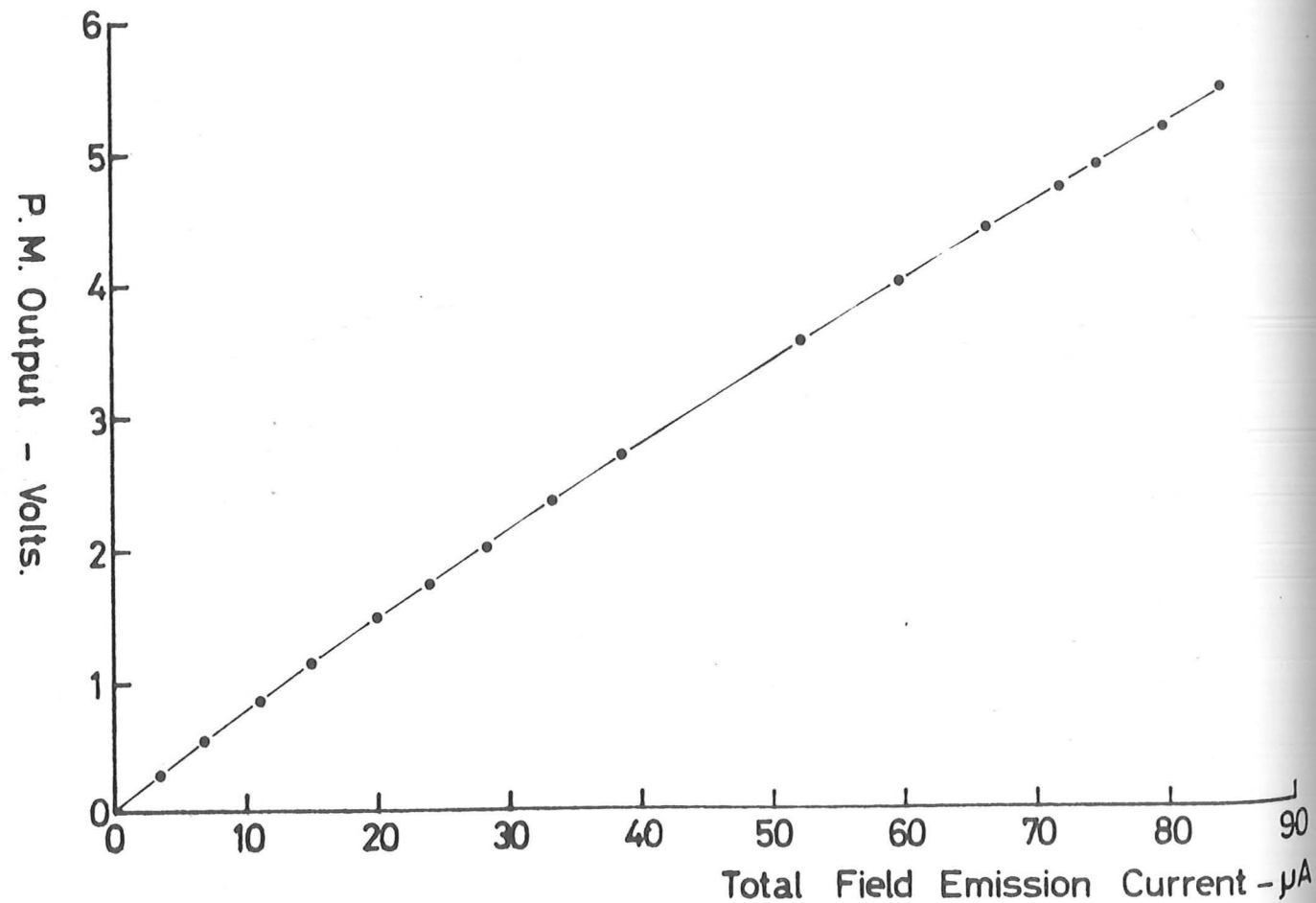


Fig 3.5 Illustrating P.M. Linearity

3.4.1 The EHT Generator

A commercial EHT generator manufactured by Brandenburg Ltd.<sup>+</sup> was used in the experiments. This had an integral filament heater supply which was convenient for flashing emitters, and had a stability nominally of 10ppm which was adequate for use later on the electron optical column.

An active grid supply for conventional thermionic electron guns built into the filament unit was not suitable for use in this new application, and so was by-passed by connecting the EHT generator directly to the filament centre tap.

A more extensive modification was made to the EHT voltage control. Originally the voltage was varied by a coarse control consisting of a fifteen position switch, and a fine control which did not overlap with the coarse settings at lower operating voltages. Since field emission current increases very rapidly with voltage, the original arrangement was clearly unsuitable. The reference circuitry of the unit was therefore changed to produce overlapping of the coarse switch positions for the full range of output voltages.

3.4.2 The Photomultiplier

A photomultiplier chain, developed in the laboratory by C.D. Bunting to give good linearity in selected area diffraction work, was used with definite advantages over the normal resistor chain, or resistor chain with capacitors between the last few dynodes.

The circuit is shown in Fig. 3.4, and stabilizes the voltage on the first and last two stages of amplification by using zener

<sup>+</sup> Brandenburg Ltd., London Road, Thornton Heath, Surrey. Model HSO530 EHT Generator and 3035S filament supply.

diodes. This has the effect of giving very good linearity as dynode voltages vary very little with anode current. Since very nearly the whole of the chain current may be drawn in the anode circuit a smaller anode load resistor may be used, which permitted experiments to be carried out with the PM output connected directly to both the pen recorder and the waveform analyser.

Fig. 3.5 shows the PM output as field emission current, the PM tube observing the whole emission pattern. In this example the chain current was approximately  $70 \mu\text{A}$ , thus no significant departure from linearity was observed with anode currents up to  $60 \mu\text{A}$ .

The use of a smaller load resistor also enables higher bandwidth to be achieved, which is important for applications in conjunction with the scanning electron optical column described in Chapter 5.

### 3.5 High Voltage Pulse Generator

The addition of a control grid to the simple field emission diode opens up the possibility of using pulsed emission in electron optical applications. Since the emitter potential may be kept constant, a pulsed electron beam can be formed which has a small energy spread and may be imaged without introducing severe chromatic aberration.

The electrode system which has been developed will be described in more detail in Chapter 4. The parameters of importance in the design of the pulse generator were the load presented by the grid, which was purely capacitive of approximately  $50\text{pF}$ , and the voltage swing required to modulate the emission. Early experiments had shown that a voltage variation on the grid of 500 volts

was sufficient to change emission from cutoff to 0.1mA, therefore the pulse generator was designed to give 1000 volts output, which was estimated to be sufficient to reduce the surface field on the emitter to very low levels. This output voltage was a convenient choice, as suitable power supplies were available to give 1050 volt lines, though the possibility of going to higher voltages was not excluded.

### 3.5.1 Experimental Requirements

In order to specify the performance of the pulse generator more closely, it is necessary to consider in more detail the experimental use and possible practical application of the unit.

The field emission electron gun is intended for use in conventional electron optical instruments with demountable vacuum systems, where its potentially high brightness would be a considerable advantage. Clearly, compatibility with the ultra high vacuum systems necessary for continuous field emission is a serious obstacle preventing this advance.

Under normal operating conditions, emitter destruction is brought about by ions, formed at the anode under electron bombardment, which are accelerated and focused back onto the cathode, and eventually destroy the emitter by sputtering. Order of magnitude calculations based on a plane, parallel electrode system have shown that whereas electron transit times are typically 1ns, ion transit times are in excess of 100ns. Thus, if a pulse of emission were drawn of shorter duration than the ion transit times, then the change of grid potential would also serve to defocus the ions, and so reduce the emitter damage due to ion bombardment.

Pulses of emission of approximately 100ns duration could be

used to build up a scanning microscope image using one pulse per picture element. Clearly, in order to gain maximum advantage from this mode of emission, the pulse duty cycle must be as large as possible.

A second, separate approach to using pulsed operation would be to draw emission for sufficient time to build up a complete micrograph, taking full advantage of the high brightness of the emitter. This picture could be stored and displayed for a much longer period before drawing emission again. Typically, a picture could be formed in 10ms, which might be repeated at a rate of one per second.

A variant of this technique would be to write one line of a picture per emission pulse, about 10  $\mu$ s duration, and to pulse with a repetition rate of 1kHz, so building up a complete picture every second.

Either of these techniques would give an artificial enhancement of field emitter lifetime by a factor equal to the reciprocal of the duty cycle.

We must now consider the effects of variations of amplitude between successive pulses. For SEM operation we may assume distinguishable contrast levels of 5% after Smith and Oatley (1955). As changes in surface fields at the emitter produce proportional changes in emission current which are typically an order of magnitude larger (Martin et al. (1960)), then for operation with one pulse per picture element, the successive grid voltage pulses must not differ by more than 2 parts in  $10^3$  if they are to be indistinguishable on the final picture.

The required specification for the pulse generator is therefore to produce pulses of up to 1kV amplitude which are repeatable

to 0.2%, with durations from 100ns to lms, and at repetition rates of 1/ sec to several hundred thousands/sec.

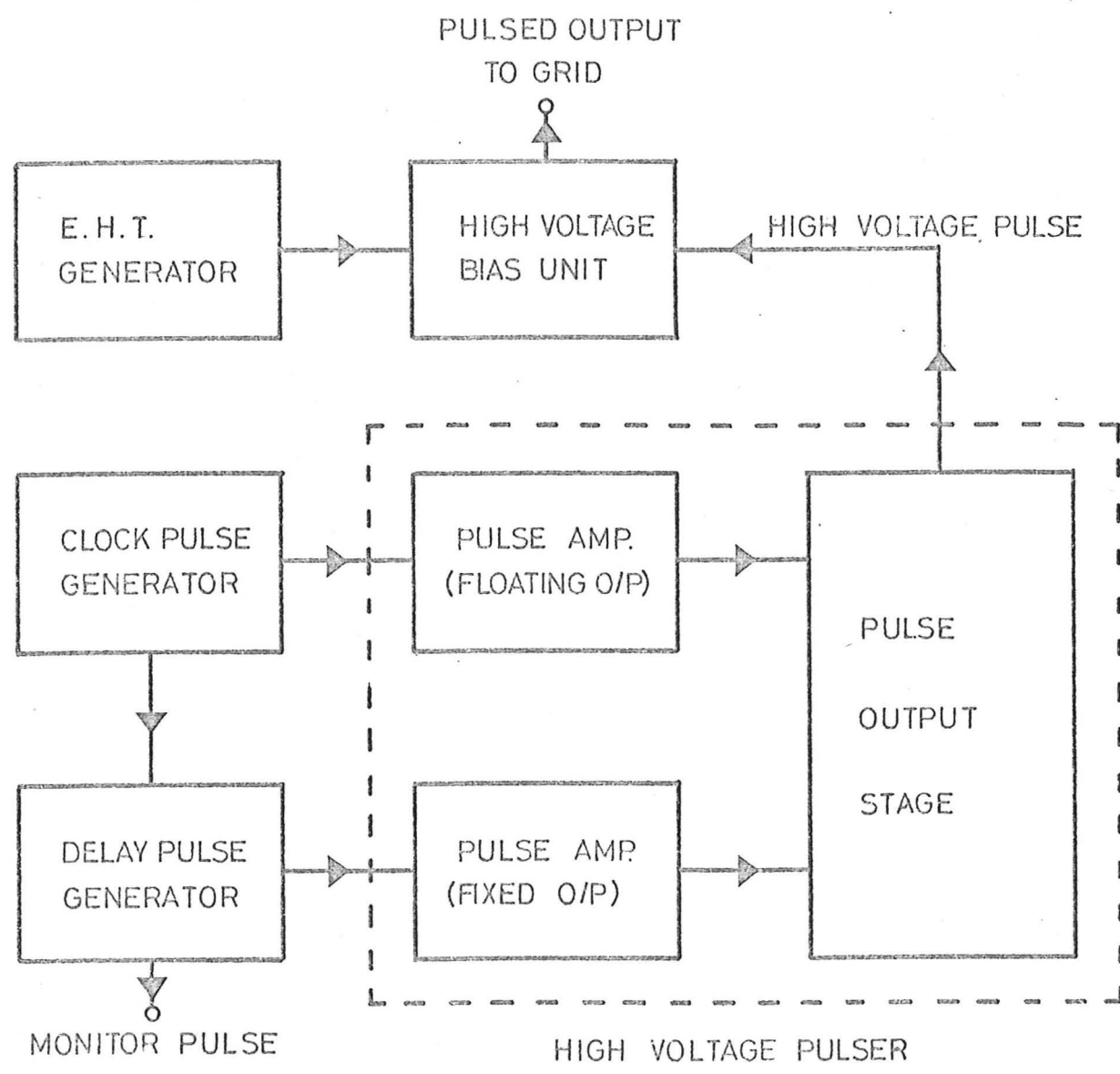
### 3.5.2 Other Work

Several pulse generators have appeared in the literature which fulfil some of the requirements listed above. The techniques used fall into two main categories:

a) Hard-valve, high voltage amplifiers. Gunn (1961) has described a high voltage pulse generator which has a class 'A' output stage. In principle these techniques could be used, however, practical limitations prevent serious consideration. Consider a rise time of 100ns into a capacitive load of 50pF. This requires a standing current in the output stage of nearly one amp at 1000 volts. Thus such a system would be very large and expensive.

b) Series switch/shunt discharge generators. This configuration is more commonly found with thyratrons performing the switching functions, see, for example Ruben (1965), Chan and Gunn (1965) and Paz (1965). Thyratrons have high stand-off voltages, fast switching characteristics and pass large peak currents, however, the permissible repetition rates are low due to the decay times of the ions, even with the best hydrogen thyratrons a rate of  $5 \times 10^4$ /sec would represent an absolute maximum.

It is possible to replace the circuit function of the thyatron with hard valves, Wouk (1957) and de Wijn (1961). This arrangement is ideally suited to a purely capacitive load since complicated extra circuitry to maintain the pulse shape is not required. Particular advantages of this type of circuit are that, compared to group (a) above the mean power supply requirements and power dissipation are greatly reduced. Moreover, rise and



TIMING SEQUENCE :

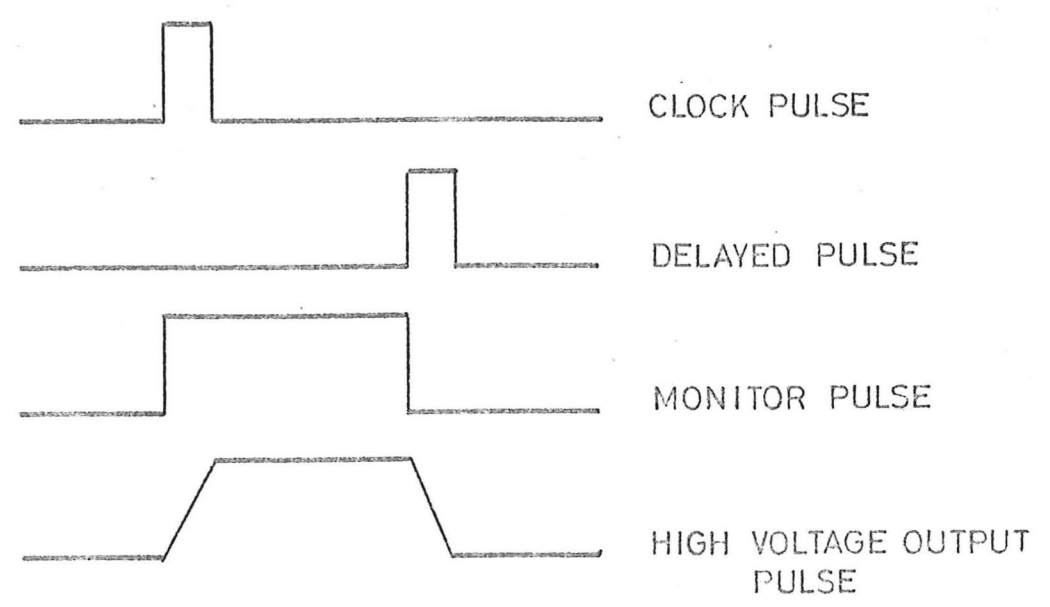


Fig 3.6 Block Diagram of H.V. Pulse Generator

fall times are not dependent on quiescent levels, but on peak valve currents, which can be considerably larger. This approach was used and is described below.

3.5.3 Circuit Functions

A block diagram of the complete pulse generator is shown in Fig. 3.6.

Valves were only used where high voltages were necessary in the pulse itself and in the drive amplifiers. To power these units  $\pm 300V$ , 0.5A lines were provided, and for the high voltage an additional + 250-450V, 200mA supply was floated above the + 300V line, giving the possibility of a 1050 volts swing between lines.

For convenience and compatibility with other circuitry, the timing pulses were generated in separate transistorised modules working from  $\pm 12V$ ,  $\pm 30V$  lines.

Operation of the circuit is controlled by the clock generator, producing an output pulse which is amplified and controls the "series switch" section of the pulser. The clock generator also triggers the pulse width unit, which gives an output pulse at the end of the chosen pulse duration, this is again amplified and used to operate the "shunt discharge" section of the pulser.

3.5.4 Clock Pulse Generator

The circuit, shown in Fig. 3.7, is based on the emitter coupled multivibrator, T1, T2, fed from current sources T3 and T4. This configuration has the advantage that its period can be switched over the very wide range from 1Hz to 1MHz by changing a single capacitor.

In normal operation this generator fires the Eccles-Jordan monostable T5, T6, which gives a 100ns prepulse output through

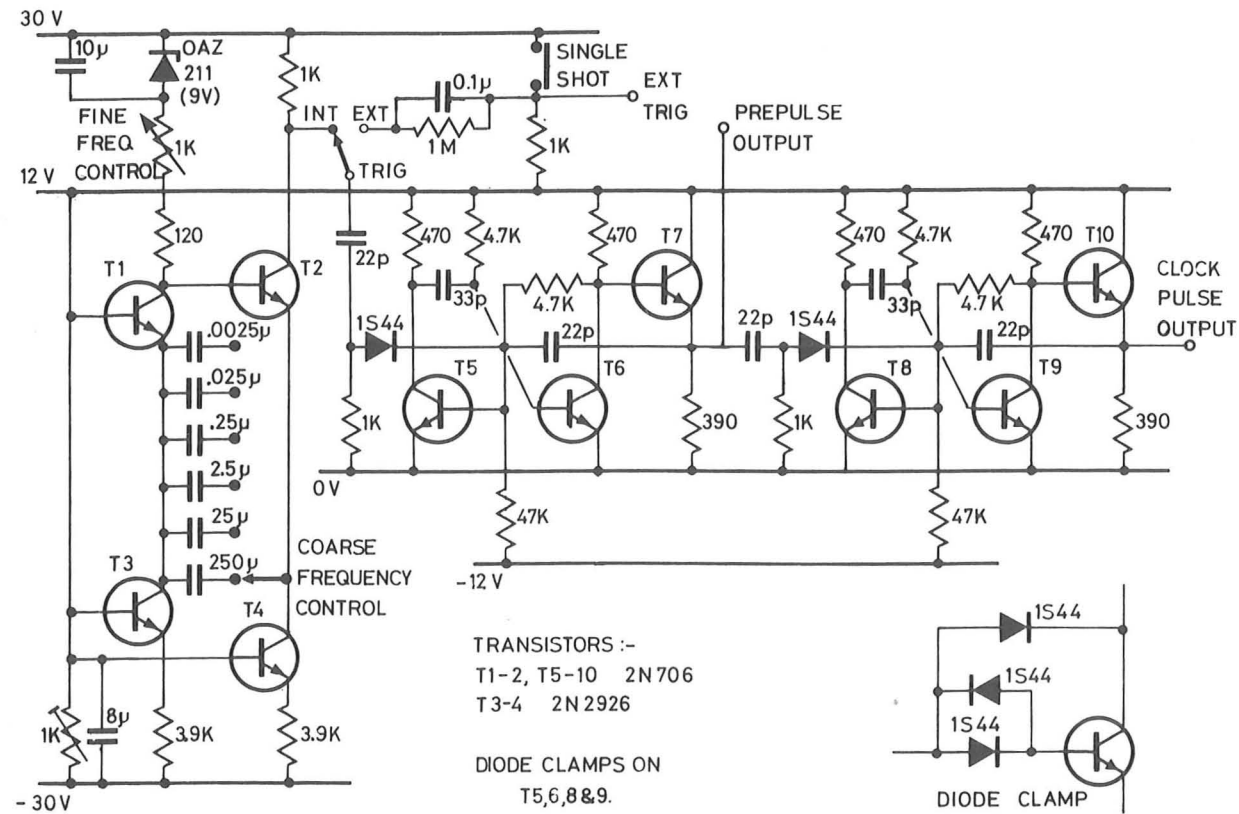


Fig 3.7 Clock Pulse Generator

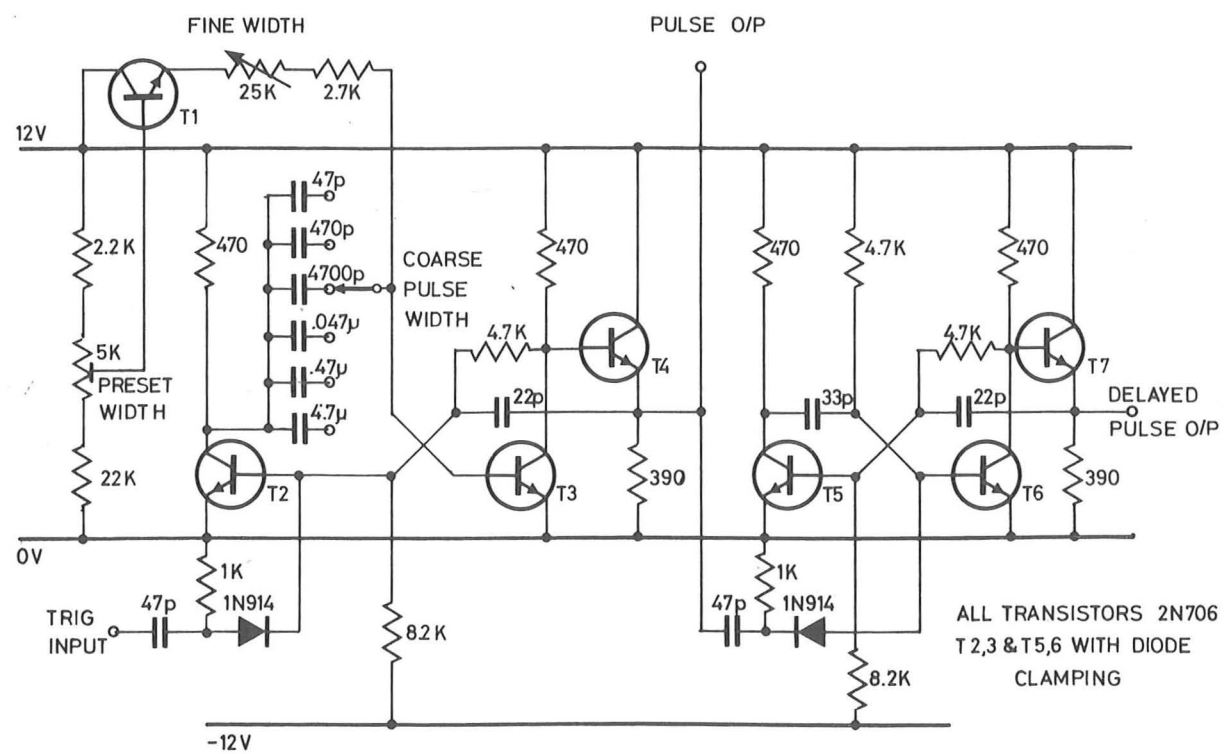


Fig 3.8 Pulse Width / Delay Unit

the emitter follower T7 for external triggering, and fires a similar multivibrator T8, T9, on its falling edge to produce the 100ns clock pulse output through the emitter follower, T10.

To give good rise and fall times the transistors are kept out of saturation by the diode clamp circuit shown, which also gives easier triggering. Outputs are taken from emitter followers to avoid loading the monostables.

Additional facilities for external triggering and single shot operation are also provided.

### 3.5.5 Pulse Width/Delay Unit

The circuit, shown in Fig. 3.11, produces a delayed pulse output of 100ns duration for each input trigger pulse. The delay may be continuously varied over the range 100ns to 100ms, and is used to turn off the high voltage pulse generator, thereby setting the width of the high voltage pulse. An additional output is taken from the delay generator, so that a monitor pulse is provided which starts with the incoming trigger, and finishes on the leading edge of the control output pulse.

The monostable T2, T3, produces the variable delay. Coarse control is obtained by switching capacitor values, and fine control by varying the capacitor charging rate. Transistor T1 provides a voltage line which may be used to preset the absolute values of pulse width.

This pulse is buffered by the emitter follower T4, and used to trigger the monostable T5, T6 on its falling edge, which provides the delayed pulse output of 100ns duration through emitter follower T7.

As before, the transistors in the monostables are kept out of saturation using clamping diodes, and the outputs are provided through emitter followers.

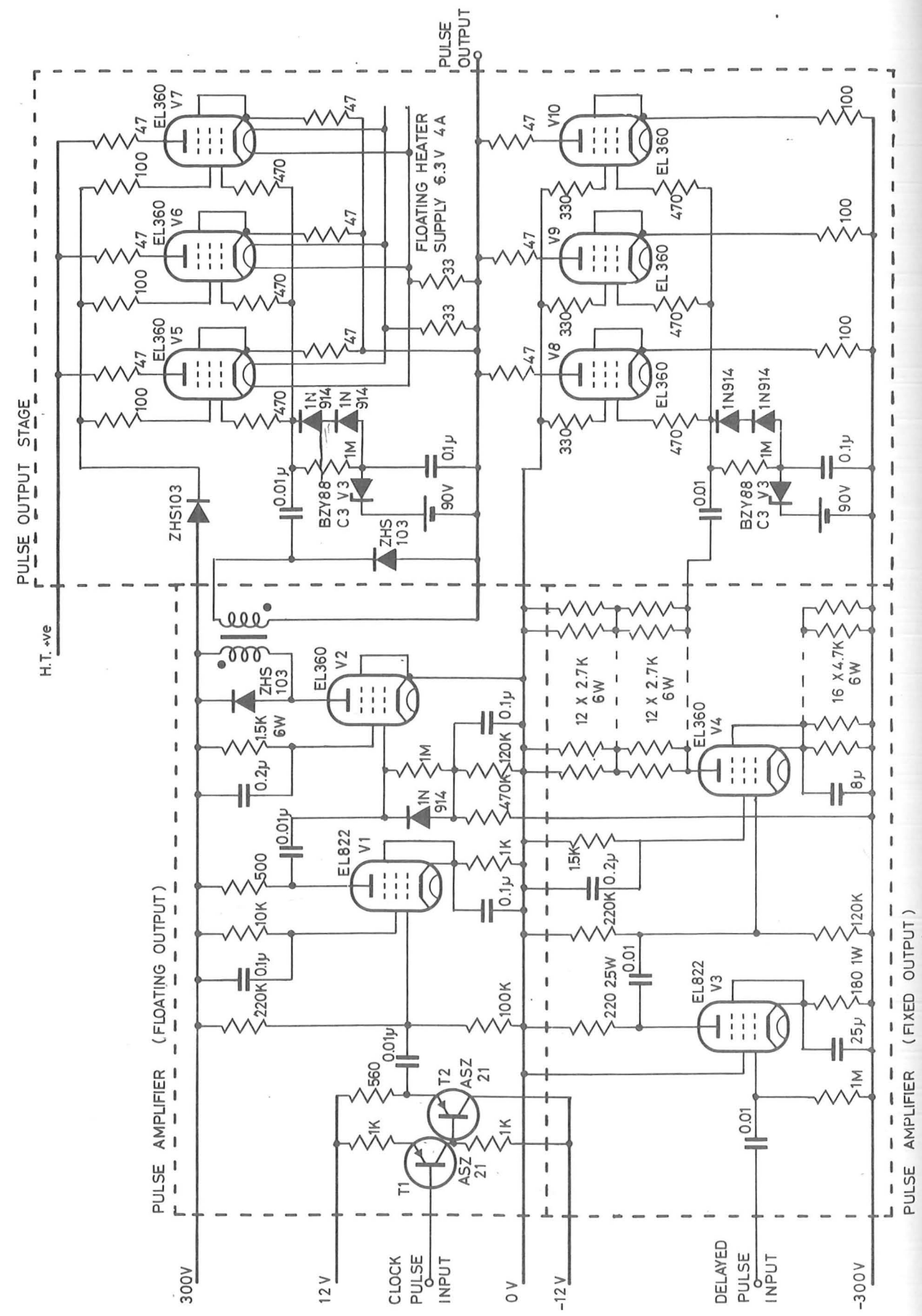


Fig 3.9 High Voltage Pulser

3.5.6 High Voltage Pulser

For convenience of construction this was divided into three units as is indicated in Fig. 3.9, which shows the detailed circuit. The pulser consists of two pulse amplifiers which drive the series switch/shunt discharge output stages from the low voltage timing pulses.

a) Pulse amplifier (fixed output). This is the simpler of the pulse amplifiers, and produces an output relative to the -300 volt line. It provides two stage voltage amplification of the delayed pulse through V3 and V4, to give a positive output pulse of 100 volts, which is required to drive the discharge valves of the output stage from cut-off into grid current. In order to maintain risetimes of less than 100ns, high powers must be dissipated in load resistors and these were constructed as arrays of 6 watt wire-wound resistors, mostly connected in parallel to minimise stray inductances.

b) Pulse amplifier (floating output). The second pulse amplifier is slightly more complicated, as it produces a drive pulse which must float with the cathodes of the series switching valves of the output stage. Isolation is achieved by using a pulse transformer having two windings on opposite sides of 12.7mm ferrite toroid (Mullard FX3008), the primary of 30 turns, and secondary of 21 turns, both wound as single layers from 36 swg enamelled copper wire. Electrical properties measured at 1kHz were as follows:

Interwinding capacitance	=	5 pF
Primary Inductance	=	830 μH
Secondary Inductance	=	400 μH
Mutual Inductance	=	475 μH

The circuit is a two stage valve amplifier as before, however, the input pulse is inverted by transistors T1 and T2, so that the output valve V2 is normally biased off. Valve V1 amplifies the inverted input pulse and provides drive for V2 from cutoff into grid current. By using the diode clamp circuit at the grid of V2 problems of bias voltage varying with repetition rate are prevented.

The negative voltage pulse applied across the transformer primary is inverted and provides a positive drive pulse of 100 volts to the output stage. Diodes are connected across both primary and secondary windings of the transformer to prevent ringing.

c) Pulse output stage. The pulse output stage is a series switch/shunt discharge configuration as previously explained. Both of the switch elements consist of three EL360 valves connected in parallel, capable of giving combined output currents up to 12 amps. The high current is necessary to produce the short rise and fall times required at the grid of the field emission triode with the total capacitive load involved.

Both switches are normally held in cut-off by battery bias between grid and cathode of -90 volts. The bias unit for the series switch must float with the output, and was constructed in a perspex box, which gave a capacitance to ground of approximately 20pF. An incoming pulse takes the grid from -90 volts to +10 volts and into grid current. By using diodes with a large value resistor in parallel, droop on the drive pulse is minimised. At the end of the pulse the grids swing below -90 volts and the diodes become conducting to rapidly restore the d.c. level ready for the next pulse.

The batteries used were very small for compact construction and to minimise stray capacitance, consequently they had a shelf life of about one month and only a limited total available charge. To extend the life of the batteries a circuit was devised in which the battery is isolated from a buffer capacitor by a low voltage Zener diode, so that after a number of pulses the capacitor is charged to the sum of battery and zener voltages. Bias is provided to the valve from the capacitor, and excess grid current is then fed back through the batteries which extended their useful lifetime to approximately nine months.

Series switch operation. The operation of the pulse output stage is initiated by the amplified clock pulse. The grids of the series switch valves V5, V6 and V7 are driven positive with respect to their cathodes, bringing the valves hard on. As the output potential rises, the grids follow as the grid to cathode voltage is maintained by the output of the pulse transformer.

The screen grids cannot simply be connected to the anodes in triode configuration as the valves must be cut off between pulses. However, the screen must rise to the anode voltage during the pulse otherwise the valve gain will drop and the output will not reach the positive HT line. This is achieved by biasing the grids through a high voltage diode. Capacitive coupling within the valve takes the screen voltage up with the cathode and the diode becomes reverse biased. As the screen overshoots the anode voltage, high screen currents are drawn which reduce the screen potential to that of the anode.

The series valves are now turned off at the end of the clock pulse, with the output at the HT line voltage.

Shunt discharge operation. After the duration set by the

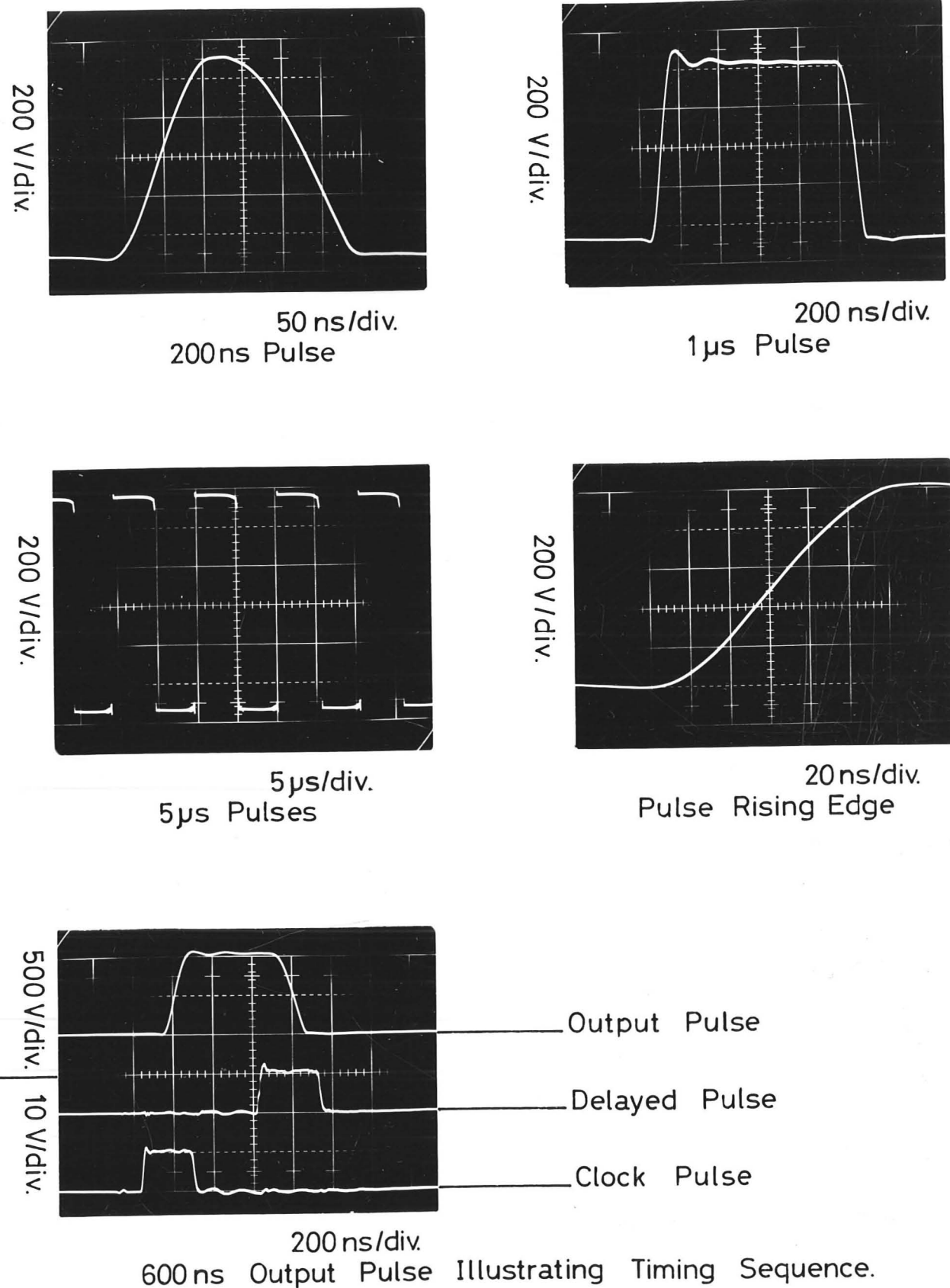


Fig 3.10 Typical Pulse Output Waveforms

pulse width unit, the amplified delay pulse is applied to the shunt discharge valves V8, V9 and V10. These are driven into grid current and the output voltage falls.

By choosing the screen grid resistors carefully, the anode voltage may be brought very close to the negative line. If the resistor is too large the screen voltages fall rapidly when the valves are switched on, and their gain drops so that an increased fall time has to be tolerated. Conversely, with the resistor too small, excessively high screen currents prevent the anode voltage dropping and may damage the valves.

As the output voltage falls the screen grid voltage of valve V5, V6 and V7 will fall also until the diode becomes forward biased. The series resistor then serves to limit the maximum diode current and prevent its destruction.

At the end of the delayed pulse, the shunt discharge valves are turned off, and the screen voltage is restored through its series resistor. The pulser is then ready for recycling.

### 3.5.7 Pulse Generator Performance

The pulse generator came very close to meeting the required specification discussed above.

Rise and fall times of 100ns were obtained though the shortest practical pulse duration for full amplitude was about 150ns measured at half maximum amplitude. Repetition rates were limited to 250kHz by excessive power dissipation in the valve V2 of the clock pulse amplifier, though this rate could be varied over the continuous range down to 1Hz.

Pulse amplitudes of 1kV were achieved between the -300 and +450 volt lines available. Larger pulses were obtained by running the HT line from a 0 - 2kV, 5mA supply, which placed severe

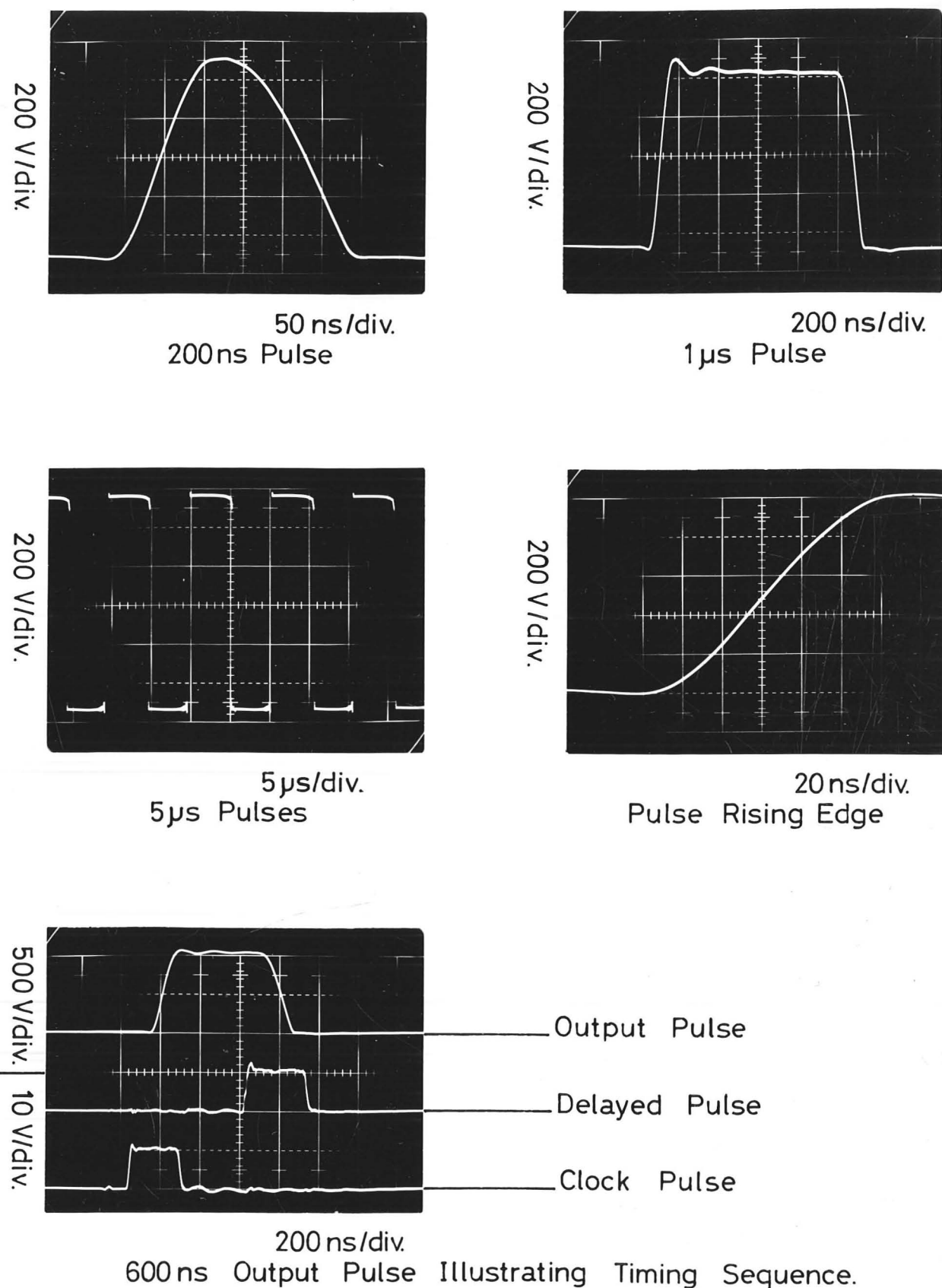


Fig 3.10 Typical Pulse Output Waveforms

pulse width unit, the amplified delay pulse is applied to the shunt discharge valves V8, V9 and V10. These are driven into grid current and the output voltage falls.

By choosing the screen grid resistors carefully, the anode voltage may be brought very close to the negative line. If the resistor is too large the screen voltages fall rapidly when the valves are switched on, and their gain drops so that an increased fall time has to be tolerated. Conversely, with the resistor too small, excessively high screen currents prevent the anode voltage dropping and may damage the valves.

As the output voltage falls the screen grid voltage of valve V5, V6 and V7 will fall also until the diode becomes forward biased. The series resistor then serves to limit the maximum diode current and prevent its destruction.

At the end of the delayed pulse, the shunt discharge valves are turned off, and the screen voltage is restored through its series resistor. The pulser is then ready for recycling.

### 3.5.7 Pulse Generator Performance

The pulse generator came very close to meeting the required specification discussed above.

Rise and fall times of 100ns were obtained though the shortest practical pulse duration for full amplitude was about 150ns measured at half maximum amplitude. Repetition rates were limited to 250kHz by excessive power dissipation in the valve V2 of the clock pulse amplifier, though this rate could be varied over the continuous range down to 1Hz.

Pulse amplitudes of 1kV were achieved between the -300 and +450 volt lines available. Larger pulses were obtained by running the HT line from a 0 - 2kV, 5mA supply, which placed severe

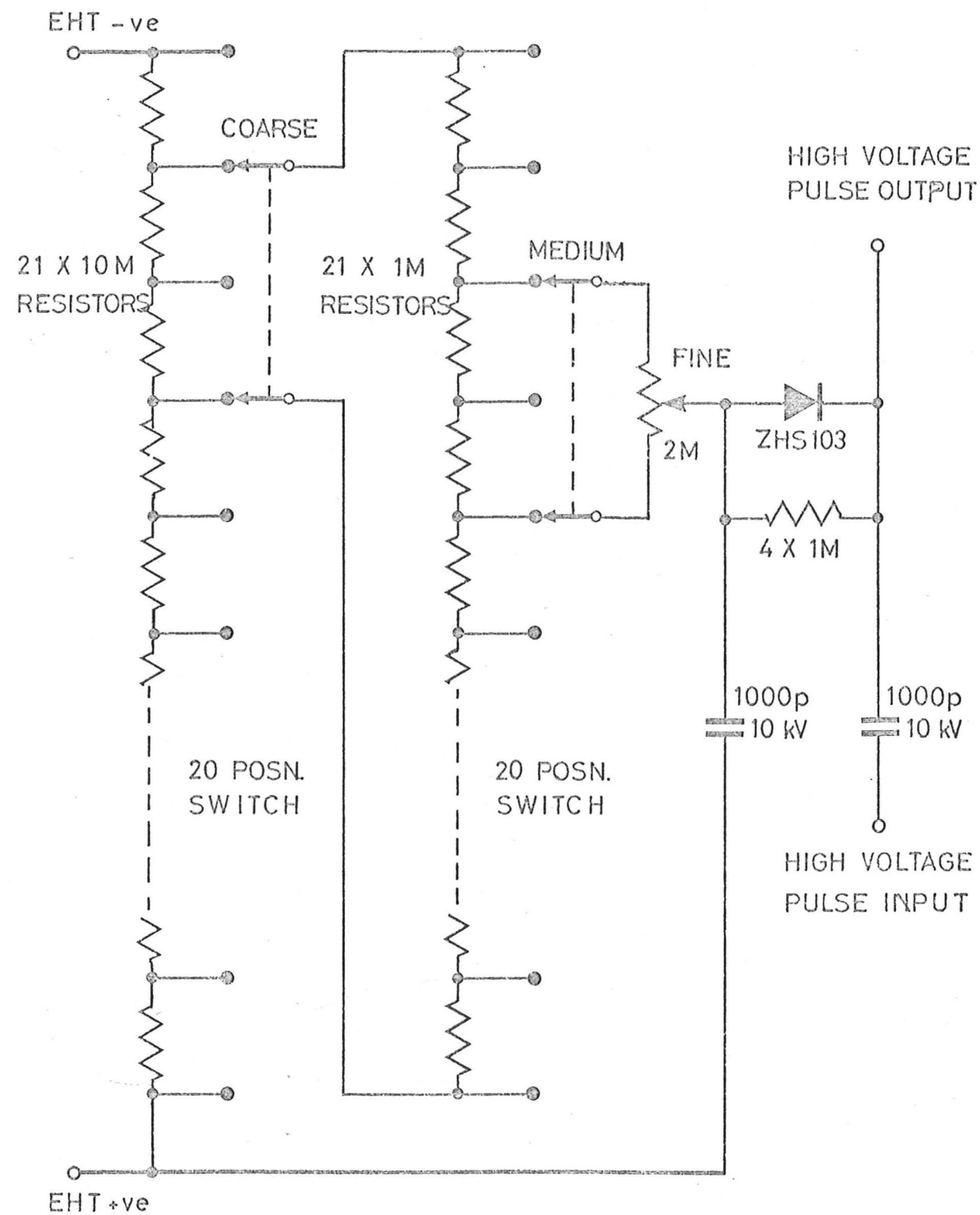


Fig 3.11 High Voltage Bias Unit

limitations on the repetition rates due to its limited current capability.

Photographs of typical output pulses taken from a Tektronix type 545 oscilloscope are shown in Fig. 3.10. These illustrate the good pulse shape obtained, and very short rise and fall times. Also included is a trace of an output pulse with timing pulses superimposed to illustrate the timing sequence.

### 3.5.8 High Voltage Bias Unit

This unit provides a d.c. grid voltage derived from the main EHT supply, onto which the high voltage pulses may be superimposed. The circuit is shown in Fig. 3.11.

Resistor chains were wired directly onto wafer switches made in the laboratory from perspex, which gave high voltage isolation up to 15kV, and had two wipers.

Using the circuit of Fig. 3.11, a continuous and uniform variation of d.c. bias voltage is possible with coarse medium and fine controls.

Incoming pulses are transmitted to the bias voltage through a d.c. isolating capacitor, and added to the bias voltage. During a pulse, the diode isolates the output from the bias chain, so that the pulse generator is not loaded. No deterioration of the pulse waveform was detectable when connected through the bias unit.

The application of the unit as shown in Fig. 3.6 could be either in conjunction with the pulser, or simply to provide a d.c. control bias without the pulse input.

EXPERIMENTS PERFORMED IN THE FIELD EMISSION MICROSCOPE4.1 Cold Field Emission

Early experiments performed in the FEM were designed to test the field emitters, and to gain practical experience in their operation. Initially no other electrodes were introduced to the vacuum system, and experiments were performed with cold field emission only. Pressure in the microscope was usually better than  $1 \times 10^{-9}$  torr.

4.1.1 Preliminary Experiments

When the first emission pattern had been obtained and the conditions for cleaning the emitter by resistive heating established, the instrumentation described in the previous chapter was progressively developed.

The characteristic (110) tungsten emission pattern was clearly recognisable on the phosphor screen and was recorded on the 35mm camera.

A recorder was set up to monitor emission current. Typical results showing the rapid variation of emission current and pattern for the field emission diode are shown in Fig. 4.1, in which the patterns (a), (b), (c) and (d) refer to the points marked on the plot of current variation. This result was obtained under constant voltage operation immediately after flashing the emitter. The fall in emission current is due to the steady adsorption onto the clean surface of the emitter of residual gas atoms. The emission pattern is also affected by loss of

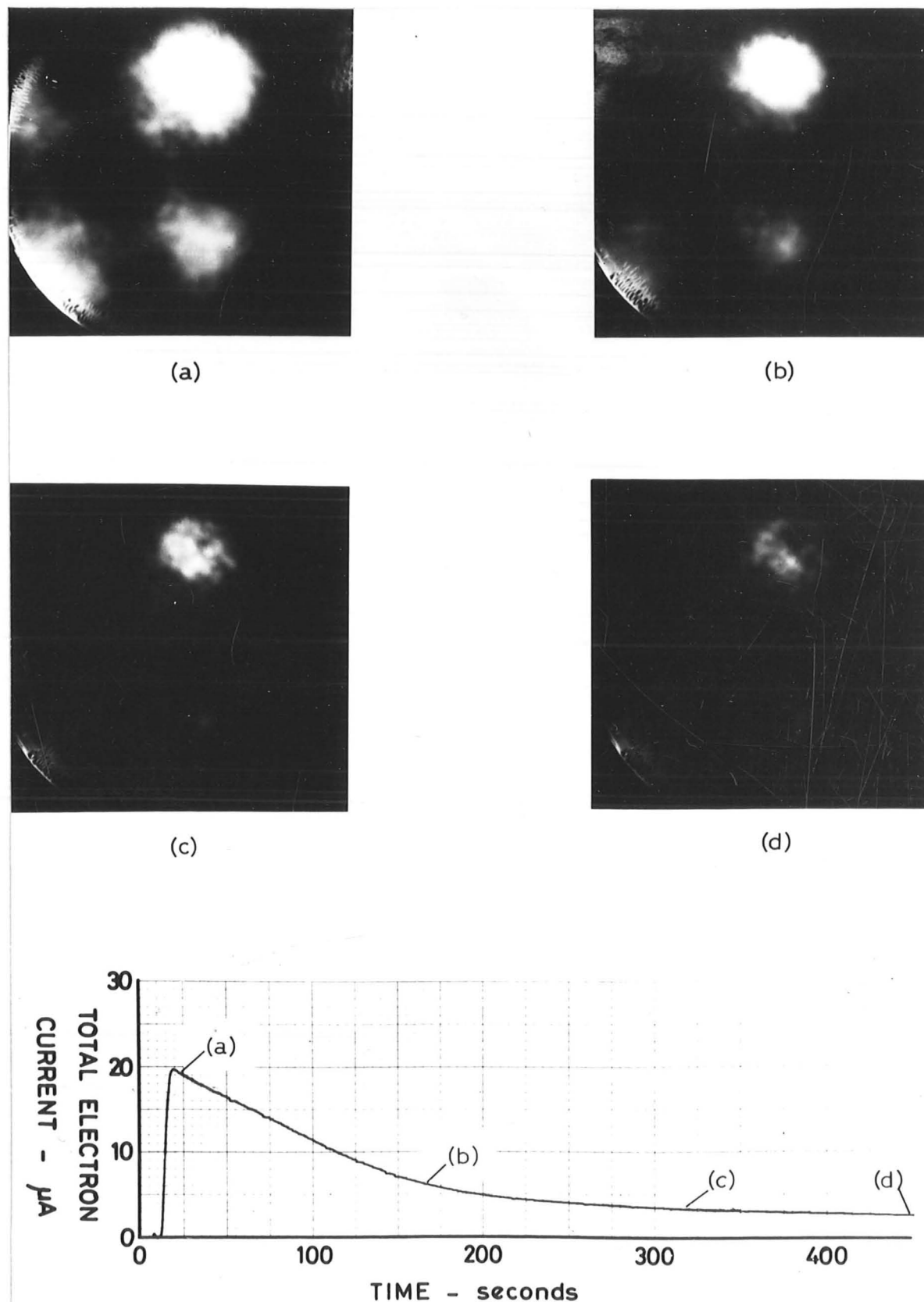


Fig 4.1 Cold Field Emission - Time Variation

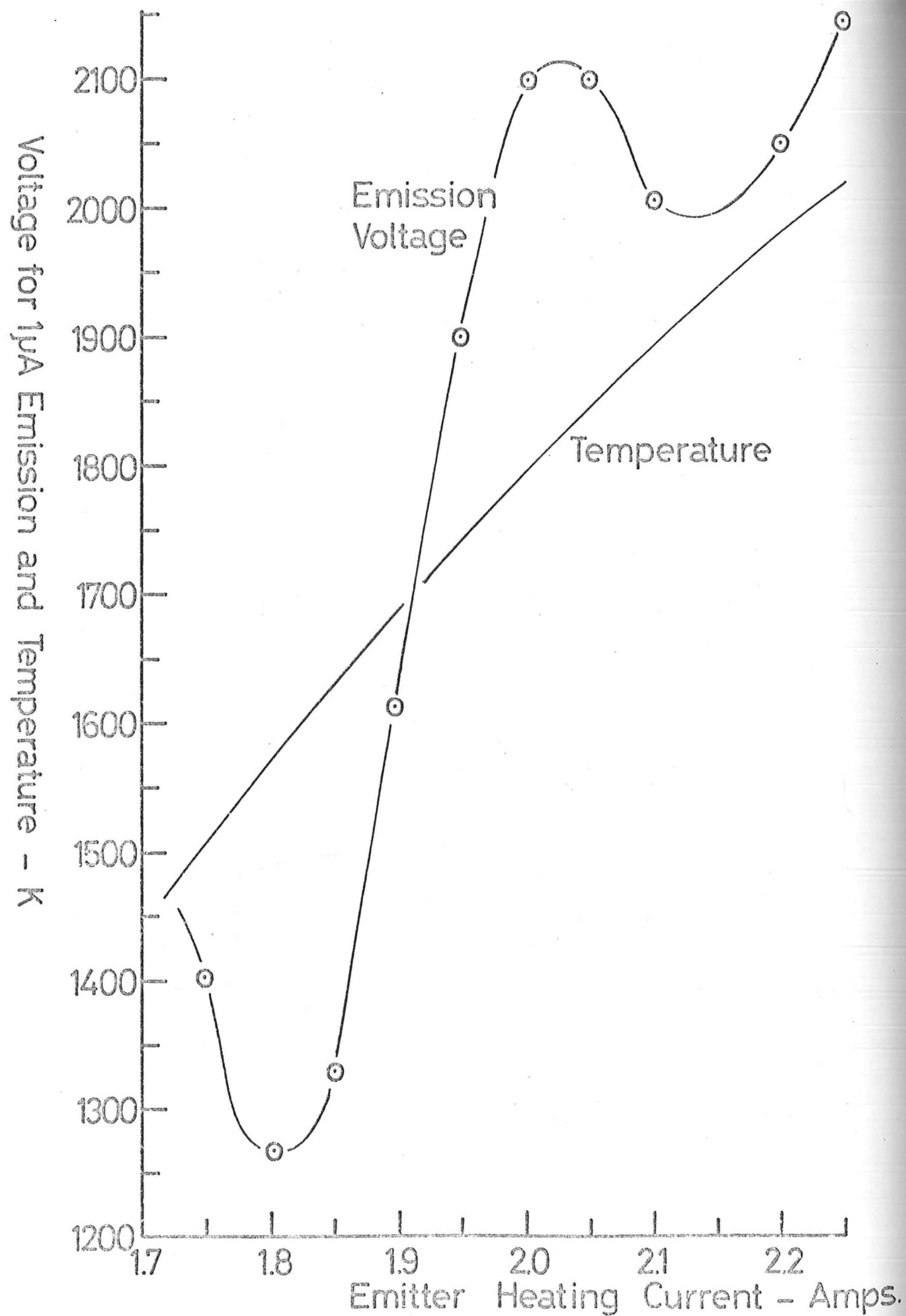


Fig 4.2 Effect on Emission of Flashing Temperature

brightness and definition.

Addition of a resistor bleed chain from the EHT unit enabled the diode voltage to be directly recorded. This enabled results shown previously in Figs. 1.2 and 1.3 to be obtained.

It was found that an emission current of a few microamps could be drawn for about an hour before it started to increase due to surface roughening from ion bombardment. The emission current became increasingly irregular and sudden small but sharp rises in emission current could be correlated with the appearance of bright spots in the emission pattern.

If the emission were allowed to continue the current built up until discharges occurred, and the emitter was destroyed.

#### 4.1.2 Flashing of Emitters

Providing emission is stopped before the onset of vacuum arc conditions, it may be reformed by "flashing". This name has been given to the process whereby the emitter is heated to about 2000K, which is sufficient to evaporate adsorbed gases, and increase the mobility of the surface tungsten atoms. Irregularities caused by ion bombardment are smoothed over by surface tension effects, and a clean, hemispherical tip results.

The flashing was accomplished by resistive heating of the emitter, passing a current of about 2 amps through its support loop.

The process was investigated by passing a predetermined heating current through the support for a fixed period of 5 seconds. Current/voltage characteristics were then determined and this was repeated with the flashing current steadily increased. Typical variation of the voltage required for 1  $\mu$ A emission is shown as a function of flashing current in Fig. 4.2.

When the flashing temperature is increased, the voltage for emission decreases rapidly as the emitter cleans. At the first minimum all contaminants have been removed except oxygen, which has a high binding energy on the (100) faces, and serves to greatly enhance the emission. The (100) faces therefore show very strong emission under these conditions. Further flashing at higher temperatures removes the remaining adsorbed oxygen and the voltage increases correspondingly as emission from the (100) regions drops.

The reason for the second minimum is not certain, but the drop in voltage may correspond to a lowering of work function on some other faces as the last traces of adsorbed gas are removed.

Higher temperature flashing permits the emitter to become more blunt under the action of surface tension forces with very high surface mobility. No further cleaning results, and consequently the emission voltage starts to increase. Clearly the optimum flashing temperature is that at which the emitter becomes atomically clean, but serious blunting does not occur. For this emitter 2.15A is appropriate, corresponding to 2000K.

The optical pyrometer was used as a measure of temperature in a separate experiment and the results are also shown in Fig. 4.2. No attempt was made to make an absolute calibration of temperature by correcting for the emissivity of tungsten, nor for the pyrex glass window through which the emitter was viewed, as this was not necessary for experimental purposes. The situation is further complicated as there is a temperature drop along the shank of the emitter which cannot readily be determined, though some estimates of its magnitude have been made, Swift (1960), Martin et al (1960). Since this effect tends to cancel the first two, the measured

temperature is not greatly in error and is probably within the range  $\pm 50\text{K}$ .

The flashing period did not seem to be critical and five seconds was found to be satisfactory.

#### 4.2 T-F Emission

The T-F mode of operation reported by Dyke (1953) offers the possibility of stable emission by electron tunnelling which does not require UHV conditions. Drechsler, Cosslett and Nixon (1958) suggested that stable T-F emission is possible in vacua as poor as  $10^{-4}$  torr, with current densities of  $10^8 \text{A/m}^2$ . Thus an early investigation of this form of emission was considered to be highly desirable.

##### 4.2.1 T-F Emission Characteristics

The T-F emission mode may readily be established by reference only to the emission pattern.

Cold field emission from a clean emitter has poorly defined boundaries between low and high work function faces. When the emitter is flashed a near hemispherical end form results in which there are no sharp boundaries. Thus the emission pattern has a "cloud like" or "cotton wool" appearance.

As the emitter temperature is increased a sharp transition takes place in the pattern and distinct boundaries develop which are characteristic of the T-F mode of emission. This corresponds to a reformation of the tip under the action of the high electric field in addition to surface tension effects, when some crystal faces grow at the expense of others. The faces which grow are generally those having a closer packed structure with high bonding energies and consequently high work functions. The junctions

between these faces usually have lower work functions, also the surface electric field is locally enhanced thus most emission comes from these regions. This effect may be seen in the emission pattern reproduced in Fig. 1.4.

In particular, the (111) face emits strongly under T-F conditions and is very stable due to the relatively close surface packing. This orientation of emitter wire is therefore very attractive for electron optical applications of T-F emission.

#### 4.2.2 T-F Emission Stability

The stability of T-F emission with respect to its tolerance of relatively poor vacuum is obtained by operating at a sufficiently high temperature that a favourable equilibrium is established between residual gas adsorption and re-evaporation, also to the rate of ion bombardment damage to the tip and its repair by mobile surface atoms of tungsten.

Unfortunately, surface mobility increases very rapidly with temperature and brings with it problems of stabilizing the emitter geometry. Two opposing effects are present, namely blunting of the emitter due to surface tension, and emitter build-up due to the electrostatic field. Dyke et al. (1960) have investigated these effects in detail, and under certain conditions they may be arranged to exactly balance. Thus enabling stable T-F operation at over 2000K. However, under normal conditions the presence of an electric field large enough to draw T-F emission is sufficient for build-up effects to predominate. Thus, the operating temperature should be as low as possible consistent with maintaining a clean emitter.

In practice, an operating temperature of 1800K (uncorrected) has been found satisfactory, and stable operation has been achieved

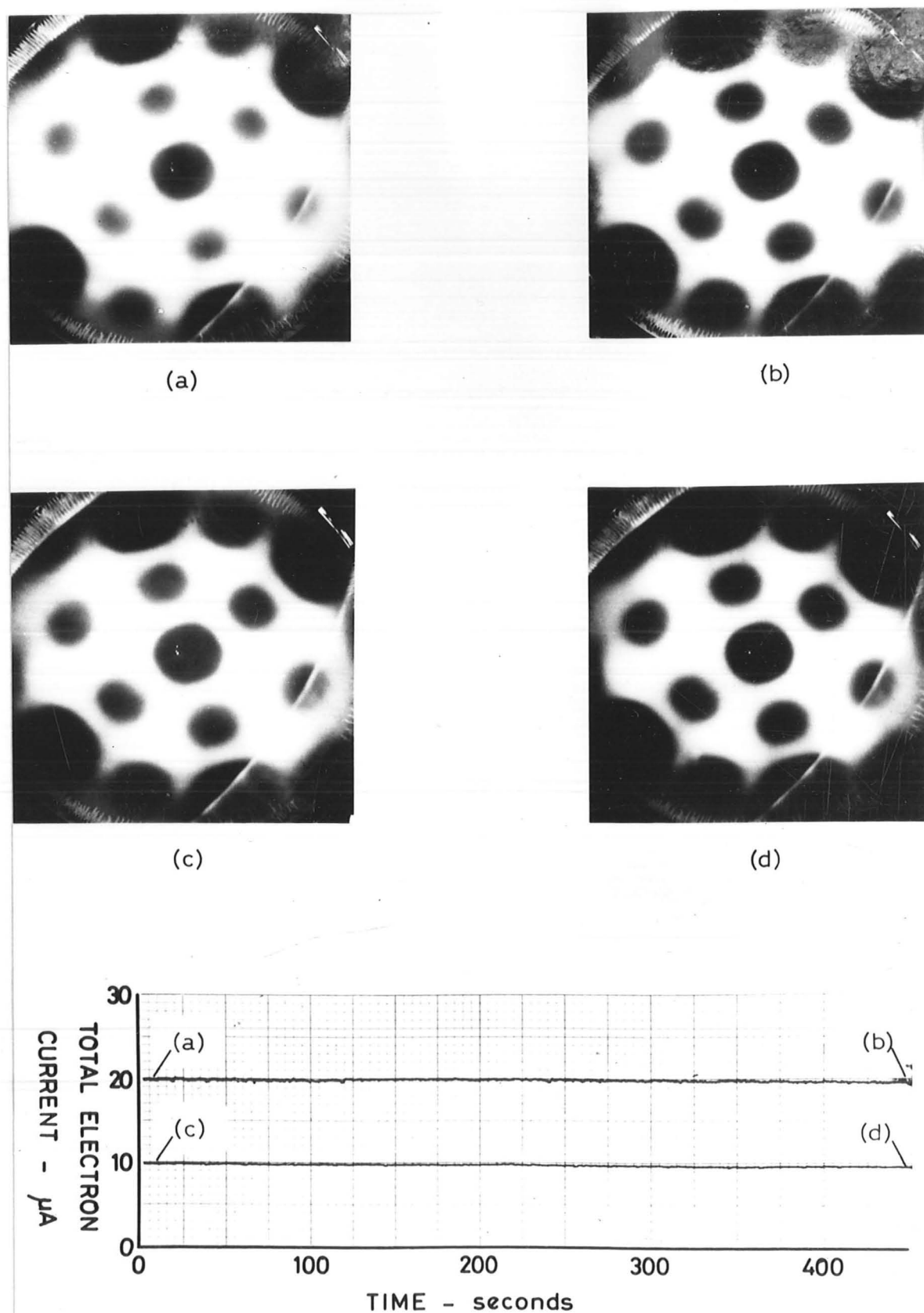


Fig 4.3 T - F Emission - Time Variation

for periods of several hours with many different emitters. The stability of this emission is illustrated in Fig. 4.3, which is directly comparable with Fig. 4.1 for cold field emission.

The maximum pressure under which T-F emission may be drawn depends on many factors including the tolerable emission current variations and the operating temperature. In practice it has been found to be very difficult to maintain T-F emission at 1800K at pressures higher than  $10^{-6}$  torr, and at this pressure the emission current under constant voltage conditions suffered random variations of typically  $\pm 10\%$ . This pressure must therefore be taken as the worst under which a T-F emitter may be satisfactorily operated.

#### 4.2.3 Establishing T-F Operation in Practice

The FEM provides an ideal environment for performing experiments, as a large amount of visual information is available from the emission pattern. Thus, as described above, it is relatively straightforward to set up T-F operation by observation of the pattern. However, in a practical application, it is very unlikely that it would be possible to observe the emission pattern directly, and alternative means of setting up the T-F emission mode were developed.

At first it was hoped that it would be possible to make emitters reproducibly, so that their temperature could be set by reference to the heater current, as is common practice with thermionic electron microscope hairpin filaments. It was somewhat surprising therefore when emitters operating in the region of 1800K showed temperature variations of  $\pm 10\%$  for the same heater current. However, the thermal losses at the tip are largely due to radiation (proportional to  $T^4$ ), so that smaller variations of

temperatures occur for thermionic emission at typically 2,700K.

The temperature of emitters may, however, be set very accurately by observation of the emission current/voltage characteristics. The plot shown in Fig. 1.4, for a T-F diode, differs from the similar FE plot by the existence of a small, almost constant emission current at low applied voltages. This plateau is due to thermionic emission from the relatively large bulk of the support filament. The emission density is in the region of  $1\text{A/m}^2$  and gives a thermionic current of a few microamps for the emitter geometry used. It is a sensitive function of temperature, thus this may be set by applying about 500 volts to the diode and increasing the heater current to give a thermionic current of typically  $3\ \mu\text{A}$ .

When the applied voltage is further increased the surface field at the tip becomes sufficient for tunnelling to take place, and the steep rise in the emission current occurs with the simultaneous appearance of the emission pattern on the screen. These effects are characteristic of emission by electron tunnelling.

#### 4.2.4 Relative Stabilities of Crystal Faces in T-F Emission

An important feature of the T-F emission mode is the marked variation in stability of individual crystal faces, as judged from the emission pattern.

a) The most stable crystal face with a large emission current density is (111). This is largely as expected due to the high degree of symmetry of the orientation, relatively close packing and hence high binding energy of the surface structure.

b) Some faces, particularly those in the region of the (111) face, appear and disappear from the emission pattern in a random manner.

## GLASS INSULATOR WITH TUNGSTEN LEADTHROUGHS

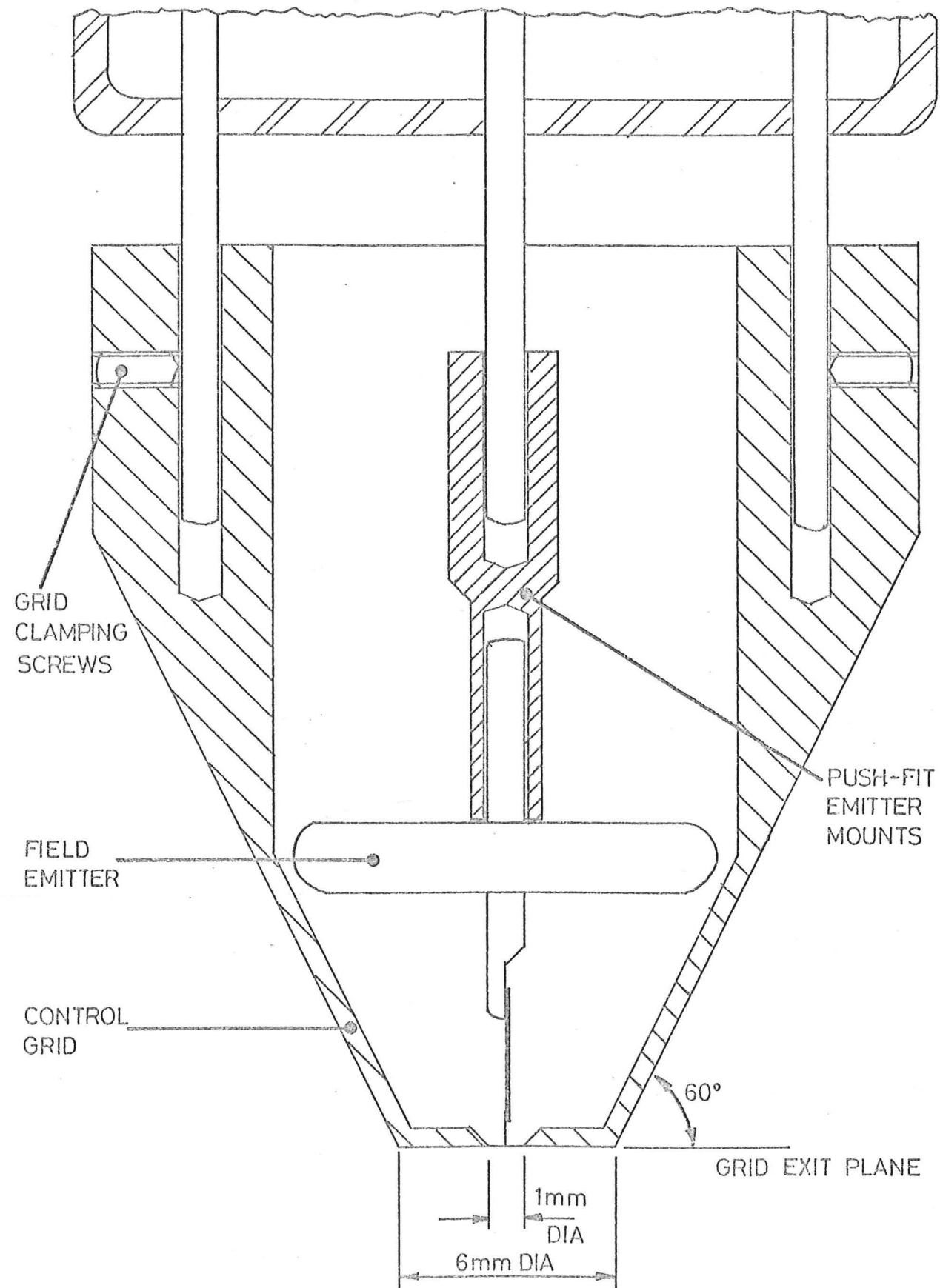


Fig 4.4 Emitter and Grid of the Triode Gun.

c) Under poor vacuum conditions adsorption occurs on the (100) face, this may be limited as discussed above by raising the emitter temperature. However, under adverse vacuum conditions emission from this face may become very intense and erratic, and cause emitter destruction.

These observations, which relate to macroscopic variations in the emission pattern, will be supplemented in section 4.5 with measurements of emission from selected crystal faces. Such measurements are relevant from the point of view of the noise which would be introduced into an electron beam generated by a T-F source.

#### 4.3 Triode Gun Configuration

From practical considerations of using field emission electron sources in electron optics, the diode configuration so far considered has distinct disadvantages. These stem from the interdependence of emitter radius, emission current and the operating voltage. Ideally, a field emission gun is required which is capable of operating at any voltage suited to the application, and in which the emission current may be varied independently.

This has been achieved, at least partially, by the development of the triode gun configuration shown in Fig. 4.4. It differs from the diode by the inclusion of an additional electrode which performs the function of a control grid. Although the design of the grid was governed largely by practical mechanical considerations, an attempt has been made to maintain its surface close to that of a diode equipotential in order to minimise deviation from the diode field structure.

The grid was constructed of stainless steel and mounted

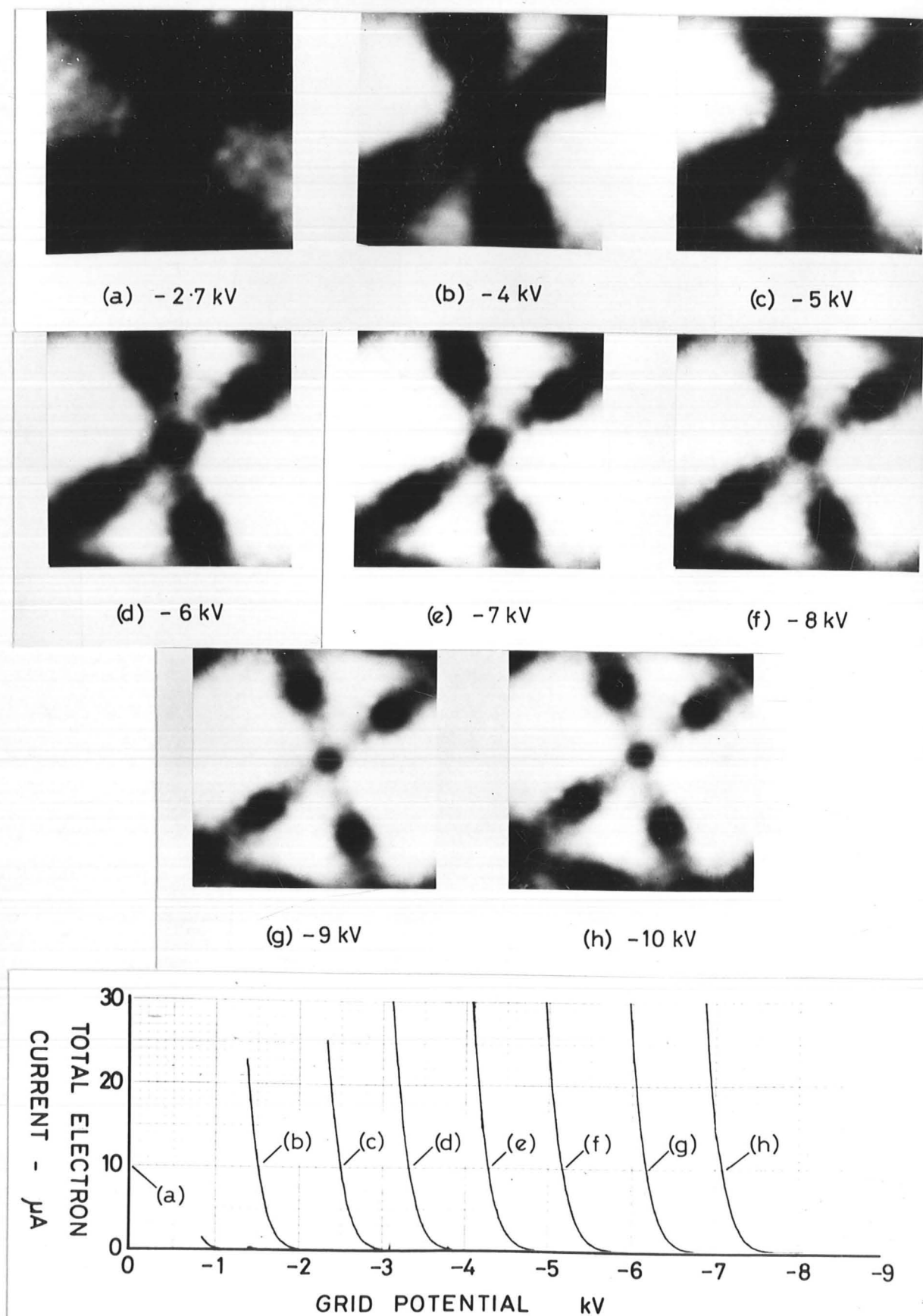


Fig 4.5 Field Emission in the Triode System

directly onto the tungsten leadthroughs of the glass insulator. Sufficient clearances were allowed to permit alignment of the grid with respect to the axis of an emitter tip by manual adjustment, when it was clamped into position by its fixing screws.

In practice the height of the filament tip with respect to the exit plane of the grid was found to have little effect on the performance. Thus the tip was normally adjusted to be the exit plane of the grid, and this position could be easily and accurately set.

#### 4.3.1 Field Emission Control Characteristics

The grid control characteristics were conveniently produced in practice by monitoring the grid voltage using a potential divider. Typical current/voltage variation is shown in Fig. 4.5 with the emission patterns corresponding to the emitter potentials indicated and 10  $\mu\text{A}$  emission.

Characteristics may be compared with these of the diode [Fig. 1.37]. Over the range of voltages investigated, emission was established with the grid 2-3kV positive with respect to the emitter, and this varied only slightly with variation of the overall gun voltage.

The performance may be described in terms of normal valve parameters. As an example, for operation at  $V_a=5\text{kV}$ ,  $I=10\ \mu\text{A}$ , these would be:

$$\begin{aligned} g_m &= 7 \times 10^{-8} \text{ A/Volt} \\ r_a &= 5 \times 10^{-9} \text{ ohms} \\ \mu &= 350 \end{aligned}$$

with an estimated accuracy of  $\pm 10\%$ .

The effects of varying the overall gun voltage on emission pattern can also be seen in Fig. 4.6.

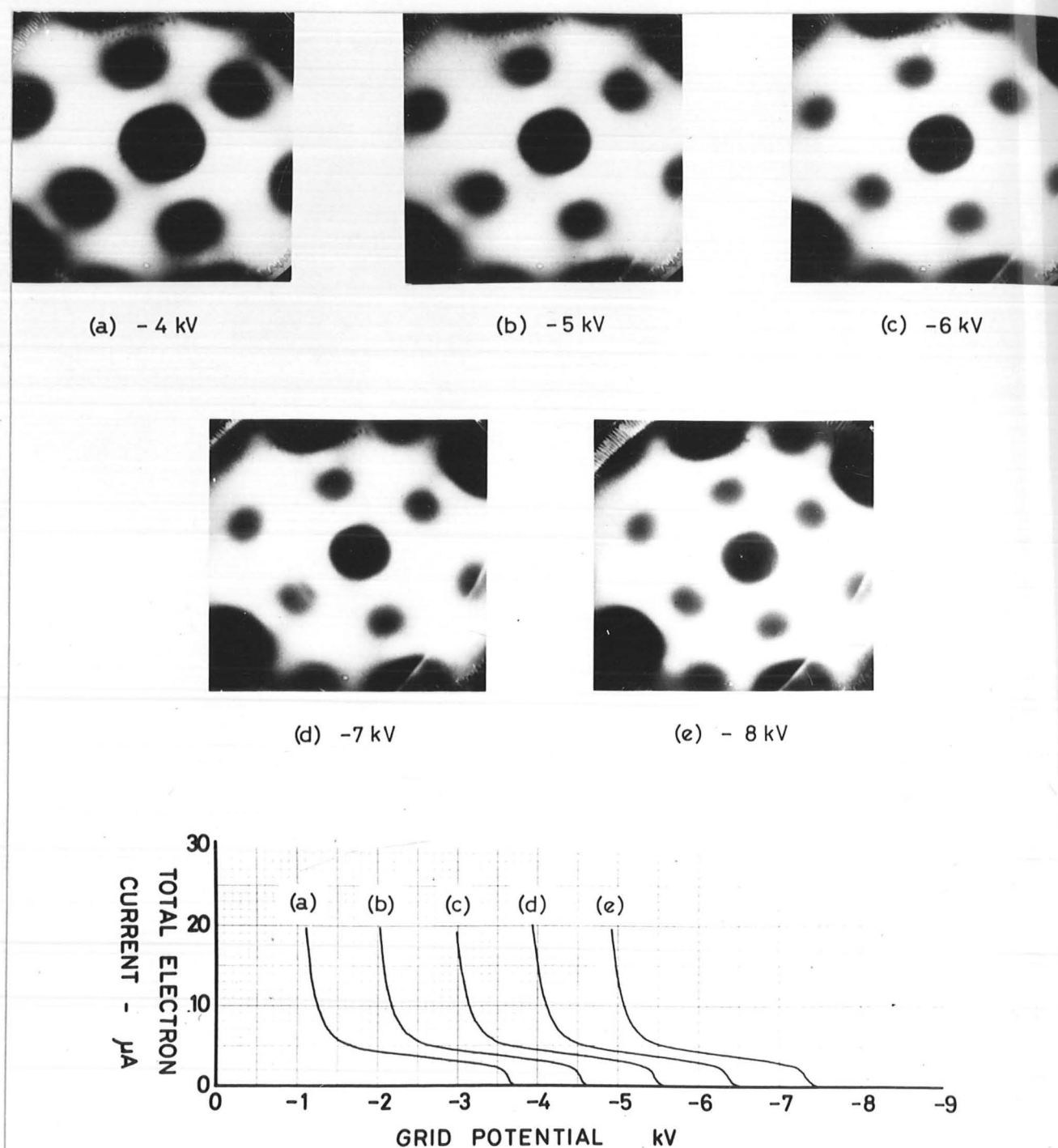


Fig 4.6 T - F Emission in the Triode System

a) The size of the pattern is reduced as voltage is increased. Gomer (1961), has reported that in a typical diode configuration the emission pattern is compressed to approximately  $2/3$  of its theoretical size. This effect is due entirely to differences in the actual electric fields and the ideal case of spherical symmetry about the tip. In the triode operating at higher voltages the axial component of electric field is enhanced, leading to additional pattern compression.

b) Brightness of the pattern increased with voltage due to higher phosphor efficiency.

c) The definition in the emission pattern is considerably improved and considerable extra detail becomes available at higher voltages. This is important as it indicates that the emitter surface is being imaged at higher resolutions, and consequently the triode structure is not introducing severe aberrations into the system.

These properties of the triode structure suggest applications in the fields of conventional Field Emission Microscopy where the improved resolution theoretically obtainable with higher voltage operation would be advantageous. Also, the possibility of improving light yield at higher voltages could be very useful in Field Ion Microscopy. The use of a similar system has been reported in the literature by Garber (1959) with the additional facility for the image gas to be introduced inside the grid, so increasing ion yields while at the same time maintaining an adequately high vacuum in the imaging region.

#### 4.3.2 T-F Emission Control Characteristics

Behaviour in T-F emission mode is essentially similar to the cold field emission. This may be seen from Fig. 4.6, which shows

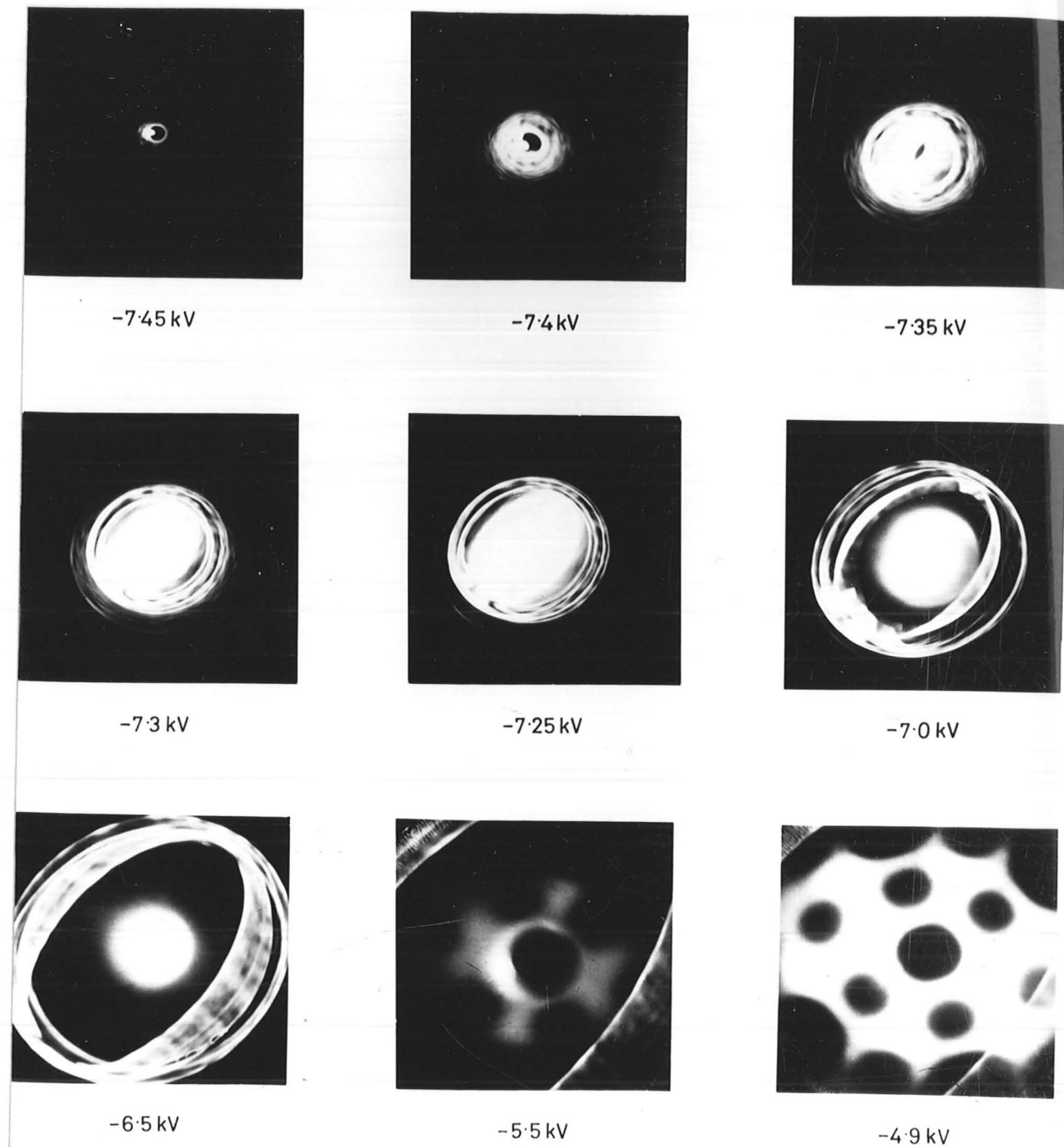


Fig 4.7 T - F Triode with Emitter at  $-8\text{kV}$   
Effect of Varying Grid Potential.

T-F emission characteristics for comparison with Fig. 4.5.

The characteristics differ from the field emission case in a similar manner to the diode, with the addition of current at low fields which has been attributed to thermionic emission from the support and heating filament. This is further justified by measurements of grid and anode currents separately, when nearly all of the thermionic current passes to the grid, and very little to the anode. At higher fields on the steeper parts of the characteristics almost all of the current flows to the anode, and little extra to the grid. Indeed, the anode current characteristics would be very similar to those with cold field emission.

Extremely interesting patterns result from the presence of the two types of emission. This is illustrated in Fig. 4.7, in which the operating points may be identified directly with curve (e) of Fig. 4.6. The surface field increases as the negative grid voltage is reduced.

At the lowest surface fields (top left of Fig. 4.7) the emission can only be thermionic and in fact, the emission pattern is formed after a crossover. This becomes apparent as the field is increased when the crossover unfolds. At the highest fields the normal T-F emission patterns emerges as the bright bands towards the edges of the pattern [also present with the diode - Fig. 1.47]. These may be attributed to thermionic emission from the base or sides of the emitter tip.

The bright, axial emission evident at moderate fields is presumably due to Schottky enhanced thermionic emission from the tip. This would explain the slight but steady increase of the thermionic emission with field in the temperature limited conditions. In view of these experiments considerable doubt must exist concerning the possibility of operating pointed emitters in the

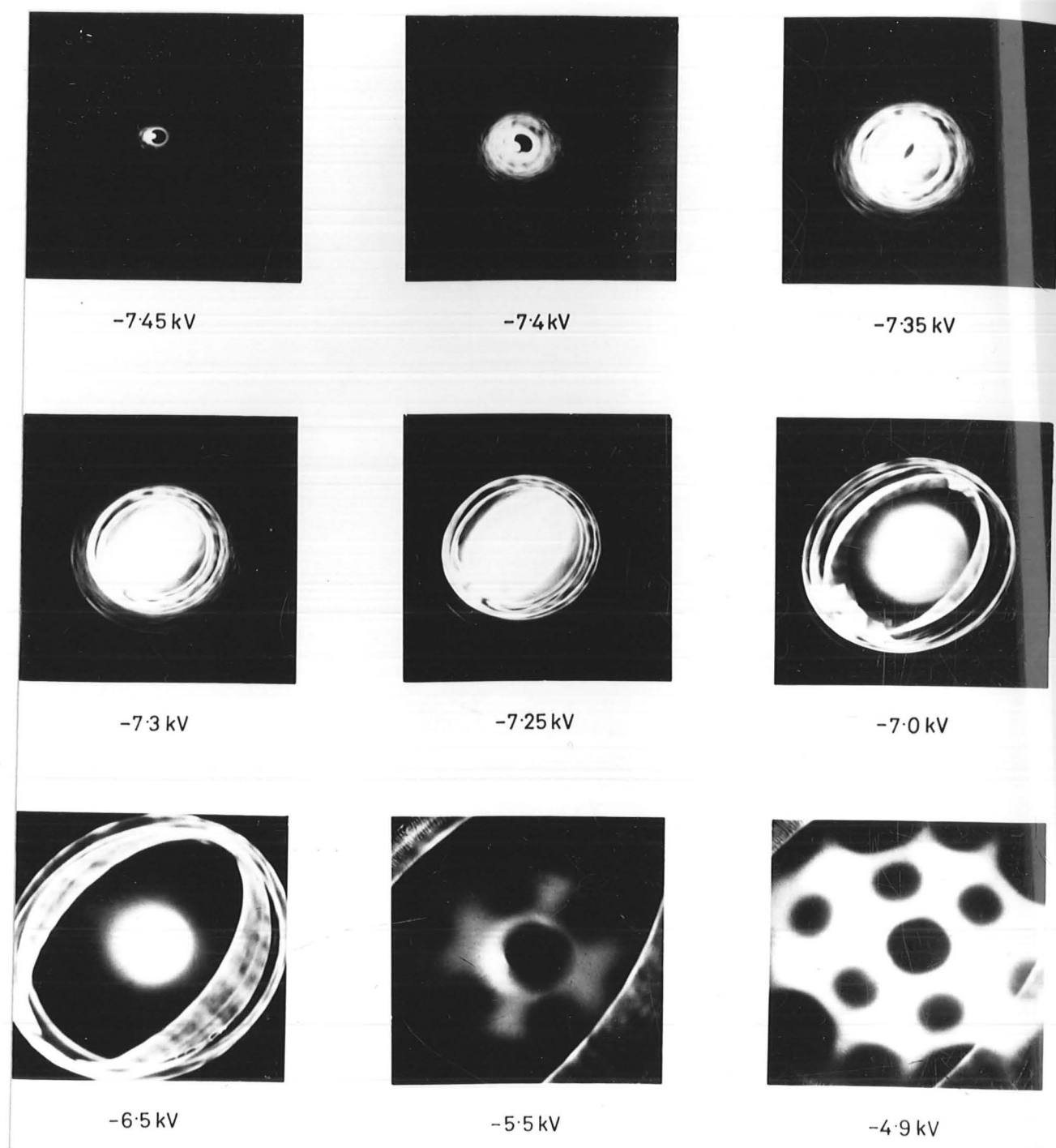


Fig 4.7 T - F Triode with Emitter at -8kV  
Effect of Varying Grid Potential.

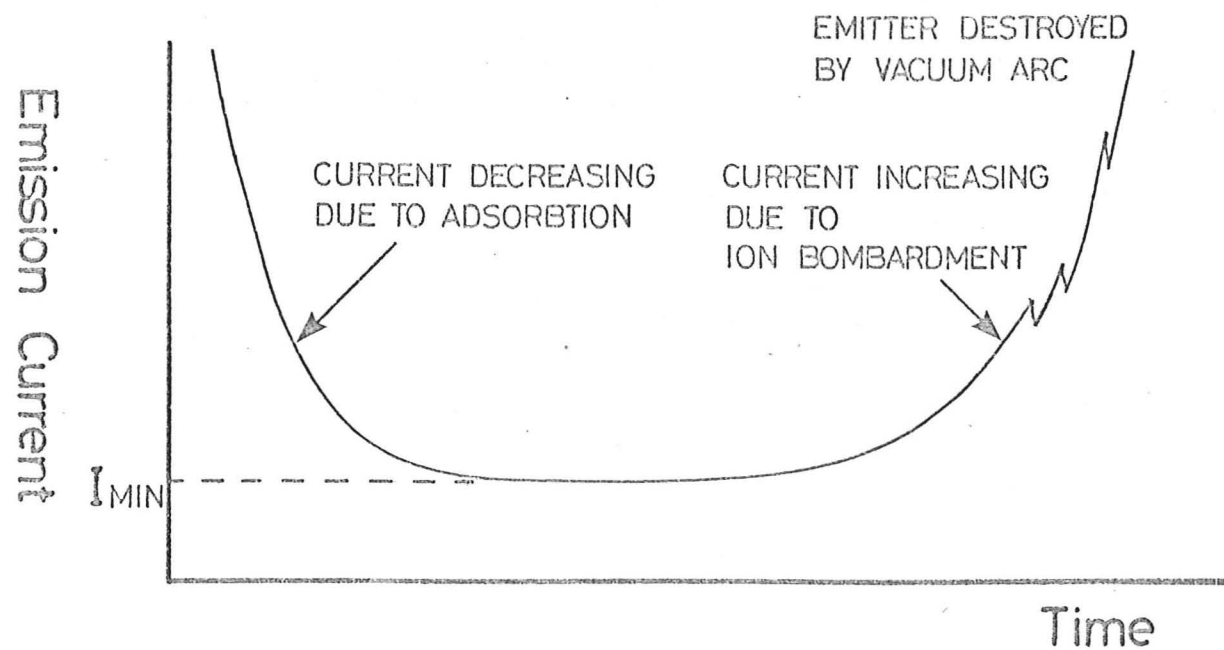
T-F emission characteristics for comparison with Fig. 4.5.

The characteristics differ from the field emission case in a similar manner to the diode, with the addition of current at low fields which has been attributed to thermionic emission from the support and heating filament. This is further justified by measurements of grid and anode currents separately, when nearly all of the thermionic current passes to the grid, and very little to the anode. At higher fields on the steeper parts of the characteristics almost all of the current flows to the anode, and little extra to the grid. Indeed, the anode current characteristics would be very similar to those with cold field emission.

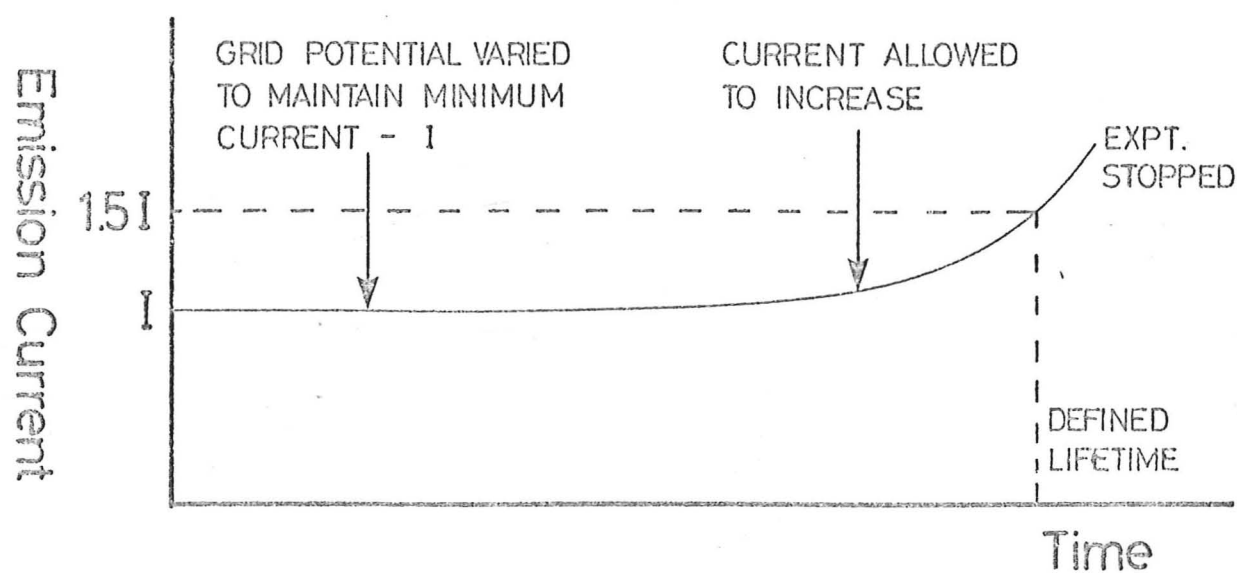
Extremely interesting patterns result from the presence of the two types of emission. This is illustrated in Fig. 4.7, in which the operating points may be identified directly with curve (e) of Fig. 4.6. The surface field increases as the negative grid voltage is reduced.

At the lowest surface fields (top left of Fig. 4.7) the emission can only be thermionic and in fact, the emission pattern is formed after a crossover. This becomes apparent as the field is increased when the crossover unfolds. At the highest fields the normal T-F emission patterns emerges as the bright bands towards the edges of the pattern [also present with the diode - Fig. 1.47]. These may be attributed to thermionic emission from the base or sides of the emitter tip.

The bright, axial emission evident at moderate fields is presumably due to Schottky enhanced thermionic emission from the tip. This would explain the slight but steady increase of the thermionic emission with field in the temperature limited conditions. In view of these experiments considerable doubt must exist concerning the possibility of operating pointed emitters in the



(a) Applied Potentials Constant



(b) Controlled Emission Current

Fig 4.8 Illustrating Emission Current Variations and Lifetime Criterion

Schottky enhanced thermionic mode with negatively biased grids, or at temperatures much in excess of  $2000^{\circ}\text{K}$  when thermionic emission would lead to excessive emission currents and rapid emitter blunting.

4.4 Measurements of the Lifetimes of Field Emitters

The lifetime of a field emitter is the time for which emission may be drawn before the emitter needs to be flashed in order to repair the effects of ion bombardment damage.

Previous reported work on measurements of emitter lives by Dyke and Dolan (1956) has been concerned entirely with extending the lifetime by improving operating conditions. Thus pressures used were considerably better than  $10^{-9}$  torr, which represents approximately the best vacuum which could be obtained in a readily demountable instrument using a field emission gun.

Operating pressures down to about  $2 \times 10^{-10}$  torr could be obtained in the FEM. For the purposes of experiments these could be deliberately worsened by leaking gas into the system. Pressures up to  $10^{-7}$  torr have been produced in this controlled manner for the experiments described below.

4.4.1 Lifetime Criterion

When operated under constant voltage conditions, the emission current of a field emission diode or triode shows considerable variations as shown schematically in Fig. 4.8(a). Results of this kind are not readily given a meaningful interpretation. The initial current is high and ill defined, also it provides little useful guide to the subsequent minimum emission current, making controlled experiments difficult to set up. Towards the end of the emitter lifetime, ion bombardment damage becomes severe and

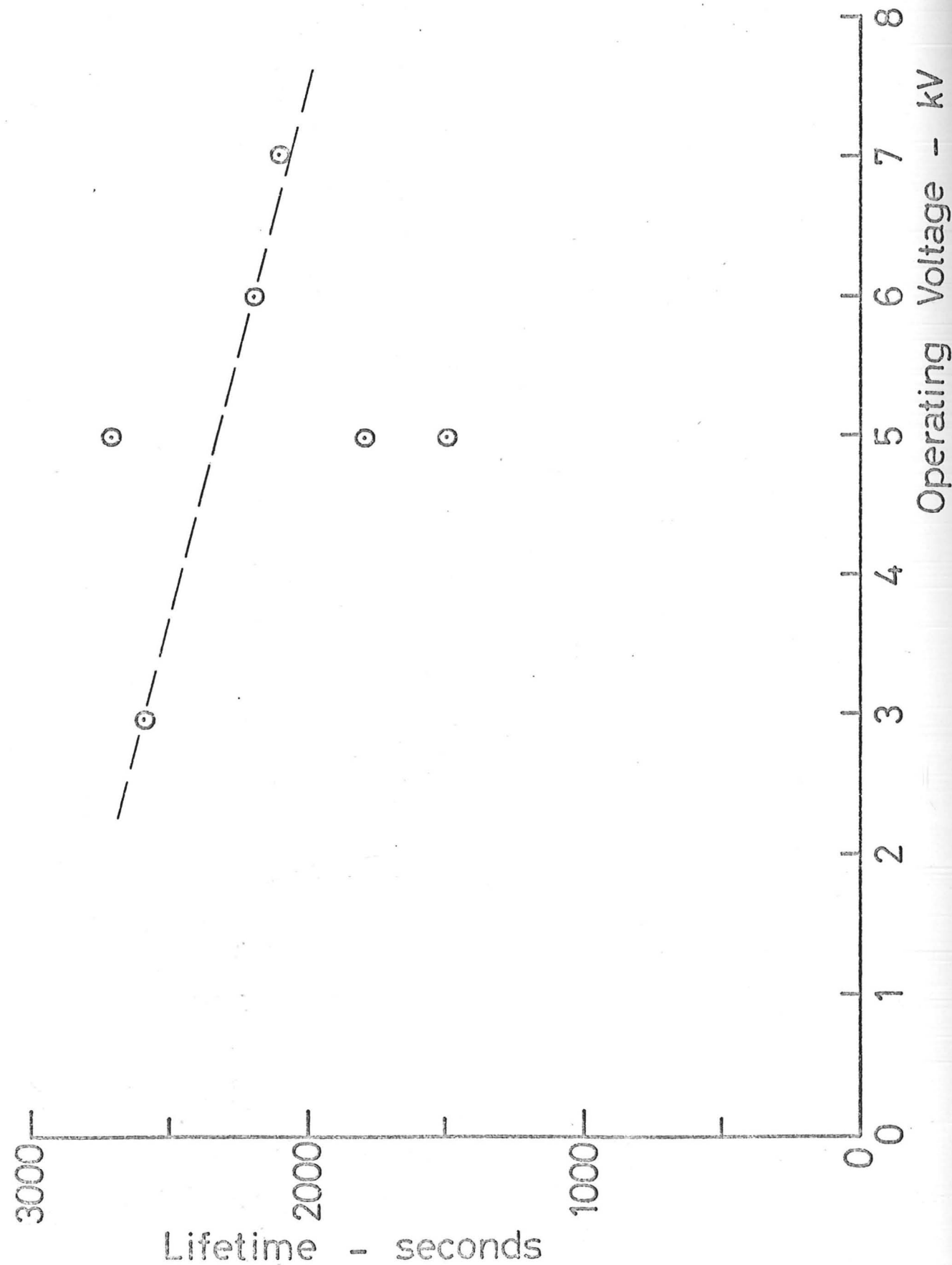


Fig 4.9 Lifetime Variation with Operating Voltage

current increases rapidly, which if allowed to continue would result in total destruction of the emitter tip.

It was necessary therefore to define the emitter lifetime in a way which allowed controlled experiments to be carried out. An experimental method was developed which proved satisfactory and gave reproducible results, it is illustrated in Fig. 4.8(b). For example, it is intended to determine the lifetime of an emitter at emission current  $I$ . The current is initially set at this level which is maintained by increasing slightly the emitter voltage (or grid voltage in the case of triode operation). When, however, the emission current starts to increase due to the cumulative effects of ion bombardment no further alteration of the conditions is made. The period of useful emission, or lifetime is thus defined arbitrarily as the time taken for the emission current to increase to 50% higher than its set minimum level. The emission is then stopped before the emitter is destroyed.

4.4.2 Variation of Lifetime with Voltage

Some early experiments were performed to determine whether lifetime would vary significantly in the triode system as the operating voltage was increased from the inherent diode operating voltage.

The results were obtained for 100  $\mu$ A emission current and are shown in Fig. 4.9. In order to reduce lifetimes to practical levels which permitted a number of experiments to be carried out, the pressure was increased to approximately  $2 \times 10^{-8}$  torr using the leak valve. Unfortunately, the mass spectrometer was not available at this stage and pressure monitoring relied on the pump control gauge and a Bayard-Alpert gauge which usually differed by a factor of three in their readings, thus an average value was

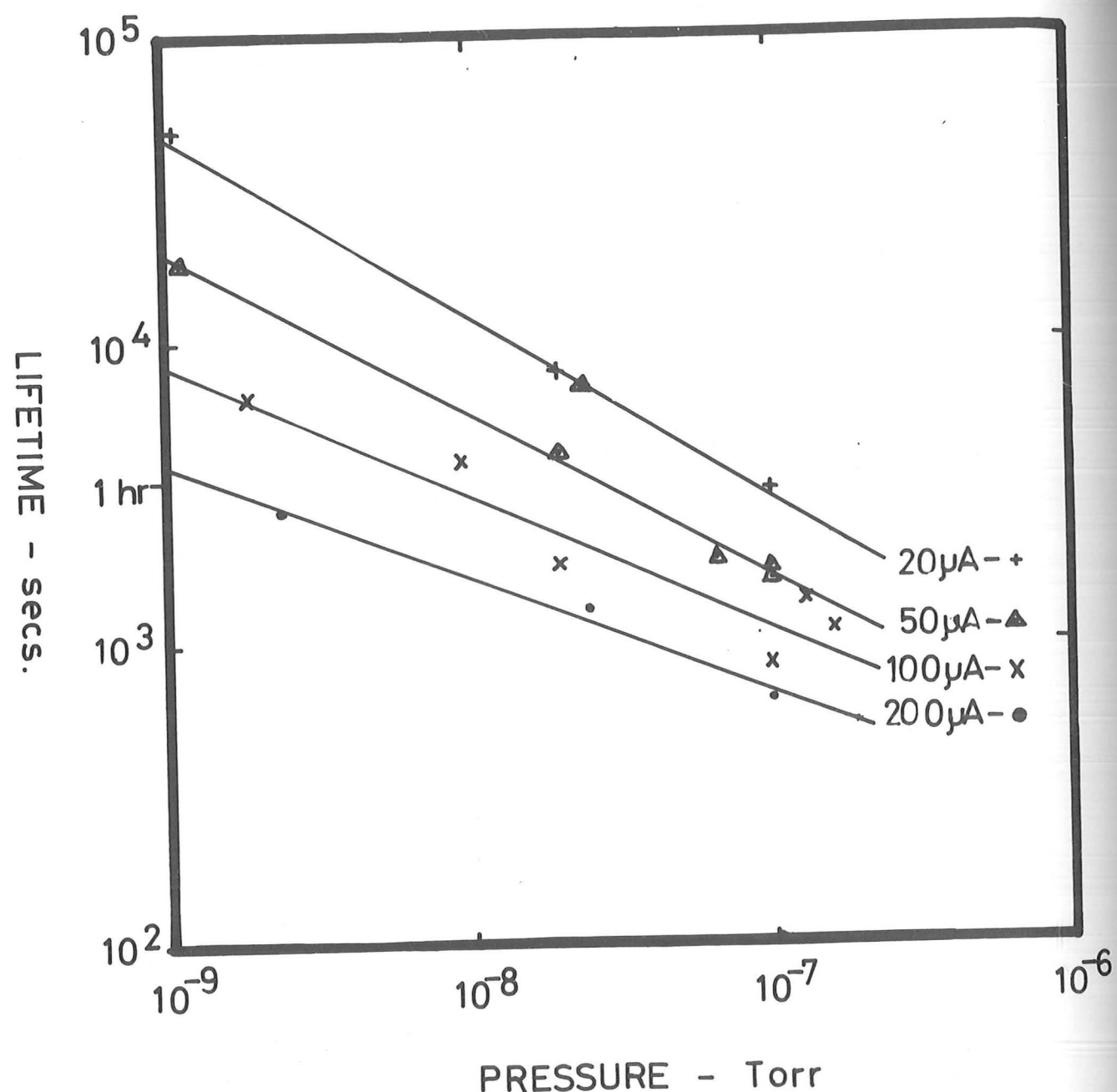


Fig 4.10 Lifetime Variations with Current and Pressure

taken to set the pressure. The mass spectrometer was later used to measure pressure, when it was found that large variations in the residual gas levels were possible using the setting up techniques described above. Thus there were larger variations in the operating conditions in this initial experiment than were achieved in later experiments.

On the basis of the results shown we can therefore conclude only that there is no appreciable change of lifetime with operating voltage over the range considered, though there is evidence of a slight trend towards shorter lives at higher voltages.

#### 4.4.3 Variation of Lifetime with Emission Current and Pressure

Experiments were carried out to measure lifetimes under conditions of varying emission current and operating pressure. The experiments recorded here were conducted at 5.0kV with the triode geometry. The total pressure was measured during operation using the mass spectrometer by summing the partial pressures of residual gases.

Results are plotted in Fig. 4.10, and show that greater lifetimes are achieved at lower emission currents, and lower operating pressures. In order to be able to operate for several hours without flashing emitters, pressures in the region of  $1 \times 10^{-9}$  torr must be obtained, and emission currents must be limited to about 20  $\mu$ A.

On the basis of the results the following empirical relationship was derived for the variation of lifetime with both emission current and total pressure:

$$L = 0.3 / [P(7 \times 10^{-2} / I^{0.2})]$$

where L is lifetime in seconds, P is pressure in torr, and I the current in amps.

#### 4.4.4 Factors Affecting Lifetime

The empirical relationship derived above does not lend itself to any obvious quantitative theoretical explanation for the variation of lifetimes. Since emitter damage is caused by ion bombardment or sputtering, it is a reasonable assumption that the lifetime is determined by the removal of a given fraction of emitter tip atoms, which would be substantially independent of the rate of removal.

This assumption is supported qualitatively by the results given in Fig. 4.10, which show that increased emission currents and increased operating pressure, which both increase rates of ion bombardment, also reduce lifetime. To a lesser extent, operation at higher voltages, which tends to increase sputtering yields, produces as a slight reduction of lifetimes as shown in Fig. 4.9. Further experimental evidence comes from the observation that lifetime measurements carried out simultaneously, and under very similar vacuum conditions, showed an approximately reciprocal relationship between lifetime and emission current.

In order to investigate more fully the mechanisms determining emitter lifetimes, an attempt was made to take into account the sputtering rates of the components of the residual gases which were present when the results shown in Fig. 4.10 were obtained.

A large number of experimental measurements of sputtering rates have been collected together in an article by Maissel (1966), and where necessary these results have been extrapolated for operating at 5kV. Additionally, as a simple check, a classical model of sputtering has been considered based on a calculation of the energy imparted to stationary tungsten atoms by moving ions of differing masses. The values obtained by the two methods were in good agreement.

Unfortunately, there was little or no improvement in the correlation between the measured results and operating conditions with the sputtering corrections included.

The above considerations have not taken into account the following three important factors:

a) Equilibrium levels of adsorbed residual gas atoms on the anode surface, which will depend on the nature of the anode and the constituents of the residual gas.

b) The probability of creating an ion by electron collision on the anode surface which will again depend on the actual gas atoms.

c) Trajectories followed by the ions in their bombardment of the emitter, which will depend again on the mass of ion.

Each of the above would be very difficult to assess quantitatively, and hence would add little to the value of the results even if such a complex analysis were possible. The experiments reported were carried out in a wide range of vacuum conditions which are typical of those which would be found in a practical application. The reader is therefore referred to Fig. 4.10 directly for an estimate of emitter lifetime under particular operating conditions.

#### 4.5 Measurements of Emission Noise and Stability

The dynamic effects of gas adsorption and ion bombardment taking place on the surface of a field emitter cause continuous variations in the electron emission current. These variations may be considered as emission noise, and in a practical application would result in noise on the electron beam.

Measurements of this noise have been made in the FEM by

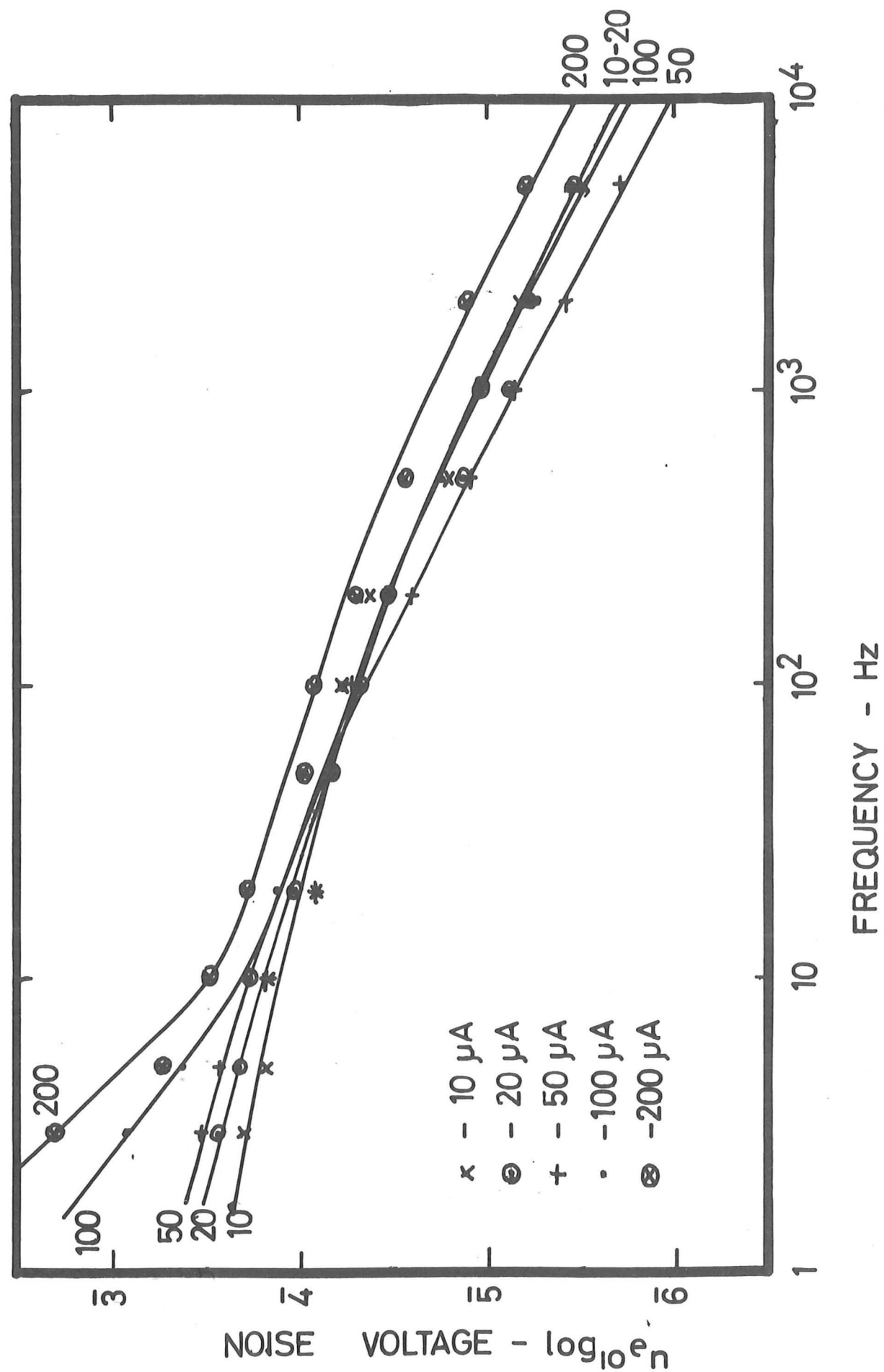


Fig 4.11 Spectral Content of Emission Noise

monitoring the emission current, and by observing the emission pattern using a photomultiplier. Direct monitoring of the emission current has the advantage that it is very simple, but is limited to the bandwidth of the recorder, d.c. to 50Hz approximately. Observation of the emission pattern by means of the photomultiplier is capable of a high bandwidth, in this case approximately 50kHz, limited by the screen phosphor response. Also, it has the advantage that the screen may be masked off so that only the intensity due to a small area on the screen is monitored, thus relative performances of individual crystal faces may be compared.

#### 4.5.1 Spectral Analysis of Field Emission Noise

Using the photomultiplier technique to observe emission, the output current was fed directly to a wave analyser. The results of experiments performed at 5.0kV in a pressure of  $1 \times 10^{-9}$  torr are shown in Fig. 4.11 as a plot of spectral noise density,  $e_n(f)$ , for various emission currents, and normalized to a mean signal level of one volt.

It may be seen that for frequencies above 10Hz there was little variation with emission current, and the noise voltage showed a variation with frequency described approximately by:

$$e_n(f) = 1 \times 10^{-3} f^{-0.8}$$

where  $e_n(f)$  is in volts/(Hz)<sup>1/2</sup>,  $f$  in Hz.

We may therefore calculate the rms noise voltage,  $E$ , due to frequencies higher than 50Hz which would not be included if the current variation were plotted directly on the recorder.

$$\text{Thus } E^2 = \int_{50\text{Hz}}^{\infty} e_n^2(f) df$$

whence  $E = 1.6 \times 10^{-4}$  volts

This contribution is so small that it would not be detectable on the recorder, which would show typically 5% peak to peak noise under these conditions, and therefore would give a true representation of the emission noise.

An interesting feature of the results shown in Fig. 4.11 is that only for very low frequencies, ie. less than 10Hz, is there any systematic increase in noise with increasing emission current. This is to be expected for noise resulting from ion bombardment of the emitter.

Adsorption and desorption of residual gas molecules from the emitter surface will also contribute to the emission noise. However, this effect depends only on the levels of residual gases in the microscope and so will be substantially independent of emission current.

We arrive, therefore, at the rather surprising conclusion that ion bombardment is a very low frequency event under these operating conditions.

It is possible to make an estimate of the maximum rate of ion bombardment of the emitter tip, by treating the anode as a source of ions and using the conservation of brightness.

For operation with 100  $\mu$ A total emission at 5kV, a pressure rise of  $2 \times 10^{-10}$  torr during emission would be typical. The ion pump on the FEM was rated at 60l/sec and this therefore represents a total rate of desorption from the anode under the influence of electron bombardment of:

$$60 \times \frac{2 \times 10^{-10}}{760} \times 2.7 \times 10^{22} = 4.3 \times 10^{11} \text{ molecules/sec}$$

where  $2.7 \times 10^{22}$  is the number of molecules of a gas in one litre at N.T.P.

Redhead (1970) has reported some experimental measurements of ionization and desorption cross-sections for some adsorbed gas systems in connection with the operation of ionization gauges, in which electrodes are bombarded by electrons with energies of approximately 200eV. The measurements show that the formation of one ion for every 50 neutral atoms or molecules desorbed, is typical. The ion energies range over about 10eV.

Taking the figures given above, we may calculate the brightness of ion source after acceleration to the emitter potential of 5kV. For an effective anode radius of 50mm, the brightness, B, is given by

$$B = \frac{(4.3 \times 10^{11}/50)}{\pi^2 \times (5 \times 10^{-2})^2} \times \frac{5 \times 10^3}{10}$$

$$= 1.7 \times 10^{14} \text{ ions/sec/m}^2/\text{sr.}$$

The maximum flux of ions, n, which can be concentrated into the area of the emitter tip, A, by an ideal focusing field is given by the conservation of brightness:

$$n = B A \Omega$$

where  $\Omega$  is the solid angle subtended at the emitter surface equal to  $2\pi$  sr. Thus for an emitter radius of 100nm

$$n = 1.7 \times 10^{14} \times \pi (1 \times 10^{-7})^2 \times 2\pi$$

whence  $n = 33$  ions/sec.

This estimate is in good agreement with the experimental results of Fig. 4.10 which suggest rates of about 5 ions/sec.

#### 4.5.2 Effects of Emitter Aging

An emitter was artificially aged in the FEM by drawing d.c. field emission for one half its estimated lifetime at 100  $\mu$ A, at

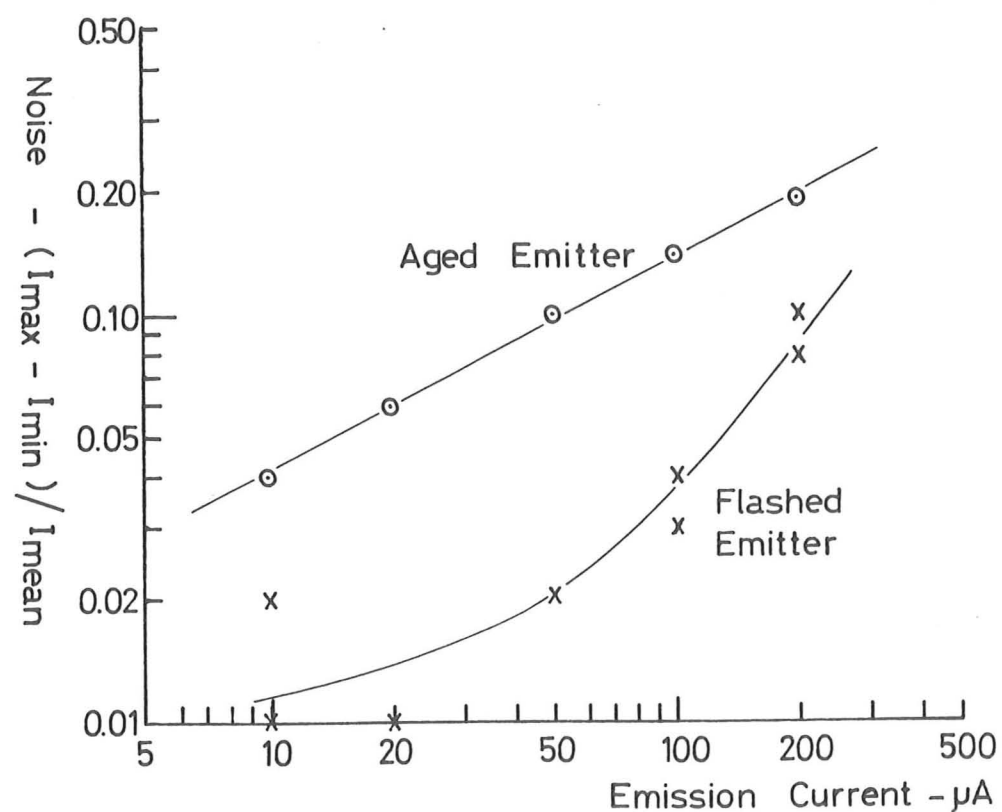


Fig 4.12 Effect of Emitter Age on Noise

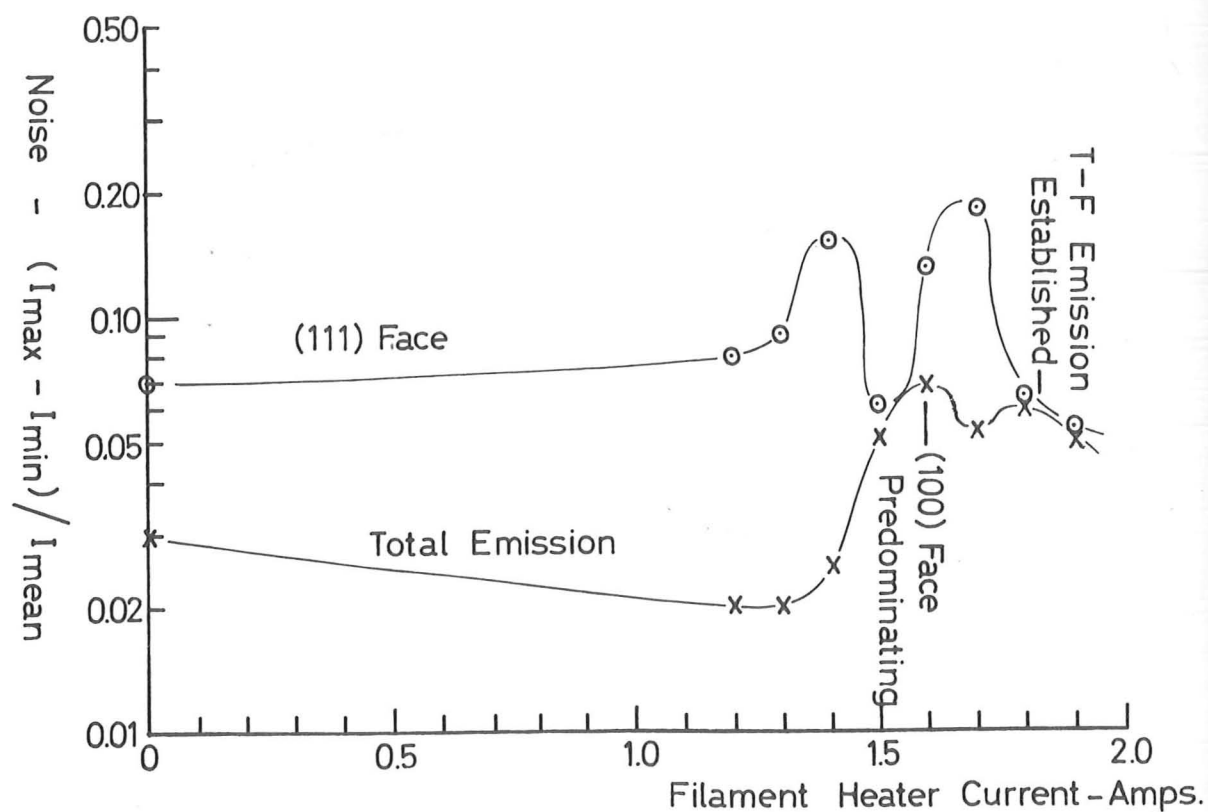


Fig 4.13 Noise Variation with Temperature

5kV, in a pressure of  $1.0 \times 10^{-9}$  torr. Results showing emission noise as a function of emission current at the same voltage and pressure are given in Fig. 4.12, both for the aged emitter and for the same emitter immediately after reflashing.

As may be seen the emission noise has increased by a factor of about four times with the aging process. It is surmized that as a result of cumulative damage, areas of the surface have become rough causing enhanced local fields. This leads not only to enhanced local emission but also to the increased probability of ion bombardment in these areas, the combined effects tending to increase the emission noise.

#### 4.5.3 Effects of Heating the Emitter

The plots shown in Fig. 4.13 are typical of noise variations with temperature for emission at  $100 \mu\text{A}$ , 5kV in a total pressure of  $1 \times 10^{-9}$  torr. In the figure both total emission, and emission from the (111) face only are considered.

It is not until the temperature approaches that necessary for T-F emission that significant changes occur. The rapid increase in noise on the total emission coincides with increased brightness of the (100) face due to adsorbed oxygen. At similar temperatures the (111) face exhibits sudden changes in noise level, which are almost certainly associated with residual gas desorption and emitter geometry changes with the onset of T-F emission.

It is characteristic of T-F emission that the noise levels are almost independent of operating pressure.

#### 4.5.4 Variations with Operating Pressure and Emission Current

Measurements of emission noise have been made over a wide range of operating pressures and emission currents. The results

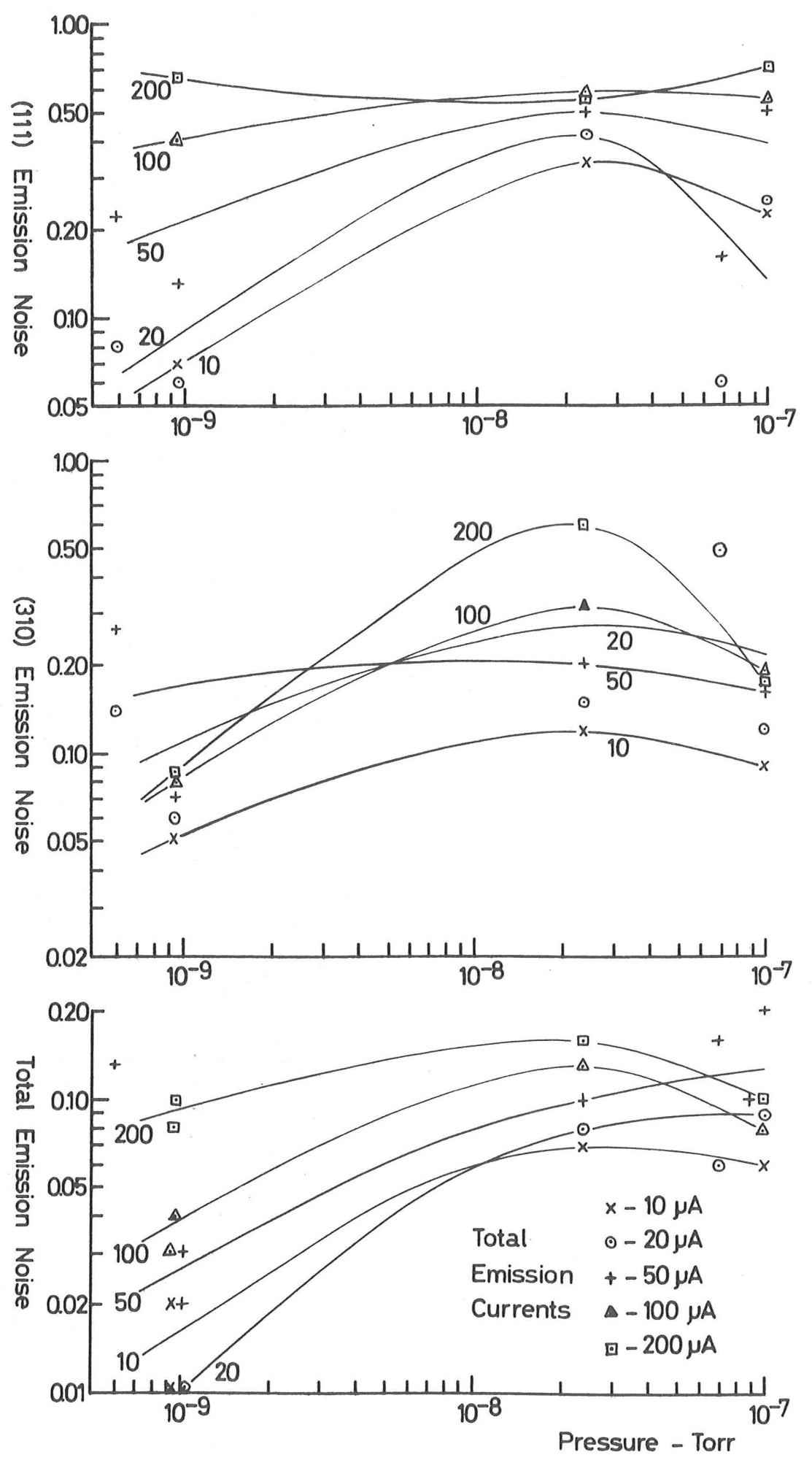


Fig 4.14 Variations of Emission Noise -  $(I_{max} - I_{min}) / I_{mean}$

are presented in Fig. 4.14 for total emission, and for emission from the (111) and (310) faces.

As may be expected with this type of experiment there is considerable variation between measurements taken in apparently similar conditions. As a result it is possible only to give an approximate value for the emission noise to be expected under given operating conditions.

For lowest noise operation in a microscope operating in good vacuum conditions ( $10^{-9}$  torr) the (310) orientation has lower noise levels than the (111) orientation. However, a peak-to-peak noise level of approximately 10% (4% rms) must be tolerated.

Generally, the noise increases with increasing operating pressure, though it does not appear that at very high pressures ( $10^{-7}$  torr) the noise reduces. This effect is almost certainly anomolous as the frequency of ion bombardment must increase with pressure, and would thus have been outside the bandwidth of the recorder.

4.6 Pulsed Emission

The pulse generator used is described in the previous chapter. Pulses of 1.0kV amplitude were applied to the control grid of the triode field emission gun.

Operation in the pulsed mode did not differ significantly from normal d.c. conditions. Pulses were applied to the grid and the positive bias increased until emission was established. Emission patterns were as obtained under d.c. operating conditions.

The output voltage swing of the pulse generator was unfortunately not quite large enough to take emitters from cut-off into high emission levels. For a duty cycle of 0.1, and mean

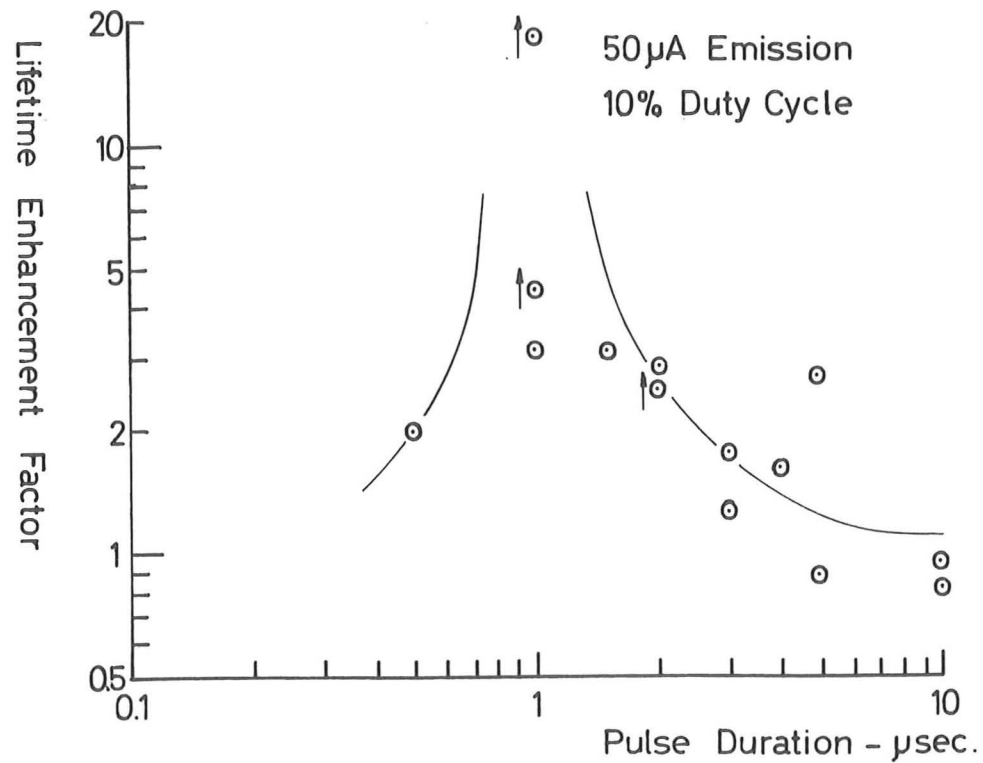


Fig 4.15 Effects of Pulsing on Emitter Lifetimes

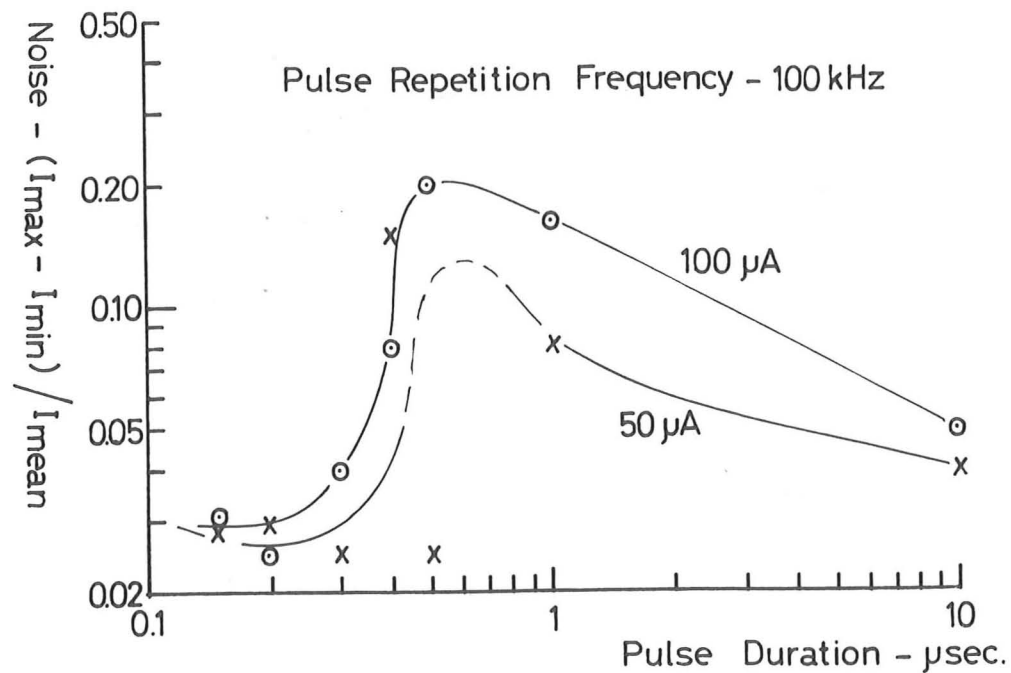


Fig 4.16 Noise Variations in Pulsed Mode

emission current of  $100 \mu\text{A}$ , there would be a d.c. standing emission current of approximately  $5 \mu\text{A}$ . Thus the  $1\text{kV}$  pulse would take the emission current from  $5 \mu\text{A}$  to  $1\text{mA}$ .

Peak current levels of an estimated  $10\text{mA}$  have been achieved for  $150\text{ns}$  duration pulses at  $100\text{kHz}$ , giving mean emission levels of  $200 \mu\text{A}$ , with a standing d.c. current of approximately  $50 \mu\text{A}$ .

#### 4.6.1 Lifetime of Pulsed Emitters

Experiments were normally performed in relatively poor vacuum in order to reduce the lifetime to more practical values, the pressure being controlled by leaking air into the system. As exact experimental conditions could not be reproduced from day to day, measurements of lifetime under d.c. operating conditions were made as a basis of comparison for the pulsed experiments.

To investigate the variation of lifetime with pulse width the mean emission current and overall accelerating voltage were kept constant at  $50 \mu\text{A}$  and  $5.0\text{kV}$  respectively. By keeping the duty cycle constant at  $0.1$  also, the possibility of effects due to emitter heating and variations in the on and off state electric fields was prevented.

For convenience, measured lifetimes are presented as a ratio of pulsed lifetime to d.c. lifetime at the same mean current. The results are plotted in Fig. 4.15, and it should be noted that in the case of experiments which had to be stopped for practical reasons, the lifetimes have been taken as the running times observed, and the points are marked with arrows.

It is clear that there is a significant effect for pulse durations in the region of  $1.0 \mu\text{sec}$ , though attempts to reproduce the conditions necessary to obtain greatly enhanced lifetimes were not always successful.

The most satisfactory explanation for the observed experimental phenomena involves a delicate balance of two factors:

1) Ion transit times from the anode, where they are generated, to the emitter are approximately 1  $\mu$ sec. Thus, operating with pulsed emission for 1  $\mu$ sec, and then considerably reducing the field at the emitter has the effect of defocusing the ions and so reducing the ion bombardment damage.

2) Ion decay times are approximately 10  $\mu$ sec - so that operation at repetition frequencies higher than 100kHz introduces the possibility of severe bombardment by ions generated during the previous pulse. Recovery times of hydrogen thyratrons, for example, are typically in the 10  $\mu$ sec range, and may be reduced by negatively biasing a suitable electrode to act as an ion collector. The grid of the FE triode would perform this function, and being highly negative could be expected to remove the much slower ions present in the system (up to mass 28) in the same order of time.

Experiments were conducted to test these hypotheses:

a) Operation with 1.0  $\mu$ sec pulses at 200kHz gave a lifetime ratio of 1.56 showing little enhancement of lifetime, thus supporting (2) above.

b) Pulses of 3.0  $\mu$ sec at 100kHz also gave a ratio of 1.56 which does not differ significantly from experimental results at 30kHz. This supports (1) above indicating that the repetition frequency has little effect when the pulse duration is greater than 1  $\mu$ sec.

Unfortunately, time was not available to pursue this investigation further. However, it is clear that a significant enhancement of emitter lifetime is possible by use of pulsed emission. Further experiments are necessary to establish more precisely the

required operating parameters.

#### 4.6.2 Noise and Stability of Pulsed Emission

Noise on pulsed emission shows a marked dependence on pulse duration. A series of experiments were performed at 5.0kV under good vacuum conditions of  $9 \times 10^{-10}$  torr. Emission noise was measured under pulsed operation at 100kHz and varying pulse durations. Results are plotted in Fig. 4.16, for mean current levels of 50 and 100  $\mu$ A.

There is a very significant change in the noise levels at pulse durations of about 400ns. For shorter pulses the noise is greatly reduced.

It was first thought that this effect might be due to resistive heating of the emitter under the very high peak current conditions. However, no sign of this effect was observed, either by directly viewing the emitter through the pyrometer telescope, or from changes in the emission pattern. If the mechanism for the noise reduction was due to heating of the emitter, this could only be brought about by the establishment of T-F operating conditions, when the emission pattern would have shown marked changes typical of T-F operation. However, no such changes to the emission pattern occurred.

It is most probable that the noise reduction corresponds to a reduction in level of ion bombardment of the emitter. This supports the explanations of lifetime enhancement for short pulses, and suggests that ion bombardment is substantially reduced for pulse durations of 300ns or less.

#### 4.7. Conclusions

The results obtained from the FEM have demonstrated its use

not only for developing and understanding the basic techniques of operating field emitters, but also as a versatile test bench for more fundamental experiments to examine the triode system, emission noise and emitter lifetime, and the effects of pulsing. The principle advantages of the instrument were derived from the ability both to operate in controlled UHV conditions and to see the emission pattern. All but very few of the experiments would have been impossible in the optical column.

Towards electron optical applications, techniques have been devised both for flashing emitters, and for establishing T-F emission directly from the current/voltage characteristics of emitters, without the need to first observe their emission patterns in the FEM. Also the triode gun geometry has been developed, allowing control of emission current and of operating voltage which are substantially independent.

Measurements of emitter lifetimes and emission noise have been made over a wide range of operating conditions, and may be used to predict these parameters in future designs of field emission guns. In particular Fig. 4.10 gives the expected lifetimes and Fig. 4.14 the noise levels.

From the results, two modes of operation appear promising from the point of view of long lifetimes and low levels of emission noise:

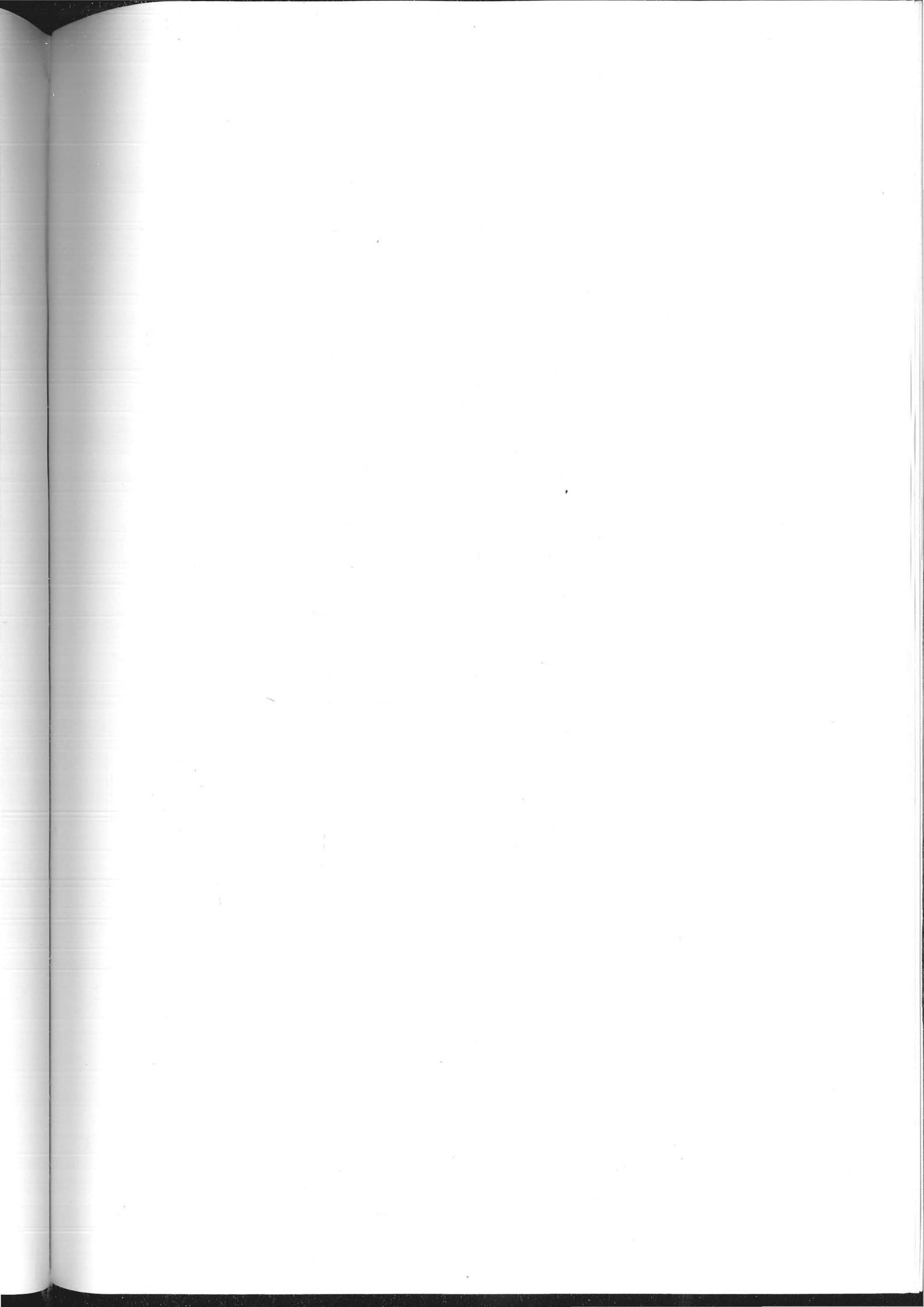
a) Cold field emission in a vacuum of  $10^{-9}$  torr, at up to about 20  $\mu$ A emission current. There is little relative advantage from either (111) or (310) orientations in this mode.

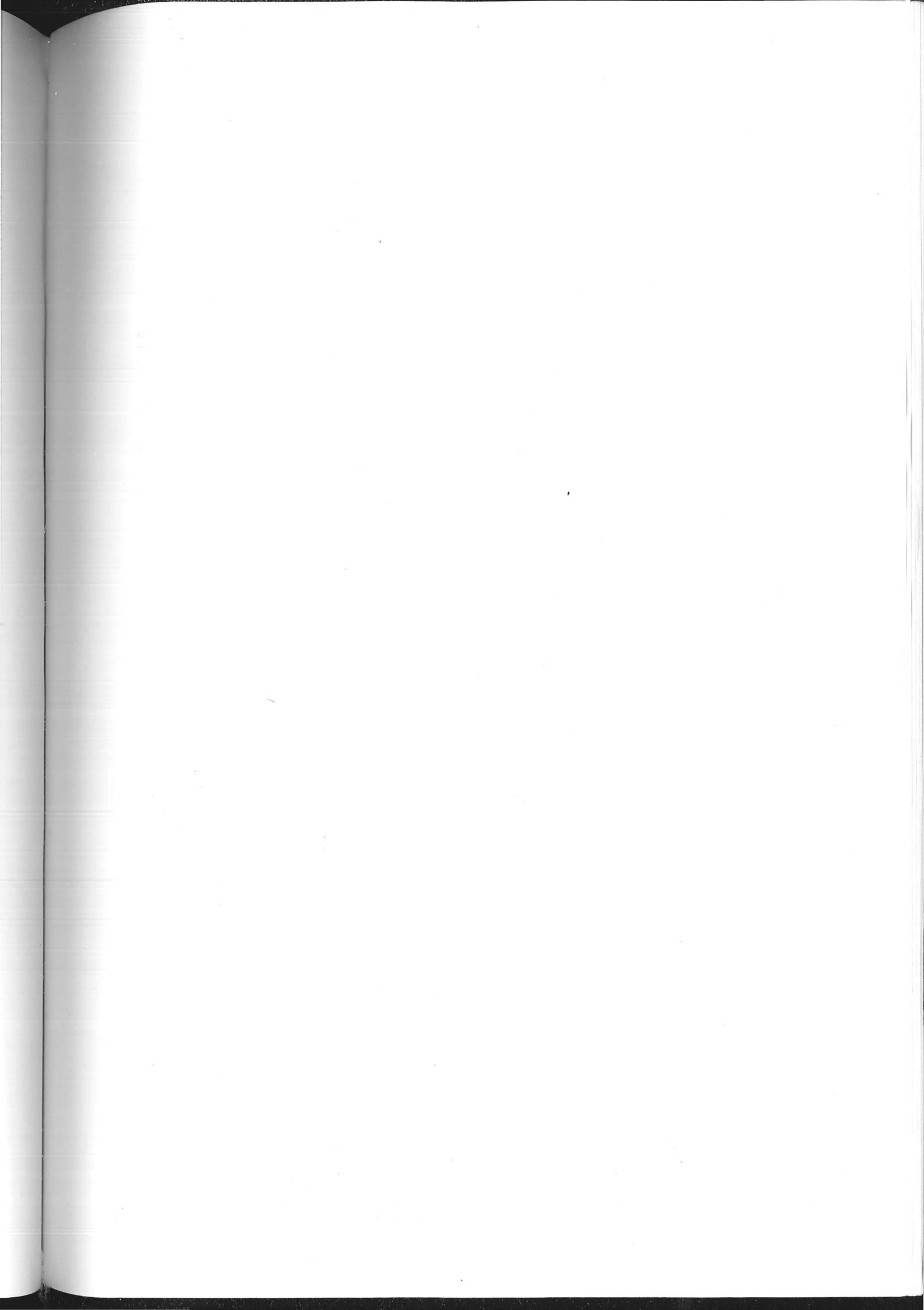
b) T-F emission in a vacuum of  $10^{-7}$  torr or better. Higher levels of emission current may be tolerated, however, only the (111) orientation is suitable.

The second mode of operation is important from the point of view of reducing the requirements of operating pressure necessary for stable emission.

A more fundamental aspect of the measurements of noise and lifetime is their relevance to the understanding of the mechanisms causing them. In particular, there is the rather surprising conclusion that the rate of ion bombardment is normally very low.

Experiments with pulsed emission in many ways complement the other results, with measurements of reduced emission noise and enhanced lifetimes under certain pulsed conditions. Unfortunately it was not possible to conduct a more detailed investigation of the pulsed emission mode of operation. It is clearly necessary to study further not only the effects of pulsing on noise and lifetime, but also to determine more precisely the conditions under which enhanced lifetimes and reduced noise occur.





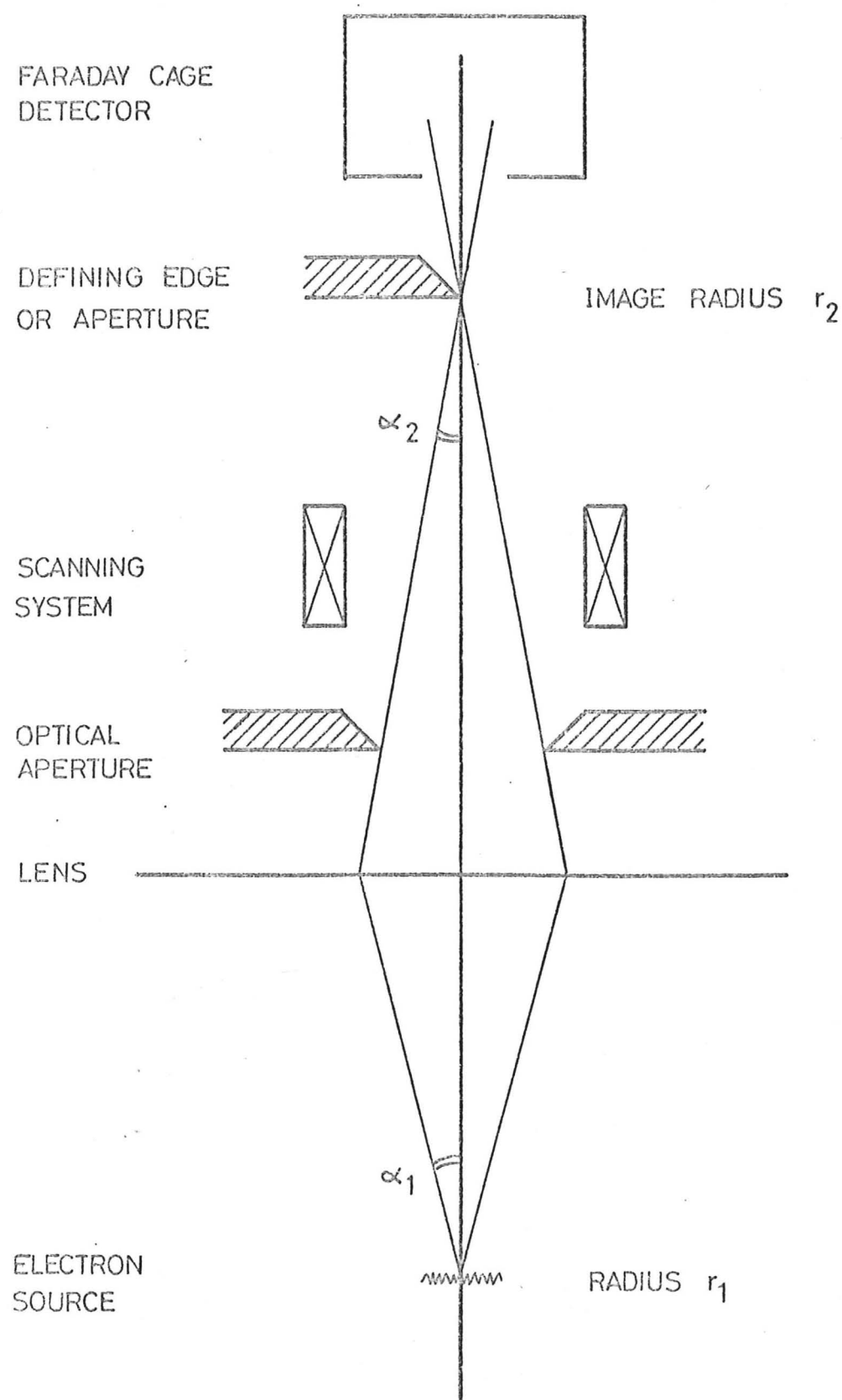


Fig 5.1 Electron Optical Column for the Measurement of Brightness

THE SCANNING ELECTRON OPTICAL COLUMN

5.1 General Concept

The basic requirement of this instrument was to provide the facilities for measuring the currents, diameters and brightnesses of electron probes, formed from field emission, and T-F electron sources.

The experimental method adopted was similar to that of Haine and Einstein (1952), and is illustrated schematically in Fig. 5.1. A lens system is used to image the electron source, and after passing through a defining aperture, the electron probe is scanned across a well defined edge to measure its diameter. Usually, the profile is displayed on an oscilloscope or chart recorder. Probe current is measured by collecting all of the beam in a Faraday cage, and hence the probe brightness may be calculated.

There are obvious similarities between these experimental requirements and the final stages of the scanning electron microscope, on which the design is based. Indeed, the SEM may be used to make brightness measurements, Smith (1956). A particular attraction of this design arises because of the small size of the field emission electron source, which permits operation of a single lens system as a high resolution SEM with little further modification.

5.2 Electron Optical Considerations

There are important differences in the use of the Haine and Einstein method with field emission, as compared with thermionic

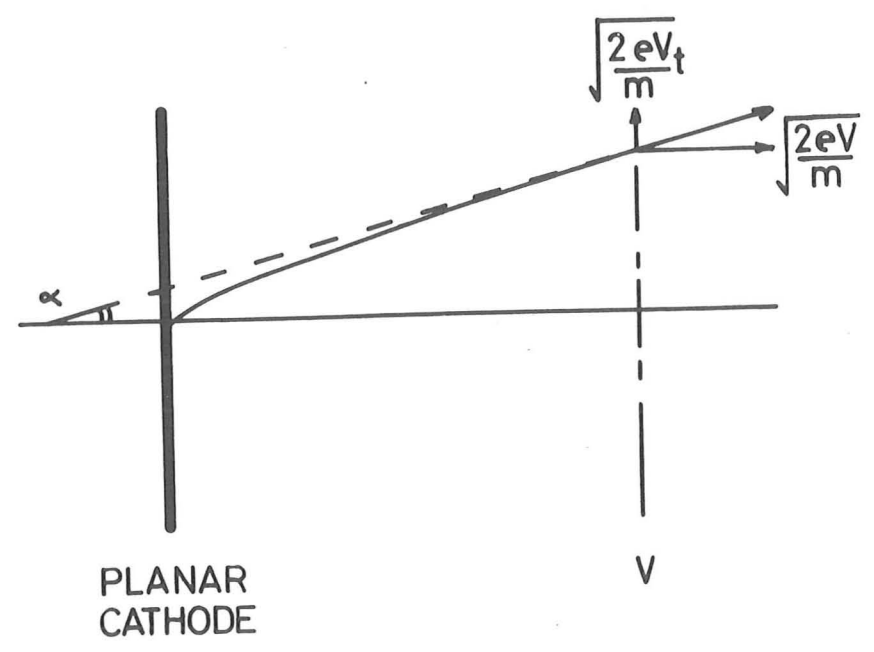


Fig 5.2 Planar Cathode

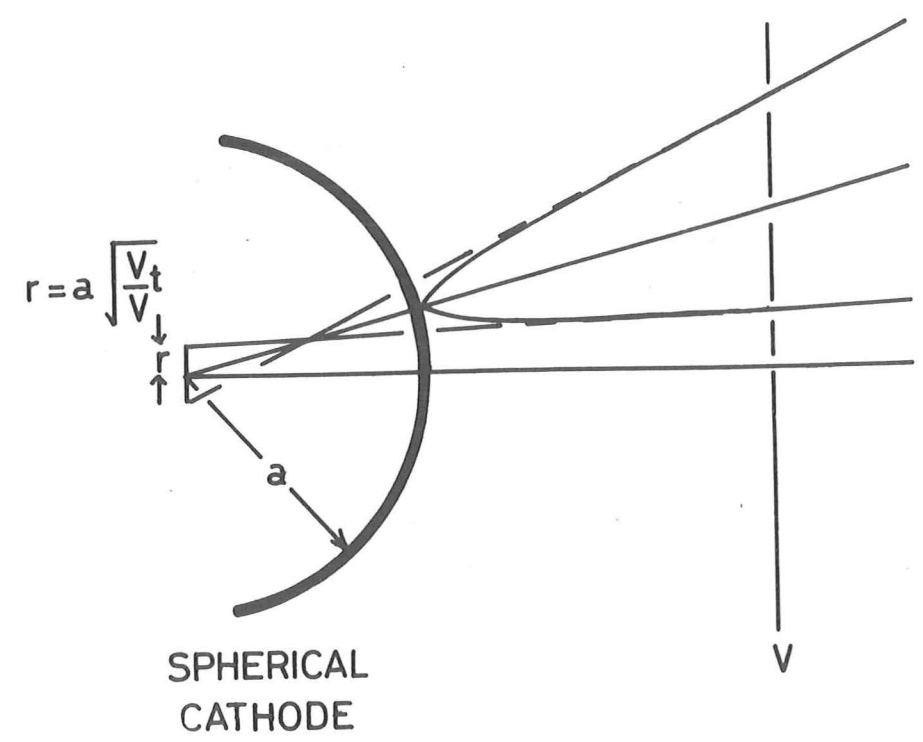


Fig 5.3 Spherical Cathode

cathodes. These arise from the size of electron source, which may be very small in the case of field emission.

5.2.1 The Conservation of Brightness

Consider the optical system of Fig. 5.1 to be free of aberrations. By simple geometrical optics, the magnification of the source  $M$ , is given by:

$$M = \frac{\alpha_1}{\alpha_2} = \frac{r_2}{r_1}$$

The brightness of the image,  $B_2$ , may be expressed as:

$$B_2 = \frac{I}{(\pi r_2^2 \pi \alpha_2^2)}$$

Where  $I$  is the current passing through the optical aperture.

Similarly, referring to the source:

$$B_1 = \frac{I}{(\pi r_1^2 \pi \alpha_1^2)}$$

Whence  $B_1 = B_2$ , the brightness is conserved, and the brightness of the probe is equal to that of the source.

In the presence of aberrations, however, the radius of the image  $r_2$  is increased,  $I$  and  $\alpha_2$  remaining constant. Thus the brightness is reduced.

5.2.2 Thermionic Emission Cathodes

In the case of thermionic emission, the cathode emits over a large area and may be regarded essentially as the planar cathode shown in Fig. 5.2. From the anode, at a potential  $V$  with respect to the cathode, the emission diverges with semiangle,  $\alpha$ , where:

$$\sin \alpha = \sqrt{\frac{V_t}{V}} \approx \alpha \quad \text{for small angles}$$

where  $eV_t$  is the transverse energy of the emitted electrons.

The brightness of an area of cathode,  $A$ , emitting with a current density,  $j_0$ , is therefore:

$$B = \frac{j_0 A}{\pi \alpha^2 A}$$

$$= \frac{j_0}{\pi} \frac{V}{V_t}$$

This places no restrictions on the area  $A$ . For thermionic emission from tungsten the emitting area will have radius of typically 50  $\mu\text{m}$ . Such a large source may readily be imaged with negligible aberrations and consequently no loss of brightness.

In the Haine and Einstein system, with a thermionic electron source, the magnetic lens contributes negligible aberrations and the full theoretical brightness may be achieved.

### 5.2.3 Field Emission Cathodes

The field emitter tip may be considered as a hemisphere of radius,  $a$ , as shown in Fig. 5.3.

For a region near to the axis, emission appears to come from a virtual source within the emitter tip of radius,  $r$ ,

$$\text{where } r = a \sqrt{\frac{V_t}{V}}$$

This expression is derived from an exact solution for electron trajectories between concentric spheres (Gomer (1961) and Everhart (1967)).

Emission current  $I$ , within a semiangle  $\alpha$ , is given by:

$$I = j_0 \pi \alpha^2 a^2$$

whence Brightness B

$$B = \frac{j_0 \pi \alpha^2 a^2}{\pi \alpha^2 \pi a^2 (\sqrt{V_t}/V)}$$

$$= \frac{j_0}{\pi} \frac{V}{\sqrt{V_t}}$$

In this case no limit has been imposed on  $\alpha$ . However, it is clear that  $\alpha$  will be limited by aberrations introduced in any practical imaging system.

It is illustrative to calculate a typical value for the virtual source radius,  $r$ . Taking  $a = 100\text{nm}$ ,  $V_t = 0.2$  volts, and  $V = 2\text{kV}$ .

$$\text{then } r = 100 \frac{0.2}{2000}$$

$$r = 1\text{nm}$$

Clearly, when imaging of such a source, aberrations in the lens will provide a large contribution to the final probe, and the theoretical brightness will not be approached.

#### 5.2.4 Single Lens Imaging of F.E. Sources

Problems associated with a single lens imaging system have been considered in more detail by Cosslett and Haine (1954). Following their method we assume that the probe diameter is determined by spherical aberration alone, with the image of the source making a negligibly small contribution.

Emission may be regarded as having an angular current density,  $i_c$ , then beam current,  $I$ , passing through the aperture is given by:

$$I = i_c \pi \alpha_1^2$$

using the notation of Fig. 5.1.

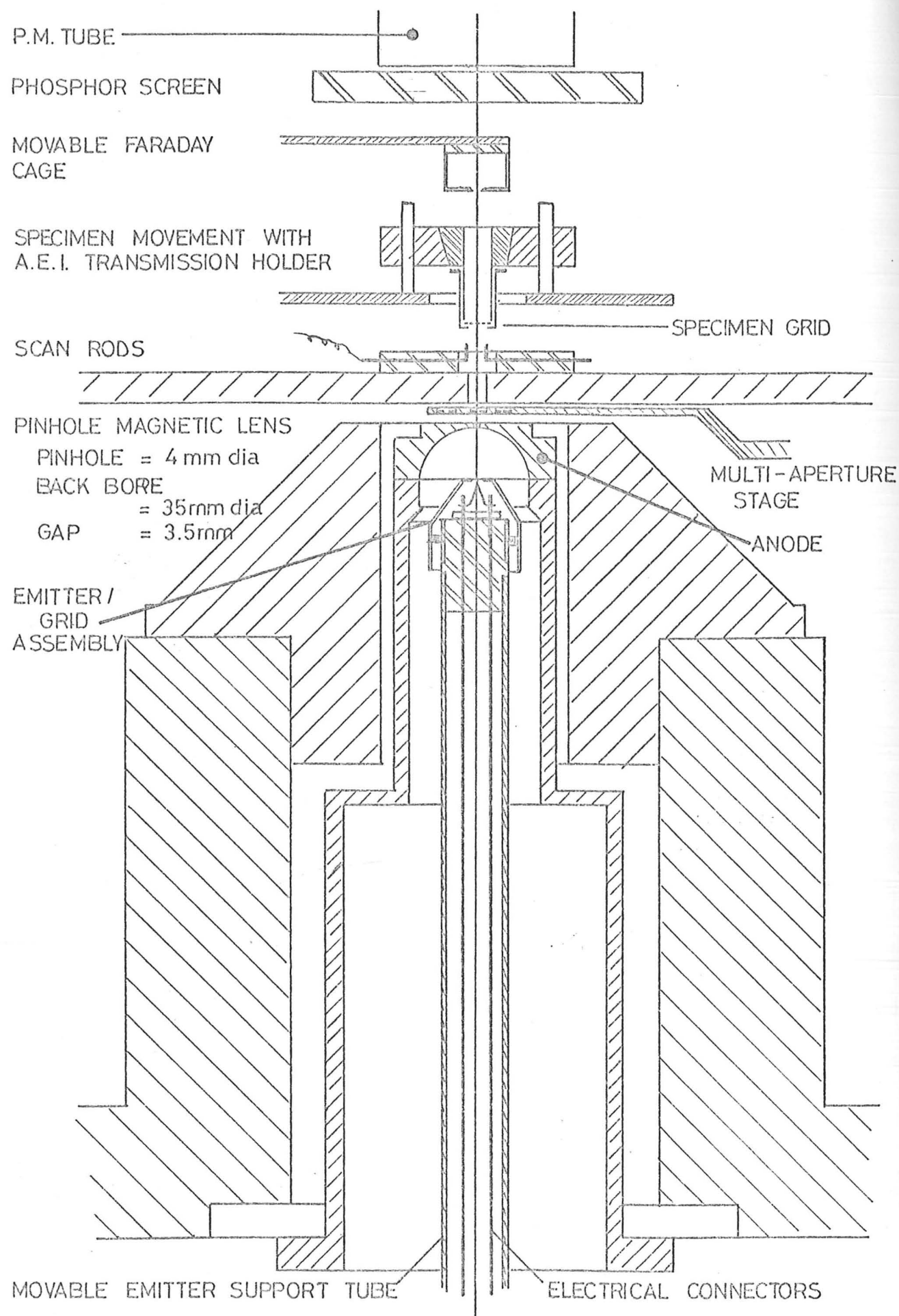


Fig 5.4 The Scanning Electron Optical Column.

As the source is imaged at the finite magnification,  $M$ , the minimum disc of confusion is taken as

$$r_s = \frac{1}{4} C_s (1 + M)^4 \alpha_2^3$$

following Cosslett and Haine (1954), and Der Shvartz (1967).

This expression is exact for thin, symmetrical lenses, and must be regarded as an approximation in this case.

Eliminating  $\alpha_1$ ,  $\alpha_2$ , and solving for  $I$  gives:

$$I = \pi i_c \frac{(4r_s)^{2/3}}{C_s} \frac{M^2}{(1 + M)^{8/3}}$$

This has a maximum value for  $M = 3$  when

$$I_{\max} = 0.56 \pi i_c \left(\frac{r_s}{C_s}\right)^{2/3}$$

From this equation, it is clear that for maximum current the magnification should have a value close to its optimum, and that  $C_s$  should be as small as possible. This requires a lens of short focal length. In order to approach optimum imaging conditions in practice, the emitter must be brought very close to the centre of the lens.

The design of the scanning electron optical column has therefore been based on the highly asymmetrical SEM objective lens. By positioning the emitter within the back bore of the lens near optimum imaging conditions have been achieved. A section through the SEOC column is shown in Fig. 5.4.

### 5.3 Mechanical Design of the SEOC

The idea that a useful practical field emission gun should be compatible with conventional, demountable vacuum systems has been expressed earlier. It was therefore decided to build the

SEOC along conventional lines using nickel plated mild steel, and rubber vacuum seals. At the same time reasonable care was taken in the design of the system to avoid unnecessary contamination.

By this construction it was possible to build the SEOC very economically. Further, the design of many of the components could be based directly on those used in the standard SEM of Oatley, Nixon and Pease (1965), and consequently will not be described here in great detail.

The electron gun was kept as a separate section of the column, which could be completely removed. As such, it was constructed to ultra high vacuum standards to permit differential pumping across the anode aperture. The electron gun is described in section 5.4.

#### 5.3.1 Vacuum System

Rough pumping was achieved by an oil rotary pump with an activated molecular sieve foreline trap, to prevent contamination of the system by back-streaming rotary pump oil.

The high vacuum pump used was a 600 l/s mercury diffusion pump to give clean vacuum, free of hydrocarbon contamination. It was fitted with a stainless steel, double liquid nitrogen trap with an anti-creep cooled surface which was built in the laboratories. This was designed to give a larger conductance than commercially available traps (1200 l/s), and long lasting nitrogen tanks (10 hours).

The main construction was built up on a large baseplate of mild steel, which had been bored out to accommodate the field emission gun and to provide pumping. The magnetic lens and a pumping tube were mounted to this and a second block of bored mild steel was mounted above to provide the specimen chamber pumping



Fig 5.5 Lens Aperture Stage



Fig 5.6 Scanning System

A robust mechanical system was thus achieved which had pumping speeds of approximately 100 l/s at both the specimen chamber and at the gun.

Vacuum seals were dry viton 'O' rings throughout, to give low outgassing rates and minimise hydrocarbon contamination. Movements were brought into the specimen chamber through sliding 'O' ring seals which were lightly greased to minimise the possibilities of leaks.

Pressures of  $2 \times 10^{-6}$  torr were readily achieved in the system after about 15 min pumping, and, after overnight pumping pressures of  $5 \times 10^{-7}$  torr were regularly obtained.

#### 5.3.2 The Magnetic Lens

The magnetic lens was based on the pinhole design of Pease (1963) which has been successfully used in this laboratory for the high resolution scanning microscopes.

An interesting feature of the new lens is the aperture stage. This was a modified Siemens unit and permitted rapid changing between three apertures. These could also be removed through the side of the lens directly, permitting easy replacement of dirty apertures without dismantling the lens. This is shown in Fig. 5.5, with the top pole piece removed.

The lens was supplied from a Hewlett - Packard constant current supply, which had measured ripple and noise on load of better than 1 part in  $10^5$ . It was capable of supplying a maximum current of 1.5 amps with the 1500 turn lens winding.

#### 5.3.3 Scanning System

With the field emission gun in the back bore of the lens, it was not possible to use a double deflection scanning system.

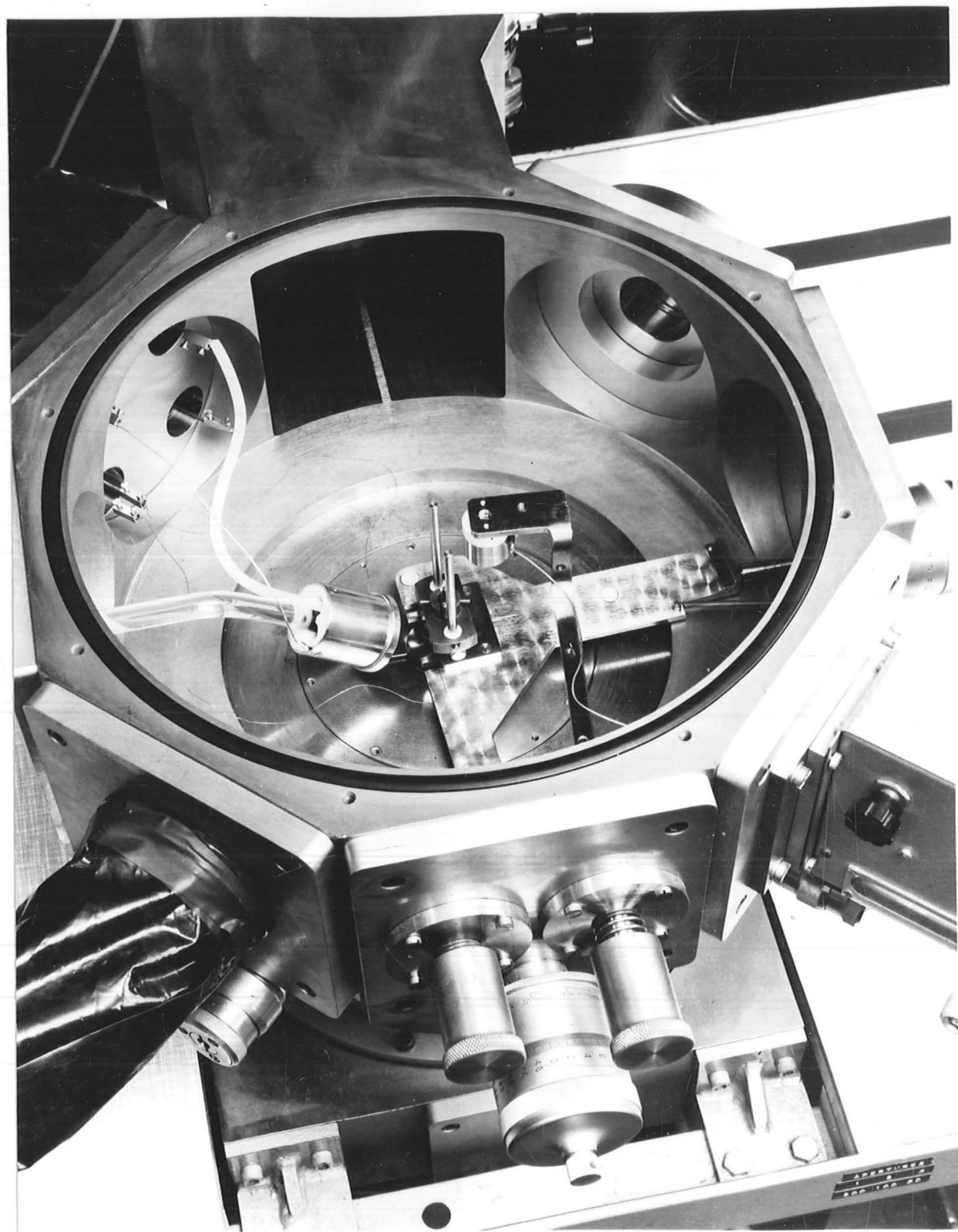


Fig 5.7 The Specimen Chamber

Thus it was necessary to scan after the lens and a short electrostatic system was devised which is shown in Fig. 5.6.

The electrodes consisted of four short rods, 2mm long and 1.5mm diameter, set parallel to the lens axis on a 4mm p.c.d. The rods were bent through  $90^\circ$  and clamped between two thin sheets of PTFE insulator. This was shielded with a copper cover to prevent charging, and this can be seen in the figure.

For convenience, one each of the X and Y scan electrodes was grounded, the remaining being driven positive and negative about earth potential.

#### 5.3.4 The Specimen Stage

A general view into the specimen chamber is shown in Fig. 5.7. The specimen table was supported on three PTFE feet which were free to slide over the top surface of the magnetic lens. It could be moved externally to two 2" micrometer heads, with sliding vacuum seals made directly onto the micrometer shaft. The shafts were fitted with hardened steel balls and the specimen table was kept in contact with these by two tension springs, one micrometer being located in a vertical 'V' slot, and the other thrusting against a flat surface.

An adaptor was made to take an AEI transmission microscope specimen holder which is also shown in Fig. 5.4. The adaptor could be adjusted to give a range of working distances. The specimen holder carried 3mm grids as used in normal transmission microscopy.

#### 5.3.5 Signal Detection

Three means of signal detection were provided, a transmission detector which was used in the probe measuring experiments, a conventional scintillator - lightpipe combination for normal SEM

operation, and a Faraday cage for measuring beam current.

a) Transmission detector. The most satisfactory arrangement was found to be a thin P11 phosphor screen settled onto lead glass, which was mounted in line with the lens axis on top of the specimen chamber lid.

By keeping the phosphor thin it was possible to see into the chamber, and to see the heated emitter for rough alignment. Preliminary alignment of the column was then achieved by observing the stationary transmission image on the screen.

In normal operation the photomultiplier was mounted over the screen, and screen intensity modulation was displayed as signal level. The arrangement is shown in Fig. 5.4.

b) Secondary electron detector. This was based on the normal SEM scintillator-lightpipe combination of Everhart and Thornley (1960). It differed slightly in that a glass scintillator, GS1, was used with a glasslight pipe, so that a mild bakeout of the vacuum system would have been possible if required. Following normal practice, the scintillator was housed in a cage which could be biased to discriminate between secondary and reflected primary electrons.

Electrical supply for the scintillator was provided by a Brandenburg Model 705 0-15kV unit. Vacuum leadthroughs were again of glass and metal construction and made for the apparatus by the laboratory glassblower.

The detector may be seen in Fig. 5.7, on the left hand side. The EHT lead was insulated with PTFE sleeving.

c) Faraday cage. The Faraday cage was mounted on a simple X - Y movement, so that it could normally be kept out of the way of the transmitted beam and, when required, aligned with the axis to measure the electron current. It was constructed of stainless

steel with PTFE insulation from the movement support arm.

The electrometer used was previously made in the laboratory to a design by Earnshaw (1960). The head amplifier was adapted to the vacuum system and, having its own vacuum leadthrough, was connected directly inside the chamber.

Both the head amplifier and the Faraday cage can be seen in Fig. 5.7.

### 5.3.6 Antivibration Mounting

It was appreciated from the outset that vibration problems in this apparatus would be more severe than in the conventional SEM, as imaging the source at a magnification of 2X requires that both emitter and specimen should not move relatively to the lens, or to each other.

However, with no knowledge of the likely magnitude of the problem, it was decided to take simple precautions initially, along the lines currently used in the SEM, which, in this laboratory was mounted on commercial, solid rubber mounts.

Preliminary measurements on a conventional SEM in the laboratory having two stages of antivibration mounting showed two principle sources of vibration.

a) Building resonance in the range 10 to 20Hz.

b) 50 and 100Hz vibrations associated with mains powered motors.

It was found that the first stage of isolation produced substantial attenuation of both sources, however, after the second stage, the building vibrations was usually worse, while the mains associated vibration was little affected.

It was concluded therefore, that a second stage of vibration isolation was undesirable. The apparatus was therefore mounted

on antivibration feet providing a single stage of isolation only. Mounts were chosen to give the lowest resonant frequency of 5Hz.

#### 5.4 The Field Emission Gun

The gun was designed as a separate unit which fitted to the column from beneath the lens. By this construction the vacuum system was separated from that of column providing for differential pumping. This feature was added towards the end of the research. Also, the complete gun with movements, etc. could be removed to effect repair or alteration. Additionally, the separate construction offered the possibility of fitting any new gun design, which might evolve from theoretical or experiment advances.

##### 5.4.1 Gun Electrodes

The field emission gun geometry is illustrated in Fig. 5.4, which also shows the relative position of the electrodes with respect to the magnetic lens.

The emitters were mounted in a socket, which was constructed so that they could simply be plugged in and were then rigidly held by their pins. Stainless steel connectors were mounted in a PTFE insulator, which was able to deform slightly to accommodate small variations of pin spacing or misalignment. This arrangement also gave direct electrical connections.

The anode was fabricated from OFHC copper, with an internal spherical surface of radius 10mm. This was the largest convenient size which could be contained within the lens bore, and so gave maximum vacuum pumping of the emitter region. Differential vacuum sealing between the gun and column pressures was effected by providing a good finish between the base of the anode and its mating face. Accurate axial positioning was achieved with a small spigot on the external diameter.

The size of the anode aperture was a compromise between a number of factors. It had to be large enough to permit easy alignment, and to minimise the effects on the beam of charging at its edges, also to be readily machined without burrs and cleaned when dirty. On the other hand, it had to be as small as possible to provide maximum isolation between the gun and column vacuum levels. A diameter of  $500\ \mu\text{m}$  was chosen, which was much larger than electron optical apertures required, and would still give adequate vacuum isolation.

For experiments using the triode gun, the control grid was fitted as shown in Fig. 5.4. Its geometry was very similar to the grid used in the FEM described in section 4.3, however, the space limitations in the SEOC led to slight modifications. Mechanical mounting was provided by clamping the grid to a fixed collar at the top of the support tube using three equispaced, radial grub screws through the base of the grid. This method of fixing permitted alignment of the grid with respect to the emitter tip, and made electrical connection.

Emitter, grid and anode could readily be removed for replacement or cleaning. Also grid and anode could be readily changed, so that different electrode geometries could be obtained if required.

Electrical leadthroughs into the vacuum system were made of glass/metal construction by the laboratory glassblower. External high voltage cable connections were made inside PTFE covers which can be seen in Fig. 5.8. Inside the vacuum, connection to the electrodes was made in two stages.

a) Flexible, self supporting, stainless steel wire from the leadthroughs to terminals mounted in PTFE at the base of the support tube.



Fig 5.8 Field Emission Gun Movements

b) Connection made between these terminals and the electrodes by copper wires fed through the centre of the supporting tube, and insulated with glass sleeving.

The design of electrical connections to the electrodes was limited by the confined space within the lens bore, and the need for an unimpaired emitter movement. The system developed was not capable therefore of very high voltage operation and breakdown was found to occur at about 10kV.

#### 5.4.2 Alignment Facilities

It was necessary to provide alignment facilities for both the anode aperture and the emitter relative to the magnetic lens.

The anode alignment was obtained very simply by providing a high compression (25%) on the gun 'O' ring seal to the column, and jacking the whole gun assembly on four screws from the base-plate. Anode alignment was not critical, and the slight movement necessary was readily achieved by this method.

Emitter alignment presented a more formidable design problem. The eventual solution is shown in Fig. 5.8. The design provides for external movement of the emitter in X, Y and Z directions, and also for limited tilt of the emitter about its tip for orientation of a high emission crystal face with the optical axis.

Motion was transmitted to the emitter by the rigid central support tube, the vacuum seal being effected by a stainless steel bellows, which was within the chamber.

Externally the support tube was attached rigidly to the outer of a pair of mating spherical surfaces. This was fabricated in brass and the inner in stainless steel, which gave good bearing properties when lightly greased, with little tendency to stick. The centre of the sphere was at the emitter tip so that movement

of the outer surface relative to the fixed inner could produce tilt of up to  $\pm 3^{\circ}$  in any direction at the tip. Movement was controlled by two small micrometers mounted orthogonally, with spring returns.

The inner spherical surface formed part of a double gimbal arrangement. Flexural pivots were used on the gimbal, these are spring hinges giving axial rotation which have the obvious advantages of zero play and backlash, with high loadbearing capacity. Tilt of the gimbals by two 2" micrometers produced transverse movements of the tip - X and Y.

Vertical movement (Z direction) was produced by sliding the gimbal supports on two parallel vertical rods. These were of hardened steel with hardened steel bushes. Two pairs of bushes were used to distribute the transverse loads, as the rods had to be slightly off centre. A 2" micrometer was used to produce the vertical movement, acting against the vacuum forces.

Although the movement presented difficult design problems, its performance was reasonably satisfactory. However, it had two particular faults which should be brought to the attention of anyone contemplating a similar device. Firstly, the gimbals gave very smooth X and Y movements but formed a relatively weak part of the structure, which led to vibration problems. This could be improved by increasing their bulk, nevertheless, the structure is relatively weak. Secondly, the Z movement tended to set when stationary and stick when next adjusted. This was, however, not too important in this application where a fine Z control was not needed.

#### 5.4.3 The Vacuum System

The gun was constructed mainly from stainless steel to UHV

standards, with crushed copper vacuum seals.

Initially, four ports between the gun and the column vacuum were used to provide pumping to the gun, but later these were blanked off and a separate pumping system was provided based on an orbital electrostatic getter ion pump (see, for example, Maliakal et al. (1964)). A prototype commercial pump was used which was supplied by A.R.E.L.<sup>+</sup>, with a rated pumping speed of 80 l/s for air. This type of pump has the advantages of light weight and freedom from magnetic fields.

In the differential pumping mode the gun was rough pumped through a 1" metal valve which could be connected into the main column vacuum system through a short length of 1" diameter plastic hose, to give a gun pressure better than  $1 \times 10^{-4}$  torr. To start the orbitron pump it was baked with a 400 watt heater tape at about 200°C for 2 hours into the roughing line. The pump was then run hot for about 10 mins to outgas the anode, and pumping action would start as cooling water was supplied to the pump.

A number of difficulties were encountered with the operation of the pump, particularly in respect of its starting characteristics, however, the method described above was almost always successful.

With a 500  $\mu$ m diameter anode aperture and a column pressure of  $1 \times 10^{-6}$  torr the theoretical ultimate pressure in the gun chamber is  $4 \times 10^{-10}$  torr. Due to restrictions of pumping to the emitter region the estimated speed is only 13 l/s, which gives a theoretical ultimate pressure of  $2.5 \times 10^{-9}$  torr.

---

+ Applied Research and Engineering Ltd., Parsons Estate, Washington, Co. Durham.

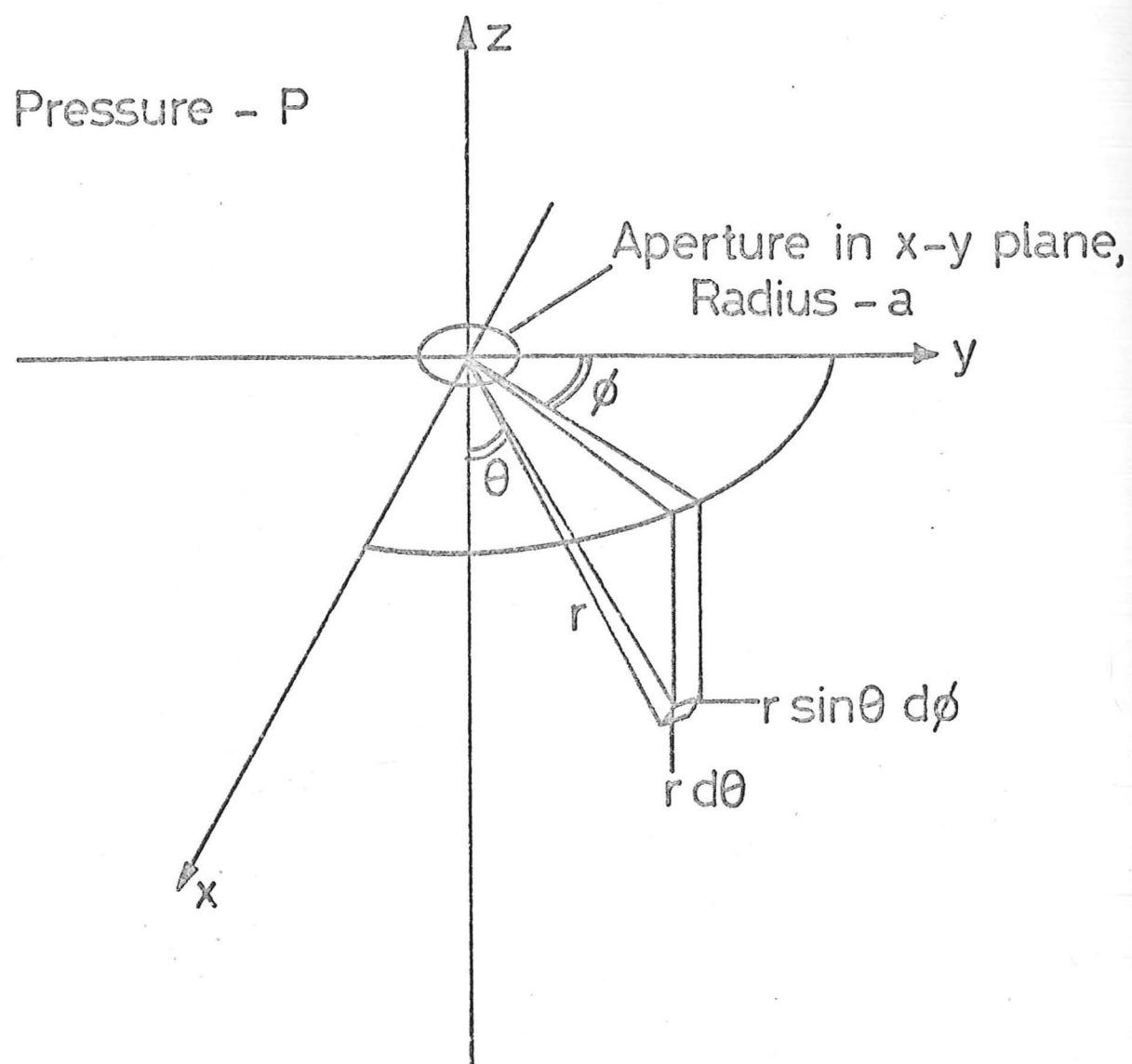


Fig 5.9

In practice, the system was not baked, and the best gun pressure recorded on a nude Bayard-Alpert gauge was  $2 \times 10^{-9}$  torr, after prolonged pumping.

Normal calculations of equilibrium pressure under differential pumping conditions do not take into account the effects of molecules streaming directly through the aperture to points in its vicinity. This is particularly important in the case of a field emitter where molecular bombardment will affect the emitter operation. It is possible to make an estimate of the magnitude of this effect.

Referring to the diagram of Fig. 5.9, gas molecules in the high pressure region, P, above the aperture, will have equal probabilities for motion in all directions. Suppose  $N\pi a^2$  molecules/sec pass through the aperture, radius a, then the probability distribution of emerging molecules will exhibit a cosine  $\theta$  variation. Since the mean free path is larger than the distances involved, the probability will fall as  $1/r^2$  for  $r \gg a$ .

Thus, the number of molecules passing through unit area normal to the direction  $(\theta, \phi)$  below the aperture will be  $n(r, \theta, \phi)$ .

$$\text{where } n(r, \theta, \phi) = K N \pi a^2 \cos \theta / r^2$$

K is a constant such that the total number of molecules/sec is equal to  $N\pi a^2$

$$\text{i.e. } \int_0^{2\pi} \int_0^{\pi/2} n(r, \theta, \phi) r \sin \theta d\phi r d\theta = N\pi a^2$$

$$\text{whence } K = 1/\pi$$

$$\text{and } n(r, \theta, \phi) = N a^2 \frac{\cos \theta}{r^2}$$

Let us assign to each molecule a mean energy such that normal

impingement would give a contribution to the pressure of  $\Delta P$ . Then above the aperture we consider the  $N\pi a^2$  molecules/sec passing through a hemisphere of radius  $r$ , heading towards the aperture, the contributions to the total pressure must add up to  $P$ .

$$\text{Thus } \frac{1}{\pi a^2} \int_0^{2\pi} \int_0^{\pi/2} n(r, \theta, \phi) r \sin \theta \, d\phi \, \Delta P \cos \theta r d\theta = P$$

$$\text{Hence } P = \frac{2N}{3} \Delta P$$

Similarly, if  $n(r, \theta, \phi)$  molecules/sec/unit area were to impinge on a surface randomly, then they would be associated with a background pressure  $P'$ , where

$$P' = \frac{2}{3} n(r, \theta, \phi) P$$

$$\text{Hence } P' = P \frac{a^2}{r^2} \cos \theta$$

Experimental values for the field emission gun are

$$P = 1 \times 10^{-6} \text{ torr, } a = 250 \text{ } \mu\text{m, } r = 10 \text{ mm, and } \theta = 0, \text{ giving}$$

$$P' = 6 \times 10^{-10} \text{ torr}$$

Thus the emitter tip is subjected to bombardment by molecules passing directly through the aperture, equivalent to an additional background pressure of  $6 \times 10^{-10}$  torr. As the total pressure in the differentially pumped gun was typically  $10^{-8}$  torr, the effects of direct molecular streaming through the aperture may be safely ignored.

### 5.5 Electronics for the Probe Measuring System

In the first instance, two scan amplifiers were built to provide suitable drives to the column deflection system, using the ramp outputs from two oscilloscope time bases. The units

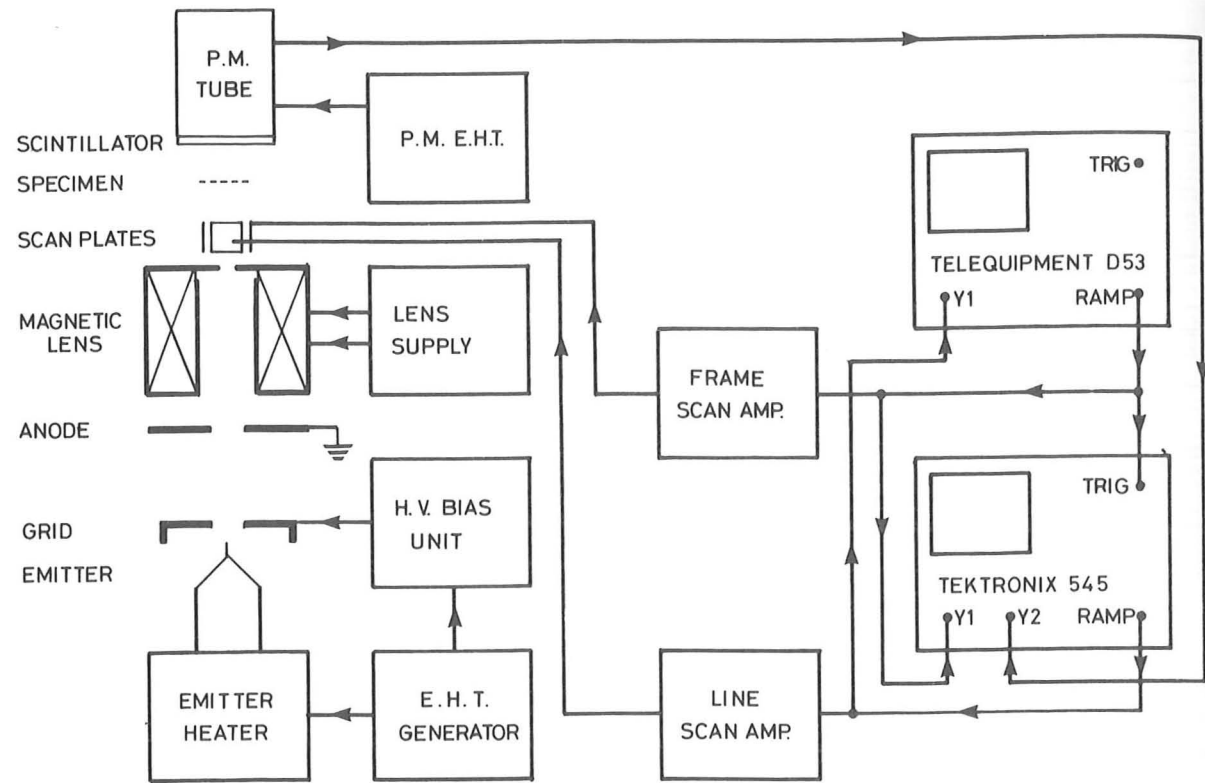
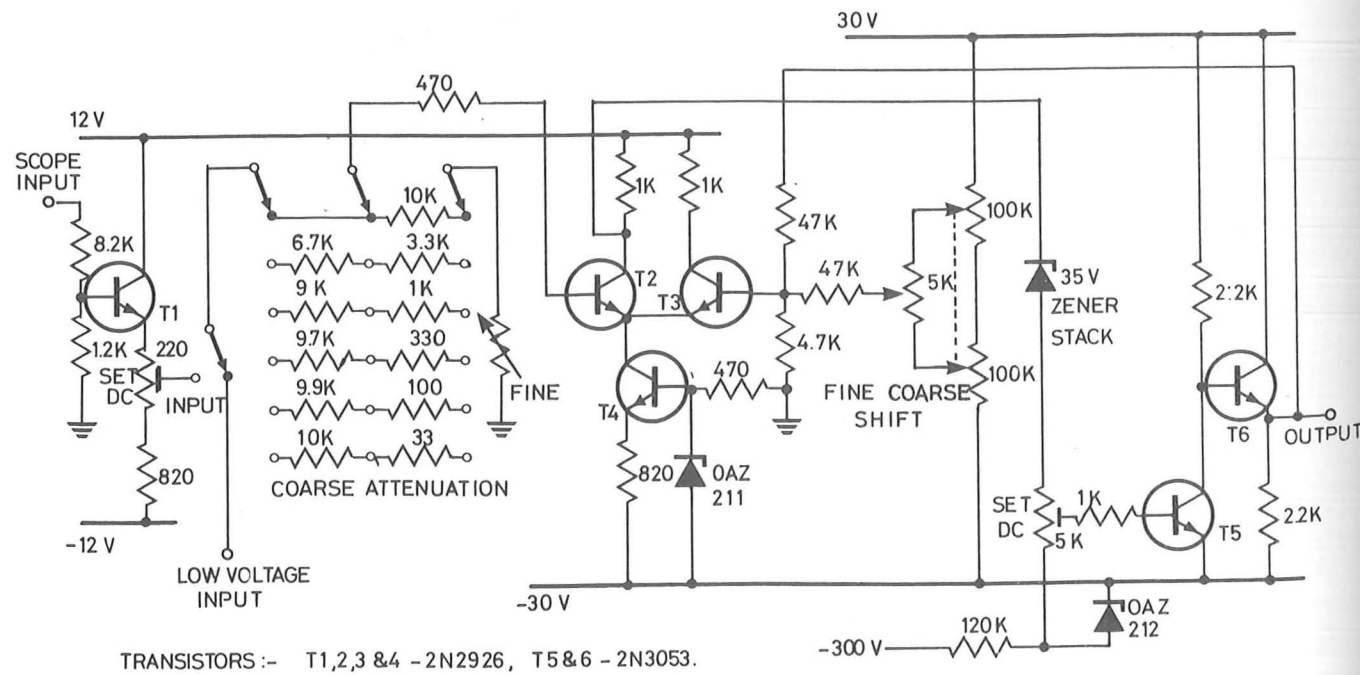


Fig 5.10 Probe Measuring System



TRANSISTORS :- T1,2,3 &4 - 2N2926, T5 &6 - 2N3053.

Fig 5.11 Scan Amplifiers

available were a Telequipment D53 and a Tektronix 545 with a type 1A1 vertical amplifier.

The system used is shown in the block diagram of Fig. 5.10. The Tektronix had the useful facility to add two input waveforms, and was therefore very suitable for use as the line generator, with the Telequipment used as frame generator on a slower scan speed.

With the interconnections shown, the frame generator was set to free run, and the line generator set to trigger from the frame output. Thus the system generated a continuous sequence of rasters on both displays. By adding the video signal from the PM tube to the frame scan within the Tektronix, a picture was displayed with vertical modulation. This mode of operation corresponds to Y modulation display of the conventional SEM (Everhart (1966), Chang and Nixon (1968)). Also, by triggering the frame generator for single shot, a single complete raster of Y modulated picture was produced.

By removing the trigger to the frame generator, and setting the line generator to free run, a continuous repetitive line scan over the same specimen feature was produced. Under these conditions measurements of probe diameters by scanning over a sharp edge were made.

The photomultiplier circuit, EHT generator, and bias unit have been discussed in Chapter 3 in connection with their applications with the PEM. It remains to discuss the operation of the scan amplifiers.

5.5.1 The Scan Amplifiers

Both oscilloscopes had high impedance, d.c. coupled positive going ramp outputs starting from ground potential. In the case

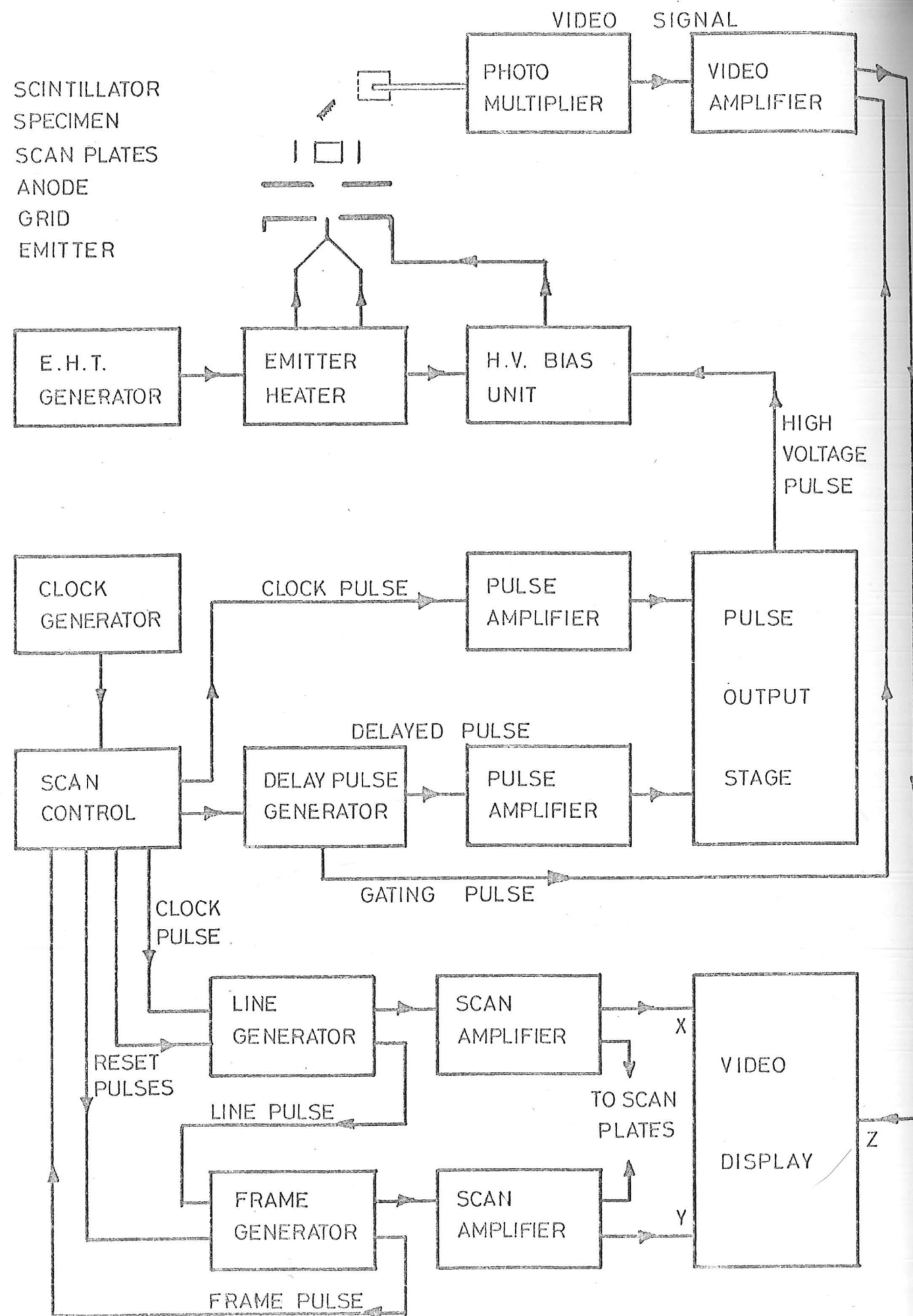


Fig 5.12 Block Diagram of S.E.M. Electronics Systems

of the Telequipment D53 this was 0 - 40 volts, and the Tektronix 545 was 0 - 90 volts. The scan amplifier was designed to take these inputs, and to provide an output about ground potential. An additional input was provided to take a low voltage ramp about ground potential from transistorized generators.

The circuit is shown in Fig. 5.11. High voltage scope inputs are first attenuated and subsequent drives taken from the emitter follower buffer stage, T1, which also provides d.c. back-off to give the attenuated ramp about earth potential. Either this input or an alternative low voltage ramp is selected and fed through a switchable, calibrated attenuator to the operational amplifier, formed from the long-tailed pair T2, T3 fed from current source T4, with output amplifier T5 and emitter follower buffer stage T6. For electrical alignment of the electron beam d.c. offset facilities are provided. The output stage, T6, has low impedance to permit high scan rates, and is capable of scan amplitudes up to the  $\pm 30$  volt lines. No detectable departure from linearity was observed for ramps of 10  $\mu$ sec or longer duration under full load, which gives a capability in excess of normal TV line rates.

### 5.6 Electronics for SEM Operation

By the addition of scan generators, scan control, and a video amplifier, the units described above and in Chapter 3 may be used to form a self contained SEM, with normal intensity or Z modulation of the picture, and full compatibility with pulsed operation. A block diagram of the system is shown in Fig. 5.12, which illustrates the interconnection of the units described. For convenience an oscilloscope was used for the video display.

The line and fram generators were based on a circuit used by

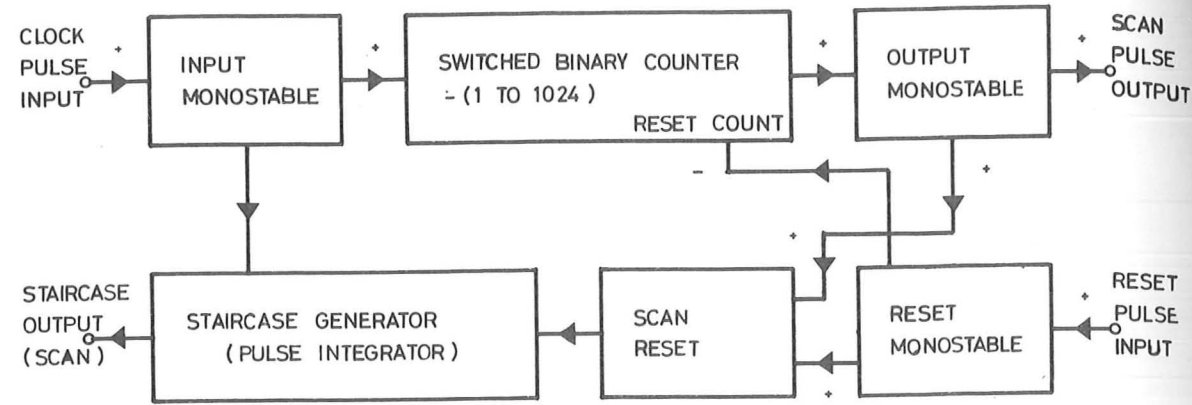
Tillett (1969), which produced staircase waveforms by integrating input pulses. This technique has obvious advantages, as it gives direct compatibility with the pulsed emission mode of operation.

The block diagram shown in Fig. 5.12 is a system which will operate on the basis of one emission pulse per picture point. It may readily be operated with d.c. emission, by simply removing the pulse amplifiers and high voltage pulser from the circuit. A remaining possible mode of operation would use one pulse per line, which may be achieved by exchanging the line generator for the scope time base as in Fig. 5.10, but retaining the frame generator. Similarly, operation with one pulse per frame is obtained by replacing both generators by scope time bases. In all modes the timing would be controlled directly by the clock generator, and the scan control would provide single frame facilities.

#### 5.6.1. Line and Frame Generators

The circuit developed by Tillett (1969) works on the basis of a diode pump into a storage capacitor. The voltage on the capacitor is followed by an FET to give the staircase output. This circuit is relatively slow, and in order to operate at higher speeds (1 pulse/ $\mu$ sec) the storage capacitor must be reduced. Unfortunately, the decay time of the capacitor due to circuit leakage is similarly reduced, but this may be countered by sampling the voltage with an MOST device, and improving the reset circuitry.

The final form of the generators is shown in Fig. 5.13, both in the form of a block diagram and as each circuit unit to avoid unnecessary repetition. The block diagram illustrates the circuit principles. Input pulses are first shaped and then fed to a ring counter, switchable over the range 1 to  $2^{12}$  (1024), and



reset externally. The staircase generator takes input pulses and integrates them to produce the staircase waveform which is reset either externally or by the counter output. By altering the magnitude of the pulses fed to the integrator as the number of steps in the staircase is changed on the switchable counter, the output is arranged to be from -5 volts to +5 volts in all positions.

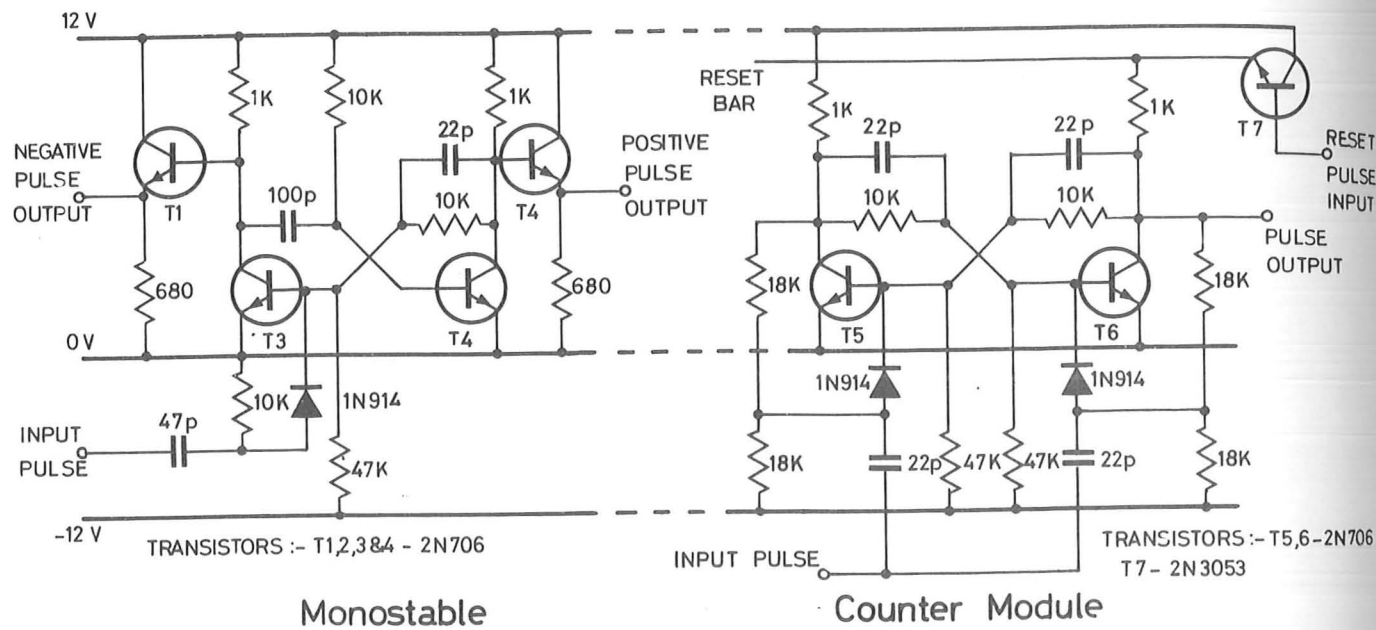
Four elements in the staircase generator are critical, these are the MOST, the storage capacitor and the diodes, which must be all chosen carefully for low leakage characteristics. The capacitor value is 1000 pF to give fast response with tolerable drive impedances. The exponential decay time of the combined circuit elements is typically 20 minutes, as measured for the completed circuit.

By using the counting technique to set the number of pulses in the staircase, the operation of the circuit is controlled directly by the clock generator. The number of steps being used to determine the resolution of the video display only. Thus, the waveform is always synchronized, and is compatible with operation in any of the modes described above.

5.6.2 Scan Control

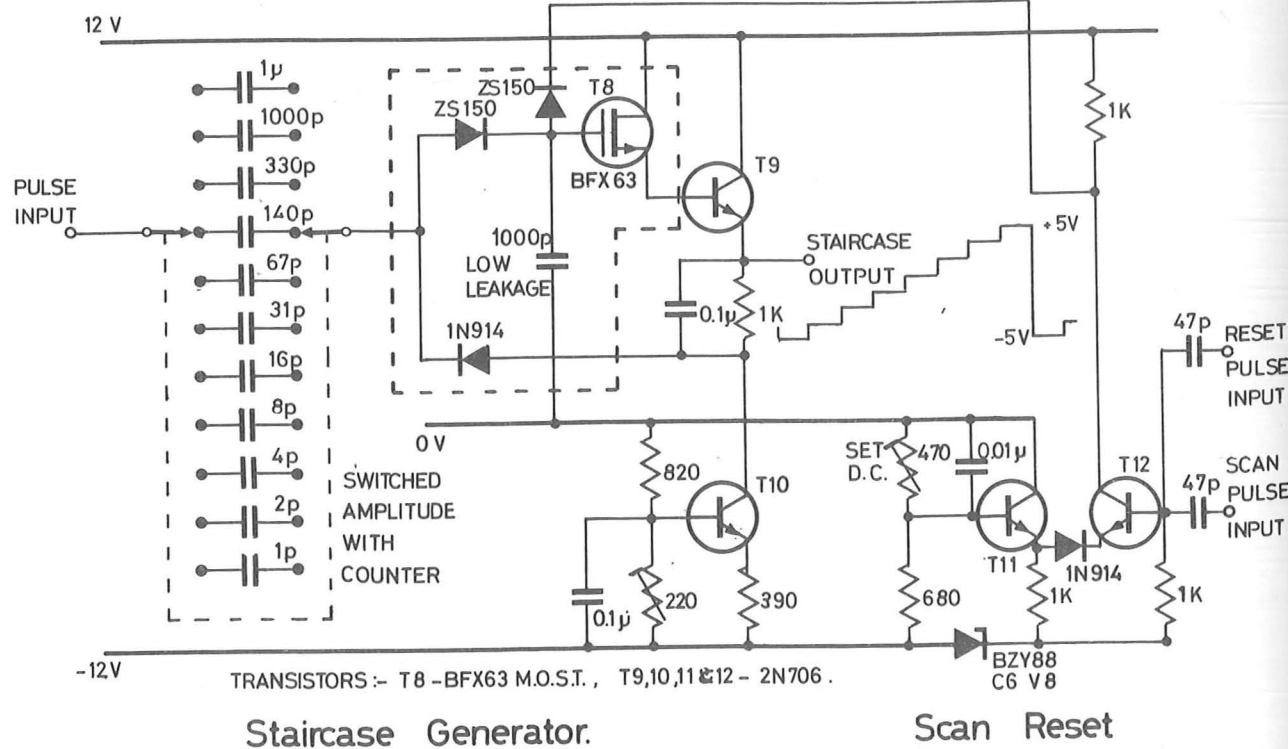
The scan control unit provides normal SEM single frame and continuous running facilities. Its inter-connections are given in Fig. 5.12.

The circuit of the unit is shown in Fig. 5.14. It either permits continuous operation by transmitting the clock pulses directly, or in the single frame mode, will transmit pulses only when externally initiated, and then only until receiving the frame pulse. A simple bistable T5, T6, is used as memory element



Monostable

Counter Module



Staircase Generator.

Scan Reset

Fig 5.13 Scan Generators

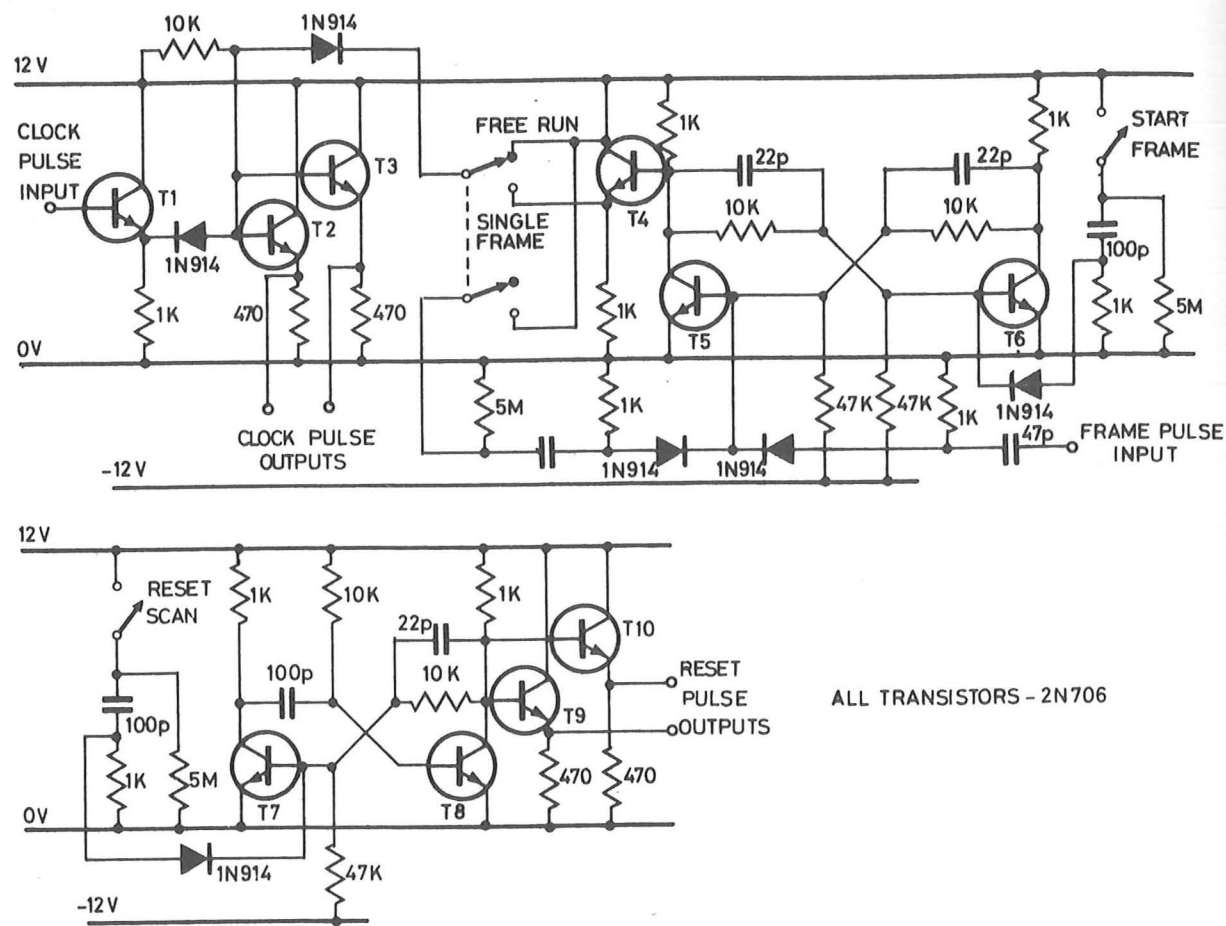


Fig 5.14 Scan Control

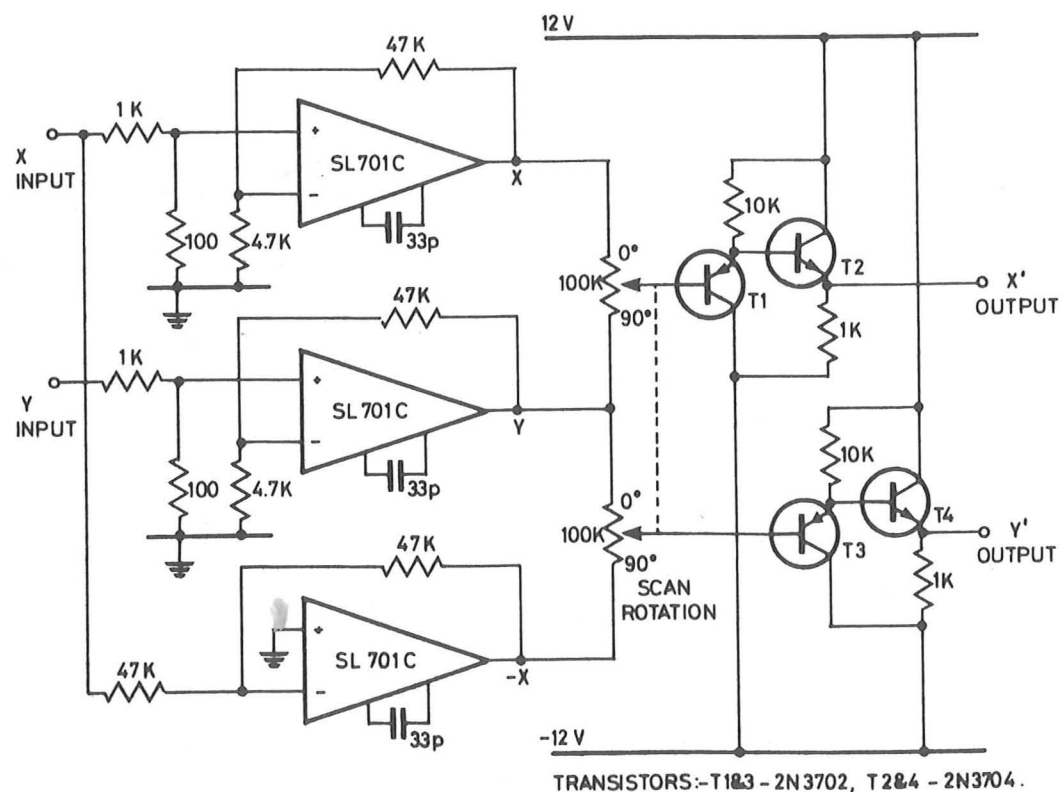


Fig 5.15 Scan Rotation

and the train of pulses is controlled by a simple diode gate, operated by the output of the bistable through the emitter follower T4.

Additionally, the unit provides reset pulses to act on the scan generator counters and ramp output, ready for the start of a single frame.

In the case of operation with one pulse per line described earlier, the clock outputs would be used to trigger the scope time bases, and the reset would set the frame generator only. For one pulse per frame, the clock pulse would trigger the scope frame generator as in Fig. 5.10, and the reset facility would be unnecessary.

5.6.3 Scan Rotation

For the particular application of probe diameter measurements, scan rotation was considered to be highly desirable. It would, in addition, provide a useful SEM facility.

Inter-connections with other units have not been included in Fig. 5.12 to avoid unnecessary complications, it is connected between the scan generators and scan amplifiers to provide rotation of the column scan raster only.

The circuit is shown in Fig. 5.15. It uses three low priced integrated circuit operational amplifiers to generate X, Y and -X, from the incoming signals. These are combined in twin ganged linear potentiometers to produce new scan waveforms X' and Y'.

$$X' = Y + (1-\alpha)X$$

$$Y' = -X + (1-\alpha)Y$$

where  $\alpha$  is the fractional rotation of the potentiometer.

The new scan directions are always orthogonal. However, the

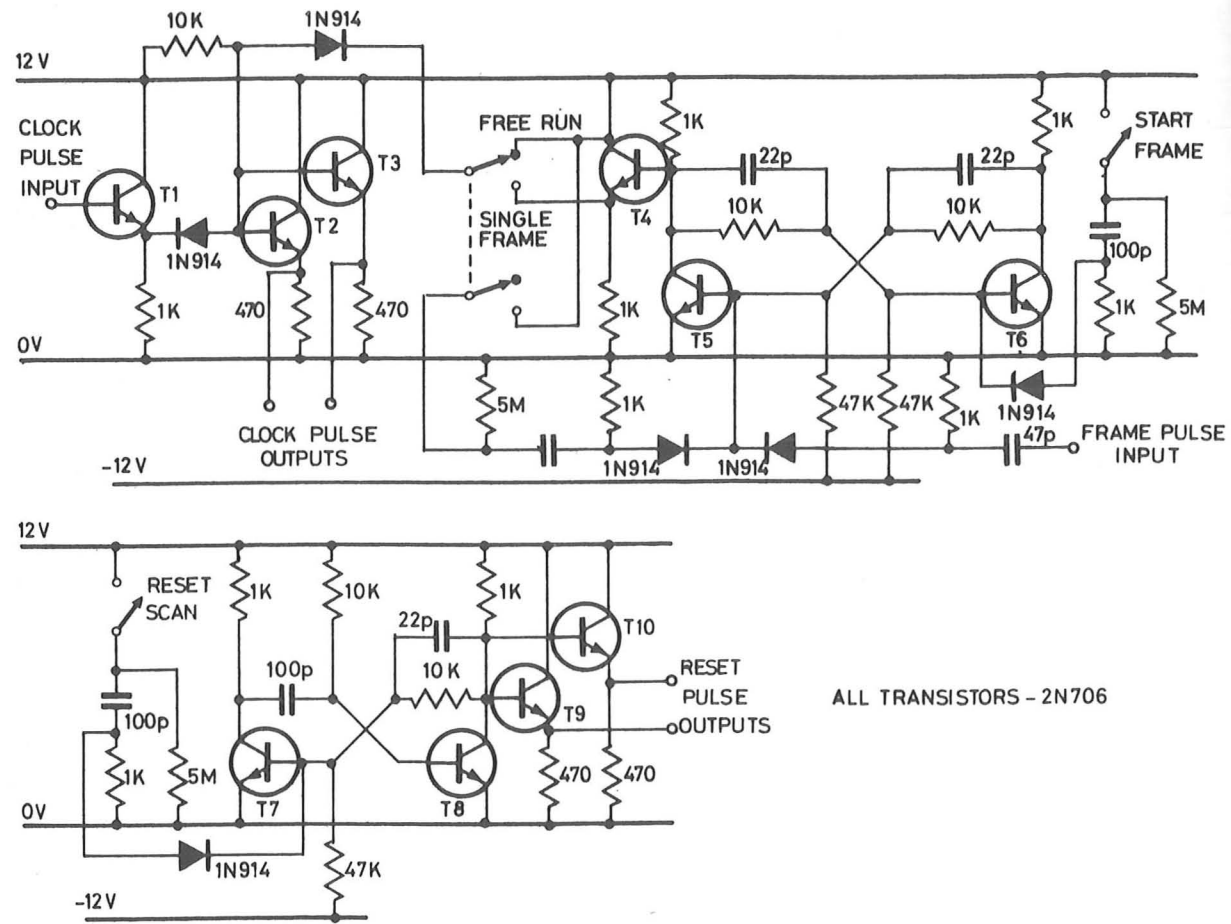


Fig 5.14 Scan Control

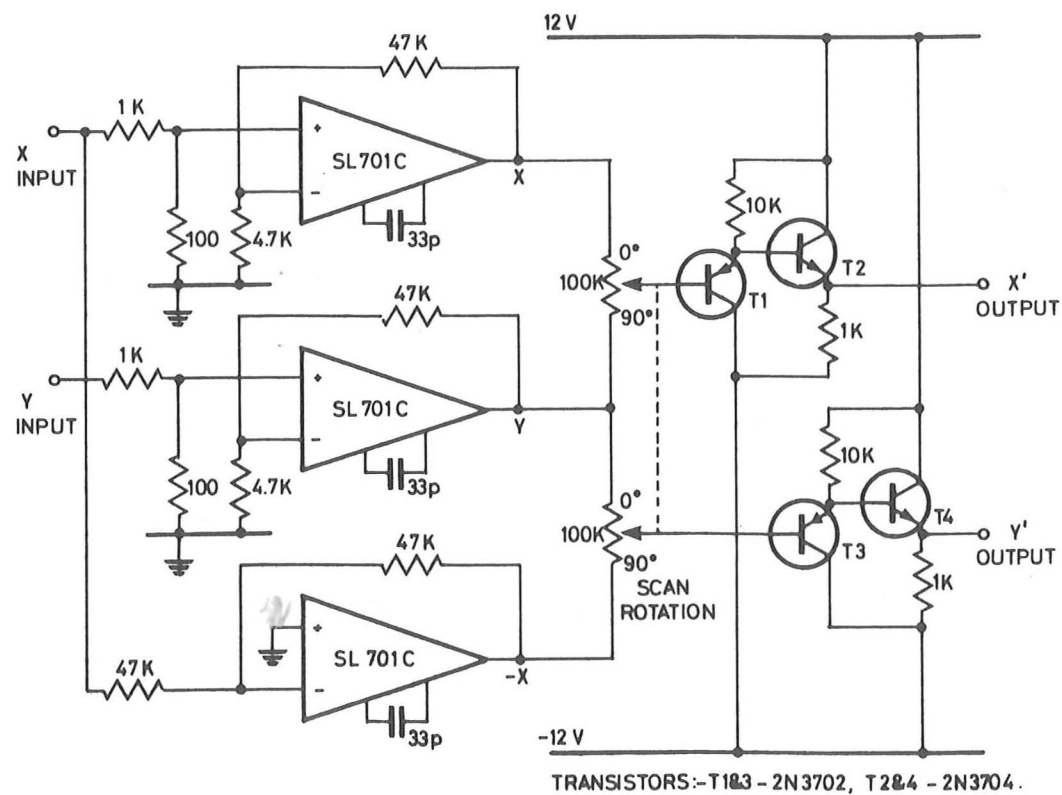


Fig 5.15 Scan Rotation

and the train of pulses is controlled by a simple diode gate, operated by the output of the bistable through the emitter follower T4.

Additionally, the unit provides reset pulses to act on the scan generator counters and ramp output, ready for the start of a single frame.

In the case of operation with one pulse per line described earlier, the clock outputs would be used to trigger the scope time bases, and the reset would set the frame generator only. For one pulse per frame, the clock pulse would trigger the scope frame generator as in Fig. 5.10, and the reset facility would be unnecessary.

### 5.6.3 Scan Rotation

For the particular application of probe diameter measurements, scan rotation was considered to be highly desirable. It would, in addition, provide a useful SEM facility.

Inter-connections with other units have not been included in Fig. 5.12 to avoid unnecessary complications, it is connected between the scan generators and scan amplifiers to provide rotation of the column scan raster only.

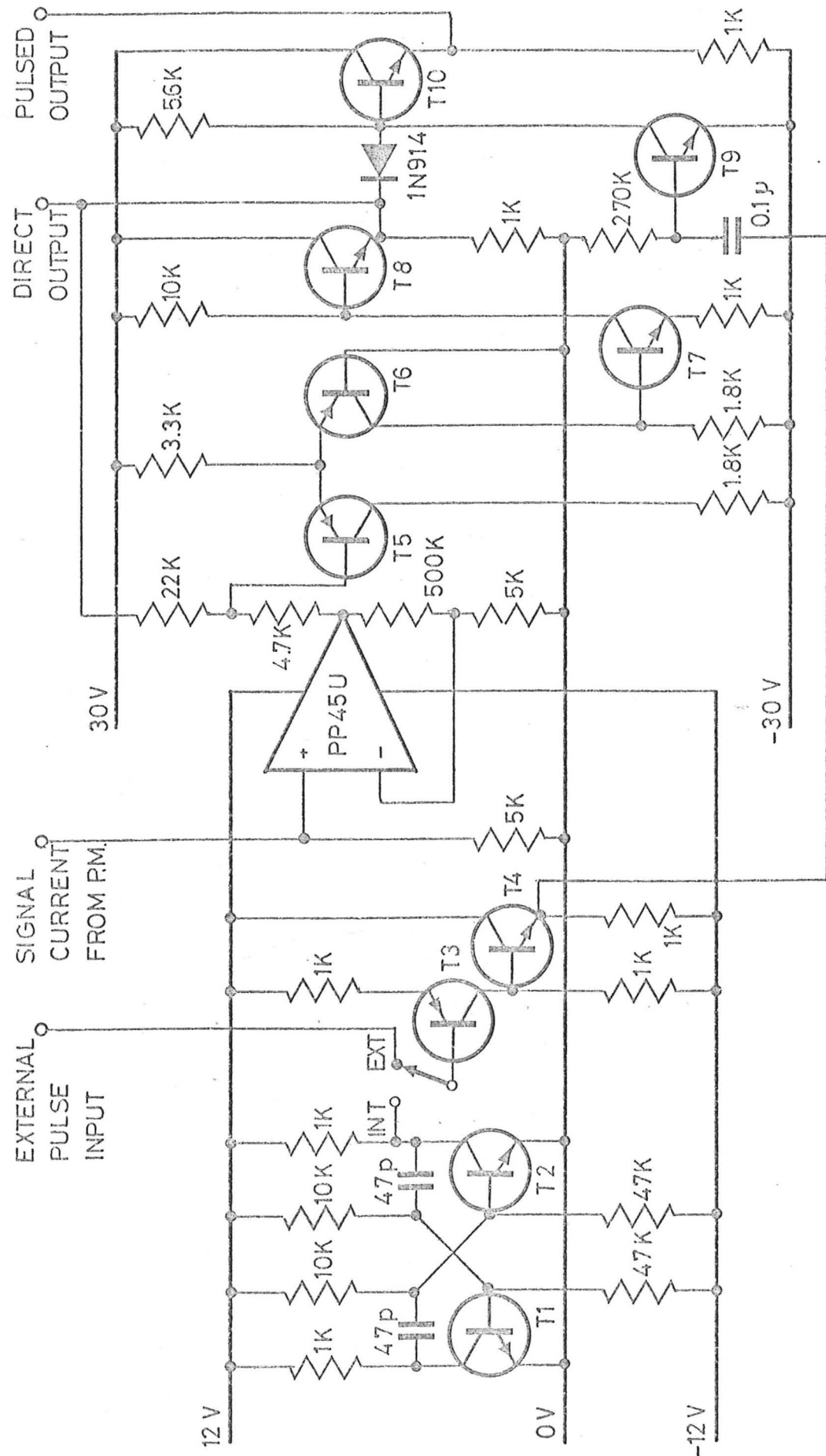
The circuit is shown in Fig. 5.15. It uses three low priced integrated circuit operational amplifiers to generate X, Y and -X, from the incoming signals. These are combined in twin ganged linear potentiometers to produce new scan waveforms X' and Y'.

$$X' = Y + (1-\alpha)X$$

$$Y' = -X + (1-\alpha)Y$$

where  $\alpha$  is the fractional rotation of the potentiometer.

The new scan directions are always orthogonal. However, the



TRANSISTORS :- T 1,2,3 & 4 - 2N706, T 5 & 6 - 2N3702, T 7, 8, 9 & 10 - 2N3053.

Fig 5.16 Video Amplifier.

amplitude of scan, R, from the centre position changes, as

$$R^2 = (X^2 + Y^2) (1 - 2\alpha + 2\alpha^2)$$

which gives a raster size depending on  $\alpha$ . For  $\alpha = 0$  and 1 the amplitude is unchanged, and it has its greatest reduction of  $1/\sqrt{2}$  at  $\alpha = 1/2$ .

The outputs from the potentiometers are buffered by double emitter followers of complimentary transistors T1, T2, and T3, T4 to maintain the d.c. levels.

5.6.4 Video Amplifier

The video amplifier circuit is shown in Fig. 5.16. A high bandwidth commercial operational amplifier (Philbrick PP45U) was used to provide initial amplification of the photomultiplier output by 100X. This gave a maximum drive voltage swing of 8 volts pk to pk. with a bandwidth in excess of 1MHz.

In order to modulate the brightness of the Telequipment D53 oscilloscope, a larger voltage swing is required, and an additional stage of amplification is used. This is a simple operational amplifier consisting of the input comparator stage T5, T6, feeding the output amplifier T7, and output emitter follower T8. Negative feedback limits the gain of the stage to 5X.

The output cannot be directly applied to the electron gun operating at approximately -5kV. This is overcome by using a.c. coupling to the gun control grid, chopping the video signal, and d.c. restoring the control grid between pulses with a clamping diode, connected inside the oscilloscope between the grid of the display tube, and the grid bias resistor. Thus a chopped version of the video waveform is delivered to the control grid of the oscilloscope display tube.

The system is particularly applicable to the pulsed emission mode. Here, the monitor pulse output of the delay unit is used to gate the video signal. This eliminates noise arising from the photomultiplier, video amplifier etc. during periods of no emission. For d.c. operation an internal, free running monostable T1, T2 is incorporated into the circuit to provide gating pulses.

A diode connected between the normal video output and T10, performs the gating function. In the absence of a drive pulse, T9 is hard on with its collector down at -30V. The diode is reverse biased and hence the pulsed output through emitter follower T10 is also at -30V. The arrival of a negative pulse at the base of T9 turns the transistor off, and the collector rises to the video output level. This is followed by T10, which takes the pulsed output to the level of the video signal.

Rise and fall times of the pulses were below 50ns, permitting compatibility with the shortest emission pulses obtainable. The output voltage could rise to 50 volts above the base level, giving maximum slewing rates in excess of 2000V/ $\mu$ s.

## CHAPTER 6

EXPERIMENTAL WORK IN THE SCANNING ELECTRON OPTICAL COLUMN6.1. Introduction

The operation of field emitters in the SEOC was limited to a large extent by the vacuum environment. Early work in the FEM (section 4) showed that it was possible to operate in the T-F mode of emission in vacua of  $10^{-6}$  torr, and this provided a basis for starting experimental work in the SEOC.

Initially, the field emission gun was not differentially pumped, but connected to the main vacuum system via the internal ports. This gave operating pressures of  $1 \times 10^{-6}$  torr at best, measured at the gun. Under these conditions the emitter was very sensitive to changes in vacuum level, and destruction would be brought about, for example, by small bursts of gas released during the operation of the sliding seals on movements and apertures. Despite these difficulties it was possible, by careful operation, to perform many useful experiments.

Before drawing emission it was necessary to thoroughly out-gas the electrodes, this considerably reduced the gas liberated by electron bombardment which might otherwise lead to immediate tip destruction. The operation of the triode was more critical in this respect, as not only did it restrict pumping to the emitter region, but also was bombarded internally by thermionic emission from the hairpin. Degassing was achieved by bringing the emitter to operating temperature, and allowing the electrodes to heat by radiation. Typically thirty minutes would be adequate, and the process could be followed by monitoring the pressure in

the gun region.

During emission, a build-up of adverse operating conditions would be indicated by either an increase of pressure in the gun, or increasingly erratic emission. In order to closely follow variations in emission current it was continuously recorded whenever possible. Typical fluctuations in good operating conditions would not be more than  $\pm 5\%$ . Using the recorder, adverse trends in emission could be seen at a glance, and appropriate action taken. This would normally involve stopping the emission, flashing the emitter to rapidly repair ion bombardment damage, and allowing the vacuum to improve before restarting.

A very useful indication of the state and temperature of the emitter was obtained by using the recorder to plot current/voltage characteristics. In the triode mode the grid must first be grounded, otherwise thermionic current will not be recorded, passing directly through the grid bias chain to the EHT generator zero volt line, and bypassing the recorder. From the characteristic, it is immediately obvious if the emitter has been destroyed as no steep, field emission section is evident, also the temperature may be checked from the thermionic section of the plot.

One problem of the T-F mode is of stabilizing the temperature, which is quite critical. As other electrodes heat up, particularly the grid, so the emitter will become hotter and could be destroyed by excessive blunting. The current/voltage characteristics may be used to ascertain the emitter temperature, even when degassing electrodes before operation. In these circumstances only a low voltage would be supplied to record the thermionic current.

FIXED FARADAY CAGE

SPECIMEN STAGE

SECONDARY ELECTRON  
DETECTOR

SCAN RODS

MAGNETIC LENS

APERTURE STAGE

ANODE

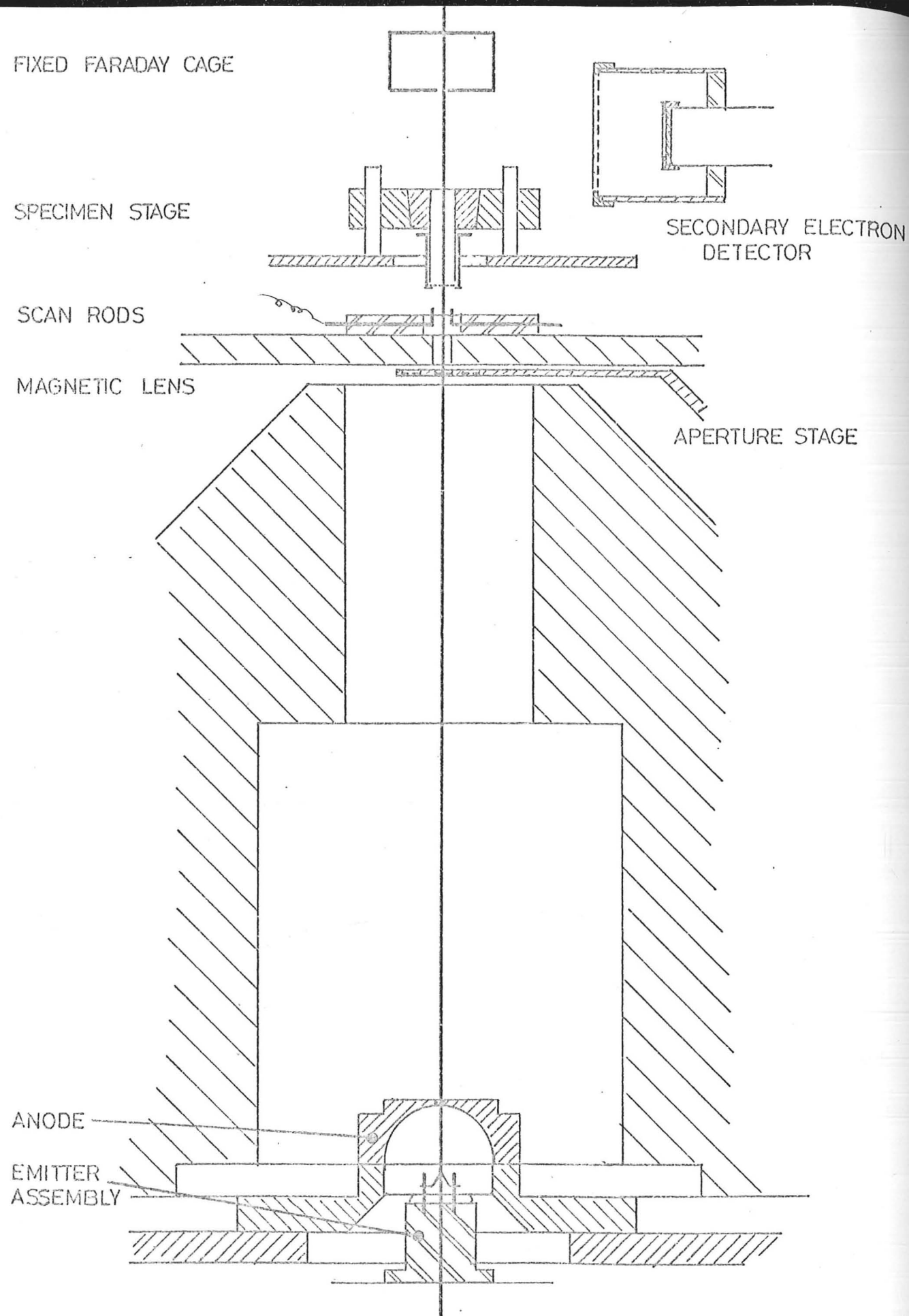
EMITTER  
ASSEMBLY

Fig 6.1 Column with Short Gun Assembly

## 6.2 Experiments with Large Emitter to Lens Separation

Preliminary experiments were carried out with a shortened form of the field emission gun shown schematically in Fig. 6.1. In this mode the emitter was completely out of the magnetic lens field, and there was little or no restriction imposed by the electrodes on the pumping speed to the emitter, so that outgassing problems were less severe.

This mode of operation was used to provide valuable first experience of operating a field emission optical system, although it was far from an optimum arrangement, and consequently the beam currents were very small.

### 6.2.1 Alignment

One of the advantages of using a lens in a strongly demagnifying mode is that small misalignments of the object cause only a very small angular misalignment at the lens, and may usually be disregarded. This is the case with the short field emission gun, in which object and image positions are similar to those in the final stage of the conventional SEM. Thus the anode alignment with respect to the lens was not critical, and the alignments necessary were of the emitter and lens aperture only with respect to the axis of the magnetic lens.

Preliminary alignment was achieved by removing the lens aperture, specimen and Faraday cage, and aligning the emitter with the anode aperture visually, by observing the heated emitter through the thin phosphor screen at the top of the chamber.

Emission was drawn and the emitter X and Y controls used to centre illumination of the anode aperture within the pinhole of the magnetic lens. The emitter was tilted to give maximum current, applying slight shift corrections as required. Emission from the

gun was thus aligned to the lens and its intensity optimised.

Preliminary centering of the lens aperture could then be achieved by focusing the illumination onto the phosphor screen, and adjusting the position of the aperture to give minimum movement of the spot, as the lens excitation was varied through focus.

In these early experiments there was no independent Faraday cage movement, and the cage was mounted on the specimen stage vertically above the specimen. Thus, when the specimen, which was a fine electron microscope grid, was moved into line with the beam, the Faraday cage cut off illumination of the phosphor screen. Adjustment of lens focus onto the specimen and final lens aperture alignment could be achieved by two means:

a) Slowly scanning the beam in one direction, the electrometer was used to monitor the current transmitted through the specimen and collected in the Faraday cage. Current was plotted against scan voltage on an X-Y recorder as the beam was scanned across the edge of a grid bar. The lens was focused to give maximum rate of change of current across the edge. Aperture alignment could be achieved by adjusting the aperture position to give minimum positional shift of the edge as the lens excitation was varied. By repeating the experiment and scanning in the orthogonal direction, the aperture could eventually be accurately centred.

This method is very similar to that used by Earnshaw (1965), and is extremely tedious. Moreover, the low bandwidth of the electrometer prohibits the observation of effects on the probe due to stray AC magnetic fields and of vibration, which are integrated and appear as an increase in the measured probe diameter.

b) By rapidly scanning a two dimensional raster over the specimen, and displaying the signal as vertical modulation of the lines of the raster on an oscilloscope, lens focusing and

gun was thus aligned to the lens and its intensity optimised.

Preliminary centering of the lens aperture could then be achieved by focusing the illumination onto the phosphor screen, and adjusting the position of the aperture to give minimum movement of the spot, as the lens excitation was varied through focus.

In these early experiments there was no independent Faraday cage movement, and the cage was mounted on the specimen stage vertically above the specimen. Thus, when the specimen, which was a fine electron microscope grid, was moved into line with the beam, the Faraday cage cut off illumination of the phosphor screen. Adjustment of lens focus onto the specimen and final lens aperture alignment could be achieved by two means:

a) Slowly scanning the beam in one direction, the electrometer was used to monitor the current transmitted through the specimen and collected in the Faraday cage. Current was plotted against scan voltage on an X-Y recorder as the beam was scanned across the edge of a grid bar. The lens was focused to give maximum rate of change of current across the edge. Aperture alignment could be achieved by adjusting the aperture position to give minimum positional shift of the edge as the lens excitation was varied. By repeating the experiment and scanning in the orthogonal direction, the aperture could eventually be accurately centred.

This method is very similar to that used by Earnshaw (1965), and is extremely tedious. Moreover, the low bandwidth of the electrometer prohibits the observation of effects on the probe due to stray AC magnetic fields and of vibration, which are integrated and appear as an increase in the measured probe diameter.

b) By rapidly scanning a two dimensional raster over the specimen, and displaying the signal as vertical modulation of the lines of the raster on an oscilloscope, lens focusing and

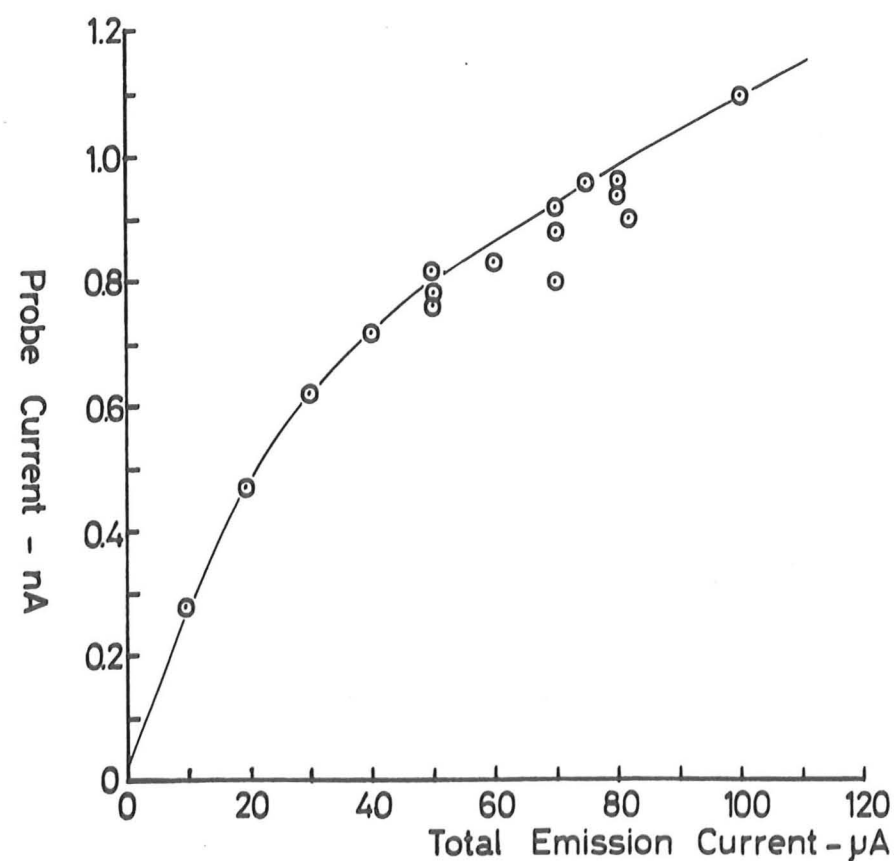


Fig 6.2 Probe Current Variation with Emission Current

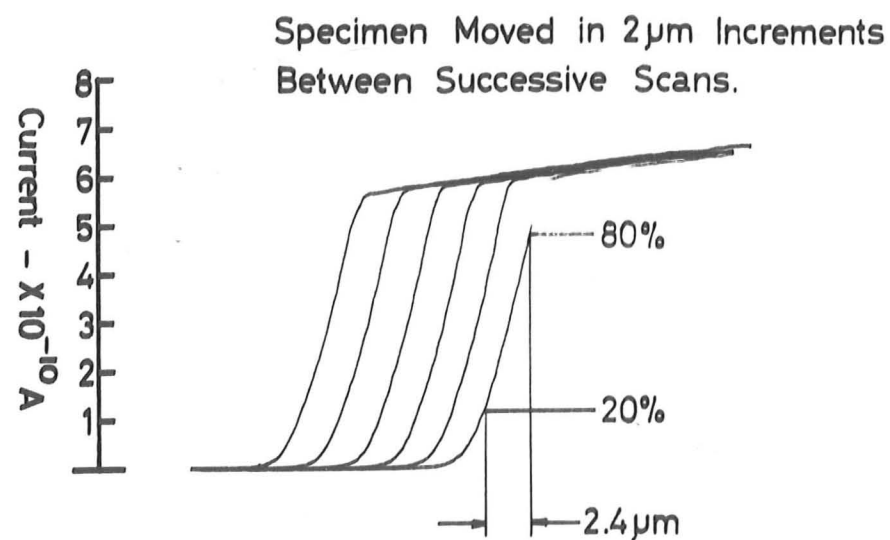


Fig 6.3 Slow Scans Across an Edge

aperture centering were made considerably easier.

This was first achieved experimentally by using the normal SEM secondary electron collector described earlier (section 5.3.5). In this mode secondary electrons generated on the grid could be collected and displayed as signal. The method, however, had disadvantages as the close proximity of the collector biased at +300 volts distorted the beam, and with the specimen normal to the beam the collection efficiency was low, moreover, secondaries generated by the transmitted beam could also reach the collector, thus the signal to noise ratio was very low, typically 2 or 3.

An improvement of about 2X in signal to noise ratio was obtained by inverting the light pipe and collecting secondaries produced by the transmitted beam on the surface of the Faraday cage. An earthed screen placed between the specimen and collector reduced the number of stray electrons directly from the specimen.

These methods were suitable for focusing and aperture alignment, however, the very poor signal to noise ratios prevented the detection of the effects of vibration and stray fields. All measurements on the probe had to be made using the Faraday cage and electrometer.

#### 6.2.2 Measurements of Angular Emission Current Densities

The experimental arrangement permitted the measurement of angular emission current density from the electron gun. Fig. 6.2 shows a plot of probe current transmitted by the lens aperture as a function of total emission current in the gun.

The relationship is not linear as might be supposed from basic considerations, and shows a marked decrease of efficiency at higher currents. The most likely explanation for this

phenomena is that under the poor vacuum conditions, the higher emission currents cause higher pressures in the gun region. This led to build-up of adsorbed gases, principally oxygen, onto the (100) faces, so enhancing the local emission in these regions, as observed in the FEM. The higher emission levels from these regions means that for a given total emission current, the proportion emitted from the (111) face decreased, and so accounted for the experimental observations.

Typical operating conditions would be with 20  $\mu\text{A}$  emission. The lens aperture was 200  $\mu\text{m}$  diameter, subtending a solid angle at the emitter of  $1.9 \times 10^{-6}$  steradians. This gave a measured angular current density of  $2.5 \times 10^{-4}$  A/sr for 20  $\mu\text{A}$  emission, and suggests that under these conditions the T-F operation has led to a remodelled emitter tip, on which the (111) emission has been enhanced by a factor of approximately 10X, compared with uniform emission into a solid angle of one steradian normally assumed.

The accuracy of these results was extremely limited as the measured probe currents would vary typically  $\pm 50\%$  between experiments under apparently similar conditions. This is again probably due to differing levels of adsorbed gas contamination in successive experiments.

Similar results to those presented above were obtained for diode operation in the region of 2 - 3kV, and for triode operation at up to 5kV.

### 6.2.3 Probe Measurements

With the beam focused onto a grid specimen, recorder plots of scans across the edge of a grid bar were obtained as shown in Fig. 6.3. In this case the grid has been moved 2  $\mu\text{m}$  by the

EXCITATION PARAMETER	WORKING DIST.	FOCAL LENGTH	PRINCIPAL PLANE	SPHER. AS.	CHROM. AB.
NI2/VP	L(MM)	FO(MM)	ZP(MM)	CS(MM)	CC(MM)
142.56	-5.00	8.47	-13.47	3.81	5.78
129.69	-4.00	8.98	-12.98	4.46	6.26
103.64	-3.00	9.63	-12.63	5.48	6.91
98.33	-2.00	10.38	-12.38	6.95	7.66
79.79	-1.00	11.19	-12.19	8.94	8.48
71.31	-0.00	12.05	-12.05	11.57	9.35
64.39	1.00	12.94	-11.94	14.94	10.25
58.66	2.00	13.84	-11.85	19.14	11.16
53.82	3.00	14.77	-11.77	24.32	12.09
49.79	4.00	15.71	-11.71	30.58	13.04
46.15	5.00	16.66	-11.66	38.03	14.00
43.07	6.00	17.61	-11.62	46.89	14.96
40.37	7.00	18.58	-11.58	57.00	15.92
37.98	8.00	19.54	-11.54	68.74	16.89
35.85	9.00	20.51	-11.51	82.15	17.87
33.95	10.00	21.49	-11.49	97.33	18.85
30.69	12.00	23.44	-11.44	133.50	20.81
28.00	14.00	25.41	-11.41	178.24	22.78
25.74	16.00	27.38	-11.38	232.47	24.75
23.81	19.00	29.35	-11.35	297.13	26.73
22.15	20.00	31.33	-11.33	373.17	28.71
20.71	22.00	33.31	-11.31	461.52	30.70
19.44	24.00	35.30	-11.30	563.14	32.68
18.32	26.00	37.28	-11.28	678.97	34.67
17.32	28.00	39.27	-11.27	809.95	36.66
16.43	30.00	41.26	-11.26	957.02	38.65

TABLE 6.1 OPTICAL PROPERTIES OF PEASE LENS

external specimen movements between successive scans to calibrate the scale.

The results shown were for the triode mode of operation at 5.0kV, diode operation giving similar results with slightly larger probes due to the lower operating voltage. The lens working distance was 25mm measured from the top face of the pinhole pole piece. Lens aperture was 200  $\mu\text{m}$  diameter as before.

The measured probe diameter, defined between 20% - 80% points in the figure is 2.4  $\mu\text{m}$ , and the probe current  $7.1 \times 10^{-10}$  amps. These give a measured probe brightness of approximately  $5 \times 10^6 \text{ A/m}^2/\text{sr}$ . This is low, however, the imaging conditions are far from optimum.

We may calculate the theoretical probe diameter from the lens parameters. These have been computed by E. Munro at this laboratory and results for the Pease lens are shown in Table 6.1, in which the working distance and position of the principle plane are measured from the outside face of the final polepiece. Under the experimental operating conditions we have:

$$C_s = 620\text{mm}$$

$$C_c = 34\text{mm}$$

With the 200  $\mu\text{m}$  diameter aperture, the semiangle,  $\alpha$ , subtended at the specimen is  $3.1 \times 10^{-3}$  radians. Following Smith (1956), the theoretical probe diameter is calculated to be 64nm.

This is considerably less than the measured probe diameter, but this was to be expected, as in the experiments effects of vibration and stray fields could not be eliminated, and would appear as increased probe diameter, also accurate lens focusing was difficult to achieve.

The poor signal to noise ratio in the secondary collection

EXCITATION PARAMETER	WORKING DIST.	FOCAL LENGTH	PRINCIPAL PLANE	SPHER. AB.	CHROM. AB.
NI2/VR	L(MM)	FO(MM)	ZP(MM)	CS(MM)	CC(MM)
142.58	-5.00	8.47	-13.47	3.81	5.78
129.69	-4.00	8.98	-12.98	4.46	6.26
103.64	-3.00	9.63	-12.63	5.48	6.91
90.33	-2.00	10.38	-12.38	6.95	7.66
79.79	-1.00	11.19	-12.19	8.94	8.48
71.31	-0.00	12.05	-12.05	11.57	9.35
64.39	1.00	12.94	-11.94	14.94	10.25
58.66	2.00	13.84	-11.85	19.14	11.16
53.82	3.00	14.77	-11.77	24.32	12.09
49.70	4.00	15.71	-11.71	30.58	13.04
46.15	5.00	16.66	-11.66	38.03	14.00
43.07	6.00	17.61	-11.62	46.80	14.96
40.37	7.00	18.58	-11.58	57.00	15.92
37.98	8.00	19.54	-11.54	68.74	16.89
35.85	9.00	20.51	-11.51	82.15	17.87
33.95	10.00	21.49	-11.49	97.33	18.85
30.69	12.00	23.44	-11.44	133.50	20.81
28.00	14.00	25.41	-11.41	178.24	22.78
25.74	16.00	27.38	-11.38	232.47	24.75
23.81	18.00	29.35	-11.35	297.13	26.73
22.15	20.00	31.33	-11.33	373.17	28.71
20.71	22.00	33.31	-11.31	461.52	30.70
19.44	24.00	35.30	-11.30	563.14	32.69
18.32	26.00	37.28	-11.28	678.97	34.67
17.32	28.00	39.27	-11.27	809.95	36.66
16.43	30.00	41.26	-11.26	957.02	38.65

TABLE 6.1 OPTICAL PROPERTIES OF PEASE LENS

external specimen movements between successive scans to calibrate the scale.

The results shown were for the triode mode of operation at 5.0kV, diode operation giving similar results with slightly larger probes due to the lower operating voltage. The lens working distance was 25mm measured from the top face of the pinhole pole piece. Lens aperture was 200  $\mu\text{m}$  diameter as before.

The measured probe diameter, defined between 20% - 80% points in the figure is 2.4  $\mu\text{m}$ , and the probe current  $7.1 \times 10^{-10}$  amps. These give a measured probe brightness of approximately  $5 \times 10^6 \text{ A/m}^2/\text{sr}$ . This is low, however, the imaging conditions are far from optimum.

We may calculate the theoretical probe diameter from the lens parameters. These have been computed by E. Munro at this laboratory and results for the Pease lens are shown in Table 6.1, in which the working distance and position of the principle plane are measured from the outside face of the final polepiece. Under the experimental operating conditions we have:

$$C_s = 620\text{mm}$$

$$C_c = 34\text{mm}$$

With the 200  $\mu\text{m}$  diameter aperture, the semiangle,  $\alpha$ , subtended at the specimen is  $3.1 \times 10^{-3}$  radians. Following Smith (1956), the theoretical probe diameter is calculated to be 64nm.

This is considerably less than the measured probe diameter, but this was to be expected, as in the experiments effects of vibration and stray fields could not be eliminated, and would appear as increased probe diameter, also accurate lens focusing was difficult to achieve.

The poor signal to noise ratio in the secondary collection

system prevented the effective observation of vibrational and stray field effects in this system, which was far from the optimum for field emission type sources, and was intended only as a preliminary experimental arrangement.

### 6.3 Immersed Emitter Configuration

The SEOC was designed principally to image FE sources at a high magnification, with the emitter positioned inside the magnetic lens back bore. This electrode configuration was discussed in Chapter 5, and it is of interest as it provides the possibility of imaging the emitter at a magnification greater than unity and very close to the optimum.

Extra difficulties involved in the operation with the emitter in the lens bore were principally the requirement to align the anode to the lens, vacuum problems associated with the limited pumping speed to the emitter region (restricted by the lens bore), and vibration of the emitter on its relatively long supports.

At this time, however, the experimental techniques were improved by the development of the differential pumping system for the gun which made the emitters relatively immune to small leaks from aperture and specimen movements, also the movable Faraday cage was incorporated which enabled the signal collection to be greatly improved by collecting secondaries generated by transmitted primary electrons at the phosphor screen.

#### 6.3.1 Alignment

The procedure adopted was similar to that developed in the earlier experiments (section 6.2.1). The column was first approximately aligned optically by observing the heated filament.

Emitter position and orientation were then adjusted to centre and

system prevented the effective observation of vibrational and stray field effects in this system, which was far from the optimum for field emission type sources, and was intended only as a preliminary experimental arrangement.

### 6.3 Immersed Emitter Configuration

The SEOC was designed principally to image FE sources at a high magnification, with the emitter positioned inside the magnetic lens back bore. This electrode configuration was discussed in Chapter 5, and it is of interest as it provides the possibility of imaging the emitter at a magnification greater than unity and very close to the optimum.

Extra difficulties involved in the operation with the emitter in the lens bore were principally the requirement to align the anode to the lens, vacuum problems associated with the limited pumping speed to the emitter region (restricted by the lens bore), and vibration of the emitter on its relatively long supports.

At this time, however, the experimental techniques were improved by the development of the differential pumping system for the gun which made the emitters relatively immune to small leaks from aperture and specimen movements, also the movable Faraday cage was incorporated which enabled the signal collection to be greatly improved by collecting secondaries generated by transmitted primary electrons at the phosphor screen.

#### 6.3.1 Alignment

The procedure adopted was similar to that developed in the earlier experiments (section 6.2.1). The column was first approximately aligned optically by observing the heated filament. Emitter position and orientation were then adjusted to centre and

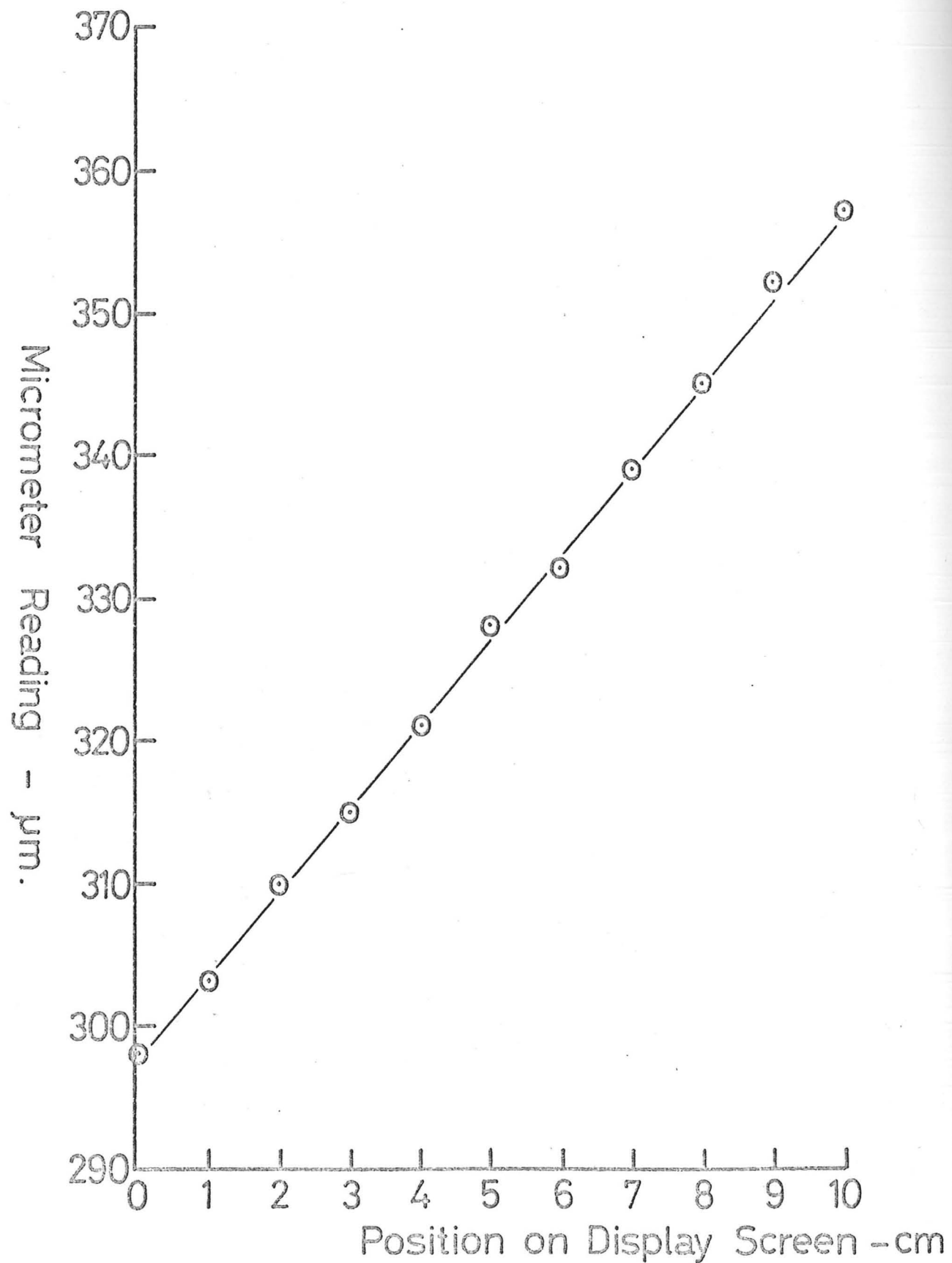


Fig 64 Illustrating Scan Linearity.

optimise illumination of the anode differential pumping aperture during emission.

The anode aperture was aligned to the lens axis using the techniques for lens aperture alignment, namely by focusing onto the screen with the lens and adjusting the anode aperture position until the focused spot did not move as the lens excitation was varied through focus.

Lens apertures were centred using the same technique of varying the lens excitation. In this case, using the improved rapid scan imaging obtained from the transmitted electron signal, focusing onto the specimen could more readily be achieved than before. The image was built up by vertical modulation of the display raster on the oscilloscope screen, and alignment was correct when this did not move as the lens was taken through focus.

#### 6.3.2 Scan Amplitude and Linearity

The scan amplitude was calibrated for each experiment by correlating specimen shift, with movement of the display of a scan across the edge of a grid bar on the screen. This was performed at low magnification, and Fig. 6.4 shows a typical plot of position on the screen as a function of specimen position. For convenience, the scan directions and specimen grid bars were arranged to lie in the directions of the specimen movements.

During experiments the scan magnification could be varied either by use of the calibrated attenuator in the scan amplifiers, or by the calibrated expanded horizontal scan facilities in the display oscilloscope. Thus the magnification of the display could readily be calculated.

It may also be seen from Fig. 6.4 that the relationship between scan amplitude at specimen and display shows little

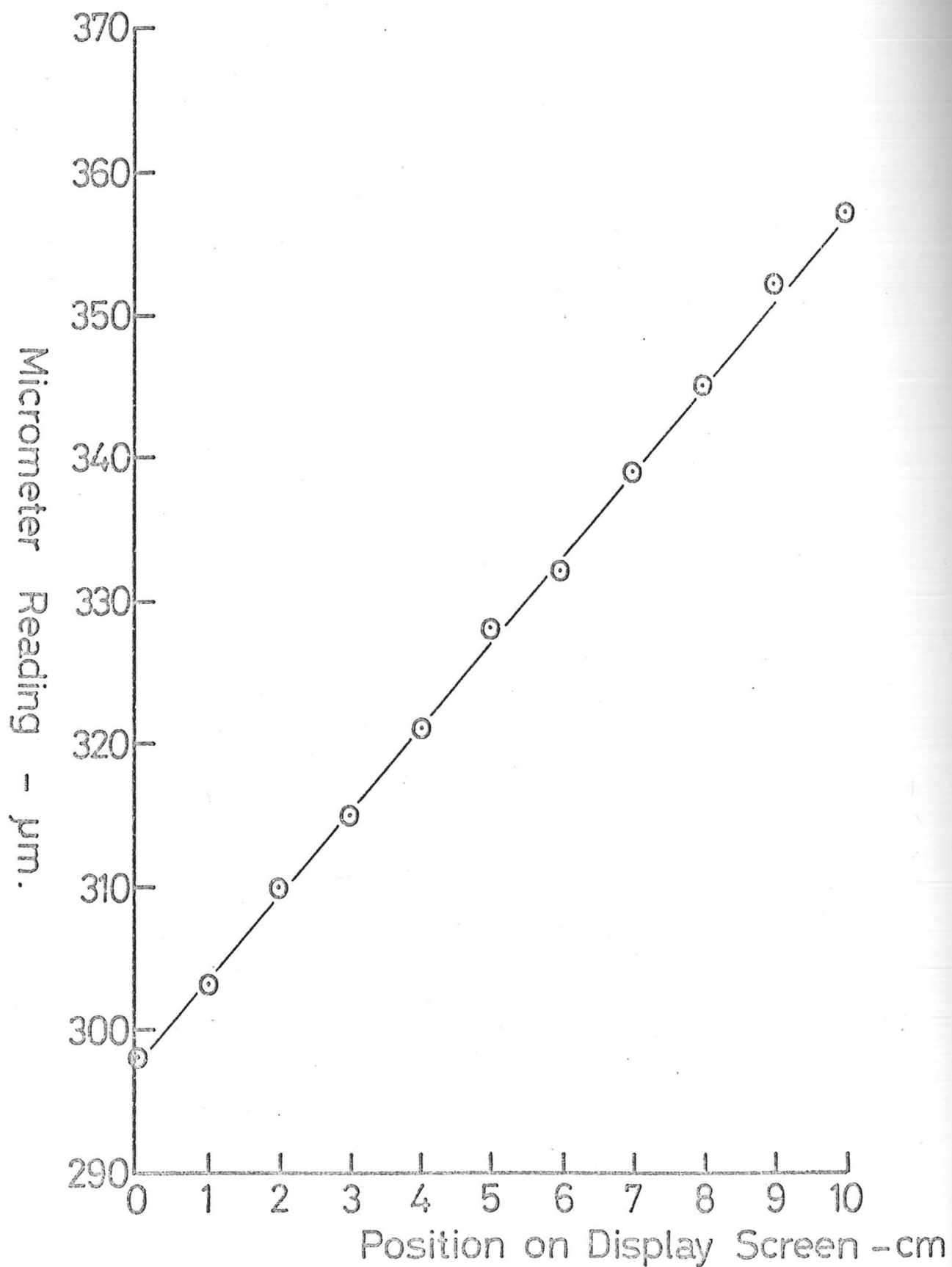


Fig 64 Illustrating Scan Linearity.

optimise illumination of the anode differential pumping aperture during emission.

The anode aperture was aligned to the lens axis using the techniques for lens aperture alignment, namely by focusing onto the screen with the lens and adjusting the anode aperture position until the focused spot did not move as the lens excitation was varied through focus.

Lens apertures were centred using the same technique of varying the lens excitation. In this case, using the improved rapid scan imaging obtained from the transmitted electron signal, focusing onto the specimen could more readily be achieved than before. The image was built up by vertical modulation of the display raster on the oscilloscope screen, and alignment was correct when this did not move as the lens was taken through focus.

#### 6.3.2 Scan Amplitude and Linearity

The scan amplitude was calibrated for each experiment by correlating specimen shift, with movement of the display of a scan across the edge of a grid bar on the screen. This was performed at low magnification, and Fig. 6.4 shows a typical plot of position on the screen as a function of specimen position. For convenience, the scan directions and specimen grid bars were arranged to lie in the directions of the specimen movements.

During experiments the scan magnification could be varied either by use of the calibrated attenuator in the scan amplifiers, or by the calibrated expanded horizontal scan facilities in the display oscilloscope. Thus the magnification of the display could readily be calculated.

It may also be seen from Fig. 6.4 that the relationship between scan amplitude at specimen and display shows little

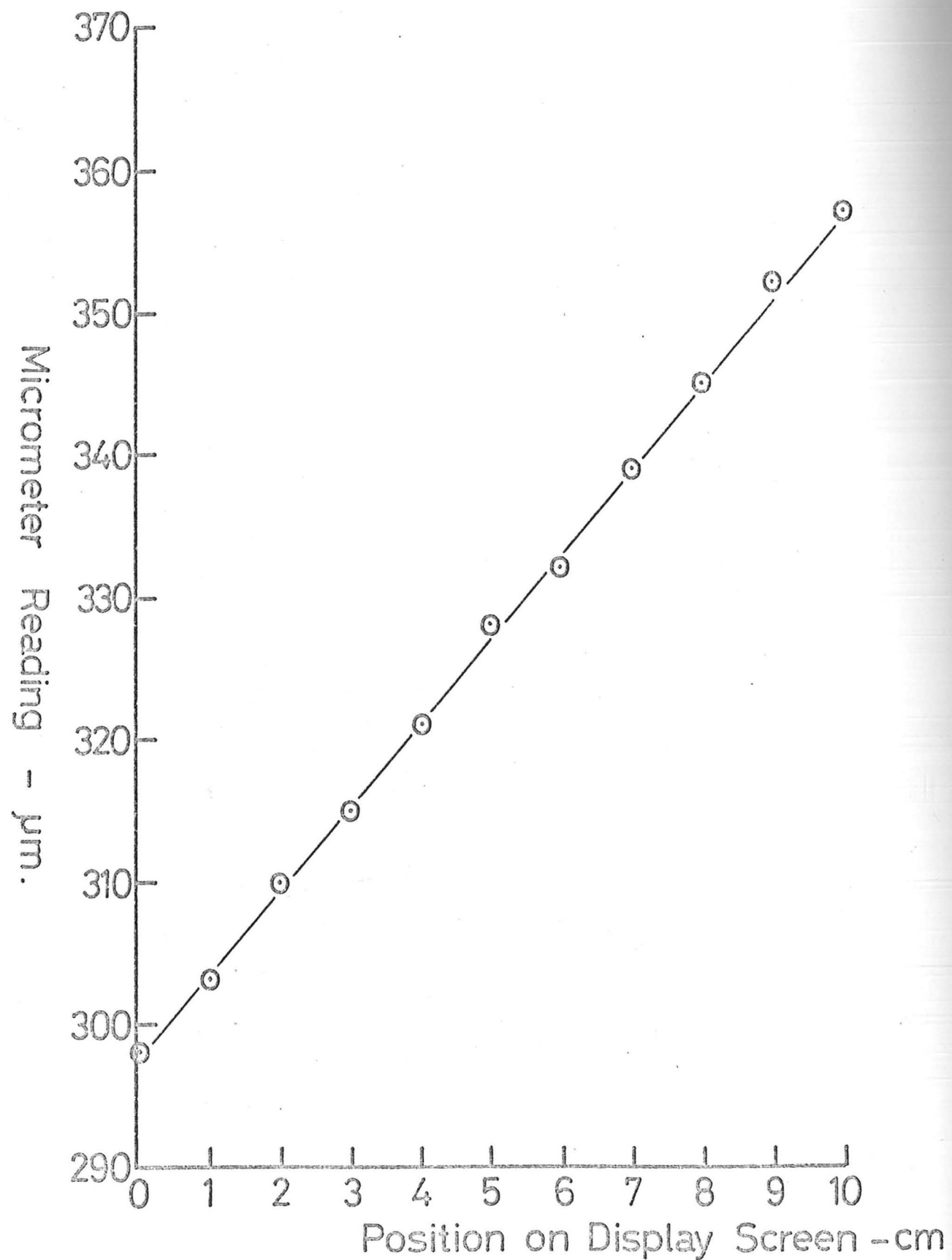


Fig 6.4 Illustrating Scan Linearity.

optimise illumination of the anode differential pumping aperture during emission.

The anode aperture was aligned to the lens axis using the techniques for lens aperture alignment, namely by focusing onto the screen with the lens and adjusting the anode aperture position until the focused spot did not move as the lens excitation was varied through focus.

Lens apertures were centred using the same technique of varying the lens excitation. In this case, using the improved rapid scan imaging obtained from the transmitted electron signal, focusing onto the specimen could more readily be achieved than before. The image was built up by vertical modulation of the display raster on the oscilloscope screen, and alignment was correct when this did not move as the lens was taken through focus.

#### 6.3.2 Scan Amplitude and Linearity

The scan amplitude was calibrated for each experiment by correlating specimen shift, with movement of the display of a scan across the edge of a grid bar on the screen. This was performed at low magnification, and Fig. 6.4 shows a typical plot of position on the screen as a function of specimen position. For convenience, the scan directions and specimen grid bars were arranged to lie in the directions of the specimen movements.

During experiments the scan magnification could be varied either by use of the calibrated attenuator in the scan amplifiers, or by the calibrated expanded horizontal scan facilities in the display oscilloscope. Thus the magnification of the display could readily be calculated.

It may also be seen from Fig. 6.4 that the relationship between scan amplitude at specimen and display shows little

departure from linearity. The plots were made at the maximum scan amplitudes and so would be expected to show greater departure from linearity than scans of lower amplitude.

### 6.3.3 Vacuum Performance

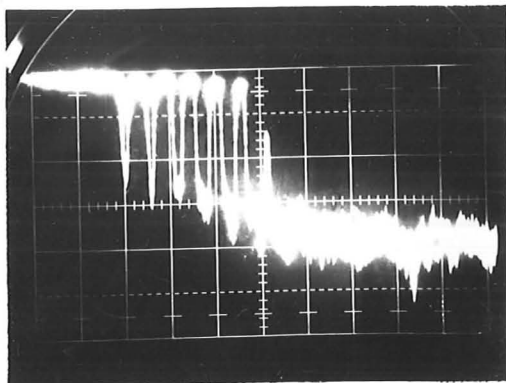
Although the change to a differentially pumped gun greatly improved the base level of the operating pressure, the restrictions on pumping speed to the emitter region due to the relatively small back bore of the magnetic lens created some new problems.

Particular attention had to be paid to thorough outgassing of the electrodes, particularly the grid of the triode gun, by bringing the emitter to operating temperature and allowing the electrodes to heat up and degas, as was described earlier. When first drawing emission a large pressure rise was inevitable. Satisfactory operation could usually be obtained by operating initially with only low current (e.g. 1  $\mu\text{A}$ ) and stopping emission to allow the vacuum to clean up as required.

The estimated pumping speed between emitter and gun chamber was 17 litres/sec. Under typical operating conditions with 20  $\mu\text{A}$  emission, the pressure in the gun chamber would rise by  $2 \times 10^{-8}$  torr. Thus the emission was creating an outgassing rate of approximately  $1 \times 10^{-6}$  torr-litres/sec., which corresponded to a pressure rise in the emitter region of about  $6 \times 10^{-8}$  torr.

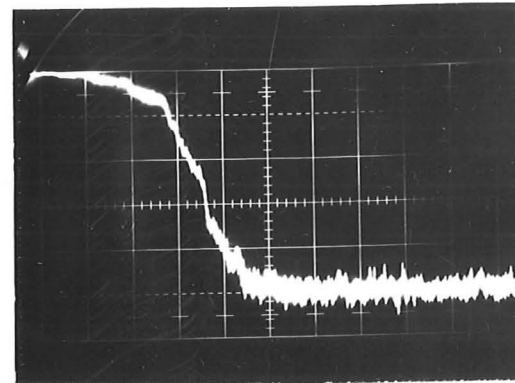
An interesting experiment was performed in which the emission was focused in the anode aperture using a very high lens excitation. The gun pressure rapidly fell to the levels achieved under conditions of no emission, and immediately rose again when the lens was turned off. This shows conclusively that the increase in pressure is due to anode outgassing and it would be a useful feature of future designs if the anode could be outgassed

Probe Current



1 div. = 190 nm

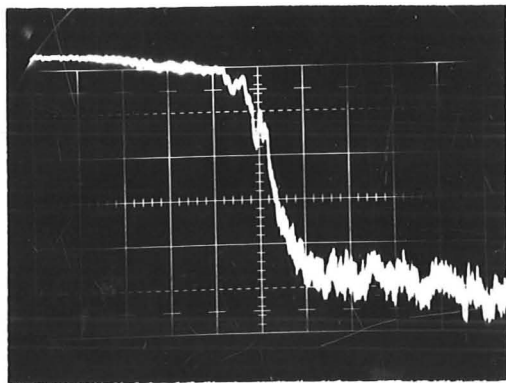
(a) Early results showing high levels of vibration at 40 Hz.



1 div. = 100 nm

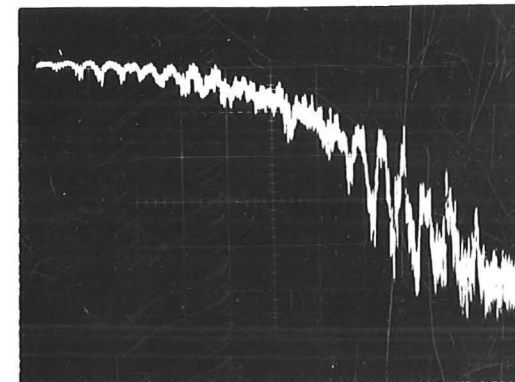
(b) Almost free from vibration. Probe diameter approx. 110 nm

Probe Current



1 div. = 100 nm

(c) Little vibration. Probe diameter approx. 60 nm



1 div. = 40 nm

(d) Typical daytime vibration levels. Probe approx. 120 nm diam.

in situ, e.g. by indirect heating, or if the emission could be focused in the anode aperture.

#### 6.3.4 Probe Measurements

The improved system for detecting the transmitted electron current using the phosphor screen and photomultiplier, enabled probe diameters to be measured directly from the oscilloscope display. Also the high bandwidth of the system (limited by the P11 phosphor to approximately 50kHz) permitted the relatively easy observation of the effects on the probe of stray A.C. magnetic fields and mechanical vibrations.

Some photographs of typical scans across the edges of grid bars are shown in Fig. 6.5. These experimental results were obtained by scanning a single line across the specimen. Direct measurements from the screen, or the photographs gave the probe diameter.

Probe current was measured in the Faraday cage as before, in this case by moving the specimen to a convenient position with the probe stationary, so that all current was transmitted. The Faraday cage was aligned for optimum collection current, corresponding to the probe entering the hole in the bottom face of the cage, which was not visible for the alignment.

For the calculation of the beam semi-angle, direct measurements of lens working distances and of aperture diameters were used. Apertures were measured on a travelling microscope and found to be very near to their nominal sizes.

Three aperture sizes were normally used, these were 200  $\mu\text{m}$ , 100  $\mu\text{m}$  and 50  $\mu\text{m}$  respectively. Varying the aperture diameter provided the most convenient means of changing the probe current, as the emission current range was limited by the difficulties

Fig 6.5 Fast Scans Across an Edge

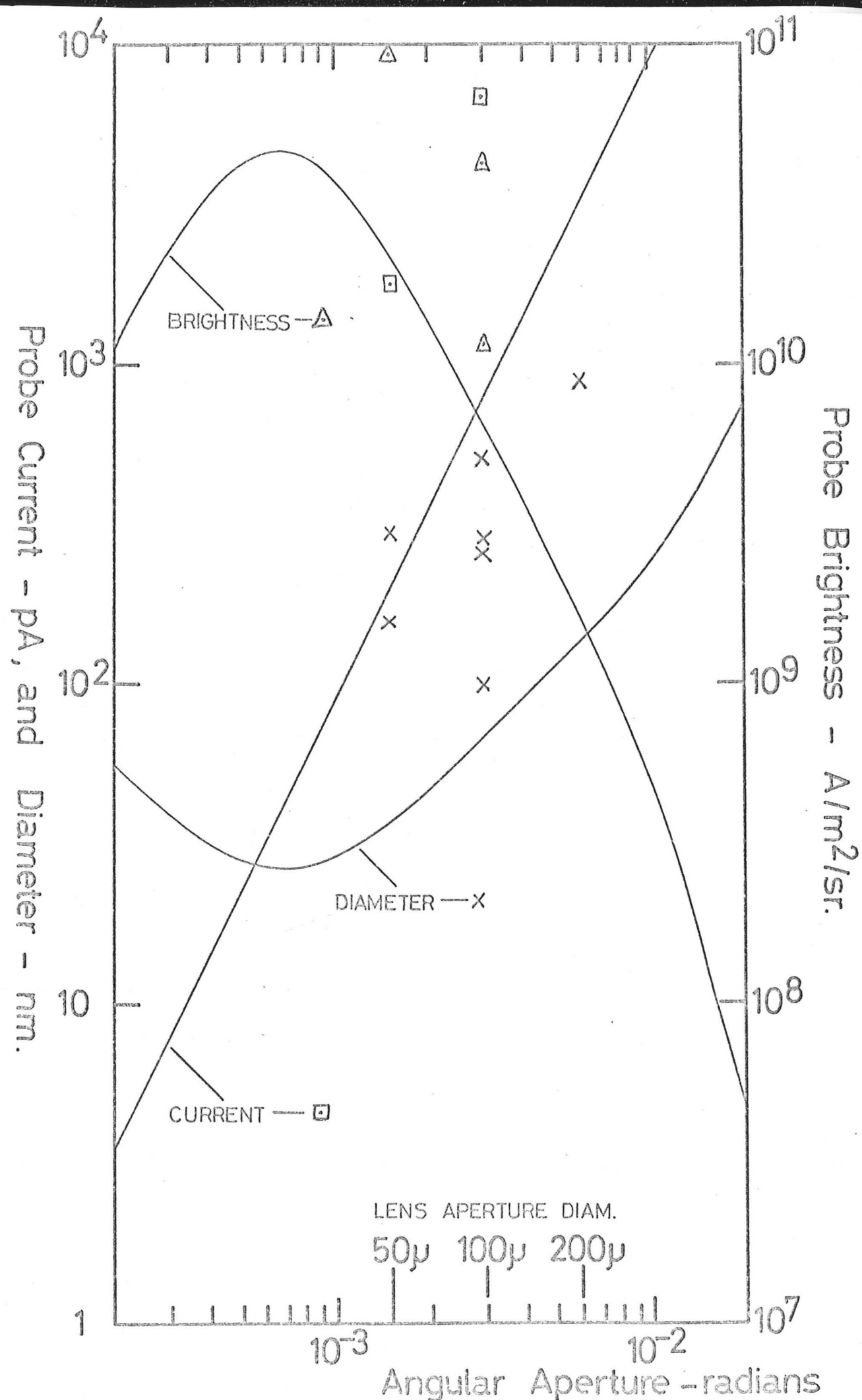


Fig 6.6 Performance of the S.E.O.C.

associated with vacuum levels in the emitter region. Some results gained from experiments for the different aperture sizes are plotted, together with the theoretical performance curves in Fig. 6.6.

Operation of the column in both the diode mode at 2 to 3kV, and triode mode over the range 2 to 7kV showed little variations in performance other than a slight general trend towards higher brightnesses and smaller probe diameters at higher operating voltages.

#### 6.3.5 Calculations of Theoretical Performance

The theoretical performance of the SEOC optical system may be calculated by extending the analysis used by Smith (1956) for the conventional SEM. Principle differences which arise are due to the relatively high magnification with which the source is imaged, requiring corrections to the spherical and chromatic aberration coefficients, and to the way in which the probe current is calculated.

Contributions to the final probe diameter may be calculated as follows:

a) Spherical Aberration. The spherical aberration coefficient is modified by the factor  $(1 + M)^4$  following Cosslett and Haine (1954), Der-Shvartz (1967) and Petrie (1962), to take into account imaging conditions with finite conjugates at magnification  $M$ . Thus the expression for the disc of confusion, diameter  $d_s$ , becomes:

$$d_s = \frac{1}{2} (1 + M)^4 C_s \alpha^3$$

b) Chromatic Aberration. By similar reasoning to that given by Petrie (1962) in which he derives the correction factor

of  $(1 + M)^4$  for spherical aberration, the correction factor of  $(1 + M)^2$  for chromatic aberration is obtained. Thus the diameter of the disc of confusion due to chromatic aberration is:

$$d_c = (1 + M)^2 C_c \propto \frac{\Delta V}{V}$$

where  $V$  is the beam voltage, and  $\Delta V$  the axial energy spread.

c) Diffraction. The diameter of the Airy diffraction disc of confusion  $d_d$ , defined as the width at half amplitude is unaffected by the conjugate positions, and is given by

$$d_d = 0.61 \lambda / \alpha$$

where  $\lambda$  is the wave length of the electrons, and is given approximately by

$$\lambda = \sqrt{\frac{1.5}{V}}$$

where  $\lambda$  is in nm, and  $V$  in volts.

d) Gaussian Image of the Source. The radius of the virtual source,  $r$ , formed within the emitter of radius,  $a$ , and operating at voltage,  $V$ , is given by:

$$r = a \sqrt{\frac{V_t}{V}}$$

where  $eV_t$  is the transverse energy of the emission.

This is imaged at magnification,  $M$ , to give a contribution to final probe diameters of  $d_g$ ,

where

$$d_g = 2M a \sqrt{\frac{V_t}{V}}$$

These four contributions to the final probe diameter are combined in quadrature (Smith (1956)). Thus the effective final

probe diameter,  $d$ , is given by:

$$d^2 = d_s^2 + d_c^2 + d_d^2 + d_g^2$$

Probe current,  $I$ , may be calculated from the angular current of emission,  $i_c$ . Referring the solid angle subtended by the aperture at the specimen to the source:

$$I = \pi \alpha^2 M^2 i_c$$

From these relationships the brightness  $B$  may be calculated, as:

$$B = \frac{4I}{\pi d^2 \pi \alpha^2}$$

Typical operation of the SEOC would be at a specimen working distance of 9mm. The emitter would be positioned 20mm below the top face of the final pole piece, which requires a focal length of 8.5mm in the magnetic lens, and gives a magnification  $M = 1.5X$ . Referring to Table 6.1, aberration coefficients for parallel illumination of the lens at the same excitation are:

$$C_s = 3.8\text{mm}$$

$$C_c = 5.8\text{mm}$$

For T-F operation at 5kV with 10  $\mu\text{A}$  emission we take  $i_c = 1 \times 10^{-5} \text{A/sr}$ , (assuming uniform emission into 1 steradian),  $\Delta V = V_t = 3 \text{ volts}$ , and emitter radius,  $a = 100\text{nm}$ .

Plots for the theoretical variations of probe diameter,  $d$ , probe current,  $I$ , and probe brightness,  $B$ , are given in Fig. 6.6. Also plotted are some experimental results.

### 6.3.6 Conclusions

Both the experimental results, and the theoretical analysis

described above show that field emission cathodes may be imaged with very high brightnesses, under the particular operating conditions of small angular aperture, consistent with small probe diameters.

There were, however, significant discrepancies between the measured and theoretical results. The most important of these was in the measurement of probe diameters, which were consistently larger than the theoretical predictions. Much of the remaining experimental work was therefore devoted to the investigation of those phenomena likely to cause an increase of probe diameter.

#### 6.4 Attempts to Reduce Probe Diameters

The single lens column differs principally from conventional electron optics by the immersion of the emitter in the magnetic field in the back bore of the lens, this being the most convenient means of imaging the emitter near to optimum magnification in a useful electron probe system. The problems associated with this geometry include increased sensitivity to mechanical vibration on long filament supports, and the possibilities of magnetic field interaction with both magnetic materials in the emitter region (e.g. niilo filament pins), and the electrostatic fields accelerating electrons from the emitter.

##### 6.4.1 Vibration

The effects of vibration could readily be identified on the oscilloscope display. The way in which vibration manifests itself may be seen in traces of Fig. 6.5.

The laboratory building was particularly bad from the point of view of residual vibration, being of steel frame construction, further, the apparatus was situated on the fourth floor. Floor

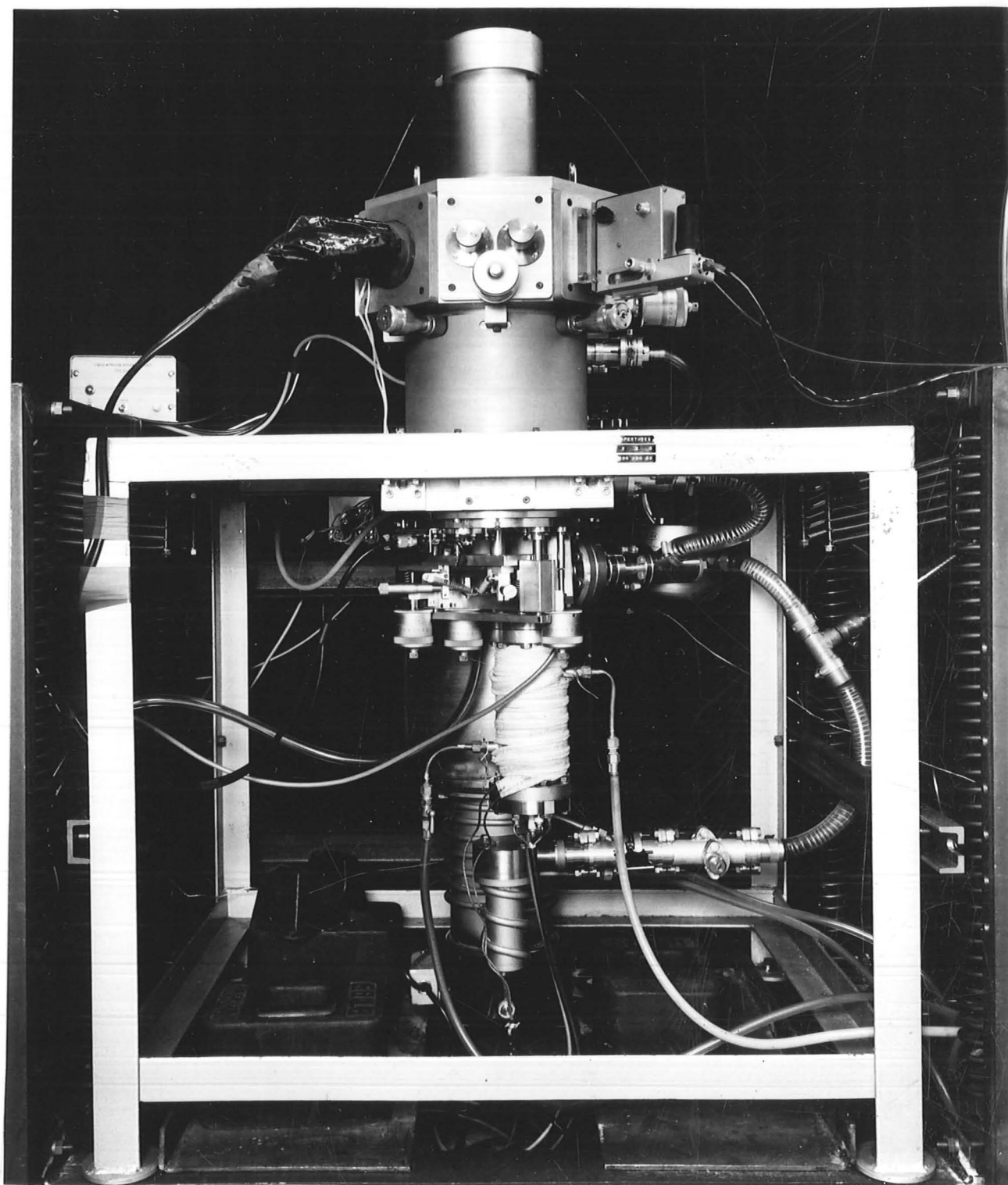


Fig 6.7 S.E.O.C. on New Antivibration Mounts

vibration had components at 100Hz and 50Hz which were associated with mains driven equipment, at a frequency varying between 10 and 20Hz which was assumed to be a fundamental building resonance. Each of these three components had typical peak to peak amplitudes of 1  $\mu\text{m}$ .

The lower frequencies, in particular, were transmitted by the rubber antivibration mounts with little attenuation. These were sufficient to excite natural resonance within the emitter, lens and specimen system at 40Hz. The effect on the apparent shift of the probe was to produce a normal background vibration level of 50 to 100nm pk. to pk. amplitude.

Although some improvement could be obtained by operating outside normal laboratory hours, this was neither a complete, nor satisfactory solution. It was therefore decided to attempt to improve the antivibration mounting of the instrument.

In order to achieve significant attenuation of lower frequencies, the resonant frequency of the support must be as low as possible. A number of possibilities were considered, including the use of compressed air mountings and metal spring supports. It soon became clear that the lowest practical resonant frequency possible with such systems is in the region of 1Hz, and in fact this is about the lowest frequency tolerable from the point of view of stability and operating convenience.

A second possibility considered was the mounting of the column on a relatively massive seismic block, which was itself supported on antivibration mounts, and so add an extra stage of vibration decoupling. Whereas this was considered a promising solution to the problem, it did not represent a simple practical solution in the short term.

	Floor	Chamber
Vertical	6mV	600 $\mu$ V
Longitudinal	1mV	500 $\mu$ V
Transverse	1.5mV	700 $\mu$ V

a) Background Levels

	Floor	Chamber
Vertical	80mV	750 $\mu$ V
Longitudinal	35mV	1.5mV
Transverse	35mV	< 1mV

b) Impact Tests

TABLE 6.2 MEASUREMENTS OF VIBRATION TRANSDUCER OUTPUTS

The system adopted was both economical, and rapidly fitted, and involved suspending the column on four large tension springs from a steel frame. This gave natural resonant frequencies in all directions of about 1Hz. The column is shown in this configuration in Fig. 6.7. I gratefully acknowledge the assistance of Mr. J.R. Cleaver for his help in the design and construction of the spring supports.

Some measured values for the attenuation of floor vibration are given in Table 6.2. These measurements were made using a Philips PR9260 vibration meter, which, although it could detect low levels of vibration, could not be used to measure the amplitude directly. The output of the transducer was therefore monitored on an oscilloscope, and measurements from this are given in the Table. For an approximate estimate of amplitudes, an output of 3mV would be equivalent to a vibration level of about 1  $\mu$ m pk. to pk. at 50Hz. Measurements were made for both background levels of vibration, and the effects of an impact test performed by dropping a ball bearing to the floor from a height of one metre.

Although the new mounting provided a significant improvement in the vibration levels, they were not a complete solution to the problem, and the low resonant frequency did add somewhat to difficulties of operating the instrument.

Vibration will always be a fundamental problem with field emission sources, where imaging of the emitter at high magnifications is desired. The solution to the problem must be both in the provision of improved antivibration techniques, for example by the use of a seismic block, and the improved design of emitter mountings and movements for maximum rigidity.

#### 6.4.2 Magnetic Materials in the Lens Field

A number of slightly magnetic materials were used in fabrications in the emitter region. Such items include the nilo filament pins, stainless steel screws, stainless steel anode mounting, the stainless steel filament mounting, and the stainless steel grid.

Of these offending items only the nilo filament pins would normally be classified as magnetic materials. A special filament base was therefore constructed using fabricated stainless steel pins supported on a mica disc. Several emitters were mounted in this base during the course of experiments.

As far as possible stainless steel items were removed. The screws were detectably magnetised in the presence of a strong permanent magnet, and so were replaced by brass. The grid was removed completely for diode operation.

Remaining items, which could be slightly magnetic were the stainless steel fabrications supporting the anode and emitter, neither of which could readily be replaced. The anode support was thought unlikely to have little effect, as it had rotational symmetry and was in any case not very close to the lens gap. The stainless steel filament pins and emitter socket fabrication were also thought unlikely to have significant effect being well behind the emitter.

Even with these precautions there was little or no detectable reductions in the probe diameters measured. This led to the conclusion that small perturbations of the lens field due to slightly magnetic items was not limiting the probe diameters at those measured.

#### 6.4.3 Electron Optical Problems

A number of electron optical problems, normally of secondary

importance in usual SEM performance, could have greater significance in the particular operating conditions of the optical column.

a) Stray A.C. magnetic fields. This phenomenon is usually more significant under low voltage operating conditions. In the SEOC the effect could readily be detected and observed on the display as it produced stationary modulation when the scan was synchronized with the A.C. mains supply. Some devices, the electrometer and oscilloscopes in particular, were found to have high stray fields which affected the beam. These were moved away from the column, and no further trouble was observed, presumably due to the very short electron paths in the column.

b) Astigmatism. Although no stigmator was fitted it was possible to scan the beam in two orthogonal directions, and so to measure the cross-section of the probe. No significant differences were detected in these experiments and it was thought unlikely that the angle of astigmatism would lie very close to the direction bisecting the scans on different occasions, when several components had been removed, cleaned or replaced.

c) Charging of apertures or specimen. Again, at lower beam voltages, the effects of contamination charging and distorting the beam become more important. In the SEOC this could occur at three points directly in the path of the beam, the anode aperture, lens aperture and the specimen.

The anode aperture was an integral part of the OFHC copper anode. This could therefore not be replaced but was carefully cleaned by polishing with wet abrasive paper, and washing in an ultrasonic cleaner with detergent, water, and then acetone. The aperture showed no visible signs of contamination when examined under an optical microscope.

Lens apertures could readily be replaced, and new apertures were fitted.

A new specimen grid was fitted which was subsequently examined in a standard SEM in secondary collection mode. It showed no signs of charging, and presented no difficulties when imaging at high resolutions.

Normal standards of cleanliness in the column were high, and after taking particular care to clean components no reduction of measured probe diameter was detectable.

d) Aperture lens aberrations. There was an aperture lens formed in the anode aperture caused by the electrostatic fields in the gun region. As most of the gun potential was dropped in a region very close to the emitter, field at the anode was low, typically in the region of  $10^4$  V/m, which gave a focal length of about 1 metre with the beam voltages used.

In an attempt to determine whether this aperture lens was contributing to aberrations in the final probe, experiments were performed with the anode removed altogether, so that the inside of the magnetic lens and lens aperture formed the anode. There was no detectable improvement in probe diameter in this configuration, and it was concluded that this effect was not limiting the measured probe sizes.

e) Aberrations due to the triode structures. Although first experiments had shown little difference between measured probe diameters in the diode and triode configurations, the possibility that the presence of the grid could cause additional aberrations in the gun was not excluded, and in a number of experiments the gun was operated both with and without the grid.

Results showed that consistently better resolutions were obtained using the higher operating voltages possible with the

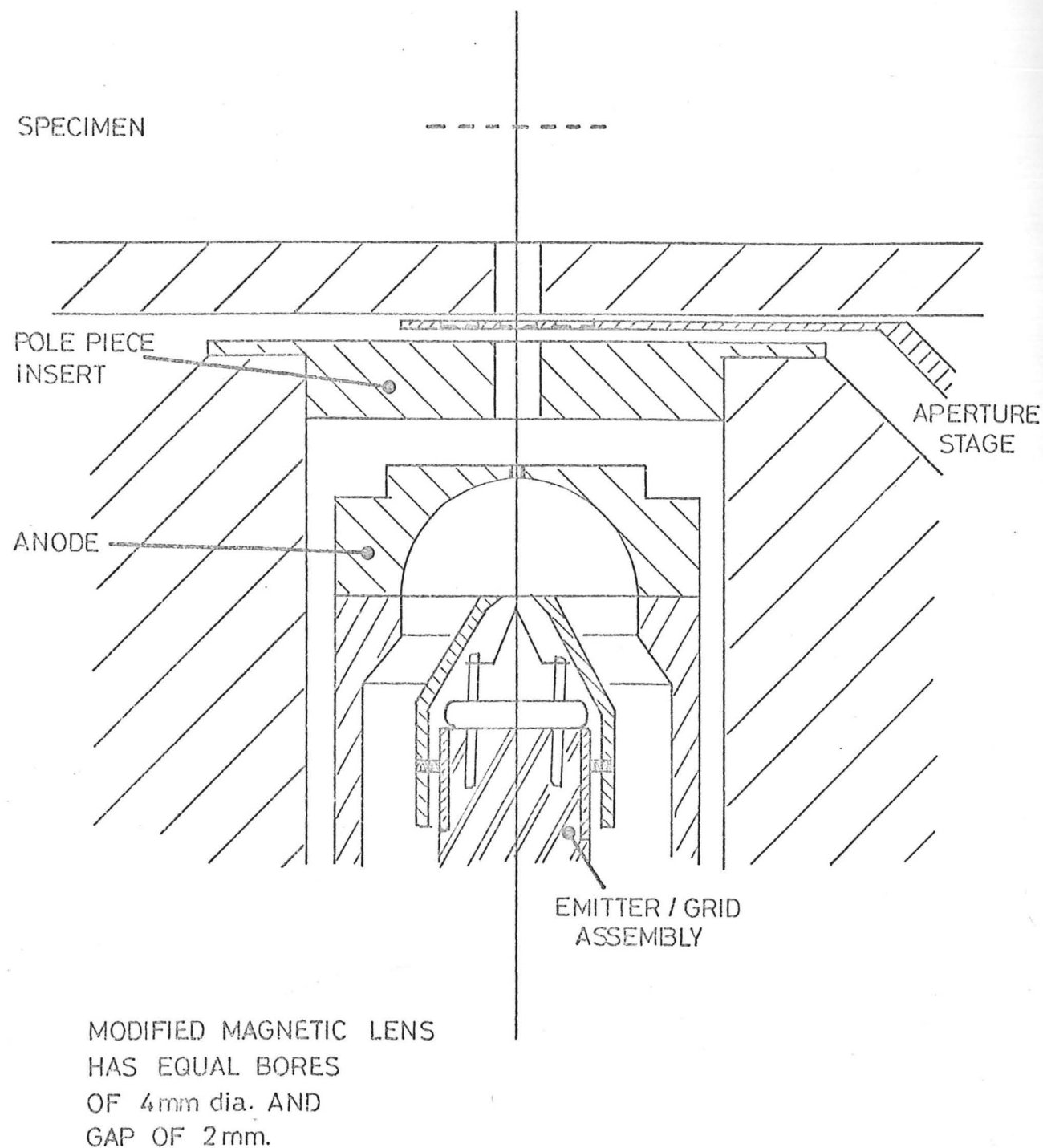


Fig 6.8 S.E.O.C. with Modified Lens.

grid, and it must be concluded that under the experimental operating conditions the grid was not causing the limiting aberrations to the probe.

f) Limitations due to chromatic aberrations. The theoretical calculations predict that the principle contribution to the final probe diameter is due to chromatic aberration for the smaller aperture diameters. The EHT and lens current supplies had been carefully checked and were found to contribute negligible ripple compared to the energy spread estimated for T-F emission.

This mode of emission has the unique property that the heating may be removed and operation may continue with cold field emission, the duration of such operation depending on the vacuum conditions. Thus it was possible in the SEOC to operate with cold FE for sufficient time to make some measurements of probe diameter, with the effects due to chromatic aberration correspondingly reduced.

When these experiments were performed there was no detectable drop in the probe diameter measured, which leads to the conclusion that some other factor was limiting the performance, over and above the contribution due to chromatic aberration.

#### 6.4.4 Interaction of Electrostatic and Magnetic Fields

With the emitter immersed in the lens magnetic field, there was the possibility of interaction between the electrostatic field of the gun and the magnetic lens field, which might produce additional aberration effects. This interaction could not readily be considered theoretically, and so the experimental system was modified to significantly reduce the magnetic field within the gun.

The modified column is shown in Fig. 6.8. A pole piece

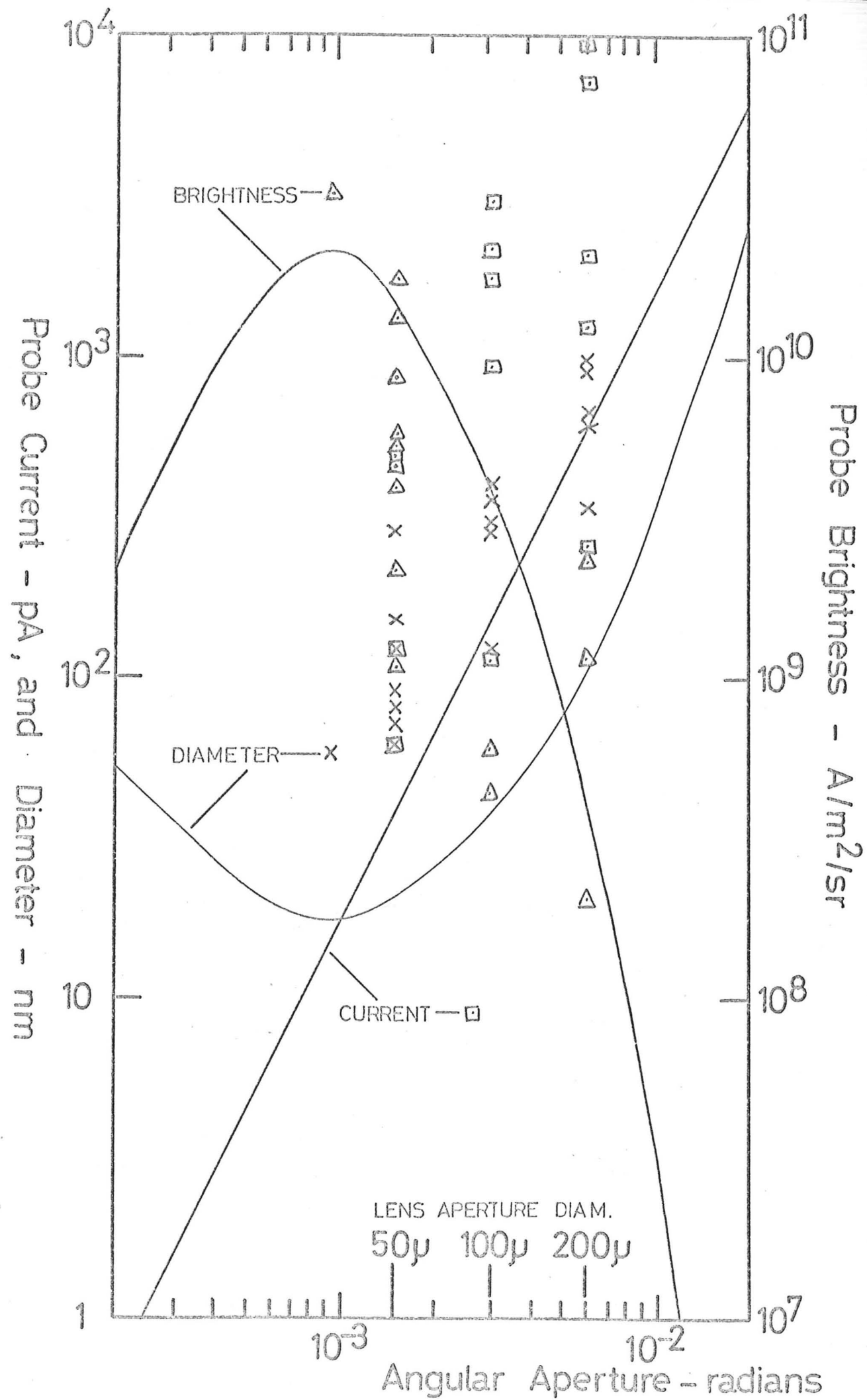


Fig 6.9 Performance of Modified S.E.O.C.

insert was fitted to the lower bore of the lens, and the gun was dropped vertically downwards. The highly asymmetric lens was therefore converted to a thin symmetrical lens, which not only removed the possibility of magnetic field effects at the emitter, but also permitted the more certain calculation of aberrations.

Theoretical performance was calculated using the formulae given in section 6.3.5. For the same specimen working distance of 9mm, the emitter had to be placed 30mm below the top of the final lens plate to accommodate the lower pole piece insert. This gave a focal length of 9.1mm, and magnification of 0.70X. Aberration coefficients were taken to be

$$C_s = 82\text{mm}$$

$$C_c = 7\text{mm}$$

from the data published by Leibmann and Grad (1951).

Plots of probe diameter, and probe brightness as functions of  $\alpha$  are shown in Fig. 6.9, for T-F operation at 5kV, 10  $\mu$ A emission. A number of experimental points are also plotted.

The experimental results show discrepancies with the theoretical predictions which are similar to those previously obtained with the emitter immersed in the lens field, (section 6.3), and that these may not therefore be attributed to an interaction between magnetic and electric fields in the gun region.

The results shown in Fig. 6.9 have a greater significance, as the approximate corrections to spherical and chromatic aberration coefficients used in the calculation of probe diameter became almost exact when applied to the thin, symmetrical lens of the modified optical system. A greater reliance may therefore be placed on these theoretical results, so that there is little doubt the discrepancies observed are real.

#### 6.4.5 Conclusions

It has been possible to eliminate a number of likely causes of increased probe diameters. However, it has not been possible to positively identify the reason for larger probe diameters than those predicted theoretically, both with the emitter immersed in the lens field, and completely out of the influence of the lens.

The ~~large~~ gradient of experimentally measured probe diameters with increasing aperture diameter in both cases suggests that the limiting aberration is similar to chromatic aberration in nature. This could include field aberrations in the emitter region due to departures of the emitter geometry from the ideal case of spherical symmetry. If such effects were due to the geometry of the emitter tip, then considerable differences would be expected between cold field emission and T-F mode when the tip geometry is known to change (see section 4.2). No changes were observed experimentally, however, which suggests that the geometry of the emitter shank may be the dominant factor.

It would have been very interesting to have continued the experimental investigation described above. Particularly so, since the progressive development of the SEOC system had led to much greater reliability of operation, and improvements in the measuring techniques. Also, full scanning microscope facilities had been developed which would not only have greatly assisted in the operation of the instrument, making possible for example, the detection and correction of astigmatism, but also have permitted a direct comparison of the SEOC with the conventional SEM.

Unfortunately, problems with emitter failures developed, and although many new emitters were tried over a period of several months, few further results were possible. Eventually, lack of time forced experimental work to be concluded.

Possible causes of the emitter failures are considered below in section 6.6.

### 6.5 Operation as a Scanning Electron Microscope

After completing of the additional electronics described in section 5.6, there was a brief opportunity to operate the SEOC as a simple scanning electron microscope, with a fully independent digital scanning system, and intensity modulated display on the D53 oscilloscope screen.

Over this short period of operation the electronic systems performed very satisfactorily, though operation with pulsed emission was not tried. The specimen was the grid which had been used in the previous measurements of probe diameter.

Unfortunately, the abrupt termination of experiments by emitter failures prevented the observation of other specimen and photographic recording of the images.

### 6.6 Analysis of Emitters Used in the SEOC

Following the continuing failure of oriented emitters in the SEOC during the latter part of the research, it is worthwhile analysing the performance obtained from all oriented emitters. This is particularly so, in view of the success of earlier experiments, which were generally performed under considerably worse operating conditions.

#### 6.6.1 Comparison of Wire Batches

The oriented emitters were constructed from two batches of oriented tungsten wire, and the troubles seemed to be associated with use of the second batch, though this was not immediately obvious at the time, as wherever possible used emitters were resharpened, so there was no clear transition from emitters made

Emitter	Total Emission Time, Seconds	Total P.I.T. Torr-Coulombs	Cause of Failure (where known)
E1	--	--	Other Use
E2	$3 \times 10^4$	$1 \times 10^{-6}$	Mechanical
E3	$2.4 \times 10^4$	$1.1 \times 10^{-6}$	Mechanical
E3B	$1.9 \times 10^4$	$7 \times 10^{-8}$	Vacuum
E4	$1 \times 10^4$	$2.4 \times 10^{-8}$	Not Known
E5	$5 \times 10^2$	$2.8 \times 10^{-8}$	Electrical
E6	$3 \times 10^4$	$1.3 \times 10^{-6}$	Mechanical
E7	$1.7 \times 10^4$	$4.6 \times 10^{-7}$	Breakdown
E7B	$4 \times 10^3$	$3.2 \times 10^{-9}$	Breakdown
F1	--	--	Electrical
F1B	$7 \times 10^3$	$7 \times 10^{-10}$	Breakdown
F2	$3 \times 10^3$	$3 \times 10^{-10}$	Not Known
F2B	$2.7 \times 10^4$	$1.7 \times 10^{-8}$	Breakdown
F3	--	--	Mechanical
F4	$3 \times 10^3$	$3 \times 10^{-9}$	Electrical
F4B	$3 \times 10^3$	$3 \times 10^{-8}$	Electrical
F5	--	--	Not Used
F6	--	--	Electrical
F7	$4 \times 10^3$	$8 \times 10^{-9}$	Electrical
F8	--	--	Not Known
F8B	$4 \times 10^4$	$2.4 \times 10^{-8}$	Not Known

TABLE 6.3 FIRST WIRE BATCH

Emitter	Total Emission Time, Seconds	Total P.I.T. Torr-Coulombs	Cause of Failure (where known)
F9	$3 \times 10^3$	$6 \times 10^{-9}$	Not Known
F10	--	--	Not Used
E8	--	--	Not Used
E9	$1 \times 10^3$	$2 \times 10^{-10}$	Not Known
E9B	--	--	Not Known
E10	$2.7 \times 10^3$	$4 \times 10^{-9}$	Not Known (poss. Electrical)
E10B	--	--	Not Known
E11	$3 \times 10^2$	$1.8 \times 10^{-11}$	Not Known
E11B	$8.5 \times 10^3$	$1.4 \times 10^{-8}$	Not Known

TABLE 6.4 SECOND WIRE BATCH

of the first batch of wire to those of the second.

Results of emission obtained with the first and second batches of oriented wire are summarized in Tables 6.3 and 6.4 respectively, with cause of eventual emitter failure where a reasonable explanation existed. As figures of merit, both total emission times obtained, and the sum of the products of operating pressures, currents and time (Total PIT) are given.

Comparison of the Tables leads immediately to two conclusions.

a) For the first batch, operating times of greater than 10,000 seconds are common, with PIT products in excess of  $10^{-6}$  torr-coulombs. In the second batch, the best effort, emitter E 11 B, required particular care in operation and even then 8,500 seconds and  $1.4 \times 10^{-8}$  torr-coulombs were all that could be achieved. Second batch performance was significantly worse than that of the first batch.

b) Unaccounted emitter failures in the first batch of emitters were only emitters E4, F2, F8 and F8B. All other emitters having a reasonably certain, known cause of destruction, either in terms of operating error, or equipment breakdown. In the second batch only emitter E10 has a failure which may be associated with an equipment fault, all other emitters having no obvious reason for ceasing to operate.

The analysis of these results shows beyond reasonable doubt that there were inherent problems associated with the second batch of wire.

#### 6.6.2 Failure of the Second Wire Batch

The oriented wire is produced by growing tungsten single crystal from normal tungsten wire, which is first seeded, and the crystal is then grown along the wire by a moving zone

technique. This type of process commonly suffers from batch variations, usually dependent on the manner in which the residual impurities present are distributed.

If the "single crystal" oriented wire has small aligned crystallites of the metal interspaced by layers of impurities, we can conclude that the average size of such crystallites will vary inversely with the level of impurities.

Consider this model applied to the tip of an emitter, which will be formed from one such small crystallite. The cohesive forces holding the tip in place will depend on the areas in contact across the grain boundary, and these will vary in inverse proportion to the square of the impurity concentration. Thus, small changes in the levels of residual impurities in the wire samples could make significant changes to the mechanical stability of emitters.

In an attempt to gather evidence which might lend support to this model, two experimental approaches were made;

a) A number of emitters and wire samples in new, used, and chemically etched conditions were examined in the conventional SEM. For this work I am indebted to Mr. L. Peters for his assistance. Unfortunately, it did not reveal any grain boundaries, though this is not conclusive as the specimens were extremely difficult to observe with surface detail. Indeed, surface roughness observed under the optical microscope with side illumination of the specimen could not be detected in the SEM. Poor depth of focus and limited magnification in the optical microscope prevented interpretation of surface detail visible.

b) The remaining length of oriented wire was subjected to a resistivity ratio measurement, in an attempt to estimate the levels of impurity present in the wire. For this work I am

grateful for the assistance of Mr. D. Stanley, and the cooperation of Professor A.B. Pippard for making available the facilities at the Mond Laboratory, Cambridge.

The ratio of resistances at room temperature and under liquid helium was measured consistently at  $4.5 \times 10^3$ . This value was relatively high, showing a high purity in the sample. It was in fact higher than measured values for single crystals of tungsten given in the literature by Haas and Nobel (1938), who reported  $2.5 \times 10^3$ .

The measured value was not, however, sufficiently large to indicate an exceptionally high purity in the sample. Also, the first batch of wire was no longer available for comparison measurement, so the results were in no way conclusive.

Whereas it has not been possible to pinpoint the cause of emitter failure, it is clear that the reason for the failure of the second batch of oriented wire lies in its metallurgical properties.

## CHAPTER 7

CONCLUSIONS AND SUGGESTIONS FOR FUTURE WORK

This research, has, of necessity, covered a broad range of subjects in an attempt to bridge the gap between the established ultra high vacuum techniques of field emission microscopy, and the requirements of electron microscopy. Conclusions have, therefore, been established within the relevant sections, and this final chapter will be reserved for a consideration of some more general aspects of the future applications of field emission cathodes.

7.1 Choice of Operating Mode

There appear, from the results of Chapter 4, to be two modes of operation worthy of immediate practical consideration, namely, cold field emission in an ultra high vacuum environment, and T-F emission under somewhat reduced vacuum conditions.

At first sight, it might be supposed that the T-F mode of operation suffers from the fundamental disadvantages of low source brightness compared with cold field emission, and large energy spread of the emission. However, the imaging of field emission and T-F sources is such that the full source brightnesses may not be closely approached, (section 5.2.4), so that the differences are of little practical significance. Also, the energy spread is only slightly worse than that normally obtained with thermionic emission, and is comparable, for example, with the typical stability of 50ppm for a 30kV EHT generator.

The principle advantage of cold field emission is the

reliability which may be achieved with this mode of operation. Emitters may be operated in a reproducible emission cycle, in which the onset of cumulative ion bombardment damage may be detected. At this stage the emitter may be flashed, and there is no obvious limit to the number of times this process may be repeated. Commercially available ultra high vacuum pumps and components offer considerable reliability of operation, as was demonstrated with the FEM, and the attainment of ultra high vacuum operating conditions may be assured.

Ultra high vacuum operation has the important disadvantage that the pumpdown time is very long, and T-F operation may well find initial application as a temporary expedient during the pumpdown cycle. In the long term, the reduced cost of vacuum components, reduced pumpdown times, and better d.c. stability of the T-F mode of emission may well lead to its general adoption.

## 7.2 Electron Optical Design

The field emission triode gun geometry described in section 4.3 permits almost independent control of emission current and operating voltage. These are desirable properties for electron optical applications, and not possible with the simple diode configuration, nor readily achieved with the combined lens and accelerator design of Crewe (1968).

Probe measurements in the SEOC (sections 6.3.4 and 6.4.4), have shown that very high brightnesses are possible with the triode gun, and there is no evidence to suggest that the presence of the grid electrode introduces additional aberrations to the system.

The design is convenient in practice, since both grid and emitter may be mounted from the same high voltage insulator, in

a manner very similar to that currently used with thermionic triode guns.

One possible disadvantage of this configuration, for higher voltage applications, is that the emitter is bombarded by ions which have been accelerated through the full gun potential. However, there is evidence to suggest that the lifetimes of emitters would not be adversely affected, not only from the results of section 4.4.2, but also from published sputtering curves, (Maissel (1966)), which show maximum sputtering rates typically at 5kV, dropping for both lower and higher voltage operation.

The triode gun could, therefore, form the basis of the design for a field emission electron optical system.

A promising column configuration would use two electromagnetic imaging lenses. The first lens would image the source at high magnification in an intermediate crossover, with the second demagnifying the image to form a probe. By varying the lens excitations, the position of the intermediate crossover position could be adjusted to provide optimum magnification of the source, to suit the particular operating conditions.

This system would have several additional advantages compared to the single lens column described in Chapter 5. By removing the emitter from the lens bore, higher voltage operation would be facilitated, also improved vacuum pumping of the emitter region would be possible, and better mechanical design of emitter movements.

### 7.3 Practical Design Considerations

It is worthwhile considering a few practical aspects of the design of field emission optical systems.

a) Differential pumping. The requirement for ultra high vacuum in the field emission gun means that either the whole instrument must operate under these conditions, or the gun must be differentially pumped. This latter arrangement has the obvious advantages that the rapid change of specimen, and facilities for in situ experiments available with present electron optical instruments would be preserved.

Although bakeout of the differentially pumped gun (section 5.4.3) was prevented by its immersion within the bore of the magnetic lens, and true ultra high vacuum levels were not achieved, the emitter was nevertheless effectively isolated from the rest of the column. Indeed, on occasions, emitters survived quite catastrophic changes of chamber pressures.

b) Emitter alignment. The development of the emitter welding jig described in section 2.3.2, enabled the orientation of emitter tips to be accurately controlled. Thus, in the design of future emitter alignment facilities similar to those described in section 5.4.2, provision for emitter tilting would not be absolutely necessary.

The design of such movements is not only difficult, but also the extra complexity of the emitter support reduces its rigidity, and so increases susceptibility to mechanical vibrations.

c) Vibration. Vibration levels encountered in the SECC imposed severe limitations on the use of the instrument. The design of future instruments must, therefore, make adequate provision for minimising the effects of vibration, by ensuring adequate rigidity of the critical components and providing adequate antivibration isolation. A possible approach to this latter problem would be to mount the whole instrument on a seismic block which was itself mounted on antivibration mountings, and so

introduce an extra stage of vibration isolation.

d) Anode outgassing. Since emitter lifetime is determined principally by bombardment of the emitter by ions generated at the anode, it would be a useful design feature to provide, for example, indirect heating facilities to the anode, and so permit thorough degassing during the bakeout cycle.

#### 7.4 New Emitter Materials

One important advance likely in the near future will be through the development of satisfactory techniques for the fabrication of field emitters from new materials. A number of materials are now becoming available which not only have lower work functions than tungsten, but also are much harder and therefore more resistant to damage from ion bombardment.

Lanthanum Hexaboride is particularly attractive in this context, and the attempts to reproduce the fabrication techniques of Windsor (1969), which are described briefly in Appendix II, illustrate the sort of difficulties which will be encountered. It should be remembered, however, that the reliable and sophisticated techniques for the production of tungsten emitters, as described in Chapter 2, are based on the results of the work of a large number of workers over a period of about a quarter of a century.

#### 7.5 Emitter Failures

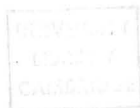
One important problem which was encountered during the research was the unexplained failure of emitters made from the second batch of oriented tungsten wire. Since it is unlikely that this will prove to be an isolated example, an examination of the metallurgical properties of oriented wire with regard to its

suitability for field emission operation will provide an important task for future workers.

#### 7.6 Pulsed Emission

One particularly interesting result of this research was the effect of emitter lifetime enhancement observed under conditions of pulsed emission, (section 4.6.1). Unfortunately, insufficient time was available for a full investigation of this phenomenon, and further research is necessary to examine more fully the factors involved, and to determine more precisely the operating conditions under which enhanced lifetime may be obtained.

With the future advancement of solid state electronics, the provision of a high voltage pulse generator for use with electron optical instruments should prove a less formidable problem than it is at the present day, and the potential advantages of pulsed operation may eventually be fully realized.



## APPENDIX I

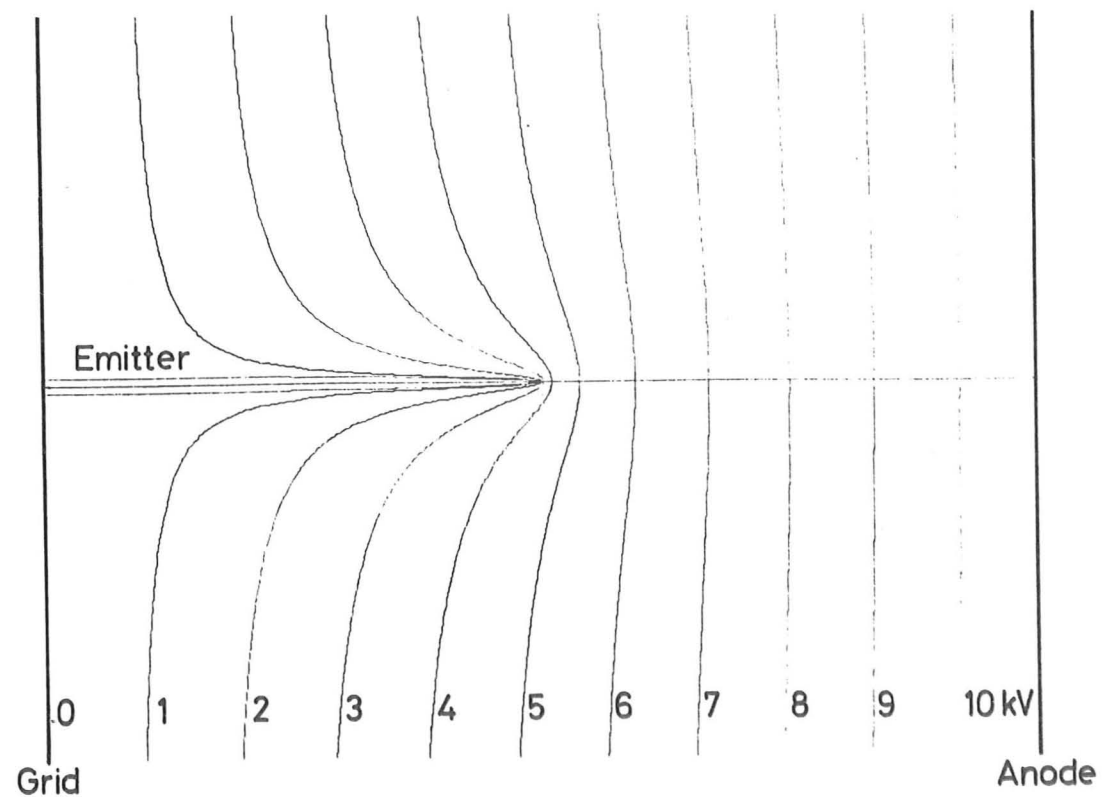
THE COMPUTATION OF ELECTRON TRAJECTORIES

Fig I.1 Equipotential Plot for 3-Electrode Gun

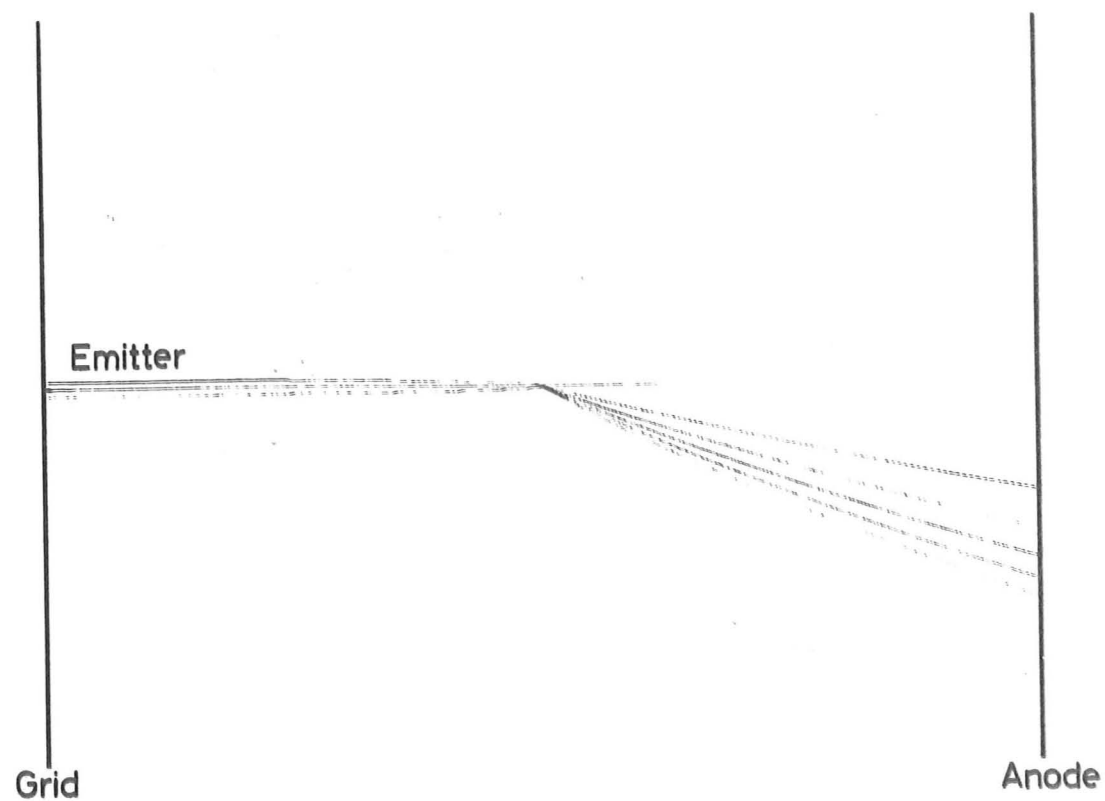


Fig I.2 Computed Electron Trajectories

An exact solution to Laplace's equation for the potential within a three electrode field emission gun was derived by Earnshaw (1965), using a transformation to the prolate spheroidal co-ordinate system. This solution was extended to consider the effects of varying the grid potential, and formed the basis for starting computational work.

It was intended to extend the analysis to calculate the performance of field emission guns, which could be immersed in a magnetic lens field, by computing the electron trajectories. However, it soon became clear that this represented a major project, and the computational work was ceased in favour of practical work.

Some results were obtained, as an example an equipotential plot is given in Fig. I.1, in which the gun geometry is included. Trajectories were calculated using the Runge-Kutta integration (Hardisty (1963)), which was available as a library routine. Some computed trajectories for electrons in the field of Fig. I.1 with zero initial energy, but started at different points on the surface of the emitter tip are shown in Fig. I.2.

## APPENDIX II

LANTHANUM HEXABORIDE EMITTER FABRICATION

Field emitters of single crystal lanthanum hexaboride have been successfully fabricated and used, by E.E. Windsor of the Mullard Research Laboratories, Redhill, Surrey. This work was brought to the author's attention early in the research period.

Lanthanum hexaboride is a particularly attractive field emitter material, since it has a low work function, and is exceptionally hard and therefore resistant to ion bombardment. Windsor had not only developed techniques for fabricating emitters, but had demonstrated emitter lifetimes significantly better than would be achieved with tungsten under similar conditions.

It was therefore decided to attempt to reproduce these techniques for emitter fabrication, in order to compare directly the properties of  $\text{LaB}_6$  emitters with tungsten. I gratefully acknowledge the help and assistance of Mr. E.E. Windsor and of Mullard Ltd.

Much of the work described above has subsequently been published, (Windsor (1969)), and so the author's work will only be described briefly.

Sintered  $\text{LaB}_6$  bar was obtained from Borax Consolidated Ltd., Carlisle Place, London SW1, and was cut into sections, 5mm square and 100mm long using a diamond saw.

Using the apparatus shown in Fig. II.1, attempts were made to traverse a molten zone along the length of the cut bars, using a high power r.f. generator, coupled into the rod by a copper concentrator. The concentrator was fixed, and the  $\text{LaB}_6$  rod could

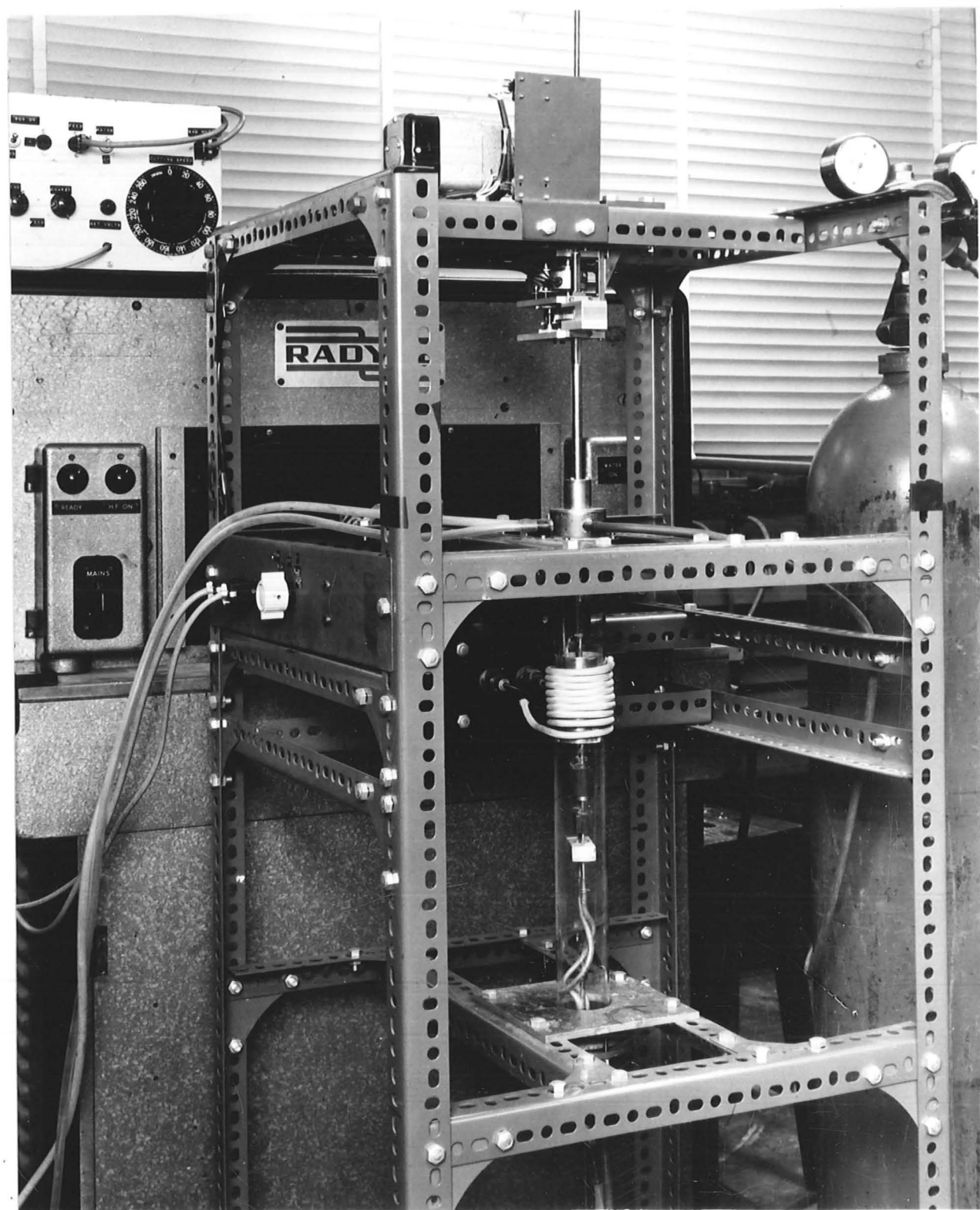


Fig II.1 Crystal Growing Apparatus for  $\text{LaB}_6$

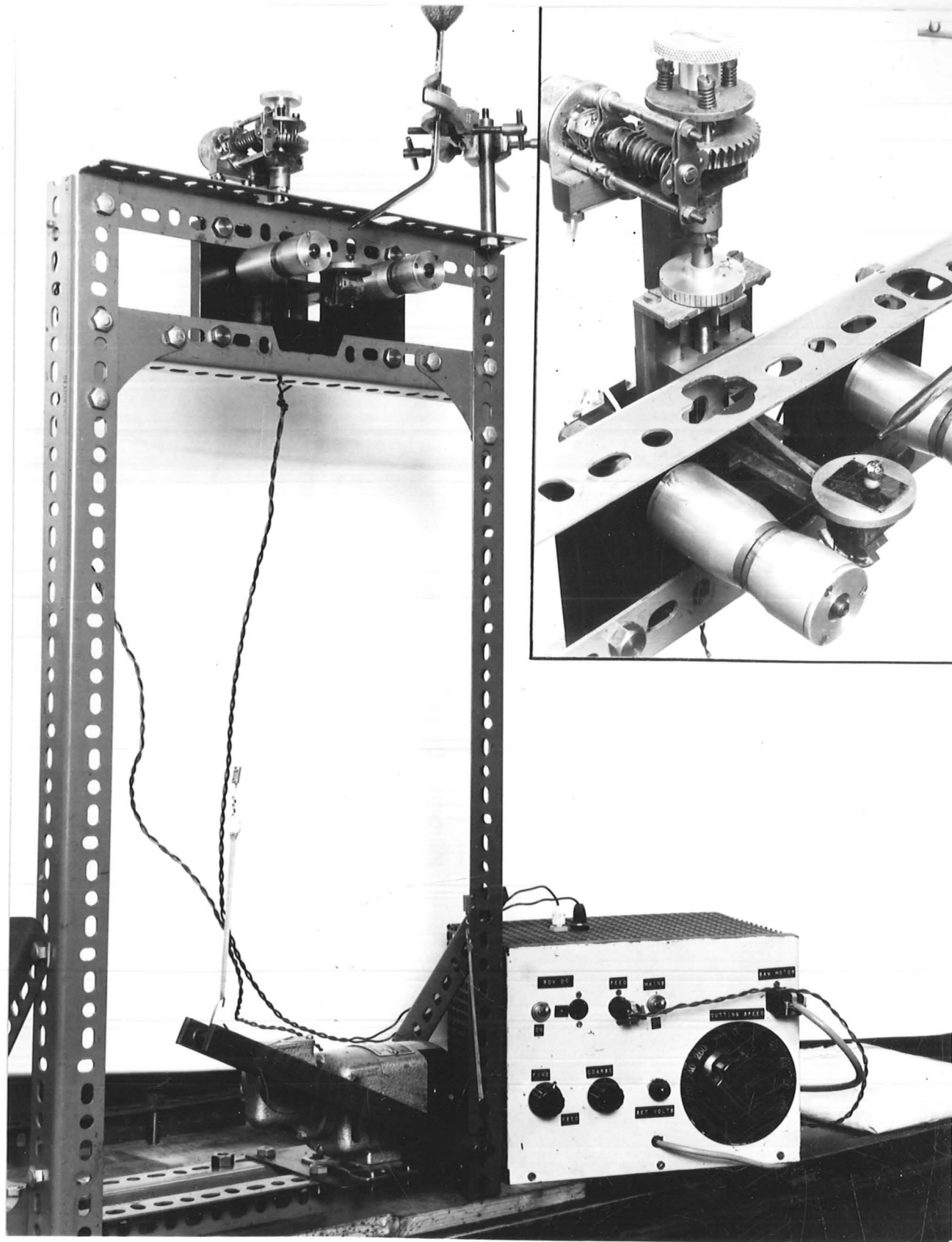


Fig II.2 Oscillating Wire Cutter

be moved through it using the motor drive at the top of the apparatus. Since  $\text{LaB}_6$  is highly reactive, the experiments were performed in an inert argon atmosphere, which was contained within a quartz tube.

The experiments were largely unsuccessful, and only on one occasion was the  $\text{LaB}_6$  completely melted. Many attempts were made, and changes of concentrator design, and the number of turns of copper tube around it produced little affect. The most likely cause of these failures is that the sintered material was insufficiently dense, being about 95% of the theoretical density, and there is good reason to expect that higher density rods would produce better results.

In order to cut the single crystal material without inducing severe damage to the crystal structure, an oscillating wire cutter was designed, and is shown in Fig. II.2 with the motor driven specimen holder inset. The cutting was achieved using 125  $\mu\text{m}$  tungsten wire, with a continuous supply of 600 grit abrasive powder suspended in light oil.

Unfortunately, the failure to establish a molten zone, and hence produce the single crystal material prevented emitters from being made.

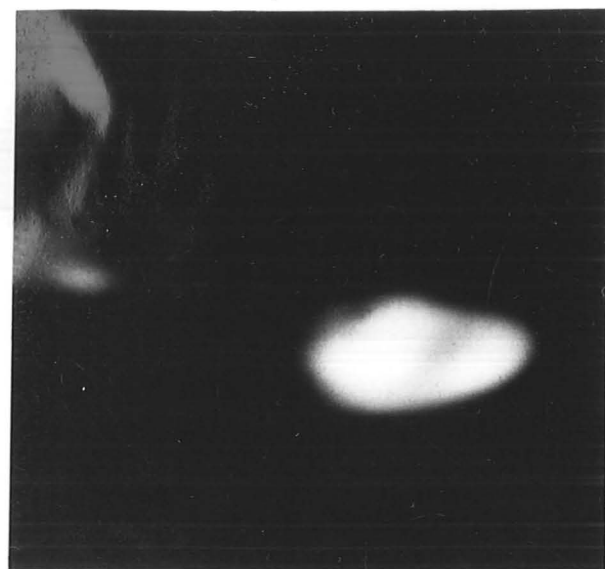
## APPENDIX III

FIELD EMISSION FROM SILICON CARBIDE WHISKERS

Silicon carbide is a potentially useful field emitter material since it is exceptionally hard. It has recently become available in the form of single crystal whiskers, which have been used directly as field emitters, (Baker (1970)), having the particular advantage that ion etching of the tip does not lead to blunting.

Fig. III.1 shows emission patterns obtained in experiments with silicon carbide whiskers, and I would like to thank Mr. F.S. Baker, of the Explosives Research and Development Establishment, Waltham Abbey, Essex, for supplying samples of the material.

In the figure, the unusual patterns (a), (b) and (c) were obtained for cold field emission at about 5kV, 20  $\mu$ A in a pressure of  $1 \times 10^{-8}$  torr. An attempt was made to establish the more familiar single crystal emission patterns, the emitter was flashed and the resulting pattern is shown in (d), where there is some similarity with the (110) pattern from tungsten.



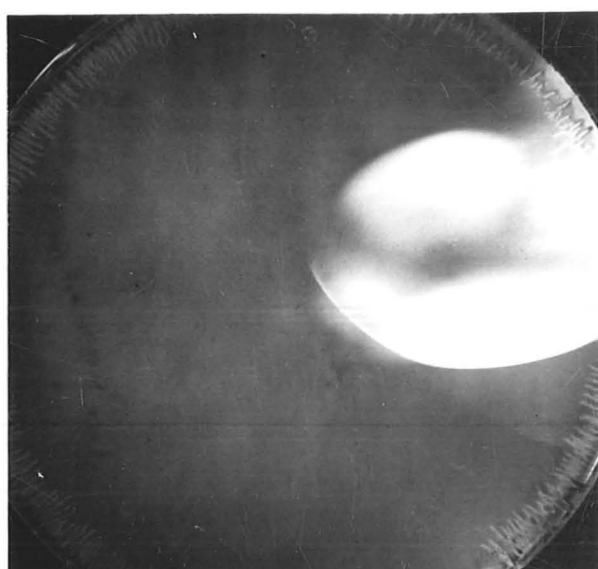
(a) Initial Pattern.



(b) After 10mins.



(c) After 20mins.



(d) After Flashing.

Fig III.1 Emission Patterns from SiC Whiskers

REFERENCES

- Albert, M.J., Atta, M.A. & Gabor, D. Brit. J. Appl. Phys., 18, 627, (1967).
- Baker, F.S. Nature, 225, 539, (1970).
- Broers, A.N. J. Appl. Phys., 38, 1991, (1967), *ibid.*, 38, 3040, (1967).
- Broers, A.N. J. Sci. Instr., 3, 273, (1969).
- Chan, T. & Gunn, M.W. Elec. Eng., 401, (1965).
- Chang, T.P.H., & Nixon, W.C. J. Roy. Microscop. Soc., 88, 143, (1968).
- Cosslett, V.E. & Haine, M.E. Proc. Conf. Electron Microscopy, London, (1954).
- Crewe, A.V., Eggenberger, D.N., Wall, J. & Welter, L.M. Rev. Sci. Instr., 39, 576, (1968).
- Crewe, A.V. Isaacson, M. & Johnson, D. Rev. Sci. Instr. 40, 241, (1969).
- Crewe, A.V. & Wall, J. J. Mol. Biol., 48, 375, (1970).
- Crewe, A.V., Wall, J. & Welter, L.M. J. Appl. Phys., 39, 5861, (1968).
- Der-Shvartz, G.V. & Makarova, I.S. Rad. Eng. & Elect. Phys. 12, 161, (1967).
- Dolan, W.W. & Dyke, W.P. Phys. Rev., 95, 327, (1954).
- Drechsler, M., Cosslett, V.E. & Nixon, W.C. Fourth Int. Conf. Electron Microscopy, Berlin, (1958).
- Dyke, W.P., Charbonnier, F.M., Strayer, R.W., Floyd, R.L., Barbour, J.P. & Trolan, J.K. J. Appl. Phys., 31, 790, (1960).
- Dyke, W.P. & Dolan, W.W. Adv. in Elect. & Elect. Phys., 8, 89, (1956).
- Dyke, W.P., Trolan, J.K., Dolan, W.W. & Barnes, G. J. Appl. Phys., 24, 570, (1953).
- Earnshaw, J.W. Thesis, Cambridge, (1965).
- Everhart, T.E. Proc. IEEE, 54, 1480, (1966).
- Everhart, T.E. J. Appl. Phys., 38, 4944, (1967).
- Everhart, T.E. & Thornley, R.F.M. J. Sci. Instr., 37, 246, (1960).

- Fasth, J.E., Loberg, B. & Norden, H. J. Sci. Instr., 44, 1044, (1967).
- Fernandez-Moran, H. J. Electron Microscopy, 16, 65, (1967).
- Fowler, R.H. & Nordheim, L. Proc. Roy. Soc., (London), A119, 173, (1928).
- Garber, R.I., Dranova, Zh.I., Mikhailovskii, I.M. & Chechel'nitskii, G.G. Instr. Exper. Technol., 1, 221, (1969).
- Gomer, R. "Field Emission and Field Ionization", Oxford Univ. Press, (1961).
- Gunn, J.B. Rev. Sci. Instr., 32, 804, (1961).
- Haas, W.J. & Nobel, J.de. Physica, 5, 449, (1938).
- Haine, M.E. & Einstein, P.A. Brit. J. Appl. Phys., 3, 40, (1952).
- Hardisty, B.M.M. Thesis, Cambridge, (1963).
- Hibi, T. J. Electronmicroscopy (Tokyo), 13, 32, (1964).
- Lafferty, J.M. J. Appl. Phys., 22, 299, (1951).
- Langmuir, D.B. Proc. IRE, 25, 977, (1937).
- Liebmann, G. & Grad, E.M. Proc. Phys. Soc., B.64, 956, (1951).
- Maissel, L.J. "Physics of Thin Films", Vol. 3, Ed. G. Hass & R.E. Thun, Academic Press London and New York, (1966).
- Maliakal, J.C., Limon, P.J., Arden, E.E. & Herb, R.G. J. Vac. Sci. Technol., 1, 54, (1964).
- Martin, E.E., Charbonnier, F.M. Dolan, W.W., Dyke, W.P., Pitman, H.W. & Trolan, J.K. Wadd Technical Report 59-20, (1960).
- Nordheim, L.W. Proc. Roy. Soc. (London), A121, 626, (1928).
- Oatley, C.W., Nixon, W.C. & Pease, R.F.W. Adv. Elect. & Elect. Phys., 21, 181, (1965).
- van Oostrom, A.G.J. Philips Research Reports Supplement No.1, (1966)
- Paz, I.M. Elec. Eng., 252, (1965).
- Pease, R.F.W. Thesis, Cambridge, (1963).
- Pease, R.F.W. & Nixon, W.C. J. Sci. Instr., 42, 81, (1965).
- Petrie, D.P.R. Fifth Int. Conf. Electron Microscopy, Vol.1, Philadelphia, (1962).
- Redhead, P.A. J. Vac. Sci. Technol., 17, 182, (1969).
- Ruben, M.J. Rev. Sci. Instr., 36, 1226, (1965)
- Smith, K.C.A. Thesis, Cambridge, (1956).

- Smith, K.C.A. & Oatley, C.W. Brit. J. Appl. Phys., 6, 391, (1955).
- Swift, D.W. Thesis, Cambridge, (1960).
- Tegart, W.J. McG. "The Electrolytic and Chemical Polishing of Metals in Research and Industry", Pergamon Press Ltd., London, (1956).
- Tillett, P.I. Thesis, Cambridge, (1969).
- De Wijn, H.W. Rev. Sci. Instr., 32, 735, (1961).
- Windsor, E.E. Vacuum, 20, 7, (1970).
- Wood, R.W. Phys. Rev., 5, 1, (1897).
- Wouk, V. IRE, Trans. Instr., I-6, 3, (1957).
- Young, R.D. Phys. Rev., 113, 110, (1959).
- Young, R.D. & Müller, E.E. Phys. Rev., 113, 115, (1959).

